ALMA MATER STUDIORUM - UNIVERSITA' DI BOLOGNA

DOTTORATO DI RICERCA IN
DISEGNO E METODI DELL'INGEGNERIA INDUSTRIALE
Ciclo XXI

Settore scientifico disciplinare di afferenza: ING-IND/06

A STUDY ON THE FLUID DYNAMICS OF DOMESTIC GAS BURNERS

Candidato:
Lorenzo Gattei

Coordinatore Dottorato:
Chiar.mo Prof. Franco Persiani

Relatore:
Prof. Alessandro Talamelli

Correlatore:
Ing. Cédric Catalogne

Esame Finale Anno 2008

To my parents

Abstract

Domestic gas burners are investigated experimentally and numerically in order to further understand the fluid dynamics processes that drive the cooking appliance performances. In particular, a numerical simulation tool has been developed in order to predict the onset of two flame instabilities which may deteriorate the performances of the burner: the flame back and flame lift. The numerical model has been firstly validated by comparing the simulated flow field with a data set of experimental measurements. A prediction criterion for the flame back instability has been formulated based on isothermal simulations without involving the combustion modelization. This analysis has been verified by a Design Of Experiments investigation performed on different burner prototype geometries. On the contrary, the formulation of a prediction criterion regarding the flame lift instability has required the use of a combustion model in the numerical code. In this analysis, the structure and aerodynamics of the flame generated by a cooking appliance has thus been characterized by experimental and numerical investigations, in which, by varying the flow inlet conditions, the flame behaviour was studied from a stable reference case toward a complete blow-out.

Nomenclature

δ_{ij}	Kronecker delta
ϵ	turbulent kinetic energy rate of dissipation
μ	dynamic viscosity
μ_e	dynamic eddy viscosity
Φ	equivalence ratio
Ψ	dissipation function
ρ	density
σ	Schmidt number
τ_c	chemical time scale
τ_f	flow time scale
τ_w	shear stress at the wall
υ	kinematic viscosity
υ_e	kinematic eddy viscosity
ξ	mixture fraction
B_i	body forces
C_{vol}	volume gas fraction
D	mass diffusivity
E_a	activation energy
h	specific enthalpy
k	turbulent kinetic energy
M	molecular weight

p	pressure
R	ideal gas constant
R_i	mass rate of creation or depletion by chemical reaction
S^h	source of enthalpy
S^m	source of mass
S_i^u	sources of momentum
S_c	global consumption speed
S_d	local displacement speed
S_i	sources of species creation
S_L	laminar burning velocity
T	temperature
t	time
U	free-stream velocity
u_τ	friction velocity
u_i	velocity components
u_r	radial velocity
w	burner flame port width
Y	mass fraction (molecule)
Z	mass fraction (element)

Contents

Introduction

Fire is a contradictory element. It is mentioned as one of the benefactors of mankind because it warms the home, cooks food or forges metals, but at the same time it represents a wild and cruel destroyer, whether runaway in a forest or feeding bullets or bombs. Even the Sun, source of light, heat and well-being can dry or burn if its power is not shielded. As for the Sun, the nature of the power of fire is its capacity to transform. Ray Bradbury started FAHRENHEIT 451 with this sentence: "It was a pleasure to burn. It was a special pleasure to see things eaten, to see things blackened and *changed*...". Therefore, fire can be so calm and peaceful, but within it is all power and destruction. It is characterized by a quick and irreversible change: wood burns, dropping ash and cinder off, dough puffs and firms up to become bread, clay hardens turning into porcelain, chemical elements react making new molecules. Hence, fire destroys a form to create another form. Moreover, the heat and well-being provided by the fire promote relaxation and communion. That's why the hearth has always represented a social occasion for sharing ideas, telling stories and singing. I like to think that nowadays the kitchen represents that hearth. The place where family groups, where life experiences are shared. Fire is still present there. Just look at the domestic gas burner.

After more than one century gas stoves can be found in the majority of Italian houses and it is possible to find a large amount of these appliances also in France, Spain, East Europe and the US. Of course the gas burner represents one of the oldest cooking appliances used to warm and heat up food. Over time its outward appearance has practically not changed at all, presenting a circular shape and flames on the perimeter. Therefore, everyone has seen a domestic gas appliance and probably knows how to use it. But how does it work? Which are the physical principles that drive its functioning? What happens when the control knob is turned and the flames cover the burner crown? These are some of the questions that I asked myself when starting this Ph.D. research. However, the most frequent question I had to answer during these years was: how does an aerospace engineer deal with such an old (and apparently simple) cooking appliance? The answer can be found in the following introduction and it will be further clarified and justified during the reading of this manuscript.

Even though the gas burner is apparently quite a common device, its functioning is still not fully understood. This appliance is indeed characterized by a complex flow field (unsteady, three dimensional, multiphase, with chemical reaction) that drives its performance. In order to understand the key role of the fluid dynamic field, a brief explanation of the functioning of the domestic gas burner is presented in the following. When the control knob is turned, the gas fuel emerges from the injector. This component can be considered the "heart" of a gas stove and it is usually placed on the bottom of the appliance. On leaving the injector, the reactive gas firstly emerges as a jet into the bowl and starts to entrain air from the surrounding ambient of the cooking hob. This gas/air mixture then flows into the burner head before being discharged through the flame ports and ignited. The unique control of the heat released by the gas burner is provided by regulating the flow of reactive gas issuing from the injector. This is performed by means of a manual valve (linked with the control knob). Therefore, there are no moving parts and all the geometrical dimensions of the internal ducts are kept fixed. This represents one of the challenges in the cooking stove design since, despite the fixed geometry, the appliance has to work properly in different countries, characterized by different fuel gases. A change in fuel typology means a change in physical properties such as density, viscosity, calorific power resulting in a complete modification of the fluid dynamics behaviour of the appliance. The same appliance also has to ensure a correct functioning in different hobs or in different positions inside the same hob layout. Therefore, although the domestic gas burner appliance can be considered a mature appliance, it still presents a difficult challenge for the designer. Finally, it must be pointed out that this is a large production appliance defined by a low price, in which the cost reduction is one of the most important targets.

Of course, it does not seem necessary to understand the physical mechanism fully, since one can always design a device which is able to provide the necessary heat. However, this may result in an unnecessary fuel consumption or in the presence of instabilities which may compromise the performances of the device or even its safety. Traditionally, this difficulty was overcome with a systematic trial and error design philosophy. This approach was probably sufficient in the past, whereas nowadays the increase of the safety and performance requirements and the availability of more and more modern numerical and experimental devices leads to a new design methodology. One approach is an experimental analysis of the gas burner flow field. Physical quantities like temperature or pressure can be easily measured almost everywhere and they do not typically require expensive sensor probes. However, if a more detailed study concerning the flow field in and around the domestic gas burner is required, then the use of optical measurements such as Laser Doppler Anemometry (LDA) or Particle Image Velocimetry (PIV) must be considered. Imaging of reactive flow fields does indeed provide new views into the complex chemical and fluid-mechanical phenomena typically found in combustion devices. Combustion imaging hence specifically

supplies information on two and three dimensional flame structures, allowing a detailed identification of the basic processes governing reactive flow. However, the application of these techniques during the development stage of a new gas burner will require expensive resources, both human and hardware, that cannot usually be expended, especially in an industrial reality. Moreover, these optical measurements present several difficulties when carrying out an investigation on a domestic stove: the optical access is limited, the circular geometry can cause distortion of the resulting image and, most of all, the use of reacting working gases will drastically increase the difficulty of measurement acquisition and the safety standard required by the lab. Another possible approach to the study of such a complex flow field is to rely on theoretical or numerical analysis. A first advantage of a numerical approach is that, sometimes, if the run cost (in time and money) is not very large, it allows a quick preliminary study of the configuration. New geometries can be tested relatively quickly, when compared to manufacturing several burner prototypes. Moreover, numerical modeling can be used for predictive purpose to test different scenarios that may be too risky or expensive to try in a laboratory. By allowing the possibility of running "what if" scenarios, numerical analysis multiplies the number of designs or circumstances before physical prototyping and testing. Computational Fluid Dynamics (CFD) have gained popularity in recent years due to a number of factors. New generations of computer hardware have more speed and more memory at a lower cost. Obviously, doing numerical modeling first can save considerably on prototype development time and costs by eliminating particular designs without actually having to test them. However, in most cases, it is not possible to completely eliminate prototype testing because of the uncertainty and limitations of the numerical model especially when it comes to new configurations that have never been tried before.

Both experimental and numerical tools described briefly above are the results of a long period of research and development, with a lot of investment in terms of money and human resources. A strong boost in their development was and it is still made by Universities and Research Centres related to aerospace engineering. This because aerospace engineering had to often deal with advanced design methodologies in order to promote the highest common standards of safety and regulation. The starting point of this investigation was represented by a collaboration between Electrolux and the University of Bologna in order to analyze existing design procedures concerning the domestic gas burner appliances, and, if possible, to develop new ones. Electrolux is a global leader in home appliances and appliances for professional use, selling more than 40 million products to customers in 150 countries every year. Electrolux products include refrigerators, dishwashers, washing machines, vacuum cleaners and cookers. This collaboration has of course influenced the overall activity carried out during this Ph.D. program. In order to be sold in the market, this kind of appliance has to be

formally certified. Manufacturers of residential and commercial gas fired burners have to inspect their appliances for certification according to the standards of the relevant authorities. These devices are therefore tested, which requires a large amount of time, for a number of operating conditions with respect to the safety of operation and to emission performance. However, these tests do not usually provide a detailed understanding of the physical processes involved in the functioning of the appliance, because they consist on a global review of some characteristics of the stove behaviour, such as for instance a visualization of the flame structure. Their result is often summarized by a simple qualitative value that does not guide the designer through the development or optimization process.

This lack of information is particularly present in the certification test regarding flame stability. Of course, the flames issuing from the domestic gas burner have to be stable and steady. In order to shorten the time to develop of the prototypes, and reduce the testing phase during the design, a better understanding of the instability phenomena of partially premixed flame is hence essential. In this context, the present research program has been characterized by the study of two flame instabilities: the flame back and the flame lift. Flame back and flame lift represent the tendency of the flame front to burn back through the burner exit ports and to detached form the burner rim, respectively. This problem is complicated by the fact that the standard design criteria adopted to avoid these instabilities go in opposite directions. If the designer tends to avoid flame back, then the possibility of flame lift occurring is increased, and viceversa. Therefore, during the development of the domestic gas burner a more exhaustive analysis is required in order to strike the right balance. It must be pointed out that the flames issuing from the burner are the result of the internal fluid dynamic processes inside the appliance. Indeed, these instabilities can be observed "outside" the burner, but they are already generated by a incorrect functioning "inside" the appliance.

Aim of this thesis is to assess the possibility to perform this investigation by means of numerical simulation tools. Main goals of the present thesis are represented by the formulation of prediction criteria concerning the flame back and the flame lift instabilities. The study has been mainly performed numerically and it has been conducted on a real domestic gas burner geometry, without introducing simplification in its shape or dimensions. However, the numerical model had to be validated and verified with experimental measurements which for this case are not available in the literature. For this reason, specific experiments must be set-up and carried out. The synergy between the experimental and numerical analysis not only increase the level of understanding of the thermo-flow physical processes that lead the domestic gas burner performances, but also allows to understand which phenomenon could be predicted by the CFD and under which conditions. The thesis presents an analysis performed on the internal domestic

gas burner aimed at a better understanding of the internal flow field of the appliance and its influence on the flame instabilities. The numerical tool was applied on a real geometry by studying different flow configuration. This investigation has been carried out together with experimental measurements performed in order to validate the model prediction and its sensibility at the flow variations. Once calibrated and validated, the numerical simulation was also applied at the study of the the flame instabilities. The flame back was investigated by means of an analysis in cold condition, without consider the reaction process due to the gas combustion. In order to obtain the necessary information to formulate a prediction criteria for the flame back instability, the numerical investigation has been supported by an experimental data set obtained in a previous industrial project. The formulated criteria is based on the balance between the unburnt mixture velocity through the burner flame port and the laminar burning velocity of the stove flame. Similarly, flame visualizations were required in order to define the flame lift phenomenon from the quantitative point of view. By means of direct flame photographs and OH chemiluminescence images the combustion model was validated on the domestic gas burner virtual prototype. The flame structure was analyzed for different flame states (from the stable flame to the lift-off instability) and compared to the corresponding numerical flame prediction. Different post-processing methodologies were presented and applied to these different flame structures in order to quantify the flame lift instability numerically. The combination of these techniques lead to the prediction criteria for the flame lift instability.

This work is performed in cooperation with two departments in Electrolux: the Cross Technology Innovation (CTI) and the Gas Technology Center (GTC). These laboratories represent the core of competence on the domestic gas burner, gained by Electrolux both from an experimental and a numerical point of view. Although many idealized problems concerning combustion were solved in simplified forms in the past, there are still many practical problems that defy a more accurate solution today. The present manuscript does not seek to replace exiting works, but to complement them, giving the reader a solid grounding on the fluid dynamics of a domestic gas burner and its instabilities: flame back and flame lift. This volume is subdivided into five chapters. Chapter 1 introduces the domestic gas burner and the fluid dynamic concepts associated with its functioning. It also includes an analysis of flame stability and the design criteria used in order to avoid the flame back and flame lift instabilities. Chapter 2 presents a detailed description of the numerical model adopted in this work. Chapter 3 provides a numerical investigation of the internal fluid dynamics of the domestic gas burner. A better global understanding of the whole appliance was also achieved by means of gas flow rate, pressure recovery and PIV measurements. These experimental results were used to calibrate and tune the numerical code as well as to point out its sensitivity to different models, to simulate the physical properties of the fluid gases. Chapter 4 presents an investigation based on a numerical Design of

Experiments aimed at formulating a prediction criterion for the flame back instability. Chapter 5 describes the analysis of the flame lift phenomenon by means of an experimental and numerical investigation achieved on a domestic gas burner crown at different equivalence ratios and heating powers. A prediction criterion for the flame lift instability is also reported in this chapter. Finally, in the conclusion, the applications of the techniques developed in the previous chapter is discussed, emphasising also possible future works related to the study of domestic gas burners.

Chapter 1

Domestic Gas Burner Design

Chapter Purpose:
This chapter gives an overview of the domestic gas burner. The working principles of this appliance will be discussed, highlighting the fluid dynamic processes involved. Special attention will be dedicated to the flame stability of the cooking stove and the empirical design criteria adopted to design the burner.

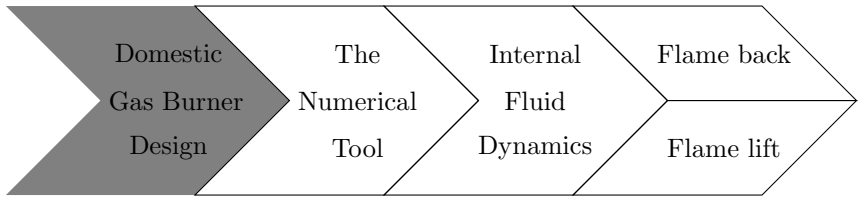

1.1 The domestic appliance

Probably the first gas appliance to be sold in Europe on a wide scale was the domestic gas range. The design of the gas range has progressed from a counter top, match-lit unit to the sophisticated range of today which may be equipped with automatic ignition, touch-control user interface and timed cooking features. The most popular range style is called "built-in" and is supplied in different pieces, with the cooking top separate from the oven in order to permit flexible kitchen arrangements and installation at convenient working heights. Built-in top burner hobs are therefore designed to be installed in a counter top and are available in different burner unit arrangements. Moreover, cooking appliances built for commercial use differ from domestic appliances mostly in size and the fact that they are built to serve special uses only.
The domestic gas burner is thus a device that is used to combust the fuel with an oxidizer to convert the chemical energy contained in the fuel into thermal energy. This energy conversion is performed by means of a combustion process. In the following sections, the classification of combustion and burner typologies will be discussed; the required features requirements that the domestic gas burner has to satisfy during its functioning will also be presented.

1.1.1 Flame definitions

In order to classify combustion phenomena and their different appliances, it is useful to introduce two types of flames: premixed and diffusion flames. These flames will be reviewed considering a laminar regime only, in which velocity is ideally parallel to the wall axis with a parabolic distribution as a function of the distance from the wall, while pressure is a function of streamwise distance.

For laminar flames issuing from a tube burner these two models of combustion are shown in Fig. 1.1. If fuel and air are already mixed within the tube, as in the case of a Bunsen burner, and the gas is ignited downstream, a premixed flame front will propagate towards the burner until it reaches its steady state position in the form of the well-known Bunsen cone. Behind the flame front, as yet unburnt intermediates such as CO and H_2 will mix with the air entrained from outside the burner and lead to post flame oxidation and radiation. Therefore the unburnt fuel stream is supplied with air (known as primary air) before combustion occurs. If all the air required for complete combustion is provided as primary air, then the flame is said to be fully aerated or fully premixed. If only part of the total air required is supplied with the primary air, the flame is said to be partially aerated, and the remaining air (known as secondary air) diffuses into the hot combustion gases downstream of the flame front.
The other mode of combustion is that in a diffusion flame or non aerated flame. Here no air is mixed with the fuel within the tube of the burner. Therefore only fuel issues from the tube, as shown in the second picture of Fig. 1.1; this

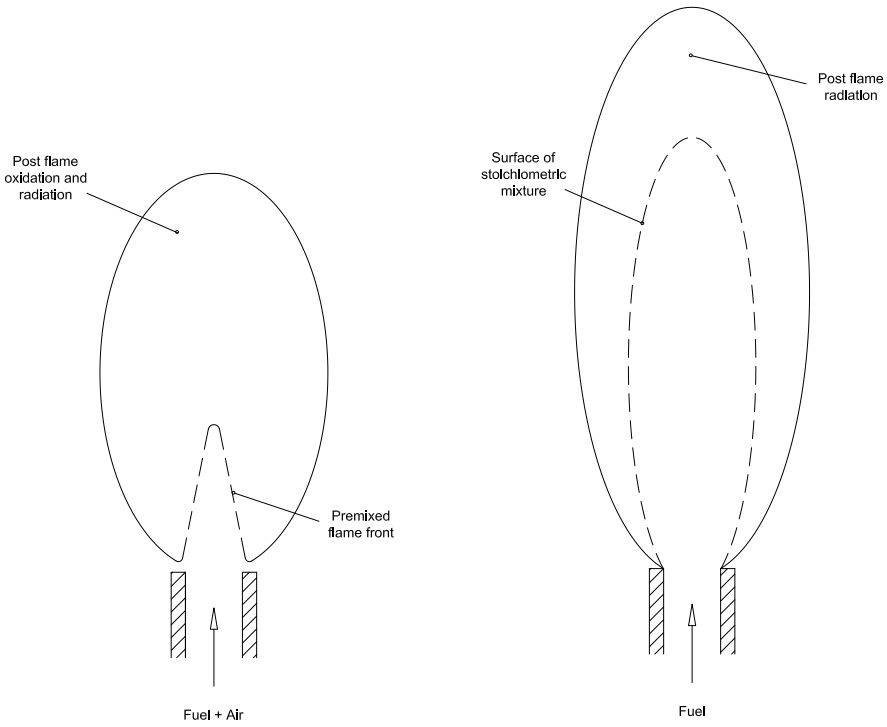

(a) Premixed flame (b) Diffusion flame

Figure 1.1: Different modes of laminar combustion.

gaseous stream mixes with the surrounding air by convection and diffusion while combustion is already occurring. Optimal conditions for this kind of combustion, however, are restricted to the vicinity of the surface of the stoichiometric mixture. This is the surface where fuel and air exist locally in a proportion that allows both to be entirely consumed. This will lead to the highest flame temperature and, due to the temperature-sensitivity of the chemical reactions, to the fastest reaction rates. In most cases combustion is much faster than diffusion and diffusion is the rate-limiting step that controls the entire process. This is the reason why the flames where the reactants are non-premixed, are called diffusion flames.
The three types of flame (premixed, partially premixed and diffusive) differ both in appearance and with respect to the dominant physical and chemical process present. All have been extensively used by combustion engineers, the properties of each being particularly suited to certain applications.

As illustrated in Fig. 1.2, premixed flames appear with a blue to bluish-green color, while diffusion flames radiate in a bright yellow. The blue colour of premixed flames is due to the chemiluminescence of some excited species (C_2 and

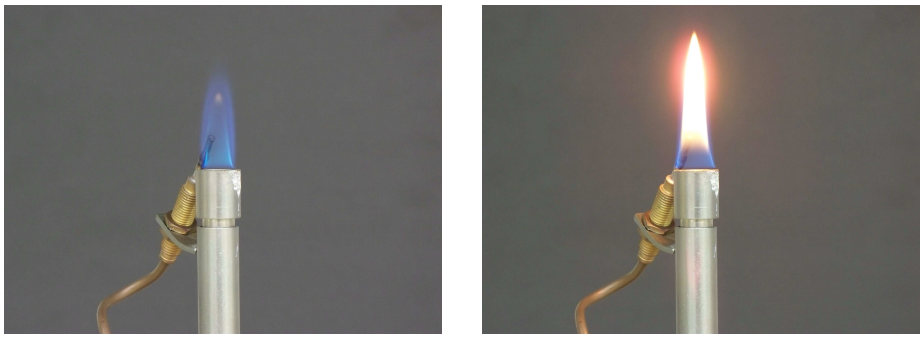

(a) Premixed flame (b) Diffusion flame

Figure 1.2: Different aspects of laminar combustion.

CH radicals), while the yellow colour of diffusion flames is caused by radiating soot particles, which dominate over the chemiluminescence that is also present in non-premixed combustion. Highly stretched diffusion flames, in fact, also appear blue since the local residence time is too short for soot particles to be formed. This leads to the conclusion that the colour of a flame is characteristic of the available residence time rather than the mode of mixing.
Premixed flames are used whenever intense combustion within a small volume is required. This is the case in household appliances and spark ignition engines. Sometimes combustion is partially premixed in order to have a better control over flame stability and pollutant emissions, as is the case in jet engine combustion chambers. On the contrary, an example of non-premixed combustion is the Diesel engine, where a liquid fuel spray is injected into the compressed hot air within the cylinder. Large combustion devices such as furnaces operate under non-premixed conditions with diffusion flames since the premixing of large volumes of fuel and air represents a serious safety problem.
Premixed flame can be divided into two other groups: partially premixed and totally mixed flames. The former describe a flame which propagates in gradients of mixture fractions [1], the latter include a combustion process propagating in stoichiometric or fuel lean mixtures (thus the flames are “fuel mixed” in that sense). Partially premixed combustion is an intermediate regime between the limiting cases of premixed and non-premixed combustion. Although combustion problems are generally approached from one of these two limiting cases, there are many practical situations where flames cannot be considered purely premixed or non-premixed, and the partially premixed approach must be used. Most of the domestic gas burners generate laminar partially-premixed flames.

1.1.2 Burner definitions

There are numerous ways of classifying burners. One common method for classifying burners is according to the flame definition presented in the previous section (i.e., how the fuel and the oxidizer are mixed):

- non-aerated burner or "nozzle mix" burner: adopting diffusive flame;
- aerated burner: adopting premixed or partially premixed flame.

Each of the different types of burner is used in various forms and configurations in order to suit particular applications. In diffusion mixed burners, the fuel and oxidizer are separated and unmixed prior to combustion, which begins when the oxidizer/fuel mixture is within the flammability range. In premixed burners, the fuel and the oxidizer are completely mixed before combustion begins. Porous radiant burners are usually of the premixed type. Premixed burners often produce shorter and more intense flames, compared to diffusion flames. These last can produce regions of high temperature in the flame, leading to non-uniform heating of the load and higher NO_x emissions.
In this work only the aerated burner will be investigated and will hereafter usually be named "domestic gas burner". Until Bunsen's invention of the aerated burner in 1855, gas was used only for lighting, since the luminous, non-aerated flame provided illumination that was far superior to candlelight. The aerated burner had, however, several disadvantages. Lightback to the injector occurred when gas suppliers did not maintain the correct gas composition. Burners were also noisy and susceptible to blockage (linting) by airborne dust. As a results of these difficulties, non-aerated burners were designed with well defined, virtually soot-free flames, and from 1945 the majority of European domestic gas appliances (excepted cookers) were fitted with non-aerated burners. The development of quiet, clean, trouble-free appliances (particularly gas fires) led to a large increase in the domestic use of gas. The advent of natural gas necessitated a revision of the aerated burner, because of the inherent problems of flame instability and sooting with non-aerated hydrocarbon burners. Conversion to natural gas therefore resulted in a large scale reintroduction of the partially aerated gas burner for all domestic gas appliances, and included the replacement of existing town gas non-aerated burners with aerated methane burners. Such changes were, however, anticipated; fundamental work had been undertaken by the gas industry from the mid-1950s onwards on both the theoretical and practical aspects of aerated burner design [2].
To be consistent with the flame terminology, the cooking appliance flame can only be described as "partially premixed" (i.e. partially on the way to stoichiometry) in regions where the mixture is fuel rich. The domestic gas burner is therefore a partially premixed device functioning under atmospheric conditions, where the formation and the homogenisation of the reactive mixture are only due to the entrainment force of the jet issuing from the injector, and to the geometrical

characteristics of the device. The mixture exits through the flame ports and the flames can be considered to be partially premixed laminar flames.

1.1.3 General layout of an aerated burner

The various parts of a domestic atmospheric gas burner are shown in Fig. 1.3. Modifications in size and shape are made to fit the desired combustion powers and heating elements. The burner assembly consists of an injector placed in a bowl, a mixing tube (venturi), a burner head (crown) and a cap.

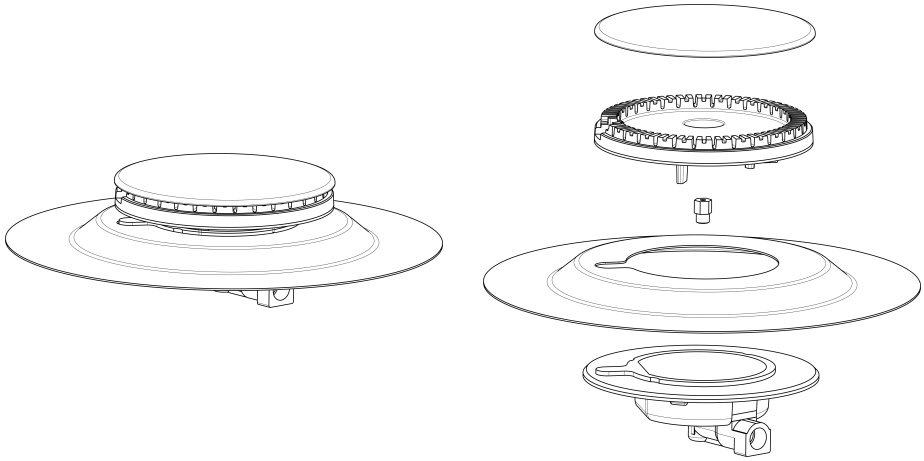

(a) Ensemble view (b) Exploded view

Figure 1.3: Parts of an atmospheric domestic gas burner. In the exploded view, from the bottom to the top the following components are shown: bowl, hob, injector, crown and cap.

Older range top burners were usually constructed of cast iron with drilled ports. Later they were manufactured in stamped metal with either drilled or slotted ports which directed the flame either horizontally or slightly upwards. Most newer ranges have round burners made of die-cast aluminum alloy in which the flame ports are directly obtained from the thermofusion process.

Referring to Fig. 1.4, when the burner is turned on the fuel enters the supply tube (1), then the gas emerges from the injector nozzle, consisting of one or more small holes (2); usually this nozzle is placed at the bottom of the appliance along the vertical axis or along the horizontal direction. The gas stream emerges from the orifice as a free jet at a rate dependent on gas pressure, orifice dimensions and gas composition. On leaving the injector, the gas entrains primary air (3) by a momentum sharing process between the emerging gas and ambient air. The gas/air mixture enters a mixing tube, which may be shaped in the form of a tapered venturi or may have parallel sides. As its name suggests, the mixing tube

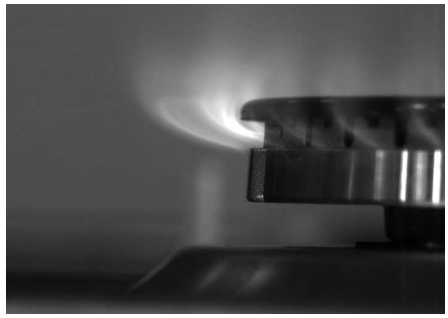

(a) Flames close up

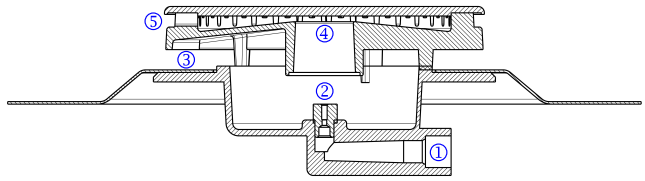

(b) Ensemble section

Figure 1.4: Traditional domestic gas burner. The section view shows its main component: (1) gas supply tube, (2) injector, (3) primary air inlet, (4) mixing tube throat, (5) flame port exit.

is designed to ensure thorough mixing of gas and air, so that a constant air/gas ratio is maintained throughout the burner head. It is normally assumed that, owing to turbulence, mixing is virtually complete at the throat of the mixing tube (4), at which point, depending on the precise geometry, the static pressure of the gas/air stream may have been reduced almost to that of the surrounding atmosphere. Further downstream, the static pressure must increase sufficiently to overcome the resistance to the flow within the burner and at the flame ports. A pressure increase can only be induced by a decrease in momentum and velocity, and this can only arise because of a gradual expansion within the burner head. It is normally achieved by a suitably shaped diffuser section in the burner. The gas/air mixture then flows into the burner head (radial diffuser) before being discharged from the flame ports (5). Of course the mixture must then be distributed uniformly to the burner ports. These flame ports can differ in size and shape according to the burner characteristic and performances. However, this work will focus on a cylindrical burner presenting two types of rectangular ports, named hereafter type 1flame port (primary flame port) and type 2 flame port (secondary flame port) respectively. As depicted in Fig. 1.3, the former are the bigger (higher) dentures on the burner crown, whereas the latter are the smaller

(shorter) ones. These ports are therefore alternatively positioned and equally spaced along the burner crown circumference.
When the mixture of gas/air is in the right proportions, the mixture will ignite. A spark device is used to light the burner.
Top burners have a maximum input rate of $3kW$ to $5kW$. Control of heat for top burner or flame size is achieved by regulating the flow of gas by means of a manual valve (control knob). Some valves have extra passageways so that finer control at low input rates may be obtained.
Other burners may have two or more separate burner heads; a smaller one positioned inside a large one. Each of these burners has its own mixing tube and they are called two-throat burners. The manual valve is constructed so that upon turndown, gas is supplied only to the smaller burner.
Finally, all gas appliances have pan supports on the top surface. The pan supports may be built-in and heated with their own burner, or they may be a separate utensil which fits over one or two top burners.

1.1.4 Burner requirements

The purpose of a domestic gas burner is to transform gas into useful heat, which is to be absorbed by an object. Attaining this purpose involves much more than the burner; the design of the burner injector, of the element to be heated and of the fuel gas passageways, is an inseparable part of the problem. In general, a burner must have the following characteristics:

- be controllable over a wide range of turndown ratios without flashback or outage (mainly applicable to gas range and manually controlled room-heater burners);
- provide a uniform distribution of heat over the area heated;
- be capable of completely burning the gas;
- ensure that there is no lifting of flames away from ports;
- provide ready ignition and cross lighting, with the flame travelling from port to port over the entire burner rapidly and positively;
- operate quietly during ignition, burning and extinction;
- be of solid construction to withstand severe heating and cooling during all the life of the appliance.

These requirements must be met under a wide variety of service conditions. Differences in gas composition and changes in pressure and specific gravity should not prevent satisfactory operation. To satisfy the above requirements, different geometrical solutions can be developed, therefore in the following a brief description of a usual appliance will be presented. However, these different design

approaches have to ensure a robust design, allowing flexibility for different working gases or different configurations of the cooking hob.

1.1.5 European standards requirements

Since legally required to do so, manufacturers of gas appliance in Europe submit their appliances for certification according to the relevant European Standards. Appliances are tested under a number of operating conditions for safety of operation (including details of construction, electrical safety, combustion performance) and thermal efficiency. For full details of test procedures and requirements, the reader should consult the appropriate European standard [3]. It is, however, worth summarizing here those tests which are of particular concern to the burner designer. The precise requirements depend on the appliance and the fuel. Appliances are classified by categories defined according to the gases and pressures for which they are designed. In the same way, gases are classified in three families (1st, 2nd and 3rd), which may be divided into groups according to the value of the Wobbe number[1]. Generally, as a gas appliance, the domestic burner refers to the 2nd (composed by groups H, L and E) and 3rd family (composed by groups B/P and P). The denominations and characteristics of the main gases used in the European countries are listed in Tab. 1.1.

Designation -	Composition (%)	W_s (MJ/m^3)	H_s (MJ/m^3)	d (Kg/m^3)
$G20$	$CH_4 = 100$	50.72	37.78	0.555
$G30$	$nC_4H_{10} = 50$ $iC_4H_{10} = 50$	87.33	125.81	2.075
$G231$	$CH_4 = 85$ $N_2 = 15$	40.90	32.11	0.617
$G32$	$C_3H_6 = 100$	72.86	88.52	1.476

Table 1.1: Characteristics of the test gases (dry gases at $288.15K$ and $101325Pa$): the composition is in volume, W_s is the gross Wobbe number, H_s is the gross calorific value and d is the density ratio of equal volumes of dry gas and dry air under the same temperature and pressure conditions.

[1]The Wobbe number is the ratio between the calorific value of a gas per unit volume and the square root of its density under the same reference conditions. The Wobbe number is said to be gross or net depending on whether the calorific value is gross or net.
The calorific value is defined as the quantity of heat produced by combustion at a constant pressure of $101325Pa$, of a unit volume or mass of gas, the constituents of the combustion mixture being under reference conditions and the combustion products being brought to the same conditions. The gross and the net calorific value consider the water produced by combustion to be condensed or to be in vapor state, respectively.

Any requirement quoted below is for these families of gases and should be used only as a guide.

- **Gas rate**. Using reference gas (mainly $G20$ and $G30$) under normal operating conditions according to the category of the appliance, the gas consumption of a burner must correspond to the manufacturer's declared (rated) heat input within certain limits of tolerance. The nominal heat input Q_n indicated by the manufacturer is given by the following expression:

$$Q_n = 0.278 \cdot \dot{V}_n \cdot H_s \tag{1.1}$$

  where Q_n is expressed in kilowatts, $\dot{V}_n$ is the volume rate of dry gas under reference conditions corresponding to the nominal heat input in cubic meters per hour, and H_s is the gross calorific value of the reference gas given in megajoules per cubic meter. Of course, the volume rate of dry gas is proportional to the static pressure applied at the gas inlet connection of the appliance in operation (injector). The static pressures at the injector are indicated in Tab. 1.2 according to the European standard for gas appliances [4].

	Pressure (Pa)		
Test gas	Minimum	Nominal	Maximum
$G20$	1700	2000	2500
$G30$	2000	2900	3500

Table 1.2: Test pressures relative to each gas category: 2H ($G20$) and 3B/P ($G30$).

- **Combustion**. For most appliances, combustion performance requirements are linked to the concentration of carbon monoxide in the combustion products. The volume content of CO in the air and water free products of combustion must not exceed a threshold value.

- **Flame stability**. The flames issuing from the domestic gas burner have to be stable and quiet. Therefore, no lightback or flame lift is permitted; these instability phenomena represent the tendency of the flame front to burn back through the burner exit ports, and to detached form the burner rim respectively.
  Concerning flame back, when the burner tap is turned to its reduced rate position the burner flames must not light back nor must they be extinguished. The hardest test for lightback certification includes:

- Configuration: the tests are carried out with a pan (in order to highlight the lightback phenomenon the pan can be substituted by a hotplate; this also ensures higher temperatures both for the appliance and for the entrained air).
- Condition: the appliance is operated initially at a reduced rate for 10 minutes.
- Working fluid: $G32$ (propylene, C_3H_6).
- Supplied pressure: $1700Pa$.

The appliance is supplied with the limit lightback gas, under minimum test pressure. On turning the tap at normal speed (operation at fairly constant speed, in a time of approximately 1 second) from the full-on position to the reduced rate position, the test checks that no lightback or extinction occurs.
Concerning the flame lift, a slight tendency to flame lift is permitted on ignition but flames must be stable 60 seconds after ignition. The hardest test for flame lift certification includes:

- Configuration: the test is carried out without a pan.
- Cold condition: the appliance is at ambient temperature at the start of the test.
- Working fluid: $G231$ (85% of CH_4 and 15% of N_2).
- Supplied pressure: $3000Pa$.

With the appliance supplied with the limit flame-lift gas, under maximum test pressure, the flame stability is verified within 60 seconds after ignition.

Within the framework already discussed for flame stability and European standard requirements, it is possible to list a number of criteria which need to be met by all gas appliances:

- Uniform flame distribution and height, giving an even heat distribution to that which is being heated.
- Complete combustion, subject to the carbon monoxide and soot emission clauses in the appropriate Standard.
- No flame lift or lightback within the full range of operative conditions.
- No excessive noise, particularly during the ignition or extinction sequence.
- The materials used and the standard of construction should be such that the burner lifetime is acceptable (at least twelve or fifteen years).

Additionally, there is now much more concern regarding the emission of nitrogen oxides (NO_x) into the indoor and outdoor environment. Although the major global sources of outdoor NO_x are power stations and automobile exhausts, gas appliances and cigarette smoke can make a significant contribution in the domestic environment. With air quality and emission Standards currently or soon to be in force in many countries, many designers are now developing "low NO_x" burners.

1.2 Fluid dynamics phenomena in the domestic gas appliance

Designers of gas cooking burners intend to create better performing appliances. Nevertheless, the less than complete understanding of the physical phenomena involved has limited burner innovation. This section covers the main fluid dynamics phenomena occurring during the functioning of the domestic gas burner. The domestic gas burner is a partially premixed appliance where the formation and the homogenization of the reactive mixture are only due to the entrainment force of the fuel jet issuing from the injector and to the geometrical characteristics of the burner. This unburnt fuel stream is commonly supplied with air before combustion occurs. However, only part of the air required for complete combustion is initially provided inside the burner: therefore the prime objective of an aerated burner designer is to ensure a correct mixture of gas and air. This mixing process drives the performances of the domestic cooking appliance and represents a key factor in the burner development process. Therefore, a brief review of the fluid dynamics phenomena involved in the formation and the homogenization of the reactive mixture are presented in the following.

1.2.1 Gaseous jet

As mentioned before, the injector of the domestic gas burner can be considered the "heart" of the domestic appliance. Its target is to provide the correct fuel flow rate and to perform the process of mixing with the surrounding air from the hob. Therefore the nozzle of a domestic gas burner converts the potential energy of the pressurized gas supply into the kinetic energy of the emerging gas jet [2]. This turbulent axisymmetric round jet is a subsonic free jet discharging into a motionless surrounding fluid. A jet of this kind is said to be submerged [5] and is shown in Fig. 1.5, which highlights three zones [6]:

- the potential core zone;
- the developing zone;
- the developed zone.

The approximately laminar (irrotational) zone within the mixing layer is often referred to as the potential core. This region is characterized by a constant velocity, equal to the nozzle exit velocity. The short potential core extension characterizing methane and butane jets is further analyzed in [7]. The core length is also dependent on the initial velocity profile and on the turbulence intensity at the nozzle exit. A subsonic free jet is therefore characterized by a potential core surrounded by a region in which mixing between jet and ambient fluid takes place [8]. The flow at the nozzle emerges into the external fluid, creating a cylindrical

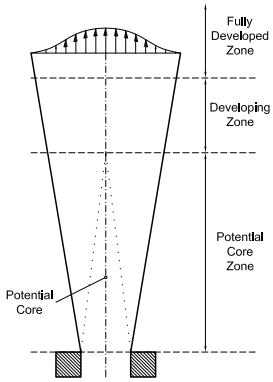

Figure 1.5: Sketch of a free jet.

shear layer that spreads out to fill the jet. As the flow exits the nozzle, shear forces are generated as a result of the velocity discontinuities between the essentially uniform velocity of the discharging flow and the surrounding motionless fluid. These forces result in instabilities which control the growth of the mixing layers: outward into the surrounding fluid and inward toward the jet centerline. Therefore, as they depart from the nozzle, the region of essentially inviscid potential flow at the core of the jet gradually decreases in width. The mechanism by which the shear layers are grow and the potential core is breaks down is further explained in [9]. A train of vortex rings, generated by the instabilities of the initial shear layer, can be highlighted at the nozzle exit. Due to these trains of growing vortices, the potential core flow is alternatively accelerated and decelerated. As the vortex rings emerge from the nozzle edge, their phase agreement across the jet disappears due to the vortex pairing mechanism, i.e. the coalescence with neighbouring rings. Moving downstream, the coalescing vortices are characterized by the following aspects: (1) increasing interval between the vortices; (2) random variation in movement and strength; (3) gradual increase of lateral fluctuations caused by the almost linear growth of the orderly wave deformations of the core of the vortex rings. In the end, the mixing region spreads inwards enough and the core no longer exists because the mixing layers that formed at the edge of the jet orifice meet at the centerline. The potential region ideally extends up to a few diameters from the nozzle orifice, and can therefore be practically considered to be within the appliance bowl.
In the developing zone the potential core has disappeared and the large shear stresses located at the jet boundary cause a decay of the axial velocity profile; therefore a continuous broadening of the velocity profile of the jet can be

highlighted. Moreover, these stresses generate turbulence and promote the entrainment of additional fluid. The velocity profile becomes "lower" and "wider" with increasing distance from the beginning of the jet. An initially fast moving jet fluid will lose momentum to speed up the stationary surrounding fluid. Due to a cross-stream transfer of momentum by turbulent mixing, the mean velocity profile spreads out downstream and develops with streamwise distance. Owing to the entrainment of the surrounding fluid, the velocity gradients decrease in magnitude in the flow direction. This causes a decreasing difference between the mean velocities outside and at the centre of the jet. Therefore, a two way interaction between mean flow and turbulence takes place. In the absence of a wall, as in the case of a jet, the production of turbulence is more evenly distributed across the flow, and it tends to peak in regions of high mean shear (high mean velocity gradient) that act as an area of turbulence production, which would otherwise decay rather quickly. Thus, turbulence is produced by local mean flow instabilities near positions of high mean shear. However the resulting turbulence tends to reduce the mean shear which created it, through mean momentum transfer.
At the end of the developing zone, the turbulent jet may be expected to develop under the auspices of a similar law, i.e. after a certain distance the jet stream becomes independent of the exact nature of the flow source. Therefore only the local environment appears to control the turbulence in the flow. In the developed zone the velocity profile is fully developed and both the axial velocity and the turbulence level decay [10]. In this region, the Reynolds stresses and higher order velocity statistics of the turbulent field reach a self-preserving state somewhat farther downstream. Furthermore, in this region the maximum velocity is inversely proportional to the distance from the inlet point, whereas the spreading is directly proportional to it. The developing and developed regions thus expand along the mixing tube of the domestic appliance.
The flow field within a domestic gas burner is that of a variable density confined jet impinging onto a plate. The impinging distance is known to influence the structure of the flow field, mostly when the stagnation plate is in the near field region of the jet. As plotted in Fig. 1.6, the flow field produced by the impingement of a turbulent axisymmetric air jet against a surface, whose diameter is large compared to that of the jet, is conveniently subdivided into three characteristic regions:

- the free jet region;
- the impingement (stagnation) flow region;
- the wall jet region.

The impingement zone is characterized by a stagnation region and by a region in which the jet turns in the radial direction. Obviously, this region is located in the proximity of the venturi neck of the burner crown mixing tube, where the mixture approaches the burner cap. Therefore, in the impingement zone,

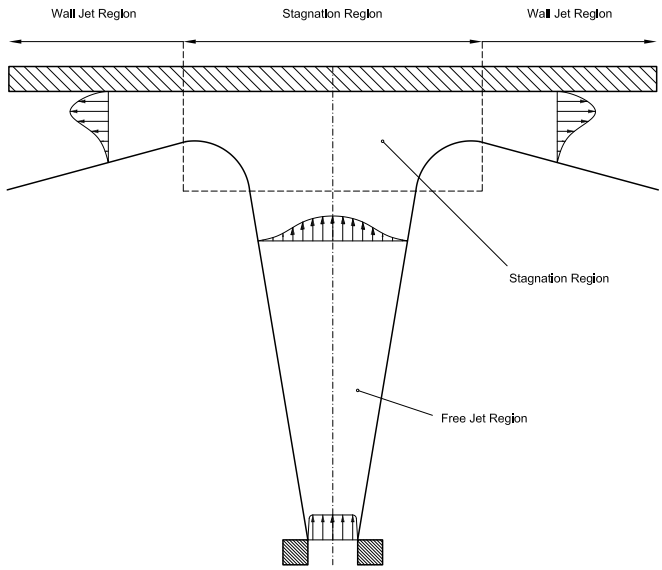

Figure 1.6: Sketch of an impinging jet.

a conversion of the axial transport of momentum and of the turbulent normal stress is achieved on the basis of the axial mean momentum transport equation. These two contributions have the following origins: the deceleration of the axial mean velocity towards the impingement plate causes the axial transport of momentum, whereas the occurring of a substantial momentum transport from the turbulent field to the mean field near the plate produces the turbulent normal stress (related to the net negative production of turbulent kinetic energy near the impingement plate). Therefore, near the wall the momentum transport is significantly enhanced: the axial convection and the turbulent normal stress are the major source terms, and their momentum is converted to that of the static pressure. As discussed in [7], the free jet region is located upstream of any strong local interaction effects due to impingement. With regards to the domestic gas burner working fluids, their jets clearly present the main free jet regions and the stagnation region. Most important of all, for these gases the self-similar profile region is mainly located at the same height of the venturi mixing tube. Moreover, in the wall jet region the effects of interaction due to impingement are no longer important, but the wall jet velocity will decrease with increasing distance from the stagnation point, due to its radial spreading. On the contrary, the wall jet consists of an inner, boundary-layer-like region adjacent to the plate, with an outer layer of free turbulent mixing. Thus, a characteristic self-similar velocity profile cannot be established because of the differences governing the growth of these two different layers. Moreover, the eddies from the shear layer of the jet

penetrate deep into the inner boundary layer, increasing the skin friction acting on the wall and, therefore, producing higher turbulence levels than the ones in the boundary layers or pipe flow.

1.2.2 Air entrainment

The mixing and homogenization of the fuel jet with the surrounding air is carried out by the air entrainment process, based mainly on the turbulent nature of the flow. In general, turbulent flows in the context of combustion problems are free shear flows. Such flows are free to develop without the confining influence of solid boundaries [11]. The fundamental types of free flow can be summarized as follow:

- wake: a developing region downstream of either an aerodynamic or a bluff body;
- jet: a fluid exiting a nozzle or orifice into a larger domain;
- mixing layer: fluid layers travelling at different speed are brought together.

The common property of the above mentioned flows is a small variation of the mean field in the main direction of motion and a large variation of the same in the direction across the flow. In all three flows, the transition to turbulence occurs a very short distance, in the flow direction, away from the point where the different streams initially meet. Turbulence causes a vigorous mixing of adjacent fluid layers and a rapid widening of the region across which the velocity changes take place. This turbulence is confined inside a well defined interface, which separates the two conditions: laminar flow (outside) and turbulent flow (inside). As the latter is convected downstream, the former is engulfed by the turbulent fluid and it becomes turbulent. This process is known as entrainment. The entrained fluid is accelerated in the case of jets, and decelerated in wakes or mixing layers.
Therefore, free shear flows are characterized by a well defined surface which moves with the fluid, separating the turbulent (eddying) fluid from the ambient (irrotational) fluid. This surface advances into the environment by a process of vorticity diffusion and subsequent amplification of the diffused vorticity by straining, because on one side, the vorticity is everywhere very small, while vorticity in the turbulent fluid is irregularly distributed and generally large. Moreover, the lateral spreading of a turbulent flow: (1) involves the conversion of irrotational ambient fluid, a process that depends in its details on the small scale diffusion of vorticity across the bounding surface; (2) is accomplished necessarily by transfer of energy from the mean flow to the turbulent motion, and the greater the rate of spread, the greater the rate of energy transfer.
The rate of conversion of the ambient fluid is controlled by the intensity of the large eddies because they fold the boundary surface. These eddies derive their

energy from the organized mean flow and cause a large increase in the rate of production of turbulent energy. The remaining turbulent motion on smaller scales merely resists the growth of large eddies by absorbing some of their energy and, in time, by leading to destroy them. Therefore, smaller-scale eddies are generated from the larger eddies through the nonlinear process of vortex stretching. Typically, energy is transferred from the largest eddies to the smallest ones on a timescale of about one large eddy turnover [12]. Entrainment is brought about by momentum transfer and total conservation [13]. Entrainment is a characteristic feature of a jet and creates a large scale, relatively slowly moving flow in the region external to the jet. Thus this process is mainly due to the intensity of the large eddies, which is set by the operation of the control cycle presented in Fig. 1.7, as assumed with the equilibrium hypothesis [14].

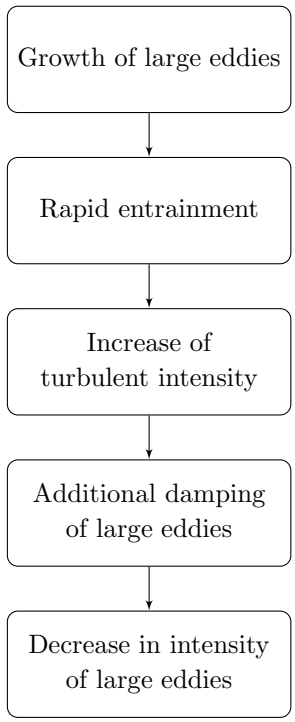

Figure 1.7: Large eddies entrainment process.

As a result, the following predictions are made concerning the entrainment behavior of turbulent jets [15]:

- in near field regions the local entrainment rate will grow with increasing downstream distance until a location is reached where the mixing achieves its asymptotic value;

- at longer downstream distances the local entrainment rate will become independent of position;
- at a low Reynolds number[2], for which the centerline growth behavior is Reynolds number dependent, the ratio of the mass flow rate, for a given downstream position, to the mass flow rate at the nozzle, will be Reynolds number dependent.

The jet structure and its entrainment effect are deeply affected by the conditions at the jet exit. In the following, the influence of the density variation, thickness of the boundary layer, turbulent initial condition and temperature are therefore considered [16].
When the ambient air density increases, the mean velocity of the entrained air decreases; hence, the effect of a decreasing density ratio leads to an increase in momentum mixing in the jet. Therefore, the denser the environment is, the more the mixing rate increases and the better the air/fuel mixture will be. However, it is important to note that the momentum mixing appears to increase fairly smoothly as the jet density is reduced. The density ratio also affects the jet stability. At a density ratio lower than a critical threshold value, the jet becomes absolutely unstable.
The jet boundary layer is represented by the region between the core top hat and the motionless surrounding fluid; inside this region, a velocity decay can be found. The influence of the boundary layer thickness on the momentum mixing can be summarized as follows for a laminar initial condition: in isothermal jets (relative density equal to 1) the larger initial boundary layer thickness results in a significant increase of the potential core length. The potential core extension becomes somewhat less dramatic as the density ratio is reduced to 0.75. As the jet density is further reduced to 0.5 (close to the methane relative density, which is equal to 0.554), the jet momentum mixing appears to be relatively insensitive to the separating boundary layer thickness. However, thick initial boundary layers result in slightly less entrainment.
The momentum mixing is reduced with turbulent initial conditions for all density ratios, whereas it is increased for both laminar and turbulent initial conditions with decreasing density ratio (with regards to the gas jet and the surrounding fluid). A separating laminar boundary layer at the nozzle exit is characterized by a natural amplification of a narrow band of disturbances that cause the jet shear layer development to be dominated by the vortex structure formation and pairing

[2]The ratio between the momentum convection and diffusion is given by the Reynolds number. It is defined as:

$$R_e = \frac{U \cdot \rho \cdot L}{\mu} \tag{1.2}$$

where U characterizes the mean fluid velocity (m/s), L is the characteristic diameter (m), ρ is the density of the fluid (kg/m^{-3}) and μ is the (absolute) dynamic fluid viscosity $(Pa \cdot s)$. Consequently, it is a measure of the ratio of inertial forces $(U \cdot \rho)$ to viscous forces (μ/L).

processes. Moreover, this spectral distribution of disturbances in the shear layer becomes narrower as the jet density is lowered, indicating a more organized vortex formation and pairing, both of which are responsible for elevated momentum mixing. On the other hand the introduction of turbulence, as disturbances of sufficient amplitude over a wide range of wave numbers, overcomes the instability mechanism responsible for the periodic concentration of vorticity and hence for the disruption of the vortex formation and pairing.
For laminar exit boundary layers, it is possible to point out an increase in the momentum mixing process at the end of the potential core due to the large scale vortex structure that engulfs large amounts of cold external air, resulting in a rapid drop of temperature. In turbulent exit conditions, the above mentioned large scale vortex structures are not present: therefore less mixing is achieved, and consequently a less rapid temperature reduction.
Laser Doppler Anemometry and Particle Image Velocimetry are applied by Serres et al. [17] to a domestic burner configuration to determine the effect of geometrical parameters and gas density on the flow field and on the entrainment process. A totally transparent new device was manufactured in quartz. This new device provides greater optical accesses for PIV measurements inside the burner. Two density ratios were studied: an isodensity (relative density = 1) and a light jet (relative density = 0.55). Several configurations were also investigated for these different gases and impinging distances: free jets, confined jets, impinging jets, and confined impinging jets (whole burner configurations). The entrainment force was verified to be more efficient for the light jets than for isodensity jets. The resulting flow fields inside the domestic appliance showed the following phenomenon: the jet impinges at high velocity, without disturbance until it approaches the plate. Therefore, the jet spreading rate is not influenced by the presence of the confinement tube. The spreading angle is about 22°. This value usually characterizes turbulent axisymmetric free jets; hence the jets first develop as free jets. From the stagnation point, the jet stream spreads radially, developing a flow pattern similar to the pattern of a wall jet.

1.2.3 Mixing

A correct prediction of the mixing is a key factor in describing the turbulent combustion process correctly. In combustion, it is often used the terminology scalar mixing, in which the scalar quantity of interest is for example the concentration of some molecular species. This mixing process refers to a molecular mixing; for different species to be molecularly mixed, they need to be intermingled on the molecular level. The molecular mixing is important in combustion because the chemical reactions of combustion proceed only if the individual molecules of fuel and oxidizer can interact directly. In particular, chemical reactions take place

upon molecular diffusion of the reactants into one another, whereas the mechanical stirring process begins at scales associated with large eddies in a turbulent flow field [18]. In a sequence of cascading events, stirring at large scales progressively creates smaller scales, due to continuous stretching and folding, ultimately tending to a state of complete mixing in the presence of molecular diffusion along the stretching interfaces between mixing fluids. Therefore, the efficient mixing in fluids involves stirring, which increases the interfacial area between the fluids being mixed, and is followed by the diffusion of the fluids. The need for stirring arises because diffusion alone is, generally, insufficiently fast to achieve the levels of mixedness (i.e. a measure of the extent of molecular diffusion) required in engineering problems. Of course, for effective mixing, turbulence is desirable (and the more turbulent, the better) because the smallest length scales get smaller as the Reynolds number increases, which promotes the final step in mixing: molecular diffusion. It is normally assumed that mixing can be considered completed at the throat of the domestic gas burner mixing tube.
The volume gas fraction formulation was adopted in this research in order to quantitatively define the level of mixing of the fuel in the air. The volume fraction or volume concentration C_{vol} is defined as the volume of gas per unit of mixture (gas and air) volume:

$$C_{vol} = \frac{V_{air} + V_{gas}}{V_{gas}} \tag{1.3}$$

where V_{gas} is the volume of gas and V_{air} is the volume of primary air (i.e. the air supplied to the unburnt fuel stream before combustion occurs).

1.2.4 Combustion

Partially premixed flames occur in many applications including gas fired domestic gas burners, IC and aircraft engines, Bunsen burners; it may also be encountered in future space applications or spaceship fires. The domestic gas burner is a partially premixed device functioning under atmospheric conditions, where the formation and the homogenisation of the reactive mixture are only due to the entrainment force of the jet issuing from the injector and to the geometrical characteristics of the device. Therefore, in the domestic gas stove, fuel and air are already mixed within the burner; as the gas is ignited downstream through the grooves, a premixed flame front will propagate towards the flame ports until it finds its steady state position. The fundamental quantity which describes this mode of combustion is the laminar burning velocity. It is the velocity with which the flame front propagates through the combustion wave into the unburned mixture in the direction normal to the wave surface. Therefore, propagation of the flame front upstream through the unburnt mixture is balanced by the downstream flow of unburnt gases, so that the flame appears stationary and its processes are in dynamic equilibrium. If either the flow rate or the burning velocity change

slightly, the shape of the flame front varies in order to restore the balance. This leads to the concept of flame stability that is of vital importance to burner designers.

The triple flame is an interesting typology to consider in approaching partially premixed combustion. A triple flame is a partially premixed flame consisting of two premixed reaction zones (one fuel rich and the other fuel lean) and a nonpremixed reaction zone. The two premixed reaction zones form exterior wings and the nonpremixed reaction zone is established in between these two wings. These three flames merge at a "triple point". The nonpremixed reaction zone is established in the region where fuel and oxidizer, from the rich and lean premixed reaction zones, respectively, mix in stoichiometric proportion. The two premixed flames are curved because their respective propagation velocities decrease when moving away from the stoichiometric condition.

The structure of a domestic gas burner flame is different from the structure of a triple flame, since it consists of a visible inner premixed flame front, represented by a bright inner cone, and an outer nonpremixed flame surrounding the cone. The former corresponds to a rich premixed flame, producing CO and H_2 as the main intermediate products, while the latter orresponds to a diffusion flame where these products burn with air. Therefore a double flame contains a rich premixed zone on the fuel-rich side and a nonpremixed zone on the oxidizer (fuel-lean) side, whereas a triple flame contains a rich premixed zone on the fuel-rich side and a nonpremixed zone and a lean premixed zone on the fuel-lean side. These differences in flame structures cause significant differences in their stability and emission characteristics. Ashman et al. [19] used a single production cooktop burner to determine the effects of loading height (i.e. the distance between the flames and the load) and thermal input on its efficiency and gaseous emissions. The thermal efficiency of the burner was found to decreases with increasing loading height. Moreover, at low loading heights, NO_x increases with increasing loading height, but CO increases with decreasing loading height. The effects of the following burner design factors on the emission of NO_2, NO_x, CO and hydrocarbon was later investigated by Junus et al. [20]: cap material, cap size, port shape, port size, port spacing, central secondary aeration, and flame insert. The approach used to arrange the experiments in this study was the factorial experimental design method and the results were statistically analyzed using the analysis of variance. Flame stability was found to be crucial: a slight instability promoted a large increase in emissions of CO, hydrocarbon, and NO_2. Moreover, port shape was found to be the most significant burner design factor affecting the emissions. A further investigation on emissions (particularly NO_2) and efficiency for gas fired cooktop burners was carried out by Stubington et al. [21], which indicated that the emission rates of hydrocarbons and CO are not reproducible when the flame impinges on the pot and grids. Therefore, the study of burner design parameters should be undertaken with non-impinging flames, and the effects of flame impingement should be considered separately. Subsequently,

a single gas burner stove, originally designed for burning natural gas with low heating value, was adopted by Ko and Lin [22] to investigate the effects of variations in gas composition on burner performance. The influence of five significant parameters, including gas composition, primary aeration, gas flow rate (heat input), gas supply pressure, and loading height, on the thermal efficiency and CO emissions, were discussed. With increasing primary aeration, the CO emission decreases, but the thermal efficiency is nearly unaffected. In the same way, with increasing loading height, the CO emission decreases, which is attributed to decreased quenching by flame impingement on the load. However, at higher loading height, the flame and combustion gases are cooled, to a greater extent, by mixing with ambient air before contacting the loading vessel, and thus the temperature driving force for heat transfer is decreased, leading to the decrease of thermal efficiency. Therefore, the balance between thermal efficiency and CO emission can be best quantified by considering the CO emission during a standard cooking task. Moreover, the use of natural gas with a high heating value instead of natural gas with a low heating value, resulted in a decrease in thermal efficiency (due to higher thermal input) and an increase in CO emission (caused by incomplete combustion). A combustion optimization study of gas stoves was performed by Hou and Ko [23] through the modification of the heating height of a single gas stove flame. To simulate the flame characteristics of a domestic gas stove, an impinging double-flame fuel-rich Bunsen flame is adopted. Impinging flame heating is therefore intimately related to the aerodynamic structure of the flame. Results show that flame structure, temperature distribution and thermal efficiency are greatly influenced by the heating height. With increasing heating height, the thermal efficiency first increases to a maximum value and then decreases. An optimum heating height, identified by the widest high temperature zone and the highest thermal efficiency, is achieved when conditions are such that both the inner premixed flame and outer diffusion flame are open and diverge. Furthermore, the optimum heating height increases with increasing methane concentration or injection velocity. Moreover, the maximum thermal efficiency occurs when the heating height is slightly lower than the tip of the inner rich premixed flame. In a subsequent analysis Hou and Ko [24] investigated the combined effects of oblique angle and heating height on the combustion characteristics. The influence of the oblique angle on flame structure is stronger for lower heating heights, but is relatively weak for higher heating heights. In general, a decrease of the oblique angle leads to a decrease in thermal efficiency. However, in the cases of lower heating heights the trend may be reversed. Furthermore, for a fixed oblique angle, as the heating height is increased, the thermal efficiency first increases to a maximum value and then decreases. A new type of gas burner with swirling flame was adopted by Hou, Lee and Lin [25] to investigate the significant parameters affecting burner performance. In these experiments, the influence of four parameters, namely primary aeration, gas flow rate (heat input), gas supply pressure and loading height, on the thermal efficiency and CO emissions, were examined. The

results showed that the swirl flow burner provides a higher thermal efficiency and emits only a slightly higher concentration of CO, than the conventional radial flow burner. These characteristics are attributed to the significant improvement in the heat transfer coefficient at the bottom of the vessel, as a result of the prolonged residence time of the combustion products in the vicinity of the vessel bottom. With the increase of loading height, the CO emission decreases owing to the reduction of quenching by flame impingement on the load. However, at high loading height, the flame and combustion gases are cooled to a greater extent by mixing with ambient air before contacting the loading vessel, and thus the temperature gradient for heat transfer is decreased, which leads to the decrease of thermal efficiency. As the thermal input increases, the thermal efficiency is reduced and the emission of CO increases. With increasing primary aeration, the emission of CO is diminished, but the thermal efficiency is almost unaffected. The addition of a circular shield enclosing the burner (i.e. semi-confined combustion flame) achieves a great increase in thermal efficiency.

1.3 Flame stability

The domestic gas burner must be capable of stabilizing the produced flame. Flame stability limits are one of the most important controlling factors in the design of a domestic appliance. Burner design would be greatly facilitated by knowing the effect on flame stability of the input parameters such as fuel/air ratio, average velocity and its distribution, laminar burning velocity.
In order to certificate the domestic gas burner, it should be installed in a suitably ventilated room and supplied with a reference gas belonging to the appliance category. After ignition, the flame must be stable and quiet. For the purposes of the European Standard [3], the following definitions must be applied:

- lightback: phenomenon characterized by the return of the flame inside the body of the burner.
- flame lift: phenomenon characterized by the partial or total movement of the base of the flame away from the burner port;

Moreover:

- flame stability: state of the flame at the burner ports when the phenomena of flame lift or light back do not occur.

There are two types of stability criteria associated with laminar flames [26]. The first is concerned with the ability of the combustible fuel/oxidizer mixture to support flame propagation, and is strongly related to the chemical rates in the system. In this case a point can be reached, for a given limit mixture ratio, at which the rate of reaction and its subsequent heat release are not sufficient to sustain reaction and, thus, propagation. This type of stability limit includes:

- flammability limits, in which gas-phase losses of heat from limit mixtures reduce the temperature, the rate of heat release and the heat feedback, so that the flame is not permitted to propagate;
- quenching distances, in which the loss of heat to a wall and radical quenching at the wall reduce the reaction rate so that it cannot sustain a flame in a confined situation, such as propagation in a tube.

The other type of stability limit is associated with the mixture flow and its relationship to the laminar flame itself. This stability limit, which includes the phenomena of flashback, blowoff and the onset of turbulence, describes the limitations of stabilizing a laminar flame in a real experimental situation.
In view of the complex flow configuration in the neighborhood of the domestic gas burner flame ports, the characterization of the stability response in terms of fundamental parameters cannot be readily undertaken. Therefore, investigations in terms of bulk characteristics of the appliance assembly were performed by

different authors. Reed [27] reported a generalized relationship for aerated gas burners to assess the effect of changes of gas characteristics on lightback, quenching diameters, blow off, yellow tip formation, inner cone size and shape, heat input and primary aeration for a given burner geometry, from a knowledge of the composition of the fuel gas and its burning velocity only. Techniques developed for detailed flame structure studies were applied by Datta et al. [28] and Datta and Reed [29] to investigate the stabilizing region of a near-stoichiometric and of a fuel-rich methane/air flame respectively on an aerated burner. The flame structure analysis showed that the maximum heat release rate in the stabilizing region of the fuel-rich flames was much smaller than in the stoichiometric ones. Their results therefore indicated that the greater stability of a fuel-rich flame, compared to a stoichiometric flame, is due to a heat interaction between the primary and secondary combustion zones in the stabilizing region of a fuel-rich flame. Moreover, the decrease in magnitude of this interaction, observed when the secondary combustion air was vitiated, is put forward as the reason for the large reduction in stability of fuel-rich flames that can be brought about by secondary vitiation. Particle-tracking experiments were performed on the burners of two commercial domestic cookers by Oostendorp [30], which indicated that in a stable burner the hot gases from the retention (pilot) flame are entrained by the main jets rather than transported by natural convection, which appears to be more important in a critical burner affected by the blow-off instability phenomenon. Moreover, it was suggested that a factor contributing to the different stability behaviors of the two burners was the different point of attachment of the main flame. Later, the results of an investigation aiming to study the effects of the burner cap design factors on flame stability were reported by Junus et al. [31]. The cap design factors studied were: the angle under the cap, the angle under the overlap, the shape under the cap, the size of the cap overlap, the height of overlap above the burner, cap material and cap thickness. To detect interactions between factors as well as the effects of each single factor, a "Factorial Experimental Design" method with statistical analysis was used. Turndown ratio seemed to be less of a problem in the experiments, compared to the ability to maintain flame stability at high primary aeration. Nevertheless, the factors which gave very high turndown ratios were usually operable only at very low primary aerations. Particle Image Velocimetry measurements were performed by [32, 33] in cold condition using air as the working fluid. This experiment was carried out in order to measure the flow field at the exit of the burner flame ports. The path of the air jets at the exit of the burner crown is shown, for both the primary and secondary flame ports, in Fig. 1.8 by means of a contour plot with superimposed stream tracers.

The footprints of the jets, corresponding to the different types of flame ports, are well visible. The highest velocities are found in the core of the jet issuing out of the primary flame port, with values of up to 2 m/s. The jets emerging from the flame port rapidly loose their kinetic energy and contribute, together with the primary air flow, to the formation of a wide region of recirculation that

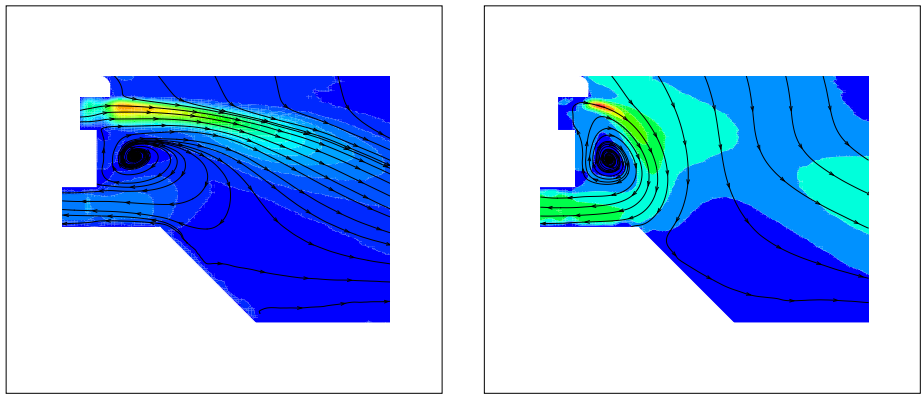

(a) Flame port type 1 (b) Flame port type 2

Figure 1.8: Flow at the exit of a domestic gas burner crown supplied with air at nominal ($2000Pa$) inlet pressure [32].

surrounds the entire gas burner crown. The path of the stream tracers shows the existence of this wide toroidal recirculation region in all the data taken along the vertical planes. These recirculation regions, located between the flame ports region and the primary air inlet, seem to entrain the totality of the primary air flow and part of the jet flow as well. The jet flows, however, feel the effects of the recirculations since their paths are clearly pointing downwards. This is more evident for the secondary flame port flow which, because of its smaller velocity, gets more entrained into the recirculation. Therefore, the weak jet from the secondary flame port is completely deviated downward because of the negative pressure gradient at the intake of the primary air. The increase of inlet pressure at the injector, and therefore in the flow rate through the nozzle, leads obviously to more energetic jets which in turn entrain more primary air, whereas the flow structure out of the flame ports remains nearly unchanged. It is possible to note that the jet issuing from the secondary flame ports directly feed the primary air entrance, but this behaviour is not representative of the flow field for a functioning application, where buoyancy effects take place due to the combustion process. Moreover, this investigation toook three different domestic gas burner geometries into account. These geometries presented different characteristics in terms of flame stability: one crown was affected by flame back, one by flame lift and the other one showed stable flames. A comparison between the flow fields out of the primary and secondary flame ports, for the three different crown burners, highlighted the fact that the velocity out of the type 2 flame ports can be correlated with the flame back effect. These results indicated that a flame instability can be highlighted with an investigation in cold condition. The possibility of predicting the flame back phenomenon in the domestic gas burner without involving the combustion process is a proof in support of the main aerodynamic

origin of this instability. However, the velocity out of the flame ports did not describe the flame lift phenomenon. Therefore, the experimental analysis stated that the flame lift instability cannot be predicted without taking into account the combustion process. Recently, Lacour et al.[34, 35] pointed out the physical phenomena responsible for the stabilisation of partially premixed flames of the domestic cooking gas burner. The structure and aerodynamics of the flame generated by a cooking model burner were characterized by Planar Laser Induced Fluorescence of the OH radical and Particle Image Velocimetry. The flame behavior was studied in conditions starting from a stable reference case and ending with blow-out by varying the flow inlet conditions and the geometry of the burner. The flame can be considered as two neighboring reactive zones, each consisting of a double edge flame with a different behavior toward flame blow-out. The stabilization of the upper double flame was similar to the stabilization of a Bunsen burner flame. The base is attached with a flame-holder mechanism and the flame tip position is controlled by the ratio between the flow velocity and the rich premixed flame speed. The bottom double flame is lifted and is stabilized thanks to local characteristics of mixing and aerodynamics. Last but not least, in the early 90's a comprehensive manual from British Gas [2] presented the most recent developments in the practice and theory of domestic gas burner design. It deals with the most important developments in burner design, without which neither the remarkable success of conversion to natural gas, nor the more recent improved efficiency, could have been achieved.

1.3.1 Flame back phenomenon overview

Aerated burners require the explosive fuel and oxidant gases to be mixed in a confined chamber before they are burned. In order to form the flame, these mixed combustion gases must pass and exit the appliance flame ports, after which they are burned. However, under certain conditions the flame can burn back through the exit ports to ignite the explosive mixture along the radial diffuser, up to the mixing tube and the injector. The resulting explosion, known as "lightback", "flame back", "flashback" or "fireback" is a well known, albeit undesirable, phenomenon, which is unfortunately common in the high temperature and high burning velocity flames burner. This instability can be prevented only by the careful design of suitable domestic gas burners.
Several definitions of flashback can be found in literature but none of them is universal, indicating that the occurrence of this instability phenomenon mainly depends on the device in which it occurs. As mentioned before, flashback occurs when the flow velocity of the reactants is of the same order as the combustion velocity so that the flame is able to propagate upstream. This low unburned flow velocity may be induced by:

- Proximity of a solid wall
  In boundary layers, the velocity is sufficiently low to allow upstream propagation of the flame front. However, this propagation is limited by wall quenching. Flashback in boundary layers seems to be predominant in non-swirling low turbulent flows, as in the domestic appliance, or low speed catalytic combustion [36–38] (the lower the Reynolds number, the thicker the boundary layer).

- Low turbulence levels
  Turbulent flame propagation in the core flow is possible when the turbulent flame velocity S_T becomes higher than the local flow velocity. Such a situation may occur in swirling flames, in which turbulence is intense and the available flame surface in significantly larger than the flame surface of a laminar flame. This situation can lead to a possible flashback on the burner axis [39].

- Combustion instabilities
  Combustion instabilities are due to a coupling between heat release, pressure fluctuations and flow hydrodynamics. The velocity fluctuations induced by an instability can be as large as the mean flow velocity and lead to a transient flashback. Therefore, if the instability reaches sufficient amplitude, the reversal of the flow can occur, allowing the flame to propagate upstream. However, this instability requires a high level of fluctuation to appear, which is usually beyond the acceptable noise levels in most combustion systems [39]. A classical example of such flash back is a turbulent premixed flame behind a step, where coherent structures control flashback [40–43].

- Vortex breakdown
  This type of flashback was experimentally observed and identified in burners adopting swirling flows. Various mechanisms control the behavior of this kind of flow. One of them is vortex breakdown, defined as an abrupt change in the swirl jet topology. Phenomenologically, the breakdown of a vortex occurs when its azimuthal velocity is larger than its axial velocity. This complex and highly three-dimensional phenomenon depends on the flow circulation (or the swirl number[3]) and on the Reynolds number [44].

Moreover, flashback can also occur by:

- Autoignition
  It occurs when the gas residence time exceeds the fuel ignition delay time,

[3]For jets emanating from long rotating pipes the swirl number is defined as the ratio between the azimuthal velocity at the wall and the bulk velocity at the pipe outlet. This definition is quite convenient since the wall velocity is directly obtained through the rotational speed of the pipe.

> leading to the ignition of the mixture in the mixing zone. Therefore, autoignition does not involve flame propagation. The autoignition delays mainly depend on local temperature, pressure and equivalence ratio [45].

Therefore the classical flashback is a result of the flame velocity exceeding the fuel/air mixture velocity in either the tube boundary layer or in the free stream. Although it is not satisfying for many of the observations in industrial and turbulent configurations [39], this instability characterizes the domestic gas appliance. Fortunately, the conditions for this delicate balance become less restrictive at a burner port. At the port, the flame is stabilized by the entrainment of outside air into the burning gases and by the quenching effect of the port walls [46]. The latter effect is most important in preventing flashback. Primarily by acting as an heat sink, the walls of the burner port effectively reduce the burning velocity of the gases to zero for a short distance (the quenching distance). Beyond this distance, the burning velocity rapidly increases to its maximum value. Therefore, flashback will be avoided as long as the gas velocity remains everywhere greater than the burning velocity. This mechanism for flashback in laminar burner flames was initially discussed by Lewis and von Elbe [47] and von Elbe and Menster [48] for methane and propane flames, and by Wohl et al. [49] for butane flames. Subsequently, the conditions required to prevent the flashback instability in laminar flows in terms of velocity gradient were quoted in [50], where a great deal of experimental data were presented. These data were integrated by Berlad and Potter [51] with a more general correlation of the boundary velocity gradient for flashback to the burning velocity and quenching distance. Moreover, the influence of shielding (inert) gases on the stability limits of Bunsen flames was discussed by [52] for iso-butane flames, indicating that the dead space (i.e. the space between the top of the burner and the base of the flame cone) becomes very small and approaches "zero" near the flashback limit; the dilution of the primary mixture by entrainment is also verified to be small. Therefore the flowing inert gases surrounding the flame caused only a superficial external cooling of the flame; this cooling effect was found to be independent of the diffusion properties of the enveloping gas. On the basis of the behavior of a Bunsen flame near quenching, Babkin [53] assumed that the reason for the quenching upon dilution could be free convection, which causes an intense mixing of the cold gas of the surrounding atmosphere with the combustion products near the edge of the burner, so that the flame is cooled, and thus quenched. Later, a study by Hieftje [54] was presented on burner design criteria and variables affecting the flashback of acetylene flames. In this work, the safe limits of operation for conventional burners were examined and presented, including experimental quenching diameters for both circular ports and slot type burners. Quenching distances, measured experimentally for a butane/air flame at rich, stoichiometric and lean equivalence ratios, were reported by Nair and Gupta [55]. The stabilization of Bunsen flames under various burner tip geometries was observed by Sohrab and Law [56] for butane/air mixtures. The burner rim aerodynamics was found to influence flame

stabilization substantially. With enhanced entrainment, the minimum velocity above which flashback no longer occurs, decreases.
A fundamental study of the flashback phenomenon for steady laminar premixed flames in locally circular tubes was carried out by Lee and T'ien [38], indicating the effects of tube radius and incoming velocity profiles on the flashback limit and the flame structure at the limit. The wall velocity gradient alone is found not to be adequate in describing the limiting condition, because the velocity profile near the wall is also important. The detailed computed flame structures give great insights into the flame flashback and stabilization process. The flame near the wall is highly curved and the flame velocity is found to exceed the one-dimensional flame speed S_L because of the pressure-flame interactive effect. These findings indicate the limitation of applying the original critical wall velocity gradient criterion as a quantitative means of evaluating flashback limits. Recently, the flashback of premixed flames along the near-wall low-velocity region at the base of a laminar boundary layer of a reactive mixture, was studied numerically by Kurdyumov, Fernández and Liñán [57], indicating that the onset of flashback decreases with the Lewis number[4] of the limiting component of the mixture. Through further investigation, Kurdyumov et al. [58] found that the Lewis number and heat losses to the wall are seen to be essential on the conditions for flashback. On the contrary, variations in the thermal expansion and activation energy of the gaseous mixture have only weak effects on this instability.

1.3.2 Flame lift phenomenon overview

A flame issuing from a domestic gas burner port can be stabilized between two limiting values of the gas flow rates. As shown in the previous chapter, when the flow rate of the gas mixture falls below a certain minimum threshold value, the flame is not capable of anchoring itself to the burner rim, and moves into the burner. This minimum threshold value of the gas flow rate is known as the flashback limit. On the other hand, when the gas mixture flow rate exceeds a certain maximum value, the flame gets detached from the burner ports. This phenomenon is called the lift-off of the flame. If the gas flow rate is increased further, a threshold value is reached, at which the flame may leave the domain of interest. This maximum value of the gas flow rate is known as the blowoff limit. Therefore, a detailed understanding of the stability of partially premixed flames is important for the design of domestic gas burners; in particular this chapter is concerned with the problem of flame-lift and blow-off of aerated burner

[4]The Lewis number is a dimensionless parameter defined as:

$$L_e \equiv \frac{\lambda}{\rho \cdot C_p \cdot D} = \frac{\alpha}{D} = \frac{rate\,of\,energy\,transport}{rate\,of\,mass\,transport} \tag{1.4}$$

In certain combustion systems, Lewis numbers are close to unity.

flames. This form of instability was dealt with by Lewis and von Elbe [47] in their boundary velocity gradient theory of flame stability. Moreover, in that period, Kurz [59, 60, 52, 61] performed blowoff studies of hydrocarbon flames on Bunsen burners with different arrangements. An important assumption stated in the boundary velocity gradient theory of blowoff, is represented by an effectively plane wave flame propagation in the stabilizing region, so that flame stretch effects are not important in this instance. In contrast, it was shown by Karlowitz et al. [62] that some part of this combustion wave can be extinguished by enthalpy loss from the reaction zone, leading to a catastrophic reduction of the reaction rate of the combustion process. This loss arises when a flame propagates in a flow field in which there is an appreciable velocity gradient: hence it arises from the shear flow. Particularly at flow rates approaching the blowoff condition, the velocity gradient is represented by the velocity of the unburnt mixture, that varies considerably in the stabilizing region within distances comparable with the thickness of the flame. The shear flow is thus the controlling physical process determining the flow rate at which a flame blows off from a burner port. Therefore, flame blowoff from the burner tip takes place due to flame quenching, as a result of flame stretch, rather than because the velocity of the unburnt mixture exceeds the local burning velocity. This flame stretch concept was applied to the blow-off of aerated burner flames by Reed [63, 27], showing that experimental stability data are in agreement with the hypothesis that blow-off is a result of excessive quenching of the flame in the stabilizing zone, arising from the effect of the shear flow in the stabilizing region. Flame propagation was observed to cease in steep flow velocity gradients and this was attributed to the stretching of the flame front caused by shear flow, whereas intermixing played only a minor role. On the other hand, Edmondson and Heap [64] carried out experiments intended to explore the extent to which intermixing in the dead space was important. Lewis and von Elbe's theory of blow-off [65] was based on a mechanism in which ambient atmosphere progressively dilutes the mixture in the stabilizing region, as the primary mixture flow rate is increased, until the flame blows off. Therefore, there were conflicting views as to the mechanism causing flame blow off. The main difference regarded the extent to which intermixing of the ambient atmosphere into the dead space of near stoichiometric flames affected the blow-off limit. Further evidence by Datta, Hayward and Reed [28] was put forward, which claimed to show that there was no intermixing of ambient gases in the dark space for the near stoichiometric aerated burner flames of all gases, because the chief reason for the lack of intermixing is the strong outward flow of the primary mixture through the dark space caused by the relative high back pressure beneath the flame, resulting from the relatively high burning velocities of near stoichiometric mixtures. This was strong evidence in support of the flame stretch theory of blow-off and against a mechanisms for blow off which considers intermixing as the major factor determining the blow-off limit. Other investigations by Datta, Hayward and Reed [28] and Datta and Reed [29] showed that

the reduction of the blow off limit of an aerated burner can be substantial in presence of vitiation. The vitiation of combustion air is an important factor in the utilization of natural gas. This is because many of the difficulties associated with the combustion of natural gas can be traced back to its low burning velocity, and any reduction of the oxygen content of the combustion air reduces burning velocity still further. Subsequently, Kawamura et al. [66, 67] reported that the critical flow velocity gradient for blowoff is caused by an excessive increase in the curvature of the base, resulting in a lowering of the burning velocity there. Therefore, flame stretch arises due to flow motion and nonuniformity and flame curvature. Flame curvature is a parameter that significantly influences the structure and propagation of premixed flames, through its contribution to flame stretch. Negative stretch (i.e. compression) increases the reaction rate and heat generation, which enhances the laminar burning velocity. A positive stretch value has the opposite effect. Therefore, flame stabilization, lift-off and blow-out are complex phenomena involving transport, partial premixing, ignition and extinction. Experimental and computational studies focused mostly on the liftoff characteristics of nonpremixed flames. Peters and Williams [68] and Pitts [69] provided reviews on theories for turbulent diffusion flame stabilization. Lifted flames in laminar nonpremixed jets were extensively investigated to gain a fundamental understanding of the lift-off and stabilization process [70–78]. During these investigations stabilized flames in the far field of a jet were observed. As liftoff height increases, a transition in the flame structure can occur, from a nonpremixed flame to a double flame containing two reaction zones, and then to a triple flame containing three reaction zones. As a result, some interesting phenomena can arise, such as the flame stabilization in a laminar mixing layer caused by triple flames. One of the first observations of triple flames was made by Phillips [79], who investigated a triple flame propagating in a methane mixing layer. However, the stabilization theories proposed by [72, 74, 80] defined the flame stabilization mechanism in terms of a balance between the local flow velocity and the tribrachial flame speed. Of course, the behavior of lifted flames stabilized near the burner exit was found to be different from the behavior of lifted flames established in the far field. Takahashi et al. [81] and Takahashi and Katta [82]investigated the stabilization of nonpremixed flames and they found the existence of a reaction kernel of high reactivity instead of a triple flame structure. This kernel provided radicals and served as a flame stabilization point in a small premixing zone, in which a balance is maintained between the residence time and the reaction time. Kim et al. [83] examined liftoff characteristics with respect to the fuel concentration gradients and noted that the flame liftoff height and propagation velocity can be controlled by varying the mixture concentration gradient. In partially premixed combustion, mechanisms from the premixed and non premixed regimes can therefore coexist. Previous investigations on the stability of partially premixed flames mainly employed spherical flames [84, 85], counter

flow flames [86], anular coflow flames [87–98] and slot burner flames [99, 90, 100–102, 83, 103]. A detailed understanding of partially premixed flames, including their applications and issues, is also presented in [104]. However, there are several differences between the domestic gas burner appliance and the standard burner configuration adopted in literature. Briefly, it is possible to consider the cooking device as a cylindrical slot burner equipped with different horizontal flame ports (i.e. different size and different location). Therefore the flames issuing from the domestic gas burner alternatively present different dimensions and locations in space (i.e. a main flame followed by an upper tiny pilot flame in a cylindrical symmetry); moreover the buoyant acceleration does not affect these flames along their streamwise centerline.

1.3.3 The dynamic balance

In order to produce a stable flame, a dynamic balance must be achieved. The flame propagates with its characteristic burning velocity into the unburned mixture. In a unbounded system, a stable combustion front can be obtained only by exactly matching the mixture gas velocity to the burning velocity. Fortunately, the conditions for this delicate balance become less restrictive at a burner port. As discussed earlier, the Bunsen burner, as also the domestic gas burner, is so configured that the fuel and air become a homogeneous mixture before they exit the tube. The length of the tube and the physical characteristics of the system are such that the mixture flow is laminar in nature. In the context discussed here, a most important aspect of the burner is that it acts as a heat and radical[5] sink, which stabilizes the flame. In fact, it is the burner rim and the area close to the tube that provide the stabilization position, because the radical reaction is retarded. If the tube is in a vertical position, a simple burner configuration is obtained as shown in Fig. 1.9.

Therefore, to have a stable flame, it is necessary to attach the flame to a flame-holder or burner, which locally interacts with the flow and combustion processes to provide a stabilizing zone. As indicate above, the domestic gas burner mixes the fuel and oxidant and it will in turn establish a particular flow pattern, characterized by laminar flow condition through the flame ports. The effect of the burner grooves on the gas mixture velocity is to reduce it to zero at the walls through viscous drag: hence the mixture velocity is zero at the stream boundary (wall) and increases to a maximum in the centre of the stream. The linear dimensions of the wall region of interest are usually very small; in slow burning mixtures, such as methane and air, they are of the order of 1mm. Since the Bunsen burner tube is usually large in comparison, as shown in Fig. 1.10, the

[5] In chemistry, radicals (often referred to as free radicals) are atoms, molecules or ions with unpaired electrons on an otherwise open shell configuration. These unpaired electrons are usually highly reactive, so radicals are likely to take part in chemical reactions.

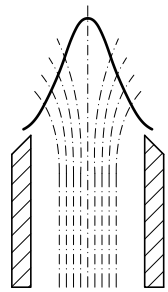

Figure 1.9: Sketch of gas mixture streamlines through a Bunsen cone flame.

gas velocity near the wall can be represented by an approximately linear vector profile.

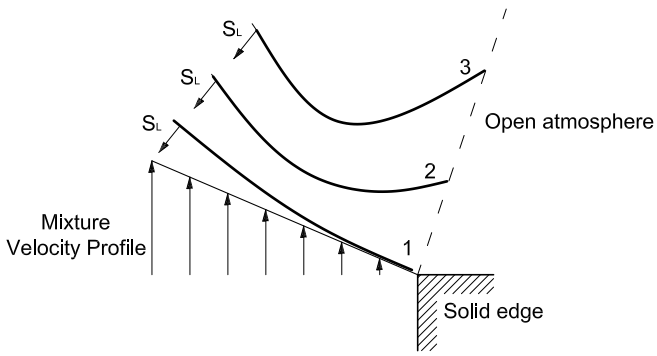

Figure 1.10: Sketch of the stabilization positions of a Bunsen burner flame.

Fig. 1.10 shows the conditions in the area where the flame is anchored by the burner rim. Since the flow lines of the mixture jet are parallel to the tube axis, a combustion wave is formed in the stream and the fringe of the wave approaches the burner rim closely. Along the flame wave profile, the burning velocity attains its maximum value. Toward the fringe, the flame is quite close to the burner rim and its actual speed is controlled by heat and radical loss to the wall; therefore the burning velocity decreases as heat and chain carriers are lost to the rim. If the wave fringe is very close to the rim (position 1 in Fig. 1.10), the burning velocity in any flow streamline is smaller than the mixture velocity, and the wave is

driven farther away by the mixture flow. As the distance from the rim increases, the loss of heat and chain carriers decreases, and the burning velocity becomes larger. Eventually a position is reached (position 2 in Fig. 1.10) in which the burning velocity is equal to the mixture velocity at some point of the wave profile. The wave is now in equilibrium with respect to the solid rim. If the wave is displaced to a greater distance (position 3 in Fig. 1.10), the burning velocity at the indicated point becomes larger than the mixture velocity, and the wave moves back to the equilibrium position [26, 105].

1.3.4 The penetration distance

Considering a flame wave inside a tube, Fig. 1.11 shows the laminar flame velocity (S_L) as a function of distance from the burner wall. This distance is called the penetration distance d_p, which is half of the quenching distance d_q [65].

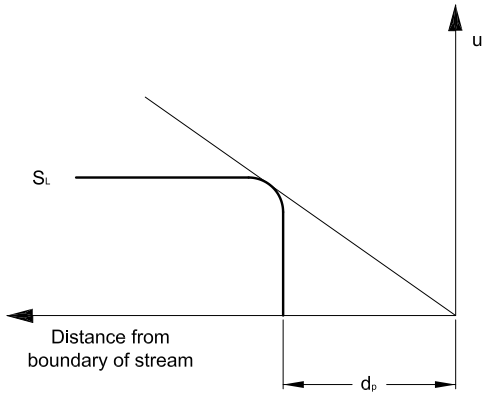

Figure 1.11: Sketch of the penetration distance of a Bunsen burner flame.

Below d_q, no flame can propagate into the tube supplying the combustible mixture gases. This parameter is characteristic of a particular fuel and oxidant and is of obvious practical importance. Quenching distances between parallel plates at a stoichiometric fuel/air ratio for butane and methane are $0.12mm$ and $0.10mm$, respectively [50].

1.3.5 Critical boundary velocity gradients

When the mixture flow in the tube is increased, the equilibrium position shifts away from the rim. As the distance from the rim increases, a lean gas mixture becomes progressively diluted by interdiffusion with the surrounding atmosphere, and the burning velocity in the outermost streamlines decreases correspondingly

[26]. This effect is indicated by the increasing retraction of the wave fringe for flame positions 1 to 3, represented dramatically in Fig. 1.12. However, as the wave moves further from the rim, it loses less heat and fewer radicals to the rim, so it can extend closer to the hypothetical edge. Nevertheless, an ultimate equilibrium position of the wave exists, beyond which the effect on the burning velocity of dilution overbalances the effect of increased distance from the burner rim. If the boundary layer velocity gradient is so large that the combustion wave is driven beyond this position, the mixture velocity exceeds the burning velocity along every streamline and the combustion wave blows off.

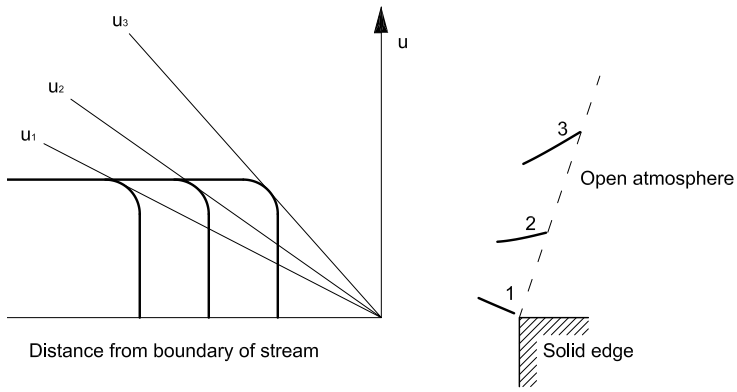

Figure 1.12: Sketch of burning velocity and mixture velocity above a Bunsen tube rim.

The diagram follows the postulated trends, in which the laminar burning velocity is the flame velocity after the mixture has been diluted, because the flame front has moved slightly past u_3. Thus, there is blowoff and u_3 is the blowoff velocity. If u_1 is the mean velocity profile of the premixed gas near the tube wall, then there is no place were the local flame velocity is greater than the local mixture velocity. Therefore any flame that finds itself inside the tube will then be blown out of the tube. So the critical flashback condition is reached if the unburned mixture velocity is represented by u_2. The profile for the mean velocity u_3 corresponds to the case in which the flame flashes back. The critical value of the boundary velocity gradient g at which the flashback condition is first reached is denoted by g_F. When the gas flow is increased, the equilibrium position of the flame shifts upward from the burner rim. Then the premixed, unburned gas becomes progressively diluted by the interdiffusion of the surrounding gas. The critical value of the velocity gradient corresponding to blowoff is denoted by g_B. The critical boundary velocity gradients g_F and g_B are given by the shapes of curves 1 and 3, respectively, in Fig. 1.12.

1.3.6 Flame stability positions

Figure 1.13 shows the comparison between the profile of the normal component of the approach velocity of the unburned gas mixture (dotted line profile) and the profile of the flame propagation velocity (solid line profile) adjacent to the burner rim, to show how the flame is anchored to the burner rim.

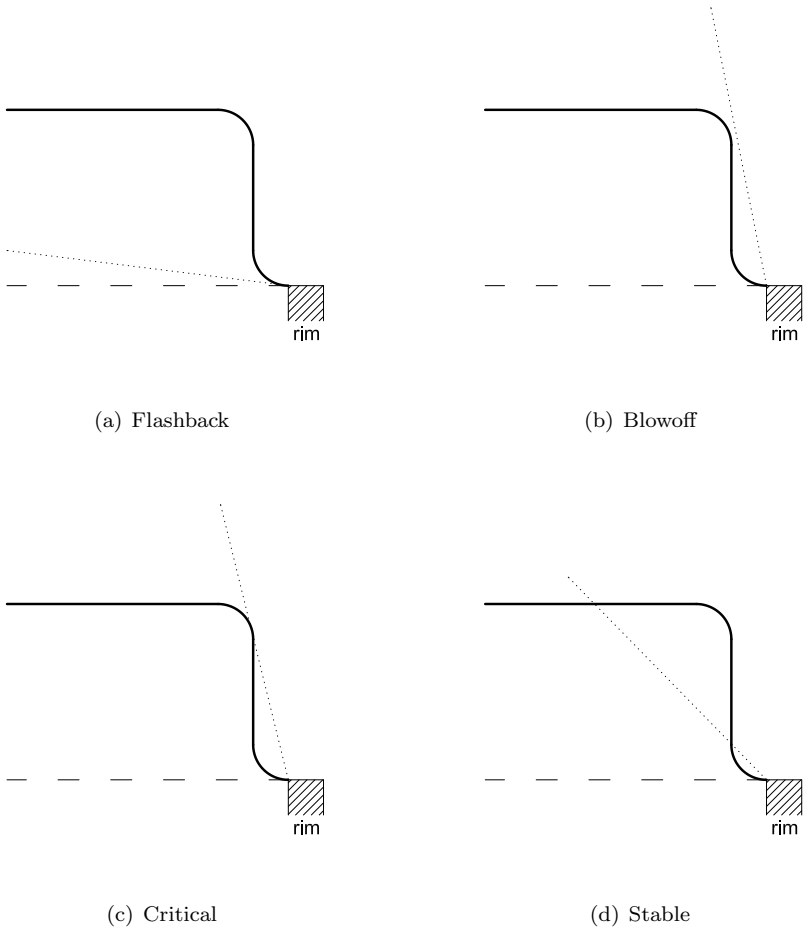

(a) Flashback (b) Blowoff

(c) Critical (d) Stable

Figure 1.13: Stability conditions between the profile of the normal component of the approach velocity of the unburned gas mixture (dotted line) and the profile of the flame propagation velocity (solid line) near a wall.

When the premixed gas flow is weak (Fig. 1.13,case a), S_L is greater than the unburned mixture not only in the near surface region but also over almost the entire cross section of the barrel; hence, the flame propagates into the barrel to produce the flashback situation. On the other hand, when the flow is very

strong (Fig. 1.13,case b), the mixture approach velocity is greater than S_L over the entire cross section, producing the blowoff phenomena. The critical condition for blowoff arises when the S_L and the mixture velocity profiles are tangent at a certain radial location (Fig. 1.13,case c). Stable combustion is finally shown as case d in Fig. 1.13.

1.4 Stability Diagrams

Stability diagrams can be used to design the domestic gas burner so as to avoid the critical conditions for flashback and blowoff. In the literature review [2, 105, 26] different stability diagrams are encountered and they are presented in the following sections.

1.4.1 Stability limits function of the boundary velocity gradients and the fuel concentration

On the basis of the theory of flame propagation, a flame is stabilized on a burner port at points in the gas stream at which the normal burning velocity is equal to the local linear velocity of the unburned gas stream. Points of such equality generally exist near the boundary of the stream. Flame stability is, therefore, dependent on boundary conditions. As discussed in the context of Fig. 1.13, flame lift or blowoff will occur when the slope of the flow velocity distribution profile or boundary velocity gradient at the stream boundary reaches a critical value. This critical boundary velocity gradient varies with the air/gas ratio of the burned mixture and with the gas composition. The same also applies to the occurrence of flame back.
Following the laws of fluid dynamics for laminar flow, the boundary velocity gradient is given by:

$$g = \frac{32 \cdot \dot{V}}{\pi \cdot R^3} \tag{1.5}$$

where g is the boundary velocity gradient (s^{-1}), $\dot{V}$ is the volume rate of flow (m^3/s) and R is the burner port radius (m).
When a stream of air and premixed gas issues from a tube, the g value must be greater than a certain critical value, g_F, in order to avoid flashback (i.e. $g > g_F$). This value g_F is called the critical boundary velocity gradient for flashback. Similarly, critical boundary velocity gradients for blowoff, g_B, are obtained with values of $\dot{V}$, corresponding to flows in which the flame just blows off the port (i.e. $g < g_B$). The values of g_F and g_B that define the flame stability of a laminar jet are determined experimentally or numerically.
Equation 1.5 was originally proposed by B. Lewis and G. von Elbe [65], who determined the critical boundary velocity gradient for flashback as a typical property of certain air/fuel gas mixtures. Further work was carried out by [106] in order to derive a formulation for the prediction of g_F when the composition of a gaseous mixture and its air/gas ratio are known, and to determine critical gradients for the separate components of the mixture. Additionally, a quite general relation of the boundary velocity gradient for flash back to the burning velocity and quenching distance was proposed by Berlad and Potter [51]:

$$g_F = 14.125(S_L/d_c)^{1.168} \tag{1.6}$$

where S_L is the laminar burning velocity and d_c is the quenching distance for cylinders, that is about three-halves of the quenching distance for plane parallel plates. This correlation provides useful information for the estimation of g_F, S_L or d_c for any flame system, when two of these quantities are known. Since the burning velocity S_L depends on the composition of the combustion gas, the value of the critical boundary velocity gradient, and hence of the gas flow necessary to prevent flashback, will vary with the fuel/oxidant ratio of the flame gases.
Expressing the blow-off data in terms of the Karlowitz similarity criterion [63] leads to an equation which correlates experimentally determined data. This equation may be written in full as follows:

$$g_B = 0.23 \cdot \rho \cdot c_p \cdot (S_L^2/k) \cdot [1 - (1 - X^{6.4}) \cdot \alpha] \tag{1.7}$$

where ρ is the mass density of the gas mixture in unburnt state, c_p is the specific heat at constant pressure of the gas mixture in the unburnt state, S_L is the laminar burning velocity, k is the thermal conductivity of the gas mixture in the unburnt state, X is the fuel concentration fraction of the stoichiometric and α is a constant equal to zero for flames with no secondary combustion and equal to unity for flames with secondary combustion. Equation 1.7 is valid for

$\alpha = 0$

or

$\alpha = 1$ and $X < 1.36$.

The only case in which there is a significant deviation from Eq. 1.7 is when there is a marked preferential diffusion [63]. It is clear from the above discussion that the velocity gradients have a definite influence on flame stability. By plotting critical the g_F and g_B boundary velocity gradients versus the mixture composition, blowoff and flashback limit curves can be obtained. A qualitative sketch of critical boundary velocity gradients versus fuel/oxidant ratio is shown in Fig. 1.14. The mixture composition is expressed in terms of gas concentration as a fraction of the stoichiometric.

For rich mixtures, the blowoff curve continues to rise instead of decreasing after the stoichiometric value is reached. The cause of this trend is that the experiments are performed in air, and the diffusion of air into the premixed gaseous mixture, as the flame lifts off the burner rim, increases the local flame speed of the initially fuel-rich mixture.

1.4.2 Stability limits as function of the mixture velocity and the fuel concentration

A laminar flame is stabilized on burners only within certain flow velocity limits; thus it is possible to present a characteristic stability diagram for a premixed flame burning at the end of a cylindrical tube, as illustrated in Fig. 1.15.

In this plot the stability boundaries are given as a function of the fuel concentrations in the mixture and the premixed (unburned) gas supply velocity. When

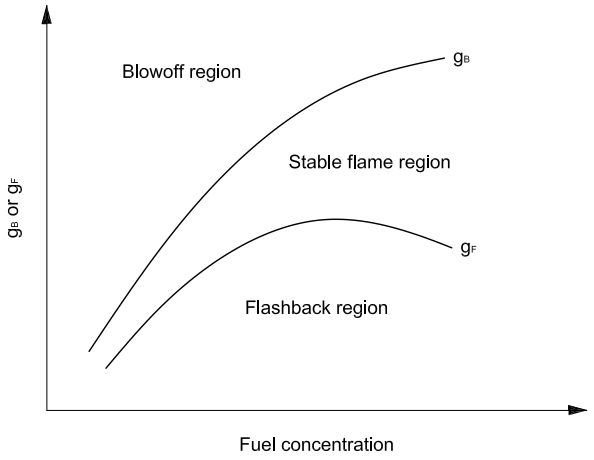

Figure 1.14: Sketch of the effect of the velocity gradient on flame stability.

the approach velocity to a seated flame (represented by the crossed region in Fig. 1.15) is decreased until the flame velocity exceeds the supply velocity over some portion of the burner port, the flame flashes back into the burner (unshaded area of Fig. 1.15). On the other hand, if the magnitude of the approach velocity increased until it exceeds that of the downward flame propagation velocity at every point, the flame will either be entirely extinguished beyond the blowoff limit or it will be lifted until a new stable position in the gas stream above the burner is reached, as a result of diluition with secondary air from the surroundings. The lift curve is a continuation of the blowoff curve beyond point A in Fig. 1.15. The blowout curve thus corresponds to the velocity required to extinguish a lifted flame. Once the flame has lifted, the approach velocity must be decreased well below the original lift velocity before the flame will drop back and be reseated on the burner rim. Between the fuel concentrations A and B, the blowoff of a lifted flame occurs at a lower velocity than the flame blowoff from the port.

1.4.3 Stability limits as a function of the primary aeration and the port loading

The discussion concerning flame stability is also aided considerably by the use of a combustion diagram, in which areas of satisfactory operation are usually depicted as a function of primary aeration and burner port loading. Primary aeration is the fraction of the theoretical air requirement (TAR, defined as the number of volumes of air required for stoichiometric combustion per volume of

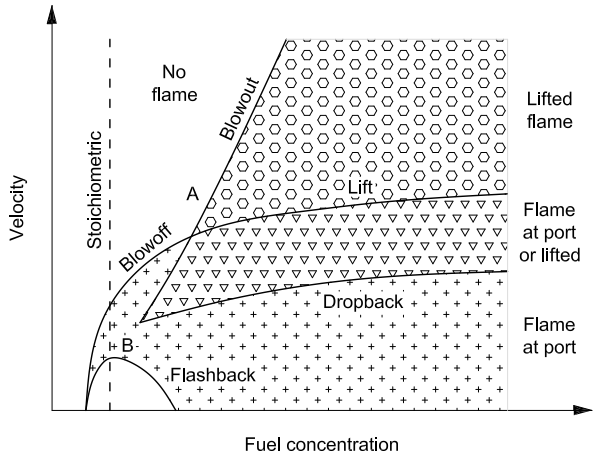

Figure 1.15: Sketch of a characteristic stability diagram for a premixed open burner flame.

fuel) supplied as primary air, expressed as a percentage. The burner port loading represents the heat input to the port area ratio.

The diagram in Fig. 1.16 depicts the following three main areas where unsatisfactory results take place:

- Flame lift: at high primary aeration, due to the increased flow rate not being balanced by a similar increase in burning velocity.
- Light back: at low heat input, due to the condition opposite that of the flame lift phenomena.
- Yellow Tipping: represents an incomplete combustion due to oxygen starvation in the flame at low primary aeration.

The exact size and location of each shaded area are dependent on the burner configuration. However, the stable working region is bounded by the yellow tipping curve at the bottom, by the flame lift curve at the top and by the flash back curve on the left side. The flash back curve peaks at a primary aeration value close to the stoichiometric condition. On the other hand, the flame lift curve decreases continually: hence, the more the primary air, the higher is the risk of lift. Moreover, high values of flame port loading are not allowed because if the aeration is insufficient the combustion process can be partially incomplete, resulting in a dangerously high value of carbon monoxide.
Careful consideration of the design parameters can minimize the extent to which any of the above three conditions may occur. In other words, the good burner

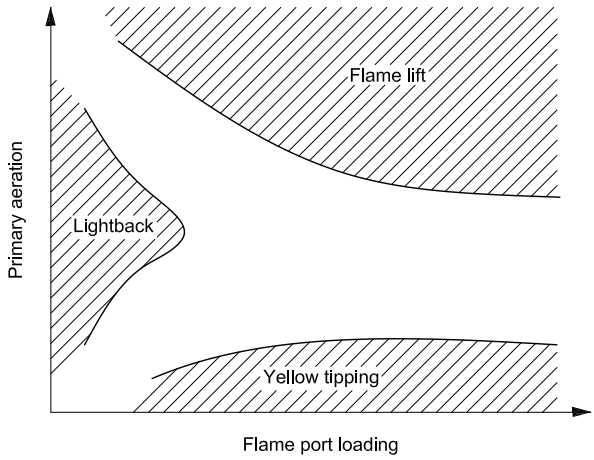

Figure 1.16: Schematic combustion diagram for a typical aerated burner.

designer will ensure that there is a large area of satisfactory operation and that the operating point is somewhere near the middle of the area.

1.5 Empirical Design Criteria

Since most of the burner characteristics are dependent on port design and port arrangement, they should be the starting point in designing a domestic appliance. Burner crown shape and size, total port area and port design and arrangement can be determined by knowing the gas input rating and the available combustion space to accommodate the burner head. Total port area may be determined by dividing the selected input rate per unit port area by the total input rate required. The number of ports is fixed by the total port area with the selection of port size. The distribution of the ports over the available burner head area determines their spacing and arrangement. A universal city gas burner should be designed to have a port loading and port size between those shown for natural gas and manufactured gases. The port loading of a universal burner should approach the recommended value for natural gas, while the port size should be almost as small as the the size recommend for manufactured gas.
The first step in the design of an appliance burner is the selection of the primary air value (Table 1.3). Further requirements are stable flames and performance flexibility when operating at the chosen primary air value.

Type of burner	Primary air
Range top	55 to 60
Range oven	35 to 40
Water heater	35 to 40
Radiant-type space heater	65
Other heating appliances	As low as 35

Table 1.3: Minimum primary air requirements for various types of appliance burners.

Attention to the following design factors reduces primary air requirements:

- distance between ports and nearest heating or impinging surface;
- direction of gas flow from ports, particularly toward adjacent surfaces upon which flames may impinge;
- temperature of surface upon which flames may impinge;
- distribution and spacing of burner ports as affecting mass and height of secondary combustion zone or outer flame mantle and availability of secondary air;
- volume and direction of secondary air flow;
- direction of venting of flue gases.

Typical characteristics of the performance of atmospheric gas burners with respect to flame stability were previously shown in Fig. 1.16. To obtain stable flames at the chosen primary aeration, the gas input rate per unit of port area must be such that the burner working point is located in the stable flame zone and, preferably, in the usual design area. To obtain flexible performance, the working point in the stable flame zone should be located as far as possible from the three curves defining flashback, yellow tipping and lifting limits.
Secondary air complements primary air; together they constitute the air necessary to complete combustion. While increased primary aeration provides better mixing of air with fuel gas, it can also result in poor combustion by indirectly increasing the amount of recirculation of combustion products. This recirculation is relatively severe immediately after ignition with a cold start.
Designing a burner for one general group of gases, e.g. natural gases, is more complicated than for one specific gas. If a universal burner is not used, an appliance requires different burners for natural and manufactured gases. These burners are usually alike except in port size; their design is a compromise. In designing a burner for one general gas type, a certain amount of flexibility must be provided to meet variations in composition. Sufficient flexibility must be provided to permit some variation in the gas composition without either an air shutter or orifice readjustment.
The span of primary air adjustment between the lifting and yellow tip limits is important in considering burner flexibility on peak or substitute gases. Even though these gases may vary somewhat in composition from the gas on which the burner is originally adjusted, satisfactory performance should be obtained without either an air shutter or orifice adjustment. Generally, the greater this span, as shown in Fig. 1.16, the better the burner's flexibility. Flexibility is greater for a design with lower port loadings. However, port loading must not be made low enough to permit flash back. Flexibility also depends on whether the primary aeration selected for design is near the lifting or yellow tipping limits. With a substitute gas having a high yellow tip limit and increased input rate on substitution, any selected design primary aeration should be near the lifting limit of the adjustment gas. With a substitute gas having a low lifting limit and decreased input rate on substitution, the selected design primary aeration should be near the yellow tip limit of the adjustment gas. Any tentative burner design may be examined for flexibility by constructing a flame stability diagram for the proposed burner. A lifting limit curve is constructed by plotting the primary aerations versus the corresponding port loadings concerning previous values of different reference burners available from the design database. A second lifting limit for the substituting gas is similarly constructed. A burner in an appliance is subjected to greater flows of air than it would be in an open room. While such flows have no effect on flash back limits, they generally lower burner flows for blow off and yellow tip limits. Yellow tip limit curves for both adjustment and substitute gases are similarly constructed. The operating adjustment point for

which the burner was designed is next located on the graph by plotting the selected primary aeration versus the port loading at which the burner is to operate. Flexibility may be evaluated by plotting the relocation of this adjustment point on substitution of one gas for another. For flexibility under the given conditions, the relocated adjustment point must be within the limit curves of the substitute gas.
In the following sections some empirical design criteria concerning the flame back and flame lift instabilities will be explained, based on the investigation performed by Jones [2].

1.5.1 Empirical Design Criteria for Flame back

Lightback occurs when the burning velocity exceeds the flow velocity through the burner, that is in the opposite to that for flame lift. Of course, the aerated burners possess this inherent disadvantage compared with non aerated ones, because lightback can occur through the flame port and the radial diffuser, down to the venturi neck: resulting in an unsatisfactory appliance performance and possibly damage to the burner due to overheating.

1.5.1.1 Effect of port geometry

The degree of quenching depends on the shape of the burner port, since heat loss to the burner must be related to the flame shape and the distance between the reaction zone and burner port. However, in the flame lift section, it will be concluded that small ports are more prone to flame lift than large ports. Therefore in practice, because of the need to guard against flame lift, it is not feasible to use burner ports that are sufficiently small to eliminate lightback. Moreover, the boundary velocity gradient theory can break down because, as port size decreases, the point of lightback remains at approximately the same distance from the port wall, and therefore it moves towards the axis of the flame where the velocity gradient is no longer constant as shown in Fig. 1.17.

Additionally, at the groove's entrance, a uniform flow at the free-stream velocity exists. As the fluid moves down the port, shear between the fluid and the wall, and between adjacent fluid particles, retards the motion, causing the boundary layer to grow until it is fully developed. Nevertheless, a port depth of at least twenty port diameters is required to ensure fully developed parabolic flow. Thus, with practical burners, where port diameter and depth are usually roughly equal, parabolic flow is only partially developed, resulting in a much flatter velocity profile, as depicted in Fig. 1.18.

Consequently, small shallow ports are more susceptible to axial lightback than small deep ports because of a flow configuration far from the fully developed condition.
Therefore, flash back will occur at increasingly greater port loadings as port size is increased and port depth is decreased. Port spacing has no effect on flashback at

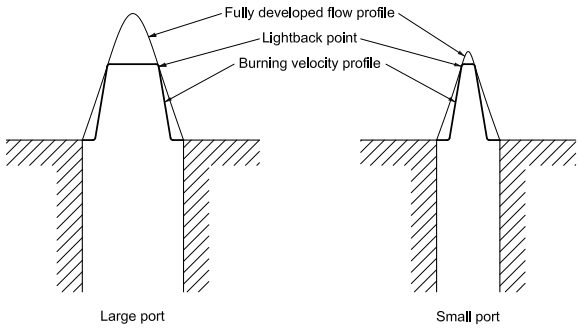

Figure 1.17: Sketch of transition from boundary to axial lightback as port size decreases.

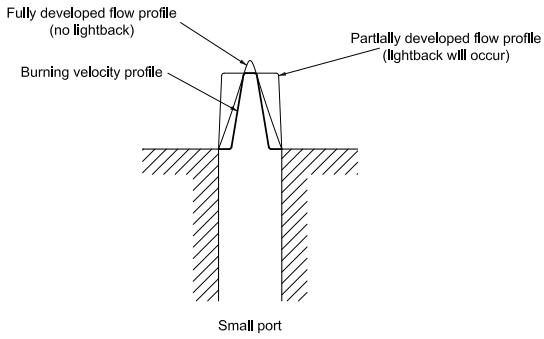

Figure 1.18: Sketch of the effect of non parabolic flow on lightback in small ports.

higher burner operating temperatures. At lower temperatures, close port spacing may possibly raise the air/gas mixture temperature. On the contrary, for a fixed total port area, increasing the number of the ports results in a cooling of the mixture; in this way the combustion process is inhibited and the propagation of the flame front is not allowed upstream toward the unburnt mixture. The risk of lightback can be eliminated by using very small ports and a low primary aeration. In practice, port sizes larger than the quenching diameter need to be used. Lightback can be avoided by providing that the flow rate is high enough and the burner ports are deep enough.

1.5.1.2 Effect of burner configuration

The presence of the pot dramatically influences lightback. Therefore lightback can be empathized by using a hotplate instead of a common pot. The pot partly

absorbs and partly releases heat, whereas the hotplate mainly release all the heat, also causing a raise in the burner and surrounding air temperature.

1.5.1.3 Effect of burner temperature

Any rise in burner temperature preheats the unburnt gas/air mixture, thereby increasing its burning velocity. While this phenomena has a slight beneficial effect with regard to flame lift, it also reduces the quenching diameter and may promote problems with flameback. Additionally, preheating will widen the flammability limits due to the accelerating effect of temperature on chemical reactions.

1.5.1.4 Effect of reactive additives

An addition of a small amount of H_2 (which itself is combustible with air) would greatly increase the flame propagation speed due to chain reaction effects. Therefore, adding H_2 to the fuel gas, the possibility of the occurrence of lightback is increased.

1.5.1.5 Effect of the gas employed

For the European standard certification [3] the critical test concerning the flame lift adopts propylene (C_3H_6) as working fluid.

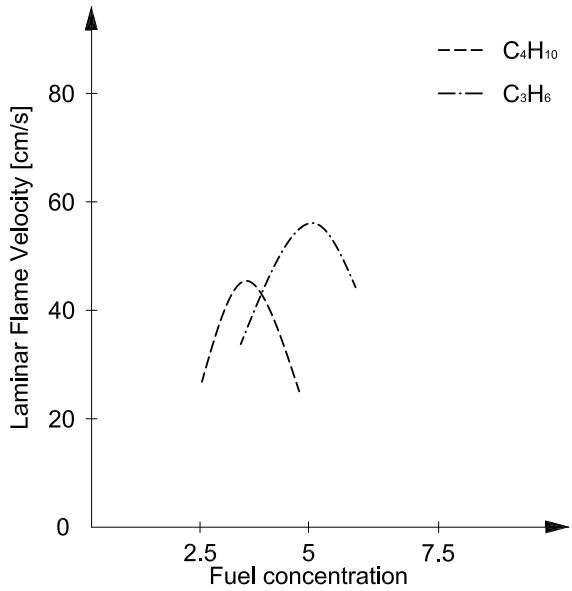

Figure 1.19: Laminar flame speed comparison between Butane and Propylene.

As depicted in Fig. 1.19, the propylene has a laminar burning velocity curve analogous to the C_4H_{10} one but it is raised to higher flame speed values.

1.5.1.6 Effect of unsteady working condition

The criterion for lightback on ignition and extinction remains the same as for conventional lightback, therefore it occurs when the burning velocity exceeds the flow velocity through the burner port. Both phenomena are due to transient changes in these two parameters during the ignition or extinction sequence. Lightback on ignition can occur at those flame ports where there are rapid fluctuations in stream velocity, due probably to turbulence within the burner. Furthermore, Fig. 1.20 shows the variation of stream velocity and burning velocity with time after ignition.

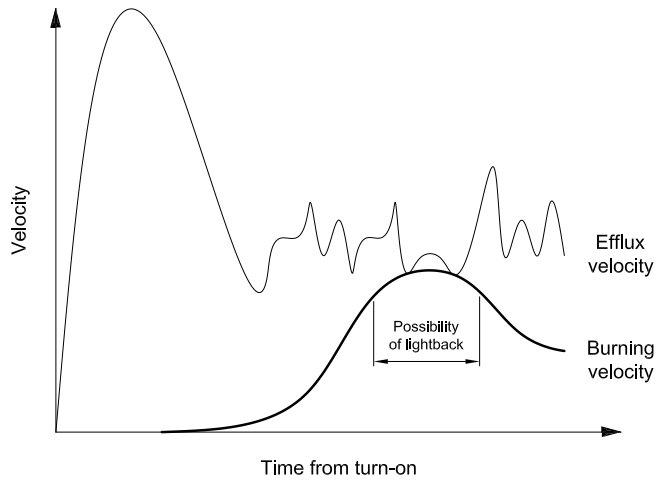

Figure 1.20: Schematic representation of a mechanism for lightback on ignition.

The stream velocity varies rapidly and randomly, while the burning velocity rises from zero (residual air in the burner), through a maximum as the mixture ratio reaches stoichiometry, and then approaches its equilibrium value. Experiments showed that the burning velocity can momentarily exceed the gas velocity during the ignition sequence, but because of the random variation in the stream velocity, it is impossible to predict accurately whether or not lightback on ignition will occur with any particular burner. Despite such uncertainty, the general guidelines state that lightback is more probable with large, shallow ports or with high burner temperatures. The latter warrants special consideration if usage patterns include reignition of a burner which may still be quite hot from a previous

ignition. Lightback on extinction occurs when the gas is turned off, if the flow velocity decreases rapidly enough to fall below the burning velocity before all the gas has been turned off. Factors to be taken into consideration, in addition to the usual criteria, are the size of the burner body and the mode of the valve closure. Physically large burners will take longer to burn off any residual gas, while a slow acting valve or a valve with a large turndown ratio may operate at low volume flow, thereby increasing the probability of lightback on extinction. Therefore, it is also important to consider whether equilibrium conditions at a turndown rate will be in this zone. Transient conditions of burner operation are a major cause for flash back.

1.5.2 Empirical Design Criteria for Flame lift

The concept of flame lift can be attributed to the stream velocity through the flame ports not being balanced by the burning velocity of the fuel/air mixture. If the primary aeration rises, both the burning velocity and the volume flow through the flame ports increase. However, the latter increases more than the former, and thus flame lift may occur. Of course, the greater the primary aeration at lift, the less susceptible is the burner to lift at its nominal operating point. If the velocity if further increased, a point will be reached at which the flames will be extinguished.

The risk of flame lift is low with a fuel/oxygen mixture, whereas it is high with a fuel/air mixture. If the fuel presents a low laminar burning velocity, then the flame lift and the blowoff phenomena will appear at a low mass flow rate. Therefore, lifting may result from too much primary air or, with no primary air, from increasing the gas velocity until it exceeds the burning velocity. The point at which the flame starts to lift from a single port burner, or at which several flames start to lift from a multiport burner, is known as the lifting limit. This characteristic is so defined that it has long been used as a measure of burner performance. It is usually expressed as percentage of primary air at which lifting occurs for a given set of conditions. Most gas appliance burners are designed to avoid lifting by the regulation of primary air (usually by an air shutter). Except under special conditions, such as when the appliance is designed to use blowing flames, lifting is undesirable. It usually indicates escape of some unburned gas or incomplete combustion. Burner applications usually require fairly definite ranges of primary aeration for good combustion. Therefore, a burner with a low lifting limit may not be able to attain the minimum required aeration without lifting, and incomplete combustion will result. Ignition of gas/air mixtures at or above the lifting limit is difficult and flame travel unreliable. Excessive lifting or blowing also decreases the efficiency of heat transfer and may produce disturbing noise.

1.5.2.1 Application to multiport burners

All domestic gas appliances are of multiport design and their port configuration influences the interaction of flames from adjacent burner grooves. Therefore the susceptibility to flame lift depends on this interaction and is obviously influenced by the port size and interport spacing.

1.5.2.2 Effect of flow rate

A multiport burner behaves somewhat differently from a single port burner because at low aerations flame interaction induces a single inner cone over the array of flame ports. As the primary aeration is further increased, separate inner cones become visible above each port.

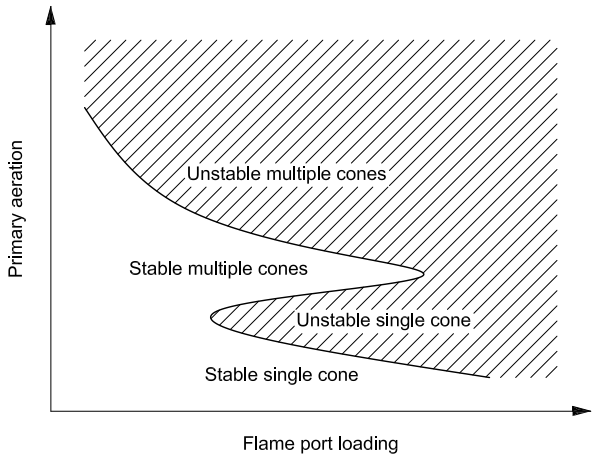

Figure 1.21: Schematic illustration of the flame lift region for a multiport burner.

The lift limit of the combustion diagram for a multiport burner is shown schematically in Fig. 1.21.

1.5.2.3 Effect of port geometry

The simplest solution to avoid flame lift is to increase the burner port size in order to decrease the unburnerd mixture velocity. For circular ports an increase in port diameter reduces the tendency to lift, i.e. a few large ports are better than many small ports. However, increasing the port size has a drawback: for the same heat power input, the higher port size involves a reduction of the specific power, thus the resulting flame is less focused and less hot.
In practice, the mixture flow from the ports is influenced by frictional losses

and vena-contracta effect; it is usual to represent these two terms as a coefficient of discharge. This coefficient is lower for small ports than for large ports. Consequently, even if the measured geometric port area remains constant, for a constant heat input the effective port loading increases as port size decreases, so that flame lift is more likely with small ports. Moreover, as the ports become more widely spaced, a reduction in interaction with neighbouring flames increases the tendency to lift. The shape and depths of the gas ports can also have an effect on flame stability. In general, ports with sharp corners are more likely to lift than ports with rounded corners. Circular ports are better in this respect than square ports and rectangular slots with a low aspect ratio (i.e. length/width ratio). Thus, with rectangular ports, for a given slot width, an increased slot length reduces the tendency to lift. However, long rectangular slots (aspect ratio > 4) can be more stable than circular ports of the same port loading. The effect of variation in port depth is shown schematically in Fig. 1.22.

(a) L <2D (b) L >2D

Figure 1.22: Sketch of flow streamlines through a burner port, showing wall attachments in deep ports.

Unless the entrance to a gas port is suitably rounded, the flow may detach itself from the port wall (Fig. 1.22, case *a*), thereby adversely affecting stability. Reattachment can take place if the port is deep enough (Fig. 1.22, case *b*). Burner ports should, therefore, have a depth/diameter ratio of more than two, if detachment is to be avoided.
Lmiting port loadings above which lifting flames will be obtained have been indicated for arbitrary reference burners, at different primary aerations and different working gases. These data are compiled for cold burners, in which lifting is most likely. The tendency to lifting decreases as the burner temperature increases.
Another way of reducing this instability phenomenon is by various design expedients to increase the limit of port loading by reducing lifting. These alternative solutions are based on the assumption that the flame lift instability is caused by an excessive secondary air at the base of the flame. This surplus of air mainly causes two effects:

- it makes the base of the flame colder, thus the laminar burning velocity is decreased. Therefore, locally the stream velocity through the flame ports is no longer balanced by the laminar flame speed, and the flame can lift.
- it produces a more premixed flame, hence the primary aeration increases and the risk of flame lift is enhanced (as explained in § 1.4.3).

The greater the aeration, the more the flame lift will occur at lower mass flow rates. In order to avoid this aeration surplus two solutions can be adopted:

- placing a deflector at the bottom edge of the horizontal ports in order to obstruct the incoming secondary air;
- using "auxiliary flames" or "pilot flames": they produce free radicals, at the base of the flame, characterized by high combustion velocities. The combustion of these radicals produces a local hanging of the flame on the burner rim (these radicals come from the molecular dissociation of the fuel gas inside the flame where the aeration is insufficient).

The pilot flame represents an extensively accepted solution in the design of domestic gas burners. However, flames issuing from horizontal ports drilled in a circular head or a head with curved surfaces, diverge from each other; thus, they have less self-piloting action than flames from a straight-sided burner. Another design solution to reduce the unburned mixture velocity and therefore raise the lifting limit for horizontal ports, is represented by placing a ledge right at their bottom edge so that the issuing air/gas stream impinges on the ledge.

1.5.2.4 Effect of recirculation current

Other factors in the appliance design may reduce the limiting port loading with respect to lifting. For example, recirculation of flue gases into the flame base, or a high velocity flow of secondary air across the port, lowers the lifting limit considerably. A square port practically always has a lower lifting limit that the circular port with a diameter equal to the side of the square.
Recirculation currents at the base of the flame in a series of long slits interfere to stabilize the flame further. For circular ports, such currents are oriented in different directions and cannot stabilize the flame to the same extent. In many combustion systems, flame stabilization is achieved after the recirculation of burnt gases, and partial premixing with hot products can also be observed.

1.5.2.5 Effect of cap geometry

The presence of the final peak at the extreme radius cap has the effect of containing the flame lift phenomenon: therefore, the moregreater is the peak, the smaller is the probability of the flame lifting off from the burner. Of course, a high peak gives worse combustion results and the possibility of flashback.

1.5.2.6 Effect of burner configuration

As in the flame back phenomenon, the presence of the pot dramatically influences flame lift. The pan acts as a flame damper and tends to contain the lift, keeping the flame attached to the burner. Consequently, for the European standard [3] validation the burner is tested without the pot.

1.5.2.7 Effect of burner temperature

During the operation of an appliance, the burner will warm up, which in turn will preheat the gas/air mixture as it passes through the burner assembly. There are two effects, both of which are light but beneficial: (1) The burning velocity of the gas/air mixture increases with temperature as mentioned before. This leads to a better flame stability at high aeration and high port loading. (2) As the gas/air mixture passes through a hot burner assembly, the mixture temperature will rise, leading to an increase in volume, a decrease in density and an increased flow resistance; therefore a decrease in air entrainment can be highlighted. Consequently the flames will become more stable as the appliance warms up. However, this effect will be absent at ignition and will decrease if the injector is also subject to a rise in temperature.

1.5.2.8 Effect of inert additives

The main purpose of using additives such as N_2 is to decrease the laminar flame speed in order to emphasize the unbalance between the mixture velocity and the burning velocity. Therefore, adding N_2 to the fuel gas, the possibility of flame lift occurring is increased. As a consequence, in the European standard certification [3] the critical test concerning the flame lift adopts, as working fluid, the methane limit gas, named $G231$, that contains 85% of CH_4 and 15% of N_2.

1.5.2.9 Effect of vitiation

The air supplied to a burner should ideally be pure, but if as a result of recirculation of combustion products, the combustion air becomes deficient in oxygen, the air is said to be vitiated. Vitiation of the primary air reduces the burning velocity of the gas/air mixture so that flame lift is encouraged [29]. Vitiation of the secondary air reduces the rate of diffusion of oxygen into the outer diffusion flame, thereby increasing flame length and the risk of incomplete combustion. Therefore, vitiation of secondary combustion air reduces the energy flux from the diffusive to the premixed zone and thereby reduces flame stability because the diffusive combustion zone acts as a pilot flame and retains the premixed zone [29].

Figure 1.23 shows schematically the effect of simultaneous primary and secondary vitiation on lift stability for a typical multiport burner, using as a base the combustion diagram used in Fig. 1.21.

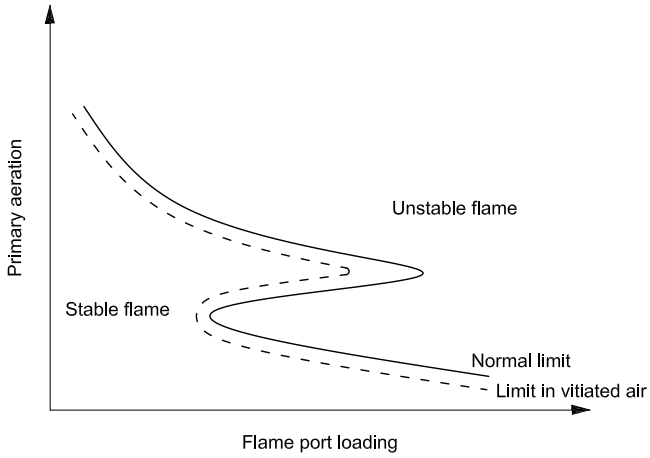

Figure 1.23: Schematic illustration of the effect of vitiation on the flame lift limit for a multiport burner.

1.5.2.10 Provision of retention flames

In order to provide a burner with the variation in heat input that is required in most kitchens, retention systems are applied to partially aerated burners. Retention flames are inherently more stable than the main flame because of their low efflux velocity; thus they are most frequently used where a high port loading is required or where there is to be a large turndown ratio (e.g. the domestic cooker hotplate).

1.6 Design of Experiments Analysis

In order to develop a new domestic gas burner, the empirical approach presented in the previous chapter was usually adopted in association with an experimental study. It is important to note the difference between experiment and test. A test is an activity performed on an existing process to verify if the process satisfies the expectations in real working conditions. On the other hand, an experiment verifies which variable influences the system result and for which values of the variables the system presents an optimal result. Therefore, during the domestic appliance design, an experimental planning aimed at obtaining the maximum amount of information with the minimum amount of experiments was considered. This approach greatly improves engineering productivity and it is the assumption according to which problems are handled from an engineering point of view, the so-called robust design. Robust design is an "engineering methodology for improving productivity during research and development so that high-quality products can be produced quickly and at low cost" [107]. The idea behind robust design is to improve the quality of a product by minimizing the effects of variation without eliminating the causes (since they are too difficult or too expensive to control). To achieve a design that has minimum sensitivity to the variations of uncontrollable factors, a Design of Experiment (DoE) approach was applied.
DoE is a statistical and mathematical strategy searching for useful information in complex systems. A careful planning of experiments increases the amount of resulting information: characterizing the process and pointing out the cause and effect relations between the input and output variables. The details of performing a DoE can be found in many textbooks [108, 109]. However, DoE theory is based on the assumption that each input might be interacting with all other inputs. This is a powerful statement. Moreover, not only all the interactions are studied, but they are all studied at the same time in one big round of tests. These considerations point out the strengths and weaknesses of the DoE approach. The strength is represented by the opportunity of investigating all the possible interactions between inputs at the same time without having any innate knowledge of how the process works. The weakness is described by the fact that there is no way to make the experiment more efficient by thinking about how the inputs really do interact. To be fair, not all DoE based investigations look at all possible interactions. Those that do, are called "full factorial" DoEs. On the other hand, "Fractional factorial" DoEs can eliminate some interactions, and therefore decrease the amount of work that needs to be done. But they are still based on the idea of full modeling, and then whittled down to improve efficiency. The savings are generally fairly meager, such as by a factor of two or four, and there is still no way to inject understanding of the fundamental process into the mix.
In order to decrease the number of tests to be performed, another technique for optimizing a process can be applied, named "Taguchi method" [110]. What DoE and Taguchi primarily have in common, is that they deal with multiple inputs and

how they interact with each other. Their primary difference lies in how they handle the interactions between inputs. DoE was invented by scientists for scientists, whereas Taguchi methods were invented by engineers for engineers. Therefore, Taguchi methods start with the assumption that we are designing an engineering system, either a product to perform some intended function, or a production process to manufacture some product or item. Since the engineer is knowledgeable enough to be designing the system in the first place, he generally will have some understanding of the fundamental processes inherent in that system. Basically, this knowledge can be used to make the experiments more efficient, by skipping all that extra effort that might have gone into investigating interactions that are know not to exist. Without going into details, it was shown that this can decrease the level of effort by a factor of ten or twenty or more. Therefore, robust parameter design uses Taguchi designs, which allows the analysis of many factors with few runs. However, the weakness ascribed to this approach is due to the fact that Taguchi does not analyze the real output of the system, but this answer is first transformed, and then analyzed. The screening or the optimization process is therefore not based on the real data, but on fitted data that might not represent the system well. Therefore, the mathematical expression linking the changes in the factors to the changes in the responses (the model) uses fitted data as responses. Several fittings, named "signal-to-noise ratios", are usually proposed and they should be chosen according to the goal of the design process, based on engineering knowledge, understanding of the process and experience.
During the development of the cylindrical burner crown range, three prototype families were manufactured and tested by means of the Taguchi approach [111]. In this design stage the right combination of materials, parts, processes and design factors was determined to satisfy the functional and economical specifications requested of the appliance. Therefore, the system variables were experimentally analyzed to determine how the product or process reacts to uncontrollable "noise" in the system; this parameter design is the main thrust of Taguchi's approach. Parameter design is related to finding the appropriate design factor levels to make the system less sensitive to variations in uncontrollable noise factors, i.e., to make the system robust. The Taguchi method was then applied in the research for the optimal values of the factors and some of their combinations that influence the onset of flame back and flame lift in the domestic gas burner. Different geometrical dimensions within the domestic gas burner crown were chosen as variables affecting these flame instabilities.
In this investigation, an experimental layout designed for three control factors, each at three levels, was adopted. This kind of experimental plan is named "L9" in the Taguchi definition, in which the "L" stands for Latin, since most of these designs are based on classical Latin Square layouts, appropriately pruned for efficiency. However, a full factorial DoE of all combinations of these factors would require 81 tests, three to the power of four. The Taguchi L9 layout recommends a subset of nine of these eighty one tests which allows, the main effects to be

determined.
For the domestic gas burner development the three prototypes families were named “L9-2”, “L9-3” and “L9-4”. Of course, they were manufactured at different times, starting from “L9-2”; the optimization process lead the designer to the “L9-3” and, finally, to the “L9-4”.

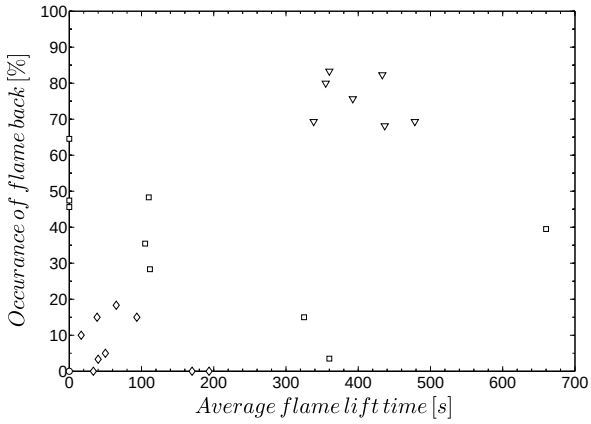

Figure 1.24: Experimental correlation concerning the average flame lift time and the occurrence of flame back for different prototype families: L9-2 (triangle), L9-3 (square), L9-4 (diamond) and the definitive crown burner (circle) located at the origin of the axes.

In Fig. 1.24, the flame back and flame lift instabilities are plotted against each other to confirm the good trend of the developing phase, where the continuous optimization process has decreased the occurence of both flame lift and flame back at the same time. It must be noted that the data for flashback and blow off reported here were obtained by visual observation of the flame. For each stability test, the proper limit gas was used.
Obviously, even adopting the Taguchi approach to test a reduced number of factor combinations, these experimental plans still requires a large amount of time and great cost in terms of prototype manufacturing and testing phase. In this scenario, the numerical simulation offers a new approach to support the product development of the domestic gas burner. The virtual prototype reduces the prototyping and testing phase in the laboratory and offers an added value in terms of technical knowledge and understanding of the burner fluid dynamic behavior. The different features characterizing the numerical tool adopted in this work will be briefly presented in the next chapter.

Chapter 2

The numerical tool

Chapter Purpose:
This chapter summarizes the characteristics of the code adopted in the numerical simulations. The main numerical models will be introduced with particular emphasis to the modelization of the combustion process.

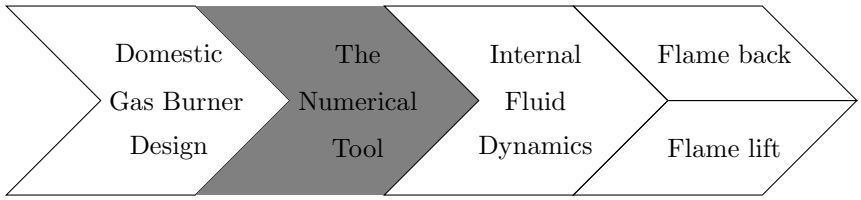

2.1 Introduction

Although most of the twentieth century investigation on fluid dynamics involved the use of the "two approach world" of pure theory and pure experiments, the advent of high speed digital computer combined with the development of accurate numerical codes for solving physical problems has revolutionized the way to study and perform fluid dynamics today. Therefore, nowadays computational fluid dynamics constitutes a new third approach in the study and development of the whole discipline of fluid dynamic.
The experiments carried out with a computer program can be considered numerical experiments. In today's CFD, computer programs for the calculation of three dimensional flows have become industry standards, resulting in their use as a tool in the design process. Numerical simulations, accomplished in parallel with physical experiments in the laboratory, can be used to help interpret such physical results and even to ascertain a basic phenomenological aspect of the experiments which is not apparent from the laboratory data. Therefore, CFD does not just provide a quantitative comparison, but also represents a tool to interpret a basic phenomenological aspect of the experimental conditions.
Therefore, the aim of this activity of research has been to develop a numerical knowledge, in order to perform design screening based on a numerical prediction of the domestic gas burner performances. This numerical prediction has been carried out with the use of a commercial finite volume CFD code. The choice to use a commercial package as a design tool was due to several reasons. Indeed, the debugging and validation of the numerical algorithm are not necessary; therefore it is possible to directly focus on the problem solving on demand. The software is not specific, but it is able to offer a wide choice of models in order to satisfy different user requests and to use the same software for different applications. Moreover, the commercial code is constantly updated, ensuring the implementation of newer models and its optimization regarding the hardware evolutions. In this way, despite of the experience and insight that would be gained in the use of an in-house CFD code, the commercial code can offer a numerical output in short time, leading to a better design and a shorter time to market.

2.2 Governing equations

The starting point for a computational investigation is a statement of the governing equations for the phenomenon under study. In this section, the complete set of detailed governing equations for gaseous reacting flows is hence presented. A fundamental assumption in the study of turbulent flow is that the gas can be viewed as a continuum, i.e. the distance between molecules of gas and the mean free path of the molecules is very small compared with the physical dimensions of the geometric scale of interest. Given this assumption, for reacting and non-reacting gaseous flows, there are five basic variables that must be considered in modeling the fluid motion: three velocity components and two thermodynamic properties (i.e. pressure and temperature). Determining the values for these five variables as a function of space and time, which is the solution of the flow field, is the purpose of the mathematical models of fluid motion. Since five variables are of interest, the mathematical model must comprise at least five independent equations. Additional constitutive equations are added if additional variables are introduced. As an example, if a third thermodynamic property must be considered, an additional equation can be added in the form of an equation of state.
The derivation of the five equations constitutes a mathematical model of gaseous, turbulent fluid flow with heat transfer. In these derivations, three fundamental laws of physics are employed: (1) conservation of mass; (2) Newton's second law of motion; and (3) conservation of energy (first law of thermodynamics).
These laws can be used to derive integral relationships for control volumes, or differential relationships for local points in space. Differential relationships in the form of partial differential equations are the most often employed form in developing numerical codes and are presented hereafter.
If the flow is assumed to be a Newtonian fluid, the first of five partial differential equations, written in Cartesian tensor notation, required to model the flow is the continuity equation:

$$\frac{\partial \rho}{\partial t} + \frac{\partial (\rho u_i)}{\partial x_i} = S^m \tag{2.1}$$

where ρ is the fluid density, u_i are the velocity components in each of the x_i directions, and S^m represents a mass source per unit volume. The first term on the left hand side of this equation represents the rate of change of density (mass per unit volume) with time and the second term denotes the change of mass resulting from convective motions.
The next three equations, summarized as one equation written in Cartesian tensor notation, are the momentum equations or the equations of motion, one for each of the coordinate directions.

$$\frac{\partial (\rho u_i)}{\partial t} + \frac{\partial (\rho u_i u_j)}{\partial x_j} = B_i - \frac{\partial p}{\partial x_i} + \frac{\partial}{\partial x_j} \times \mu \left[\frac{\partial u_i}{\partial x_j} + \frac{\partial u_j}{\partial x_i} - \delta_{ij} \frac{2}{3} \left(\frac{\partial u_k}{\partial x_k} \right) \right] + S_i^u \tag{2.2}$$

These equations are sometimes referred to as the Navier–Stokes equations. In these equations, p is the local pressure, μ is the dynamic viscosity of the fluid, S_i^u are the momentum sources per unit volume, and B_i are body forces acting on the fluid. The first term on the left hand side of this equation represents the rate of change of momentum per unit volume with time and the second term represents the transport of momentum resulting from convective motion. On the right hand side of the equation, the terms combined with μ are viscous shear forces resulting from the motion of the fluid.
The fifth equation, the energy equation, is in terms of enthalpy:

$$\frac{\partial(\rho h)}{\partial t} + \frac{\partial(\rho u_i h)}{\partial x_i} = \left(\frac{\partial}{\partial x_j}\right)\left(\Gamma_h \frac{\partial h}{\partial x_j}\right) + \frac{\partial p}{\partial t} + \frac{\partial u_i p}{\partial x_i} + \Psi + S^h \tag{2.3}$$

where h is the specific enthalpy, Γ_h is the ratio of turbulent viscosity and the Prandtl number, Ψ is the dissipation function, and S^h is the source of enthalpy generated on a volumetric source basis. As in the previous equations, the first term on the left hand side of this equation represents the rate of change of enthalpy per unit volume and the second term represents the transport of enthalpy resulting from convective motions. The first term on the right hand side represents the molecular diffusion of enthalpy based on Fourier's law of heat conduction. The pressure terms on the right hand side of the equation represent reversible work done on the fluid, while Ψ represents the irreversible work, or dissipation of energy resulting from the shear stresses, acting as a source of internal energy and always positive. This term is given by the expression:

$$\Psi = \mu\left[\frac{\partial u_i}{\partial x_j} + \frac{\partial u_j}{\partial x_i} - \delta_{ij}\frac{2}{3}\left(\frac{\partial u_k}{\partial x_k}\right)\right]\frac{\partial u_i}{\partial x_j} \tag{2.4}$$

The above mentioned set of equations represents the mathematical model of a fluid motion. The ability of modern computers to store and rapidly manipulate large quantities of data has allowed the development of flow simulations that complement, and sometimes even replace, traditional laboratory experiments. The analysis of a system, as the domestic gas burner, involving fluid flow, heat transfer and associated phenomena such as chemical reactions by means of computer based simulations is known as Computational Fluid Dynamics (CFD).

2.2.1 Numerical techniques

The application of CFD to real life flow systems requires the ability to handle turbulent flows. The description of turbulent process using CFD may be achieved using a variety of numerical simulations. Three levels of turbulent reacting flow computations are distinguished. The first level, Reynolds Averaged Navier Stokes simulations (RANS) represents the oldest approach to turbulence modeling. Therefore, RANS techniques were developed to solve for the mean values of all quantities. The balance equations for Reynolds or Favre (i.e. mass

weighted) averaged quantities are obtained by averaging the instantaneous balance equations. The averaged equations require closure rules: a turbulence model to deal with the flow dynamics in combination with a turbulent combustion model to describe chemical species conversion and heat release. Solving these equations provides averaged quantities corresponding to averages over time for stationary mean flows or averages over different realizations (or cycles) for periodic flows like those found in piston engines (i.e. phase averaging).
The second level corresponds to Large Eddy Simulation (LES). Turbulent flow produces fluid interaction at a large range of length scales. In this context, the turbulent large scales are explicitly calculated, whereas the effect of smaller ones is modeled using subgrid closure models. The balance equations for large eddy simulations are obtained by filtering the instantaneous balance equations. LES of reacting flows determine the instantaneous position of a "large scale" resolved flame front but a subgrid model is required to take into account the effects of small turbulent scales on combustion.
The third level of combustion simulations is based on direct numerical simulations (DNS) where the full instantaneous Navier-Stokes equations are solved without any model for turbulent motions: all turbulence scales are explicitly determined and their effects on combustion are captured by the simulation. Developed in the last thirty years thanks to the development of high performance computers, DNS have changed the analysis of turbulent combustion, but are still limited to simple academic flows. Therefore, because of the complexity of general combustion problems, and the limitation in capabilities of present computer systems, DNS applications are focused primarily on the study of fundamental flow structures.
In industry, the considerable expense of adopting LES and DNS simulations motivates the use for a reliable technique to reduce the cost of the design and development phases. In the present work, this technique is represented by the RANS approach.

2.2.2 Favre averaging

Due to the steady-state assumption used in the domestic gas burner flow simulations, auxiliary relationships are required to account for the effects of turbulence on the transport processes. These relationships are developed by filtering the conservation equations into mean and fluctuating components, as follows [112]:

$$\phi = \bar{\phi} + \phi' \tag{2.5}$$

where ϕ is any conserved scalar variable. In addition, in combustion modeling, an alternative method of averaging the flow field variables, known as Favre-averaging, is defined using the following relation:

$$\tilde{\phi} \equiv \frac{\overline{\rho\phi}}{\bar{\rho}} \tag{2.6}$$

where ρ is the density. As shown in this relation, Favre averaging is denoted using $\tilde{\phi}$ instead of $\bar{\phi}$. An advantage of Favre-averaging, or density-weighted averaging, is the elimination of density–velocity cross-product terms in the momentum equations, which is an effective way to account for the effects of density fluctuations due to turbulence [113].
The substitution of these variable decompositions in Eq. 2.5 for velocities in the equations of motion and continuity, and time-averaging the subsequent relations results in the following steady-state forms:

$$\bar{\rho}\frac{\partial \tilde{u}_i}{\partial x_i} = \tilde{S}^m \tag{2.7}$$

$$\bar{\rho}\frac{\partial(\tilde{u}_i\tilde{u}_j)}{\partial x_j} = B_i - \frac{\partial \bar{p}}{\partial x_i} + \frac{\partial}{\partial x_j}\mu\left[\frac{\partial \tilde{u}_i}{\partial x_j} + \frac{\partial \tilde{u}_i}{\partial x_i}\right] - \frac{\partial\overline{(\rho u_i' u_j')}}{\partial x_j} + \tilde{S}_i^u \tag{2.8}$$

The terms $\overline{(\rho u_i' u_j')}$ represents thus the Reynolds stress tensor. The modeling of these terms in the time-averaged conservation equations is known as turbulent closure, which is a major challenge of turbulence modeling in CFD. Reviews of turbulence and its associated closure problems with respect to computational modeling have been given by Wilcox [114]. However, the following sections present a description of the turbulence and combustion closures adopted in this work.

2.3 Turbulence modeling

Most common turbulence models employ the Boussinesq hypothesis[112] to model the Reynolds stress terms, where stresses are assumed to be analogous to viscous dissipation stresses. Therefore, this method involves an algebraic equation for the Reynolds stresses which include determining the turbulent viscosity, and depending on the level of sophistication of the model, solving transport equations for determining the turbulent kinetic energy and dissipation.
In this work as turbulence closure has been adopted the k–ϵ formulation. This model has become the most widely used approach for the solution of practical fluid dynamics problems because of its general applicability. It focuses on the mechanisms that affect the turbulent kinetic energy, k. In this approach, the turbulent kinetic energy is related to its rate of dissipation, ϵ, by the Prandtl–Kolmogorov relationship, in which the kinematic eddy viscosity is given by:

$$\upsilon_e = \frac{f_u C_\mu k^2}{\epsilon} \tag{2.9}$$

where f_u and C_μ are constants of proportionality that are correlated with particular kinds of flow fields, such as jets or wakes.
However, the k–ϵ model does not represent the final answer in turbulence modeling, because of its various shortcomings. An important example of one of these shortcomings is that the turbulence is assumed to be isotropic, i.e. all normal stresses are identical. With this limitation, secondary flow field effects cannot be accurately predicted. This can be especially important in highly swirling flows [115]. A second major shortcoming of the k–ϵ model is that it does not relax to laminar flow conditions at low-Reynolds numbers. Therefore, the k–ϵ model assumes a high-Reynolds number, fully turbulent flow regime and auxiliary methods are required to model the transitions between laminar flow behavior and turbulent flow behavior. An important example of this is the transition from the thin viscous sublayer flow region along a wall to the fully turbulent, free stream flow region. The accuracy of the near wall representation of the flow field is crucial in the successful prediction of wall-bounded turbulent flows, although predictions of the flow away from the wall are generally not very sensitive to the near-wall turbulence model [116].
From this point of view, the internal flow features in a domestic gas burner are dominated by the gaseous jet issuing from the injector which needs to be model accurately. Therefore the jet (i.e. injector) can be considered as the burner engine. This highly turbulent jet requires a turbulent model to capture the air entrainment effect. Nevertheless, downstream to the venturi neck of the burner crown, a relaminarization of the flow in the expansion chamber up to the flame ports has been achieved. Actually, the flame which develops out of the flame port shows the characteristics of a laminar partially pre-mixed combustion type. It is quite problematic to correctly model both a turbulent jet emerging from

the nozzle and a laminar flow in the remaining part of the burner. In order to perform a correct numerical prediction of these phenomena, two approaches have been considered: modifications of k–ϵ for low-Reynolds number situations and hybrid wall functions. The numerical code automatically selects a low Reynolds number wall treatment or a wall function, depending on the local flow field and near-wall mesh spacing. Of course, this simulation strategy was chosen after a preliminary sensitivity analysis performed in the first part of the project[117]. As a result, a good agreement with numerical prediction and experimental result was achieved with the k–ϵ Low Reynolds turbulence model by using hybrid wall functions as near wall treatment. The k–ϵ High Reynolds number provided even better results, but it only implemented standard wall functions and they cannot be applied within the mesh spacing range of the domestic gas burner model.

2.3.1 Low Reynolds number approach

The high Reynolds number k–ϵ and other models cannot deal with any flow where viscosity is important (characterized by low turbulence Reynolds number), such as in the wall viscous sublayer and the buffer zone. In order to make it possible to integrate equations up to the wall, near wall modifications are needed to account for viscosity effects, but also for other, non viscous (kinematic) wall effects, such as wall blocking and pressure reflection. The modifications of linear eddy viscosity models make no distinctions between viscous and nonvisous wall effects and involve relatively simple viscous modifications solely in terms of local turbulence Reynolds number, hence the common notion low Reynolds number modifications. Therefore, with low Reynolds number approaches, the turbulence model is modified to include terms that account for the transition from fully turbulent to laminar flow behavior [118]. In the case of the k–ϵ model, new terms have been included in the partial differential equation for k or in both the equation for k and the equation for ϵ. Wall damping needs to be applied to ensure that viscous stresses take over from turbulent Reynolds stresses at low Reynolds number and in the viscous sub-layer adjacent to solid walls. These terms are in the form of damping functions that are a function of the distance from the wall, the molecular viscosity and local values for k and/or ϵ.
Moreover, it is worth to note that the k–ϵ turbulence model overestimates the diffusion of a round jet [119] and it needs to be tuned for the considered case. The standard k–ϵ model should be modified to account for observed discrepancies between the model prediction and the experimental results. Furthermore, this standard model predicts the plane jet flow correctly, but it overestimates the spreading rate of circular jets [120]. To avoid this problem, the coefficient C_μ adopted in the k–ϵ turbulence model formulation has been tuned and its recommended value has changed from 0.09 (default value) to 0.06. Obviously, a wider spreading angle indicates an higher mass flow rate entrained from the jet. Therefore, according to the spreading overestimation of the model, the C_μ=0.06

case presents a lower air entrainment than the default one (C_μ=0.09).

2.3.2 Wall functions approach

The common way to treat wall boundaries is to avoid the molecular layer and buffer zones adjacent to a wall and to bridge the solutions at the first control cell (assumed to be fully turbulent) with the wall properties. This is achieved using the so called wall functions, a set of semi-empirical functions which have been derived from experimental evidence and similarity arguments. In this way, only one grid point is required to model the transition from the wall boundary to the fully turbulent flow field. The analytical expression used for this wall function is the universal law of the wall suggested by Prandtl [112],

$$U^+ = \frac{1}{\kappa} lnEy^+ \tag{2.10}$$

where U^+ and y^+, respectively, represent the velocity distribution in the wall layer and the distance to the wall from the adjacent cell centroid:

$$U^+ \equiv \frac{U}{u_\tau} \tag{2.11}$$

$$y^+ \equiv u_\tau \frac{y}{\nu} \tag{2.12}$$

and

$$u_\tau \equiv \sqrt{\frac{\tau_w}{\rho}} \tag{2.13}$$

In these equations, U is the free-stream velocity, E and κ are constants used in the correlation equation, and τ_w is the shear stress at the wall. The adaptation of this technique by Launder and Spalding [120] has become the standard wall function approach. Modifications to the standard approach have sought to improve its accuracy for a wider range of problems, such as dividing the near-wall region into layers [121–123] and sensitizing the law of the wall to the pressure gradient [124].
Therefore, the main assumptions involved in the standard wall function formulation are as follows:

- Variations in velocity, etc. are predominantly normal to the wall, leading to one-dimensional behavior.
- Effects of pressure gradients and body forces are negligibly small, leading to uniform shear stress in the layer.
- Shear stress and velocity vectors are aligned and unidirectional throughout the layer.

- A balance exists between turbulence energy production and dissipation.
- There is a linear variation of turbulence length scale.

The resulting Eq. 2.10 thus gives the cross stream profiles in terms of the normal distance y^+ from the wall. The wall function approach has been found to be a robust, computationally efficient and reasonably accurate method for establishing wall boundary conditions in turbulent fluid flows. However, this standard formulation is a poor approach in flow regions where the Reynolds number is low, where fluid properties are changing rapidly, where strong body forces or pressure gradients are present and where boundary walls have blowing or suction [125]. Therefore, at low Reynolds number, the log-law is not valid so the above mentioned boundary condition cannot be used. For this reason, in the domestic gas burner numerical model an hybrid wall function has been applied. This approach has been used only with the low-Reynolds number turbulence models and is detailed in [126]. It adopts a special wall boundary condition that removes the burden of having to ensure a small enough near-wall value for y^+ (by creating a sufficiently fine mesh next to the wall). The y^+ independency of the hybrid wall condition is achieved using either an asymptotic expression valid for $0.1 < y^+ < 100$ or by blending low-Reynolds and high-Reynolds number expressions for shear stress, thermal energy and chemical species wall fluxes. About the details concerning the numerical methodology for this wall boundary condition, the reader can referred to [127].

2.4 Combustion modeling

The proper simulation of turbulent combustion processes requires an effective scheme for simultaneously modeling both the mixing and the reactions of relevant chemical species. As a starting point, a partial differential conservation equation can be written for each of the chemical species of interest, in the following form:

$$\frac{\partial}{\partial t}(\rho Y_i) + \frac{\partial}{\partial x_i}(\rho u_i Y_i) = \frac{\partial}{\partial x_i}\left(\frac{\mu_e \partial Y_i}{\sigma_m \partial x_i}\right) + R_i + S_i \tag{2.14}$$

where Y_i is the mass fraction of the ith chemical species, σ_m is the ratio of effective diffusion coefficient for the ith species and the turbulent momentum diffusivity, R_i is the mass rate of creation or depletion by chemical reaction, and S_i represents other sources of species creation, such as addition from the dispersed phase. An equation of this form must be solved for N - 1 species, where N is the total number of chemical species present in the system. In writing conservation equations for species in turbulent, reacting systems, time-averaging is required, and Favre averaging is recommended [128]. These equations can be discretized using the same methods discussed previously. The chemical production or depletion term, R_i, can be determined (on a mass/volume basis) by the law of mass action as follows:

$$R_{i,kin} = -M_i k \prod_l \left(\frac{\rho Y_l}{M_l}\right)^{\nu_l} \tag{2.15}$$

where M_i is the molecular weight of the ith species, M_l is the molecular weight of the lth reactant, Y_l is the mass fraction of the lth reactant species, k is the specific reaction rate constant and ν_l is the stoichiometric coefficient of the lth reactant species. The reaction rate constant k, is, in general, expressed by the modified Arrhenius equation (with T^β)

$$k = AT^\beta exp\left(\frac{-E_a}{RT}\right) \tag{2.16}$$

where A is the pre-exponential factor, β is the temperature exponent, E_a is the activation energy for the reaction, R is the ideal gas constant and T is the temperature. Combining these two relations results in:

$$R_{i,kin} = -AM_i T^\beta exp\left(\frac{-E_a}{RT}\right) \prod_l \left(\frac{\rho Y_l}{M_l}\right)^{\nu_l} \tag{2.17}$$

Time-averaging of this equation can be accomplished by substituting the sum of a mean and fluctuating value for each of the variables and then decomposing the instantaneous variables into their main and fluctuating components.
Of course, modeling turbulent chemical reaction terms in a comprehensive combustion code requires use of simplifying assumptions. In employing simplifying

assumptions to achieve feasible solutions of chemical reaction equations, coupled with the turbulent fluid mechanics, three modeling approaches are usually adopted, which can be classified according to the two hypothetical time scales associated with chemical reactions in turbulent flow:

- the reaction time scale;
- turbulent mixing time scale.

The reaction time scale is the typical time required for the species of interest to react completely to equilibrium. The turbulent mixing time scale is the typical time required for large scale turbulent eddies to break up and reduce to the scale where molecular interactions can take place.
In the first modeling approach, which is a limiting case scenario, the reacting species are assumed to be premixed, or the turbulent mixing time scale is assumed to be very fast compared with the reaction time scale. In this case turbulent mixing can be ignored, and the finite rate chemistry and associated reaction rates can be based on mean flow properties. Bowman [129] and Bray [130] have reviewed literature for this approach. This limiting case is not applicable for non-premixed turbulent hydrocarbon diffusion flames, however, which is the focus of this work, and will not be discussed further.
In the other two modeling approaches, the turbulent mixing time scale is either on the same order or much longer than the reaction time scales for the major species of interest. However, when the turbulent mixing time scale can be assumed to be much longer than the reaction time scale, the reaction time scale can be ignored and the modeling focuses on turbulent mixing rates. On the other hand, when the turbulent mixing and reaction time scales are on the same order, both must be considered in the modeling approach. In the following section these two last modeling approaches will be discussed in detail due to their applicability to the partially premixed flames of a domestic gas burner.

2.4.1 Eddy Break Up Model

On the contrary to the Arrhenius model, the simple idea of the EBU model is to consider that chemistry does not play any explicit role, whereas the turbulent motions control the reaction rate. It is based on a phenomenological analysis of turbulent combustion assuming:

- high Reynolds number ($R_e \gg 1$);
- high Damköhler number[1] ($D_a \gg 1$).

[1] The Damköhler number is defined for the largest eddies and corresponds to :

$$D_a = \frac{\tau_f}{\tau_c} \tag{2.18}$$

Where τ_f and τ_c are respectively flow and chemical time scale. For large values of the Damköhler number ($D_a \gg 1$), chemical times are shorter than the integral flow (turbulence) time.

The EBU method, first presented by Magnussen and Hjertager [131], employs the formulation suggested by Spalding [132] assuming that in most technical applications the chemical reaction rates are fast compared to the mixing, so that turbulent mixing is guaranteed to be the controlling rate. Therefore, to account for the effects of turbulence on the chemical reaction, the reaction rate is determined by the rate of intermixing of fuel and oxygen containing eddies, i.e by the rate of dissipation of the eddies. Therefore, this combustion model relates the rate of reaction to the dissipation rate of turbulent eddies containing products and reactants. The reaction rate is hence viewed as a collection of fresh and burnt gaseous pockets transported by turbulent eddies. The dissipation rate of turbulent eddies is assumed to be proportional to the ratio between the turbulent kinetic dissipation and the turbulent kinetic energy, ϵ/k [132]. One proportionality constant is used for eddies with reactants, and another for eddies with products. However, the mean reaction rate is mainly controlled by the turbulent time scale $\tau_t = k/\epsilon$ and temperature fluctuations. This is an estimation of the characteristic time of integral length scales of the turbulent flow.
Mathematically, the above statements can be translated in the following equation, where three different reactions rates are calculated and the smallest rate is assumed to be the governing rate. Since the purpose of the turbulent combustion modelling is to find a formulation to describe the source term R_i which appears in the transport equation, according to the EBU model the volumetric chemical consumption rate is thus given by:

$$R_{i,tur} = -\rho \frac{1}{\tau_t} A_{EBU} min \left[Y_F, Y_O \frac{\nu_F M_F}{\nu_O M_O}, B_{EBU} Y_P \frac{\nu_F M_F}{\nu_P M_P} \right] \tag{2.19}$$

where the subscripts F, O and P represent fuel, oxidant and product respectively; A_{EBU} and B_{EBU} are dimensionless empirical coefficients with nominal default values adjusted for the application of interest. The first two arguments in the square brackets of Eq. 2.19 represent the rates of dissipation of turbulent reactant eddies and determine the local rate-controlling mass fraction, while the third reaction rate is the rate of dissipation of turbulent eddies with products and it is intended to inhibit the reaction where the temperature is too low[127]. Since this product dependence for the reaction rate is a deviation from the pure fast chemistry assumption, the assumption here is that without products the temperature will be too low for reactions. The micromixing time scale is taken to be k/ϵ, the dissipation time scale.
An essential feature of turbulent combustion models is their realizability. Typically, realizability conditions involve requirements on the behavior of the solution far from the flame front and on the integral of the reaction rate. The EBU model is always realizable and leads to an exponential decay of the reaction rate with distance from the flame front [133]. Models of this type have been used for a wide range of applications including laminar or turbulent reaction systems, and combustion systems including premixed or diffusion flames. The EBU model

is hence attractive because the reaction rate is written as a simple function of known mean quantities without additional transport equations. A great deal of the CFD studies make use of the EBU model because it is easy to implement and it is also available in most commercial CFD package.
The partially premixed flames issuing out of the domestic gas burner ports could be simulated without adopting a turbulence model due to their laminar regime. Since k and ϵ are required to compute the turbulent time scale τ_t, the EBU closure is generally used in association with a turbulence model. Moreover, the numerical simulation does not concern only the flame region, but it regards the whole appliance functioning (i.e. from the gaseous jet issuing by the injector to the flame out of the burner ports). In this work, the EBU combustion model is hence used together with the k-ϵ turbulence model.
However, this combustion model tends to overestimate the reaction rate, especially in highly strained regions, where the ratio ϵ/k is large (flame holder wakes, walls and so on). Moreover, despite its success, the basic form of the EBU model has an obvious limitation: it does not include any effects of chemical kinetics. Therefore some adjustments of the model have been proposed to incorporate chemical features and, in commercial codes, the EBU model is sometimes coupled to the Arrhenius law to limit the mean reaction rate using chemistry features.

2.4.2 Eddy Break Up Model with Combined time scale

Attempts to simultaneously account for mixing and finite chemical reaction rates (turbulent mixing and reactions with similar time-scales) in comprehensive combustion codes are based on variations of the EBU model. The turbulent time scale τ_t used in this model decreases with decreasing distance from solid surfaces. This leads to over prediction of reaction rates in near wall regions. The combined time scale apporach described in [134] alleviates this problem by adding the chemical time scale (τ_c) to the turbulence time scale (τ_t) for the purpose of evaluating the reaction time scale (τ_r). The chemical time is defined as a function of the kinetically controlled reaction rate (as introduced by the Arrhenius reaction presented above in Eq. 2.17), the mass fraction of the reactant and the density:

$$\tau_c = \frac{\rho Y_l}{|R_{i,kin}|} \tag{2.20}$$

Thus the reaction time rate τ_r is given by:

$$\tau_r = \tau_t + \tau_c \tag{2.21}$$

Finally, the consumption rate applied in this investigation is given by:

$$R_i = -\rho \frac{1}{\tau_r} A_{EBU} min \left[Y_F, Y_O \frac{\nu_F M_F}{\nu_O M_O}, B_{EBU} Y_P \frac{\nu_F M_F}{\nu_P M_P} \right] \tag{2.22}$$

The only difference between this equation and Eq. 2.19 is the reaction time scale. The reaction rate predicted using this model is generally less than that for the EBU model. Therefore, sustaining the reaction is more difficult with this model than with the eddy break-up model.

2.4.3 Reaction Mechanism

In this study, for $G20$ combustion the two step reaction mechanism of Westrbrook and Dryer [135], with CO as an intermediate, has been used. This represents one of the most commonly adopted in CFD applications [136]. Of course, all kinetic rates are taken from Westrbrook and Dryer [135].

$$CH_4 + 1.5O_2 \rightarrow CO + 2H_2O \tag{2.23}$$

$$CO + 0.5O_2 \rightarrow CO_2 \tag{2.24}$$

In this mechanism one semi-global scheme for oxidation of the methane has been considered. Moreover, the CO oxidation is represented by one global reaction because the combustion of hydrogen is very fast compared to the CO oxidation. Therefore, the numerical simulation does not consider H_2O formed by H_2 oxidation mechanism as well is known (a scheme of 12 elementary reactions) [137].

2.5 Numerical model

The most widely used general numerical techniques for solution of the equations of fluid motion in CFD codes can be summarized as discretization methods. In these methods, the derivatives in the partial differential equations are approximated by algebraic expressions corresponding to discrete distances in the flow domain. The algebraic expressions can be derived using finite difference approaches (usually based on Taylor's series, polynomial expansions), and finite element approaches (based on calculus of variations, and the method of weighted residuals). Finite difference methods used in turbulent combustion modeling have been reviewed by Ramos [138] and finite element methods have been reviewed by Chung [139]. In a way that is more physically intuitive, the discretization equations can also be derived using the integral form of the conservation equations instead of the differential form. This method of derivation, called the finite volume approach, is also equivalent to a variant of the method of weighted residuals, called the subdomain or control volume formulation [140]. The finite volume approach has become the preferred approach for many computational fluid dynamics applications, including most comprehensive combustion codes, because it is amenable to a variety of grid structures. Therefore, this finite volume method is adopted by the main commercially available CFD codes, such as *Star-CD*, the software used in this work. This code, developed by *CD-Adapco*, is a segregated solver in which the equations of motion are solved directly for velocity and pressure (the 'primitive' variables) with the introduction of an additional equation for pressure by means of the SIMPLE approach [140].
However, aim of the discretization methods is hence to obtain a set of algebraic equations that can be solved to predict the mass, momentum and energy transport at discrete points in the flow domain. This collection of points is referred to as a grid. The grid structure can be as simple as rectangular cells, or as complex as tetrahedral elements constructed in a fashion that follows a curvilinear surface. As the mesh point values are the sole quantities available to the computer, all mathematical operators, such as the partial derivatives of the various quantities, will have to be transformed by the discretization process, into arithmetic operations on the mesh point values [141].

2.5.1 Grid generation

Due to its generality the finite volume model can handle any type of mesh, structured as well as unstructured. Unstructured grids have progressively become the dominating approach to industrial CFD, because of the impossibility to generate automatically block-structured grids on arbitrary geometries [141]. For very complex geometries, the most flexible type of grid is hence the unstructured typology, which can fit an arbitrary solution domain boundary. Therefore, the domestic gas burner space domain has been discretized by subdivision of the continuum into

elements of arbitrary shape and size. Of course, the computational domain needs to be discretized using grid cell that should provide an adequate resolution of the geometrical and expected flow features. Of course grid generation plays a crucial role in the overall CFD process and the importance of grid properties cannot be emphasized enough. In order to reduce design costs and time to market, the grid design has to ensure a suitable global topology of the mesh to help satisfy the specific geometrical variations of each domestic gas burner virtual prototype. An automatic surface meshing strategy is hence adopted to provide for meeting the demands placed on automatic unstructured meshing in industrial settings. The software code in support of the grid generation process used in this work was *pro-AM*, developed by *CD-Adapco*. Moreover, thanks to the native CAD readers, a direct geometry transfer with repaired and closed surface meshing becomes a quick and automated process. Subsequently, the fluid volume of the burner (i.e. the volume occupied by the air-gas mixture and bounded by the wet surface) is extracted with Boolean operations in the CAD code. This operation was done in order to ease the surface and volume mesh generation in Star-CD package and to save time in the process.
Therefore, in order to capture the geometrical details of the appliance domain, a body-fitted approach has been used by *pro-AM*, in which the cells are designed to keep a regular shape. In this approach, the interior of the domain must be built up to satisfy the geometrical constraints imposed by the domain boundaries, thus a trimmed (polyhedral) unstructured mesh has been adopted. The body-fitted meshing capabilities of *pro-AM* offer a wide choice of computational cell shapes, in this analysis the trim methodology is based on hexahedral element (6 faces element) which represent the best choice when the elements are aligned with the main direction of the flow. In the case of domestic gas burner, they applied particularly well considering cylindrical based hexahedral element. To provide further flexibility in generating complex meshes, *pro-AM* accepts hexahedral fluid cell shape plus a variety of degenerate shapes formed by collapsing various cell edges. Therefore the automatic mesh process consists of straight-edged cells of various forms (predominantly hexahedral) that are shaped and joined face-to-face in an arbitrary manner to fill any volume.
Of course, the grid must be fine enough to provide an adequate resolution of the important flow features, as well as geometrical features. This may be achieved by local grid refinement. Unstructured meshes are especially well suited for this purpose because one of the advantages of unstructured grids is the possibility to perform local refinements in a certain region, without affecting the grid point distribution outside that region. This opens the way for flexible grid adaptation by local refinement based on criteria associated either to some flow gradients or to some error estimation (i.e. jet entrainment region, primary air inlet, flame ports, flame zone).
In order to analyze the suitability of the mesh and to give an estimation of the numerical error in the simulation, a grid dependency study has been performed

in the first part of the project [117], in which three significantly different grid resolutions have been used. In that study, it was shown that the grid resolution used was sufficient to obtain almost grid independent solution.
Moreover, there are several different levels of complexity concerning the geometry of a given combustion system, ranging from zero dimensional up to fully three dimensional. The highest level of geometrical complexity involves multi dimensional modeling. However, geometrical simplifications are often used to reduce the computing requirements for simulating combustion systems. Wherever possible, three dimensional cylindrical problems are simulated by angular slices instead of modeling the entire cylinder. In this way, the domestic gas burner can be modeled as a slice of a cylinder by using symmetric boundary conditions. In the context of the numerical simulations performed during this work, two grid typologies have been considered, named hereafter $Mesh\ A$ and $MeshB$.

2.5.1.1 Mesh A

The computational domain of $Mesh\ A$ is sketched in Fig. 2.1, showing that only one quarter of the geometry has been solved. A finer and more regular mesh in critical regions with high flow gradients (i.e. jet shear layer) or regions with significant change in geometry (i.e. flame ports) can be pointed out. Moreover, Fig. 2.2 presents a close up view concerning the numerical domain around the flame ports in which a local grid refinement is applied only in the smaller grooves. Therefore, the computational domain is defined by a quarter of the burner and the grid is composed by 960000 cells.
In addition to grid density, the quality of the mesh depends on various criteria such as the shape of the cells, distances of the cell faces from boundaries or spatial distribution of cell sizes. As a result, the proposed grid avoids highly skewed and warped cells and non orthogonal cells near boundaries. The adopted mesh also ensures that the extension of the computational domain is able to capture relevant flow and geometrical features. The outflow plenum is placed far away from the region of interest and its spherical shape guarantees a good residual convergence [142].

Of course, the same burner crown has been simulated with different working gases, hence different injectors has to be modeled. Therefore, in Fig. 2.3 the numerical grids concerning the nozzle $D-119$ and $E-86$ have been shown to be used in association with $G20$ and $G30$ respectively.

As already mentioned, the value of y^+ at the first node adjacent to the wall has been chosen carefully. For an adequate boundary layer resolution, depending on the Reynolds number, a range between five and ten mesh points has been ensured between the wall and y^+ equal to 20, which likely results in thirty to sixty points inside the boundary layer [143].

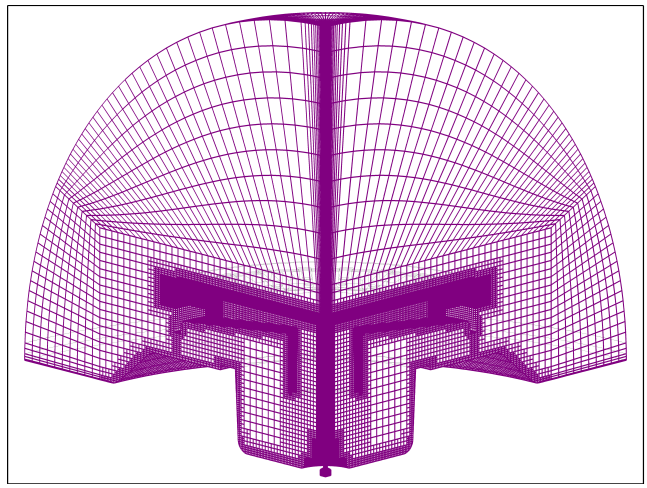

Figure 2.1: Grid of the computational domain.

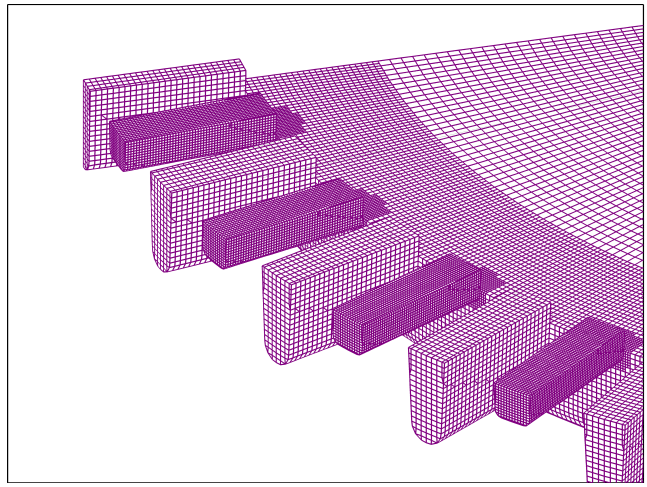

Figure 2.2: Close up view of the flame port region in the computational domain.

2.5.1.2 Mesh B

This computational domain has been used for the numerical simulations adopting the combustion model. Therefore, geometrical simplification have been used to reduce the computing requirements for simulating combustion systems, hence the three dimensional cylindrical problem is simulated by an angular slices of 11.25 degrees instead of modeling the entire cylinder. In this way a main flame port and two half of secondary flame ports have been modeled by using symmetric boundary conditions. This is still a three dimensional problem, but only a 1/32 of the geometry needs to be solved. $MeshB$ present a reduced numerical domain

(a) $D-119$ (b) $E-86$

Figure 2.3: Close up view of the two different injectors grid.

not only in the angular extension, indeed he injector, the bowl and the mixing tube are not modeled and just part of the radial diffuser has been discretized. The final computational domain was composed by 1300000 cells.
The numerical domain is shown in Fig. 2.4. As mentioned above, the finite volume model adopted in this work is characterized by straight-edged hexahedral cells that are shaped and joined face-to-face in an arbitrary manner to fill the domestic gas burner volume.

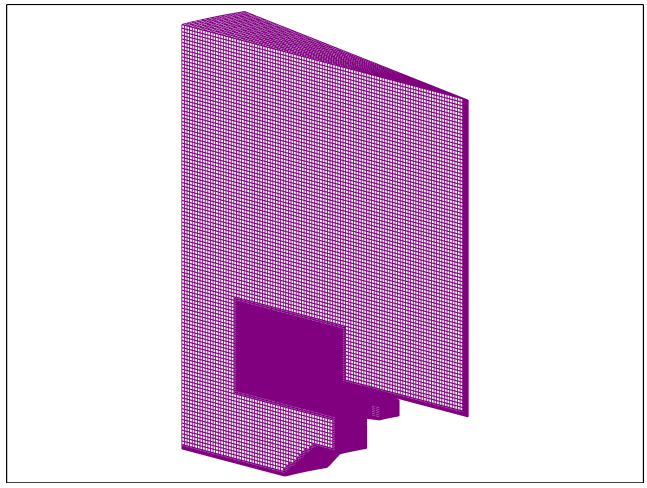

Figure 2.4: Grid of the computational domain.

Fig. 2.5 presents a close up view concerning the numerical domain around the flame ports in which a local grid refinement applied only in the smaller grooves can be pointed out. In this figure the domain inlet is also shown, represented by part of the radial diffuser upstream to the flame ports.

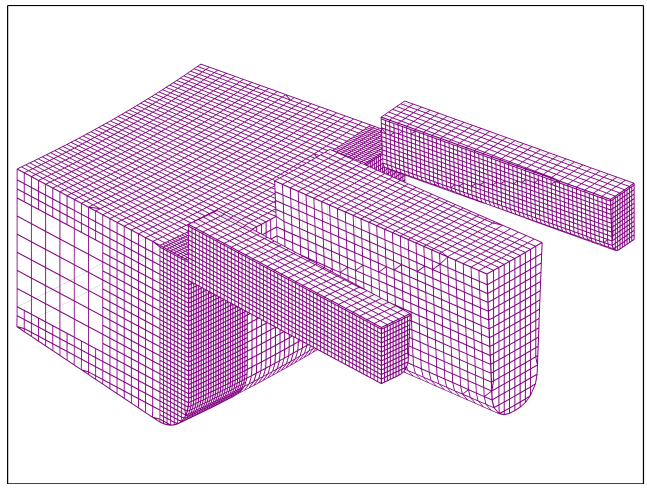

Figure 2.5: Close up view of the flame port region and numerical inlet in the computational domain.

2.5.2 Finite volume models

The numerical simulations performed on the domestic gas burner have been adopted a finite volume model in which the flow was assumed to be an axisymmetric steady compressible flow. The manner in which the convective and diffusive fluxes are expressed is one of the key factors determining accuracy and stability, for steady-state simulation concerning the domestic gas burner. A preliminary sensitivity analysis performed in the first part of this work involved a validation of the different numerical discretization schemes available in *Star-CD* by means of experimental measurements [117]. This investigation pointed out a better numerical prediction achieved by the low (first)-order scheme named Upwind Differencing (UD). The UD scheme produced solutions which obeyed the expected physical bounds without give rise to an appreciable smearing of gradients (numerical diffusion). However, in the present work these simulations can be divided in two main categories, hereafter named $Model\ A$ and $Model\ B$. Default initial conditions implemented in the code have been used for each model.

2.5.2.1 Model A

This finite volume model has been used in association with the grid typology $Mesh\ A$. This model does not take into account the combustion modelization. Indeed, when CFD codes first became commercially available, the chemistry sub models were very primitive and greatly increased the computation time, often beyond the capability of the available hardware. Therefore, a common approach to simulating combustion problems was to model them as non reacting flows. This has sometimes been referred to as “cold flow” modeling, which is really a

misnomer as the flame was often simulated as a flow input of hot inert gases to the combustor [144]. Nonreacting flow modeling may grossly oversimplify a problem, but it can give considerable insight into the flow patterns inside the domestic gas burner. In addition, most of the experimental measurements were provided in cold conditions in order to validate the internal flow dynamic. Moreover, the combustion model was not implemented for these numerical simulations also to provide the efficiency of the numerical model for flame instability prediction in cold condition.
For the study of the numerical convergence, the maximum of absolute global residual was set to 10^{-6} to obtain full convergence on the residuals.

2.5.2.2 Model B

Model B has been used in association with the grid typology *Mesh B* and the EBU combustion model. The reaction model is applied only once a convergent simulation in "cold condition" has been achieved. Subsequently, starting from the solved flow field without combustion, the reaction mechanisms are activated and the reactant can numerically burn. The numerical trick to burn the reactive mixture is represented by identifying an ignition region inside the numerical domain, in which specify the proportion of the leading reactant burnt, the ignition temperature and the duration of the ignition process. Of course, the combustion has to be a steady and self sustained process. The ignition is required just to "light up" the flame in the model. Nevertheless, the selection of the ignition region represents a non trivial step in the model setup because a wrong selection of this zone can lead to a quenching of the flame. For this reason, in the domestic gas burner numerical the selection of the ignition zone has to be determined based on the real physical behavior of the flame. Therefore, two ignition regions have been selected, each one located in front of the pilot flames (i.e. small flame ports), on the bottom of the cap. In these zones, the post processing of the flow field pointed out recirculation regions that can help the conservation of the combustion process and the feeding of the unburnt fresh mixture to the reaction zone.
For the study of the numerical convergence, the maximum of absolute global residual was set to 10^{-5} to obtain full convergence on the residuals.

2.6 Boundary conditions

In the computational procedure the flow was assumed to be an axisymmetric steady compressible flow. The model took advantage of the symmetry of the geometry by imposing symmetry boundary conditions on the sides (gradients perpendicular to the plane are zero).

2.6.1 Inlet

Regarding the finite volume model *Model A*, at the inlet boundary condition, a pressure condition was specified in order to simulate the same experimental inlet pressure and verify the mass flow rate through the injector with the available experimental data. Moreover, in order to obtain an accurate simulation, the specification of the turbulence properties (turbulence intensity and length scale) at the inlet of the computational domain required a proper tuning of the model [117] because there were no experimental data available. The turbulence intensity level, defined by the ratio of the fluctuating component of the velocity to the mean velocity, was imposed at 5% [143]. For internal flows a constant value of turbulent length scale, as an equivalent parameter for the dissipation ϵ, should be derived from a characteristic geometrical feature [143], hence a turbulence length equal to 30% of the nozzle hydraulic diameter has been adopted.
Concerning *Model B*, a velocity condition was specified in order to simulate a defined inlet mass flow rate and mixture composition.

2.6.2 Outlet

At the outlet, an open boundary condition (pressure) was imposed, moreover zero temperature and turbulence gradients were prescribed.

2.6.3 Solid walls

The boundary conditions imposed on the solid walls are consistent with both the physical and numerical model (i.e. adiabatic walls or imposed temperature). Therefore, to provide data for determining the temperature distribution along the different components of the domestic gas appliance, an experimental investigation has been carried out on a real cooking top.
The temperature mapping of the gas hob was performed by means of thermocouples type k [145] for different configurations in order to measure the temperatures during the working condition with working fluid $G20$ and $G30$ [146]. Each test is performed by changing the inlet pressure (i.e. the heat power) of the appliance every 35 minutes: starting from the nominal pressure of the working gas, then the maximum and the minimum at the end. The cooktop geometry was analyzed for three geometrical configurations:

- without grid and pot (ideal configuration);
- with grid only;
- with grid and pot (filled with cold water).

These temperature measurements have required a preliminary modification regarding the burner and the hob in order to insert the thermocouples. Their locations inside the burner and the hob are illustrated in Fig. 2.6.

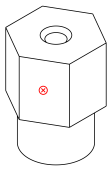

(a) Injector wall

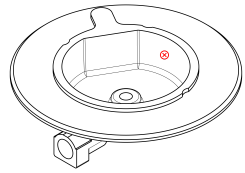

(b) Bowl wall

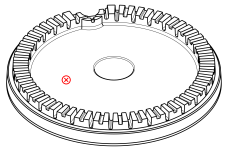

(c) Crown wall

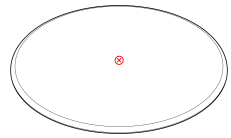

(d) Cap wall

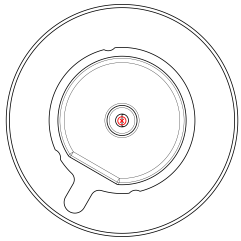

(e) Inlet gas

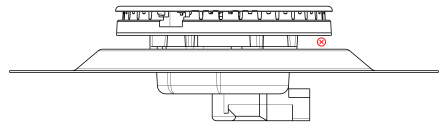

(f) Primary air

Figure 2.6: Sketch of the thermocouple locations on the domestic appliance components (the cross sign points out the exact position).

However, the thermocouples have been placed in the following locations around the appliance in the following locations: injector wall, bowl wall, crown wall and cap wall. Moreover, additional thermocouples have been located at the inlet gas (directly in the gas stream before the injector) and primary air entrance (the air temperature under the crown should be subjected directly to the air entrained by the gas jet and only indirectly by the flame radiation because of the thermocouple is placed under the crown and hence covered by the flame).
The data are presented in normalized form by dividing for the same maximum temperature (T_{max}) acquired during the experiments. This analysis hence allows to gain a better understanding of the heat transfer distribution on the domestic gas burner. By considering Fig. 2.7, the experimental temperatures on the domestic gas burner crown have been plotted in function of time by varying the gas inlet pressure; these data are shown for the different configurations, adopting $G20$ as working fluid. The temperatures present the same trends for the ideal configuration and that one with the grid: the minimum pressure causes the minimum flame height and hence an increase of heat conducted through the cap and the burner body. The presence of the pot, or even better, the water inside the pot, acts as a sink of heat and causes a decrease in the temperature gradients observed when the inlet pressure is changed.

As depicted by Fig. 2.8, the same temperature trend for the working gas $G30$ can be pointed out. However, the butane presents higher temperatures than the $G20$ experiments; e.g. the crown is characterized by an increase of $35K$, $65K$ and $55K$ for the ideal, with grid and with pot configuration, respectively.

The plots presented in this section show the importance and the key role of the thermal convection, conduction and radiation on the domestic appliance. The simplicity of these end results does rise the question of considering this thermal behavior also in the numerical simulation. In order to consider this kind of phenomenon the numerical model should be thus improved. This necessary future work is being programmed to include the solid part in the virtual prototype (i.e. to take into account the heat transfer between the fluid and solid) and the radiation effect too. By implementing the solid part on the numerical model also means to avoid the boundary condition on the walls. This step on the setup of the model can represent a difficult task to accomplish especially when the designer has to simulate a brand new geometry, for which just the virtual prototype has been generated and the real temperature distributions are unknown.

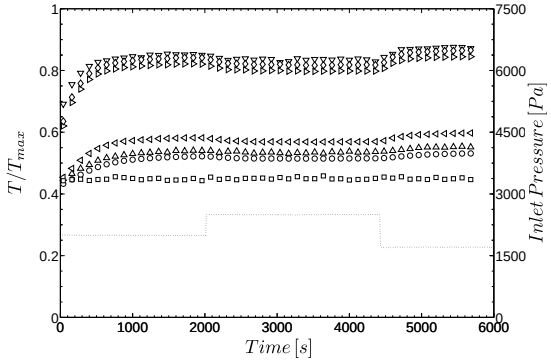

(a) Without grid

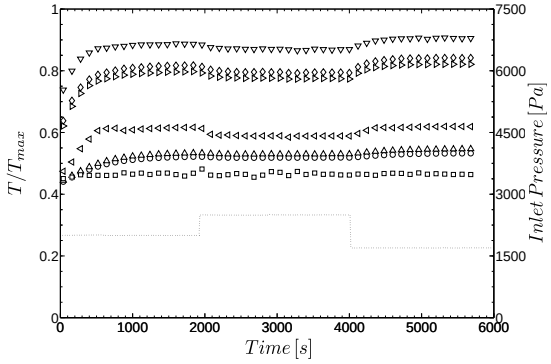

(b) Without pot

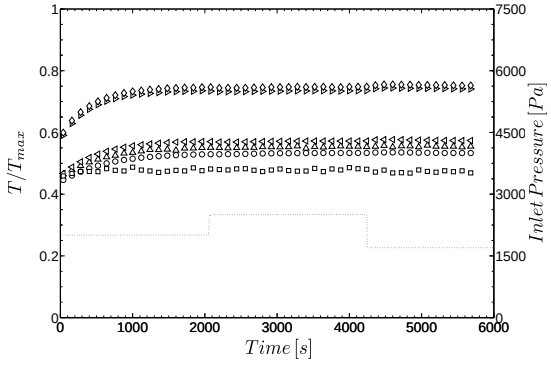

(c) With pot

Figure 2.7: Experimental temperatures on the domestic gas burner crown: injector wall (triangle up), bowl wall (triangle left), crown wall (triangle right), cap wall (triangle down), $G20$ inlet gas (circle), primary air (square) and inlet pressure (dotted line).

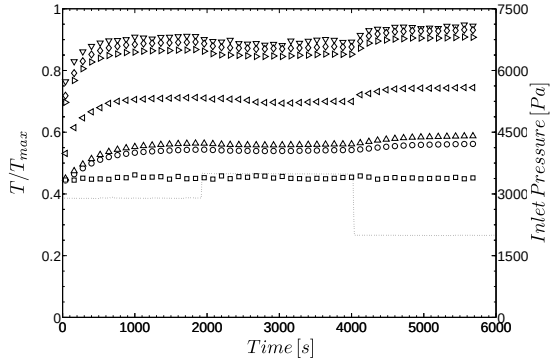

(a) Without grid

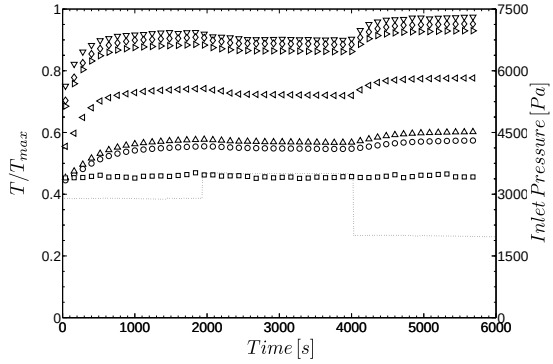

(b) Without pot

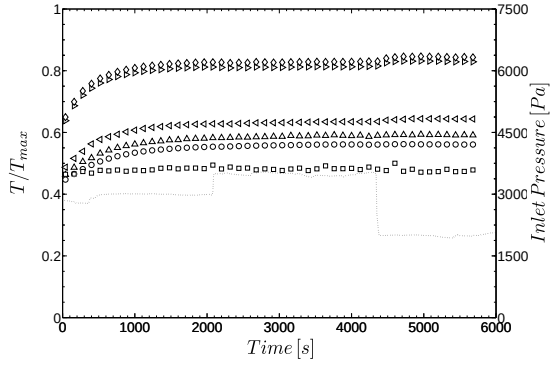

(c) With pot

Figure 2.8: Experimental temperatures on the domestic gas burner crown: injector wall (triangle up), bowl wall (triangle left), crown wall (triangle right), cap wall (triangle down), $G30$ inlet gas (circle) and primary air (square) and inlet pressure (dotted line).

Chapter 3

Internal Fluid Dynamics

Chapter Purpose:
This chapter describes an experimental and numerical investigation regarding the internal fluid dynamics of the domestic gas burner. Different measurements were acquired in order to gain an insight into the thermo flow processes of the appliance.

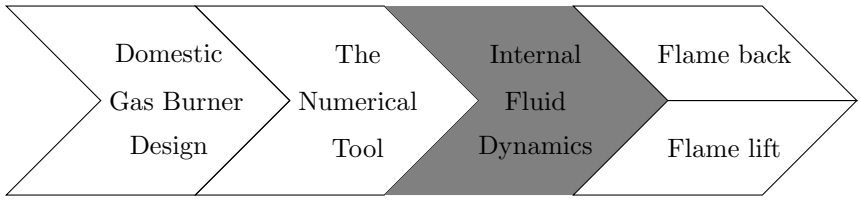

3.1 Introduction

In discussing CFD analyses, errors and uncertainties it is useful to make some clear distinctions between the meaning of the terms validation, verification and calibration. The definitions used in this work follow closely the definitions given in [147, 148].

- Verification is the procedure to ensure that the program solves the equation correctly.
- Validation is the procedure to test the extent to which the model accurately represents reality.
- Calibration is the process of adjusting the values of the coefficients of a particular numerical model to provide better agreement with the experimental data.

Therefore, a validation of the code is performed on some features of the domestic gas burner internal flow field. Of course, in most combustion simulations, simplifying assumptions must be made to get effective solutions in the time available for a given problem. The main actual simplification of this investigation is the exclusion of the chemical reactions, thus the combustion process is not modeled. Therefore, the numerical simulation was performed with the virtual prototype *Model A* presented in § 2.5.2.1. The numerical analysis is presented in association with experimental measurements performed to support the numerical prediction. Obviously, this experimental investigation was required due to the complex flow field of the domestic appliance and the lack of relevant available data in literature.

3.2 Gas flow rate

The gas flow rates $\dot{V}$ through the two injectors $D-119$ and $E-86$ predicted by the model were compared to the flow measurement as reported in Tables 3.1 and 3.2 respectively. The prediction of the volume gas flow rate was provided for different inlet pressures and temperatures. The relative error was verified to be always less than 5%.
Considering the mass flow through the injector, as the inlet pressure is increased, the flow velocity in the throat increases, hence the mass flow increases. Therefore, over the range of pressure covered, the volume flow rate through the injector is linearly correlated to the upstream gas pressure, as plotted in Tables 3.1 and 3.2. This linear behavior can be useful for further data interpolation.

Working Fluid	Pressure	Temperature	Exp. $\dot{V}$	Predicted $\dot{V}$	Error
-	(Pa)	(K)	(l/h)	(l/h)	-
Air	1700	288	213	209	-2%
Air	2000	288	229	228	0%
Air	2500	288	250	255	2%
$G20$	1700	288	278	276	-1%
$G20$	2000	288	300	301	0%
$G20$	2500	288	331	338	2%
$G20$	2000	353	340	348	-2%

Table 3.1: Validation of the mass flow rate by means of the $D-119$ injector model.

Working Fluid	Pressure	Temperature	Exp. $\dot{V}$	Predicted $\dot{V}$	Error
-	(Pa)	(K)	(l/h)	(l/h)	-
Air	2000	288	98	97	-1%
Air	2900	288	118	119	0%
Air	4500	288	145	149	3%
$G30$	2000	288	70	72	3%
$G30$	2900	288	83	87	4%
$G30$	4500	288	101	106	5%

Table 3.2: Validation of the mass flow rate by means of the $E-86$ injector model.

Of course, in order to establish a flow through any duct, the exit pressure must be lower than the inlet pressure. The inlet pressure imposed upstream of the gas burner injector therefore represents a small pressure difference between the inlet and the outlet section and will cause a small fuel wind to blow through the duct at low subsonic speed. The local Mach number will increase slightly through

the convergent portion of the nozzle, reaching its maximum at the throat. This maximum will not be sonic, indeed it will be a low subsonic value, lower than 0.582 times the inlet pressure that represents the threshold for a sonic condition [149]. Consequently, downstream of the throat, the subsonic flow encounters a diverging duct and thus the Mach number decreases.

For these kinds of flows through a convergent-divergent nozzle, such as the $D-119$ or $E-86$, there are infinite numbers of isoentropic solutions, where the pressure and area ratios between the injector outlet and inlet, represent the controlling factors for the local flow properties at any given section. This is in direct contrast with the supersonic case where only one isoentropic solution exists (i.e. choked flow) for a given duct, and the section area ratio becomes the only controlling factor for the local flow properties.

3.3 Pressure recovery

The static pressure along the lower side of the cap was computed at different radii to quantify the pressure recovery in the expansion chamber. As shown in Tab. 3.3, this investigation was performed by imposing reference and limit test pressures at the injector. Both the $D-119$ and $E-86$ injectors were adopted in order to simulate the different jet issuing from a different injector shape.

		Reference			Limit
Test gas	Injector	(Pa)	(Pa)	(Pa)	(Pa)
Air	$D-119$	1700	2000	2500	5000
Air	$E-86$	2000	2900	3500	5000

Table 3.3: Matrix of experiments concerning the pressure recovery along the radial diffuser.

For this investigation, the adopted working fluid was air in order to avoid the discharge of reactive gases in the surrounding ambient during the associated experimental analysis. Obviously, these measurements were acquired in cold conditions. The static pressure was calculated by the numerical code in four locations placed at different radii along the radial diffuser: $x/R = 0$, $x/R = 0.2$, $x/R = 0.4$ and $x/R = 0.7$ (R represents the burner crown radius), as depicted in Fig. 3.1. The experimental measurements at different radii were obtained by using four different burner caps, presenting a single hole at different radii.

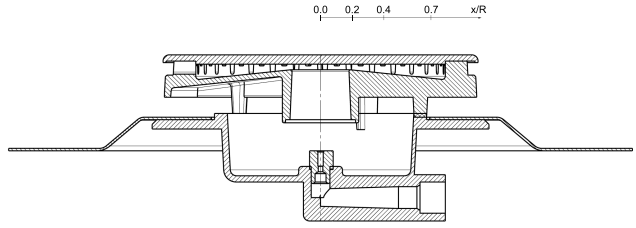

Figure 3.1: Domestic gas burner sections relative to the pressure acquisition positions: the burner cap presents a single hole located at different radii for each figure.

The static pressure in the expansion chamber calculated by the CFD model is in very good agreement with the experimental results as shown in Fig. 3.2 and Fig. 3.3 for the $D-119$ and $E-86$ injectors respectively. The data presented in the plot are normalized by adopting a common reference pressure value (P_{ref}). In the impinging jet region, the jet turns in the radial direction, therefore a conversion of the axial momentum is achieved due to the deceleration of the axial mean

velocity towards the impingement plate (i.e. the burner cap). This momentum is converted to that of the static pressure (p_s), where the term static pressure is used to describe the pressure exerted by a static, or still, mixture mass. Therefore, as shown in Fig. 3.2 and Fig. 3.3, at the impinging point ($x/R = 0$) the axial velocity is zero, thus the total pressure coincides with the static pressure that reaches its maximum value. However, the pressure distribution on the impingement surface is independent of the inlet pressure except in the case of the subatmospheric region, where it becomes stronger and shifts further away from the stagnation point as the inlet pressure is increased [150]. Subsequently, the static pressure decreases in the region of high-speed flow and increases in the region of low-speed flow. Therefore at the throat ($x/R = 0.2$), the minimum static pressure is achieved since the flow speed is the highest. On the other hand, along the diffuser the section surface increases, therefore according to the continuity equation the velocity must decrease, leading to a rise in static pressure. In order to overcome the resistance of the flow within the burner and at the flame ports, the static pressure must increase. Consequently, it is possible to point out a slight increase in the static pressure, of the order of some Pascal, after the radial coordinate $x/R = 0.4$.
Note that all the cases sketched in Fig. 3.2 and Fig. 3.3 are originated by subsonic flows at the gas burner injector. As expected, the local values at different inlet pressures collapse in the same location, indicating the subsonic nature of the flow through the injector and the same proportional relationship with the mass flow rate. This result is particularly important and useful because it can be adopted during the design process of the appliance to verify the pressure recovery, at inlet pressure values different from the reference ones.

The pressure prediction concerning the stagnation region always presents the worst agreement with the experimental data. A variety of turbulence models were employed to solve RANS equations for the axisymmetric impinging jet. Among them was the standard k-ϵ turbulence model, which has been shown to be inaccurate in calculating flow field and heat transfer characteristics, especially as it overpredicts to a great extent the turbulent viscosity and Nusselt number in the stagnation region. Moreover, the predictions obtained through the k-ϵ model resulted in far too high turbulence levels near the stagnation point [151]. There have been speculations as to the cause of the overpredictions of the turbulent kinetic energy and heat transfer rate in the stagnation region computed by the turbulence models; the isotropic eddy viscosity assumption is thought to be the chief cause of overprediction: namely this assumption has no ability to effectively capture the important effects of turbulence anisotropy in convective heat transfer applications involving flow impingement and separation [152]. Boussinesq's eddy viscosity concept implies that turbulence is isotropic, but in the stagnation region the flow is anisotropic, which cannot be accounted for by the numerical model. The anisotropy increases as the impingement plate is approached [153]. As a result, the overestimation of the turbulent kinetic energy leads to a large eddy

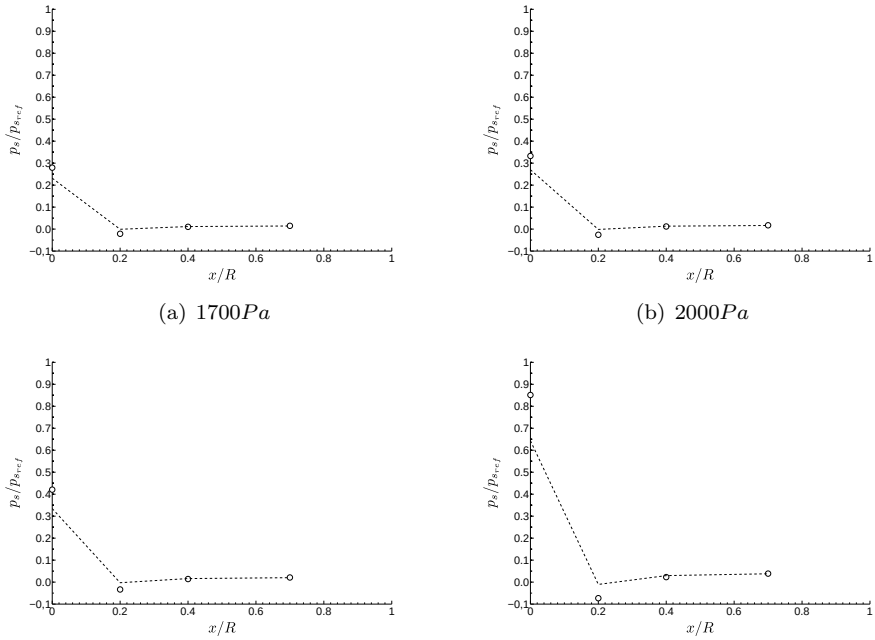

(a) $1700Pa$ (b) $2000Pa$

(c) $2500Pa$ (d) $5000Pa$

Figure 3.2: Validation of the static pressure distribution along the expansion chamber for different inlet pressures in the $D-119$ injector (normalized values). Dashed lines: CFD simulation.

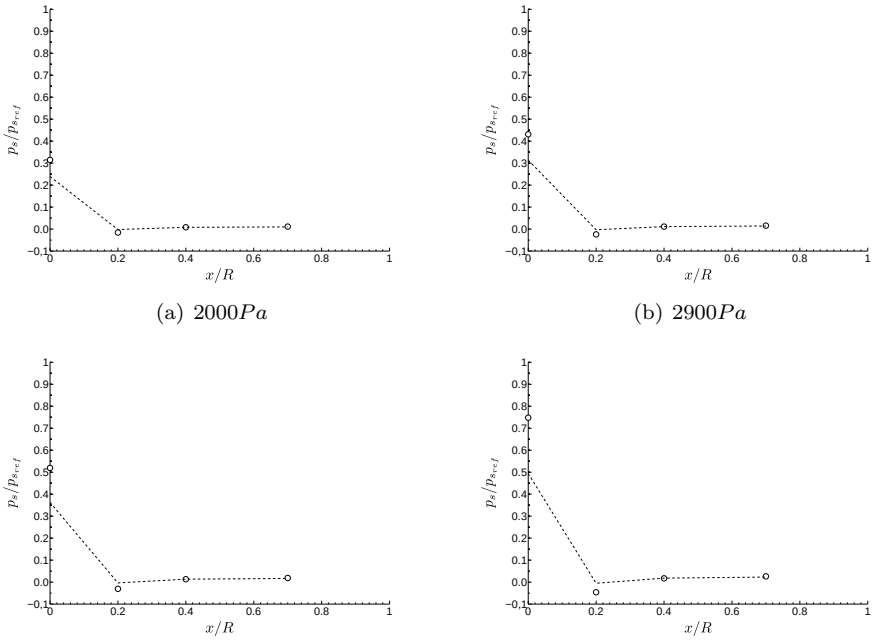

(a) $2000Pa$ (b) $2900Pa$

(c) $3500Pa$ (d) $5000Pa$

Figure 3.3: Validation of the static pressure distribution along the expansion chamber for different inlet pressures in the $E-86$ injector (normalized values). Dashed lines: CFD simulation.

viscosity in that region; this increases the mixing effects [154]. Therefore, the turbulent kinetic energy is grossly overpredicted on the jet axis, which implies the prediction of an excessive entrainment of the freestream fluid. The extra entrainment leads to underprediction of the peak radial velocities [153], which results in the underprediction of the static pressure at the stagnation point.

3.4 Flow field

An analysis of the flow out of the flame port in cold conditions was performed by means of velocity profiles out of the primary and secondary flame ports. Figure 3.4 shows the normalized radial velocity profiles at x/R = 1.06 for a domestic gas burner equipped with a $D - 119$ nozzle supplied with air at minimum, nominal and maximum inlet pressure. The normalization procedure was performed by means of the same radial velocity which represents the maximum value in the whole flow field. Moreover, the vertical coordinate was normalized by the burner flame port width. The plot points out the good agreement between the numerical prediction and the experimental result, not only in trend, but also in absolute values, always within the tolerance range indicated be the root mean square. The experimental analysis was outsourced to an external institute [32].

In order to acquire a better understanding of these data, Fig. 3.5 sums up the validation of the velocity profiles by plotting just the maximum velocity.

In the same way, Fig. 3.6 presents the radial velocity profiles at x/R = 1.06 for the same burner equipped with a $D-119$ nozzle supplied with the N_2He mixture at the same inlet pressures. The agreement between numerical and experimental values highlighted a good trend both for flame port type 1 and flame port type 2. On the other hand, as in the case of the air velocity profile validation, the primary flame port is overestimated by the numerical model, whereas the secondary flame port is underestimated. This unbalance in the prediction of the numerical velocity profiles is underlined in the N_2He simulations.

Fig. 3.7 summarizes the global agreement between PIV and numerical maximum velocity for the three different inlet pressures. By comparing Fig. 3.7 and Fig. 3.5, it is possible to highlight that for the same pressure settings, the jet out of the flame ports presents a higher velocity profile for the N_2He mix than for air. This confirms that a lighter jet (i.e. a jet generated by a gas with density lower than the surrounding air density) entrains more air than an iso-density jet (i.e. a jet generated by a gas the density of which is equal to the surrounding air density) [16].

The numerical setup relative to these two working fluids (air and the N_2He mixture) presents the same settings, the only difference being the viscosity model, since for the N_2He mixture the viscosity is kept constant. However, the sensitivity analysis performed in [155] showed that there is no relevant difference between the velocity profiles when varying the viscosity model. Nevertheless, the only parameters really imposed by the user in these simulations, are the turbulence parameters at the inlet boundary. The tuning of these turbulence parameters could help to obtain a better prediction of the velocity profile of the N_2He mixture, but it would be confined only for the use of the N_2He mixture as working fluid. Therefore, the tuning of these parameters cannot be yet performed for butane or methane (even for their limit gases) because of the lack of experimental

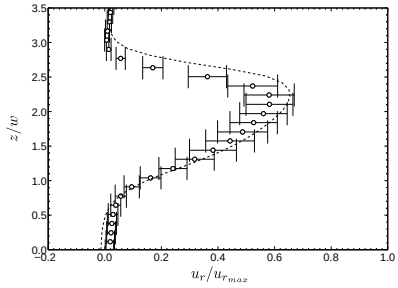

(a) Flame port type 1 (1700Pa)

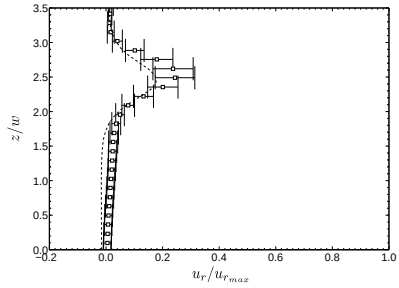

(b) Flame port type 2 (1700Pa)

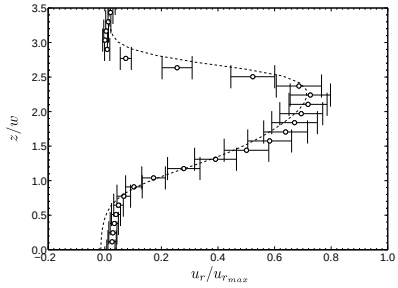

(c) Flame port type 1 (2000Pa)

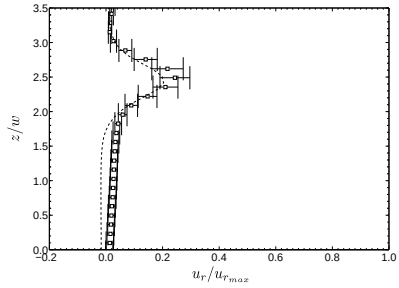

(d) Flame port type 2 (2000Pa)

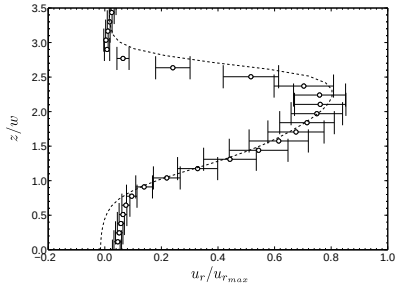

(e) Flame port type 1 (2500Pa)

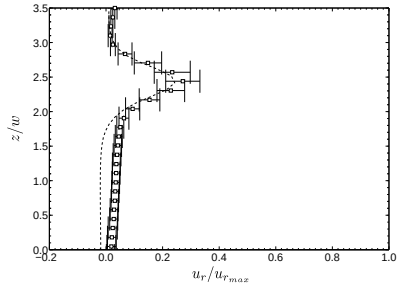

(f) Flame port type 2 (2500Pa)

Figure 3.4: Validation of the velocity profiles at x/R = 1.06 with $D - 119$ nozzle supplied with air at minimum (1700Pa, top), nominal (2000Pa, center) and maximum inlet pressure (2500Pa, bottom)[32]. Dashed lines: CFD simulation.

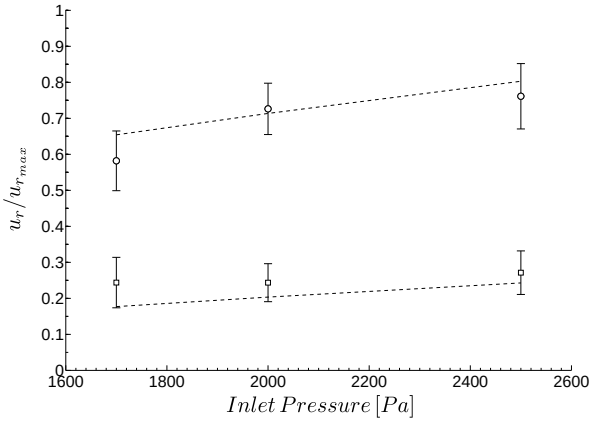

Figure 3.5: Agreement between PIV and numerical maximum velocity with air as working fluid. Markers: PIV experiments for flame port type 1 (circle) and type 2 (square)[32]. Dashed lines: CFD simulation.

fluid dynamic data for them. Gas chromatography, LDA velocity profiles in hot conditions, Laser Induced Fluorescence (LIF) or other experimental techniques applied to gas burners in association with their real working gases, are the answer for a better prediction demand.

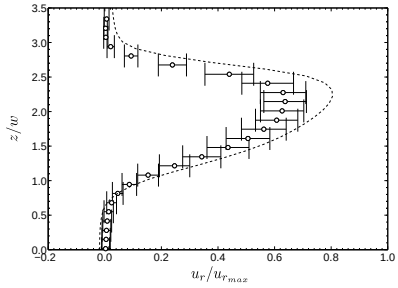

(a) Flame port type 1 (1700Pa)

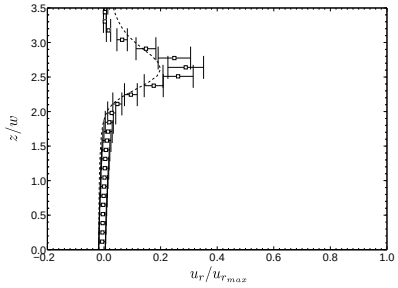

(b) Flame port type 2 (1700Pa)

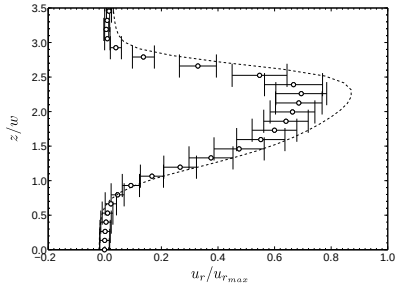

(c) Flame port type 1 (2000Pa)

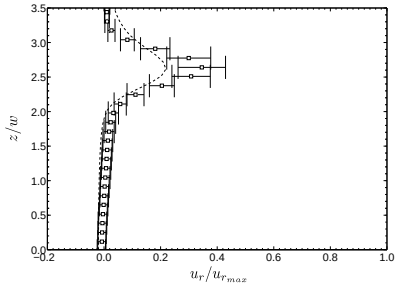

(d) Flame port type 2 (2000Pa)

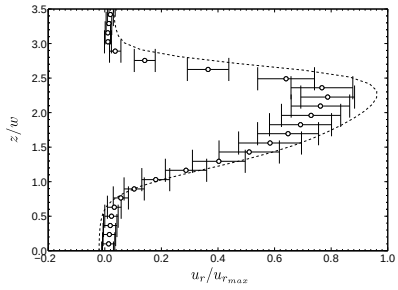

(e) Flame port type 1 (2500Pa)

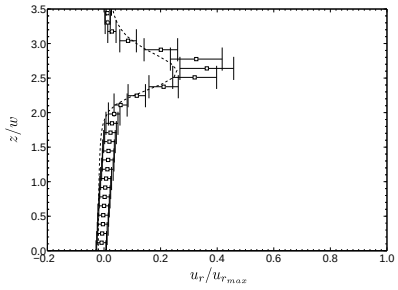

(f) Flame port type 2 (2500Pa)

Figure 3.6: Validation of the velocity profiles at x/R = 1.06with $D-119$ nozzle supplied with N_2He mixture at minimum (1700Pa, top), nominal (2000Pa, center) and maximum inlet pressure (2500Pa, bottom)[32]. Dashed lines: CFD simulation.

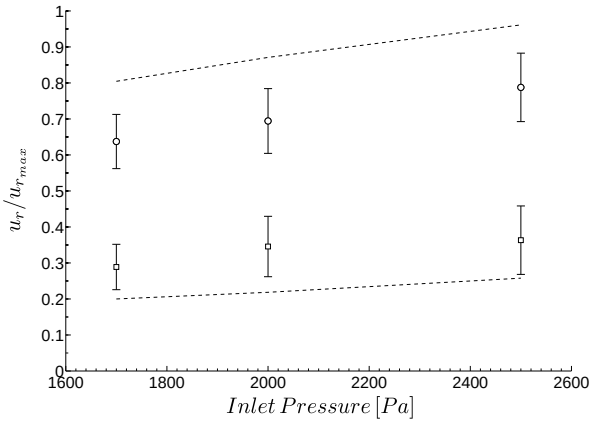

Figure 3.7: Agreement between PIV and numerical maximum velocity, with the N_2He mixture as working fluid. Markers: PIV experiments for flame port type 1 (circle) and type 2 (square)[32]. Dashed lines: CFD simulation.

Chapter 4

Flame back

Chapter Purpose:
This chapter reports a flame stability criterion for the flame back instability. The cooking appliance is investigated by means of a design of experiments analysis.

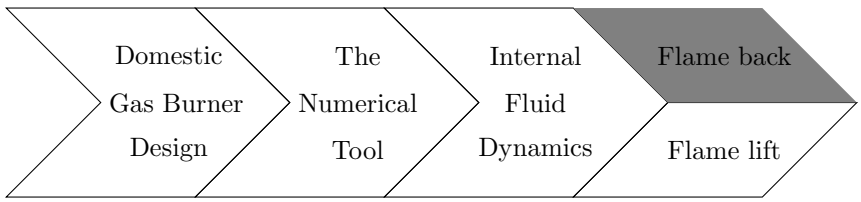

4.1 Introduction

In order to minimize the danger or occurrence of flashback, some burners are empirically designed for specific fuel/oxidant gas combinations. However, the lack of applicable theory or empirical characterization has made proper design difficult, especially because of the flexibility that the domestic appliance has to ensure for local country gas distribution restrictions (different composition of gases and supply pressures) and within reasonable costs. Therefore, the stabilization mechanisms of the domestic gas burner flames relative to the flame back instability are investigated by using previous experimental measurements performed during the development phase of the cylinder gas burner crown (see § 1.6). This data set was numerically replicated in order to use the flame back experimental results in association with the numerical prediction of the domestic appliance internal flow field. The numerical simulation was carried out by adopting $Model\ A$ as finite volume model. Of course, the unstructured grids developed for the different domestic gas burner prototypes, present the same creation strategy as $Mesh\ A$. In order to replicate as much as possible the European standard [3] conditions for the flash back instability, the adopted working fluid was $G30$, with a $E-86$injector at a nominal pressure of $2900Pa$. Moreover, the numerical model used the $G30$ fuel gas instead of its $G231$ or $G32$ limit gases. The CFD code is actually able to simulate these limit gases, but there is a lack of experimental data in literature concerning their laminar burning velocity. The goal of this correlation is to describe the dynamic balance reported in § 1.3 by comparing the laminar burning velocity and the unburned mixture velocity. Finally, a prediction criterion for the flame back instability based on the velocity dynamic balance is presented.

4.2 Laminar Burning Velocity for Butane

The burning velocity can be represented by the volume of the air/fuel mixture, at its own temperature and pressure, consumed in unit time by unit area of flame front. It is independent of flame geometry, burner size and flow rate. Therefore, the burning velocity is essentially a measure of the overall reaction rate in the flame and it is important both in the stabilization mechanism and in determining rates of heat release. The laminar burning velocity of a flame is affected by flame radiation and hence by flame temperature, by local mixture properties such as viscosity, thermal conductivity and diffusion coefficient, and by imposed variables of pressure, temperature, air/fuel ratio and heat of reaction of mole of mixture [156].

As discussed in the context of Tab. 1.1, the main working fluids of a domestic gas burner are $G20$ and $G30$. Although $G20$ is a pure methane gas, $G30$ is a mixture of $iso-$ and $n-$ butane gas. Of course the investigations present in literature, concerning the laminar burning velocity, mainly refer to common gases and not their mixtures. Therefore, $G30$ is assumed to be characterized by the laminar burning velocity of the $n-$ butane, hereafter simply referred to as butane.

The experimental data set for butane is provided by Warnatz [157]. As shown in Fig. 4.1, these measurements are only available for a narrow range of volume gas concentrations (C_{vol}), mainly around the stoichiometric concentration. Unluckily, the domestic gas burner application adopts a very rich mixture at the flame ports, therefore the laminar burning velocity close to the flame ports must be totally extrapolated from the experimental data. The interpolation and extrapolation curves adopted in this analysis are presented in Fig. 4.1.

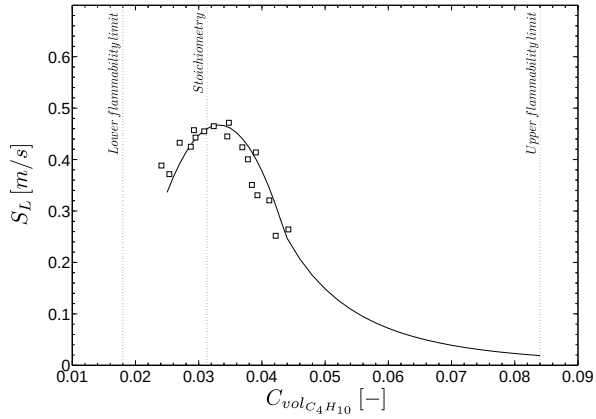

Figure 4.1: Butane laminar burning velocity: experimental points by Warnatz [157] (square marks), interpolation curve (solid line), extrapolation curve (dashed line).

The interpolation curve adopted in this analysis is the following second order polynomial curve:

$$S_L = f(C_{vol}) = a_1 \cdot C_{vol}^2 + a_2 \cdot C_{vol} + a_3 \tag{4.1}$$

where C_{vol} is the volume gas concentration and the polynomial coefficients have the following values: a_1 = -1444, a_2 = 91.27 and a_3 = -0.9873.
On the other hand, the extrapolation curve is the power curve defined by the following formulation:

$$S_L = f(C_{vol}) = b_1 \cdot C_{vol}^{b_2} \tag{4.2}$$

where C_{vol} is the volume gas concentration and the polynomial coefficients have the following values: b_1 =0.000001 and b_2 = -3.975. This extrapolation curve was generated in order to have a laminar flame speed slightly superior to zero at the upper flammability limit and to be continuous with the interpolated experimental data. Practically all experimental studies of flammability limits suggest that the laminar burning velocity at the flammability limit is not zero, but it is on the order of a few cm/s [158].
Moreover, it is generally acceptable to assume that a mixture with maximum flame temperature is also a mixture with maximum flame speed. The initial temperature effect on the laminar burning velocity indicates that the flame speed increases with preheating for all hydrocarbon/air mixtures. For a premixed laminar flame, the initial temperature effect on the laminar burning velocity can be taken into account following the relationship [159]:

$$S_{L_{T_1}} = S_{L_{T_0}} \cdot \left(\frac{T_1}{T_0}\right)^{1.74} \tag{4.3}$$

where T_1 is the target temperature, T_0 is the reference temperature, $S_{L_{T_1}}$ is the flame speed at the temperature T_1 and $S_{L_{T_0}}$ is the flame speed at the reference temperature T_0.

By applying Eq. 4.3 to the laminar burning velocity curve, it is possible to point out the relevant increase of this velocity for the gas burner nominal working condition, as shown in Fig. 4.2. Note that a temperature of $573K$ around the domestic gas burner flame ports was considered (see § 2.6.3).

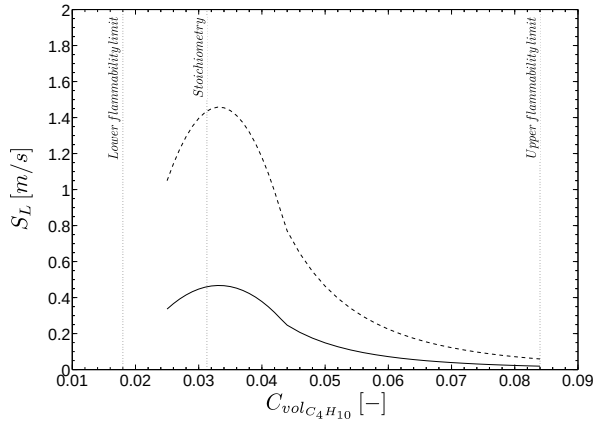

Figure 4.2: Butane laminar burning velocity at $298K$ (solid line) and $573K$ (dashed line).

4.3 Flame back correlations

As a result of the DoE numerical analysis, a dynamic flame stability criterion is presented in order to highlight the flame instabilities by comparing the laminar burning velocity with the unburnt mixture velocity at the flame port exits. The flame back experimental data is intrinsically more difficult to quantify than the flame lift because this phenomenon can only be identified experimentally in a qualitative way, and it remains mainly at the discretion of the operator who carries out the measurements. The experimental data for flame back reports in percentages, the number of times the phenomenon was observed when tested in all the configurations (3 repetitions). As mentioned in § 1.3, the flame back phenomenon can be characterized by the velocity through the type 2 flame ports. Indeed high burning velocity flames (i.e. butane flames) are particularly prone to lightback and high gas velocities are necessary to maintain stable flames. Such high gas velocities create a turbulent flow unless very small or very well designed flame ports are adopted. The CFD/experimental comparison gives us a range of averaged velocities at the small flame ports correlated with the quantification of the flame back phenomenon, as depicted in Fig. 4.3.

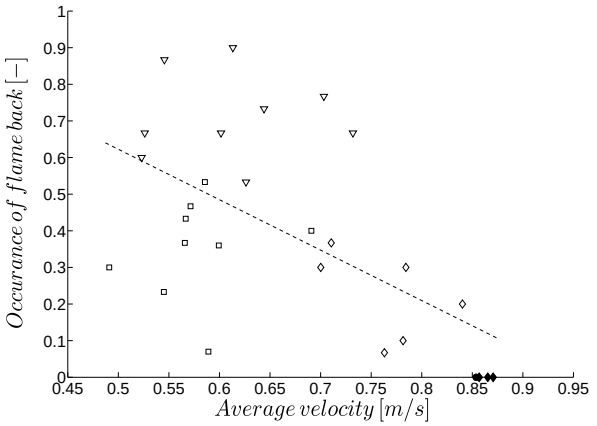

Figure 4.3: Experimental occurrence of flame back against the averaged velocity at type 2 flame ports for different prototype families: L9-2 (triangle), L9-3 (square), L9-4 (diamond) and the definitive crown burner (circle). The closed symbols represent the burners not affected by the flame back instability.

The dispersion of the data provides information regarding the applicability of the correlation by means of a dynamic stability criterion, in order to predict the flame back phenomenon.

From the numerical simulations, Fig. 4.4 depicts the velocity magnitude through groove type 2 for each burner model, plotted versus the volume gas concentration. In this figure, it is possible to highlight an isolated group, which do not present flame back according to the experimental measurements.

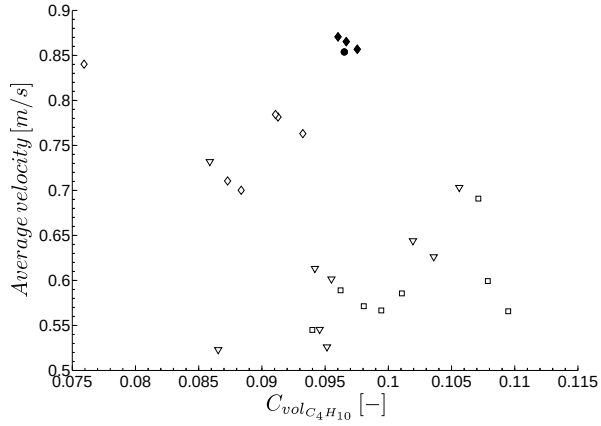

Figure 4.4: Numerical correlation for C_4H_{10} in hot conditions between the volume gas concentration and the averaged velocity at type 2 flame ports for different prototype families: L9-2 (triangle), L9-3 (square), L9-4 (diamond) and the definitive crown burner (circle). The closed symbols represent the burners not affected by the flame back instability.

Furthermore, to establish design rules to prevent this kind of phenomenon, it can be useful to plot this diagram by using dimensionless number such as:

- Reynolds number: it represents the ratio of inertial forces to viscous forces.
- Euler number: it expresses the relationship between the flow pressure and the kinetic energy.

The Euler number is a function of density, and thus, indirectly, it provides the information about the gas volume concentration; it is also inversely proportional to the pressure drop along the flame ports.

As shown in Fig. 4.5, in order to avoid the flame back instability, it is therefore possible to define some design rule criteria such as:

- Reynolds number > 75
- Euler number < 1

Fig. 4.6 presents the stability diagram function of the boundary velocity gradient and the fuel concentration for the butane numerical simulations. As opposed to Fig. 5.4, it is now possible to point out a flashback limit curve (dashed line in Fig. 4.6) that divides the stable and the unstable zone.

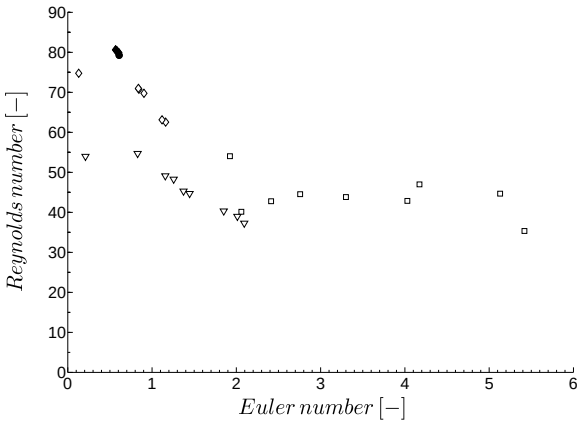

Figure 4.5: Dimensionless numerical correlation for C_4H_{10} in hot conditions between the Euler number and the Reynolds number computed for type 2 flame ports for different prototype families: L9-2 (triangle), L9-3 (square), L9-4 (diamond) and the definitive crown burner (circle). The closed symbols represent the burners not affected by the flame back instability.

This analysis therefore suggests a further investigation of the flame back phenomenon in order to highlight a prediction criteria for this instability.

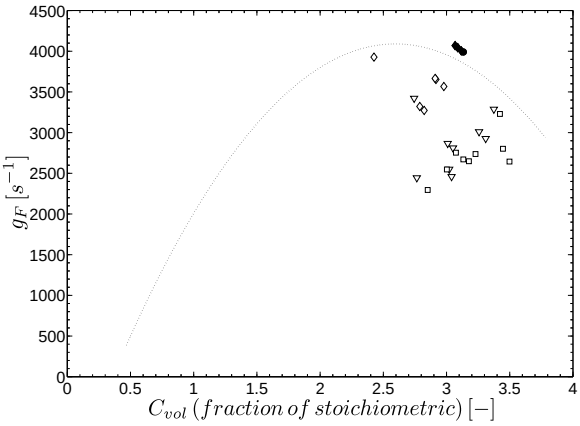

Figure 4.6: Numerical correlation for C_4H_{10} in hot conditions between the volume gas concentration (fraction of stoichiometric) and the critical boundary velocity gradient for type 2 flame ports for different prototype families: L9-2 (triangle), L9-3 (square), L9-4 (diamond) and the definitive crown burner (circle). The closed symbols represent the burners not affected by the flame back instability.

4.4 Flame back prediction criteria

In order to develop domestic gas burners that reduce to a minimum the lightback tendency and maintain laminar flames at very high gas velocities, the following prediction criterion is presented. For $G30$ at nominal pressure conditions the reactive mixture composition through the flame ports was checked to be higher than the stoichiometric concentration. Since the laminar burning velocity for the butane was extrapolated on the upper flammability limit side, the stability criterion between the laminar burning velocity and the velocity magnitude of the unburned mixture will be based on extrapolated data. As highlighted in the previous section, flame back occurs when the burning velocity exceeds the flow velocity through the burner. However, this threshold cannot be established only by the velocity magnitude value. For this reason, the prediction criteria cannot be based on a static balance between different velocities. Therefore, the criteria will be represented by a dynamic balance, in which the velocity and other physical quantities, such as concentration and temperature, will be taken into consideration. In order to evaluate S_L, the gas volume concentration, pressure and temperature, were therefore monitored at different radii (x/R = 0.96 and x/R = 0.98) out of the flame ports. Figure 4.7 plots the radial velocity magnitude at x/R = 0.96 in correspondence to the secondary flame ports as a function of the gas volume concentration for the three prototypes families "L9-2", "L9-3", "L9-4" and for the definitive rapid burner design. This plot is basically the same plot shown in Fig. 4.3 and Fig. 4.4, but the velocity depicted here is not inside the type 2 flame ports, but outside them; it also presents the laminar burning velocity curve, at $298K$ and extrapolated in hot conditions (600 - $625K$).

It was evaluated in order to point out the balance between S_L and the velocity magnitude, as a possible way of characterizing the behavior of different burners in the context of the flame back phenomenon. From Fig. 4.7, it is possible to highlight the interpolation and extrapolation curves for the laminar burning velocity at $298.15K$. Moreover, to underline the uncertainty regarding the influence of temperature on S_L , a dash-dotted curve is plotted. Figure 4.7 also highlights in red the burner designs for which the flame back phenomena was experimentally observed, leaving in green the burners which did not present flame back. The Figure shows that the burners where the flame back phenomena did not occur are clustered together and that their velocity magnitude is higher than the extrapolated range of flame speed. On the other hand, the burner designs for which flame back was observed can be split in two groups:

- Burner for which the volume concentration of butane is outside the range of flammability limits. These prototypes, located outside the flammability limits, are not considered due to the physical impossibility of generating the flame (i.e. flame extension).

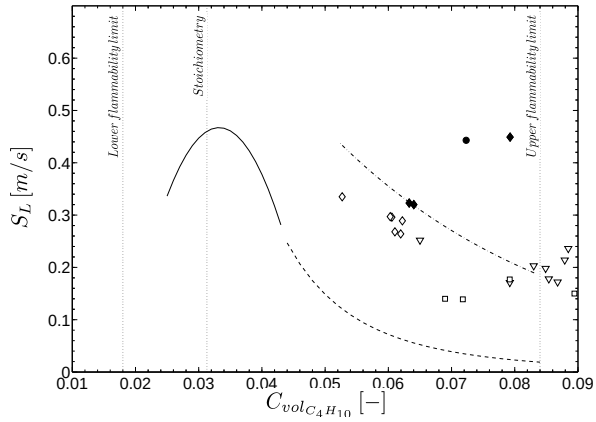

Figure 4.7: Butane stability diagram for flame back at x/R = 0.96 for different prototype families: L9-2 (triangle), L9-3 (square), L9-4 (diamond) and the definitive crown burner (circle). The closed symbols represent the burners not affected by the flame lift instability. Lines: experimental C_4H_{10} laminar burning velocity in cold condition (solid); extrapolated C_4H_{10} laminar burning velocity in cold condition (dashed) and extrapolated C_4H_{10} laminar burning velocity in hot condition (dash dotted).

- Burner within the range but for which the velocity magnitude is lower that the extrapolated flame speed.

Figure 4.7 clearly shows that the computation of SL as a function of the data extracted from the CFD model can be used as a dynamic criteria to highlight flame back.

Similarly, Fig. 4.8 shows the same situation depicted in Fig. 4.7, but for x/R = 0.98, where obviously all the characteristic velocities of the burners shift to the left because of the secondary air entrainment that makes the mixture lean. The boundaries of the stable flame regimes bounded by the limit of flame back may thus help to provide useful guidelines for the design of practical devices aiming to achieve a more stable operation with the $G30$ working fluid.

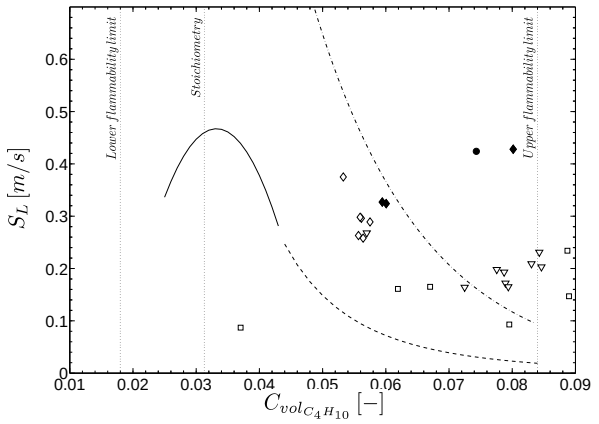

Figure 4.8: Butane stability diagram for flame back at x/R = 0.98 for different prototype families: L9-2 (triangle), L9-3 (square), L9-4 (diamond) and the definitive crown burner (circle). The closed symbols represent the burners not affected by the flame lift instability. Lines: experimental C_4H_{10} laminar burning velocity in cold condition (solid); extrapolated C_4H_{10} laminar burning velocity in cold condition (dashed) and extrapolated C_4H_{10} laminar burning velocity in hot condition (dash dotted).

Chapter 5

Flame lift

Chapter Purpose:
This chapter presents an experimental and numerical analysis of the partially premixed flames of a domestic gas burner. The structure of these flames was investigated to verify the flame lift instability in different conditions. A prediction criterion for this instability phenomenon is also presented.

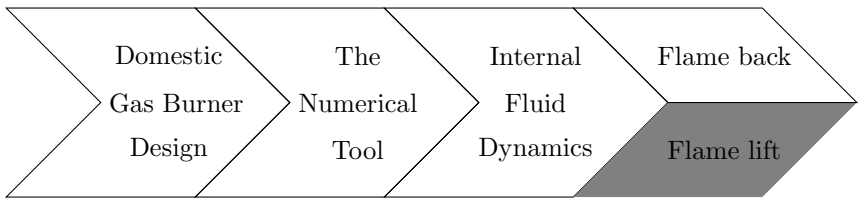

5.1 Introduction

This investigation focuses on the flame lift in domestic gas burners. As explained in the previous chapter, this instability was initially studied by means of a correlation between the experimental dataset and the numerical prediction regarding a DoE preliminary analysis (see § 1.6). To replicate as much as possible the European standard [3] conditions for the flame lift certification, the numerical simulations were performed in isothermal condition, by using $G20$ as working fluid, and a burner equipped with a $D-119$ injector at a nominal pressure of $2000Pa$. As mentioned in § 2.5.2.1, 3D automatic trimmed meshes were generated for the different geometries of the prototypes families and they were used in association with $Model\ A$. The aim of this work was to point out the instability by means of the velocity dynamic balance. Unluckily, adopting this approach in association with numerical simulations in cold conditions lead to unsatisfactory results.
In order to improve the understanding of the flame lift phenomenon, the effects of partial premixing and the input of heat power on the cooking appliance flames were analyzed. This approach allowed the identification of trends that are experimentally observed and numerically predicted. To obtain the data for a specified equivalence ratio, a smooth rich flame is stabilized first. The fuel concentration is then steadily reduced and the flame behavior is monitored. The data clearly show the complex nature of the various possible burning regimes in the cooking appliance. In this context, the results of numerical simulations carried out with $Model\ B$ on laminar partially premixed flames with simple methane-air chemistry are presented. These results were obtained for fuel-rich to stoichiometric conditions, and provided unique information regarding the onset of the flame lift-off and its progressive degeneration into the blowout condition. More specifically, computational confirmation of previously observed experimental trends is presented by focusing on the flame established at the main port of a cylindrical domestic stove. The study was conducted by post-processing the numerical data in order to gain a better understanding of the flame lift phenomenon and to obtain a predictive criterion for this instability.

5.2 Laminar Burning Velocity for Methane

Available experimental data for CH_4, obtained for atmospheric pressure at $298.15K$, was provided by Warnatz [157] as depicted in Fig. 5.1. In this figure it is clear that very lean and very rich mixtures fail to support a propagable flame. This means that if the mixture contains too little fuel or too little oxidant it fails to maintain a propagating flame, as confirmed by the upper and lower flammability limits. Furthermore, the flame speed at the flammability limits falls to zero quite steeply. For most mixtures, the maximum flame speed occurs at the stoichiometric composition; in particular, it occurs slightly on the richer side of the stoichiometric point. Unfortunately, the dataset does not cover the entire flammability range, therefore the experimental points not only have to be interpolated, but also extrapolated on the edge of the flammability limits. Fig. 5.1 proposes the fitting curve used in this work for the methane simulations.

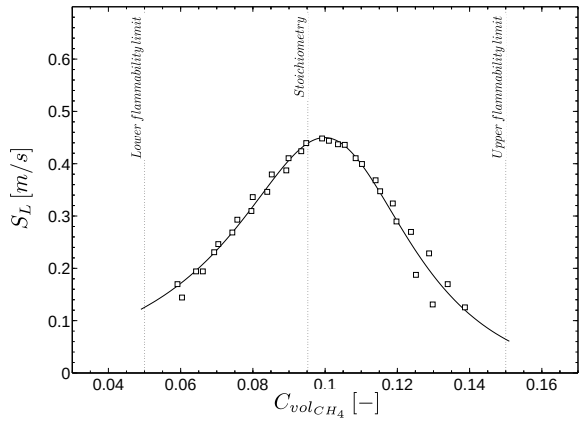

Figure 5.1: Methane laminar burning velocity: experimental points by Warnatz [157] (square marks), interpolation curve (solid line).

The fitting curve adopted in this analysis is the following rational curve, that represents a ratio between a fifth order polynomial function and a fourth order polynomial function,

$$S_L = f(C_{vol}) = \frac{p_1 \cdot C_{vol}^5 + p_2 \cdot C_{vol}^4 + p_3 \cdot C_{vol}^3 + p_4 \cdot C_{vol}^2 + p_5 \cdot C_{vol} + p_6}{C_{vol}^4 + q_1 \cdot C_{vol}^3 + q_2 \cdot C_{vol}^2 + q_3 \cdot C_{vol} + q_4} \quad (5.1)$$

where C_{vol} is the volume gas concentration and the polynomial coefficients have the following values: $p_1 = 0.4674$, $p_2 = 0.6002$, $p_3 = 0.3368$, $p_4 = -0.6354$, $p_5 = 0.07762$, $p_6 = 0.003993$, $q_1 = 4.036$, $q_2 = 12.42$, $q_3 = -2.687$, $q_4 = 0.1533$.

By applying Eq. 4.3 and considering the temperature through the flame ports around $523K$ (see § 2.6.3) it is also possible to show the methane laminar burning velocity in hot conditions as shown in Fig. 5.2.

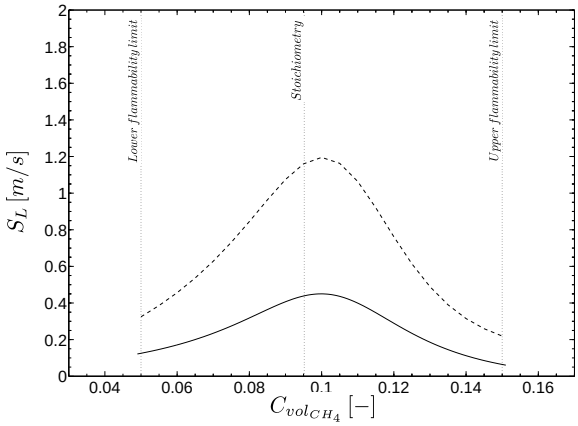

Figure 5.2: Methane laminar burning velocity at $298K$ (solid line) and $523K$ (dashed line).

5.3 Flame lift correlations

The flame stability analysis concerning the "L9-2", "L9-3" and "L9-4" prototype families is reported for the flame lift instability. Figure 5.3 reports the experimental data (flame lift duration time) against the numerical prediction concerning the difference in velocity between the primary and the secondary flame ports.

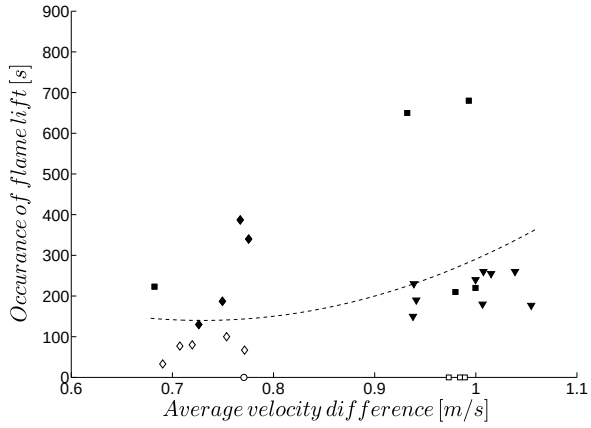

Figure 5.3: Experimental occurrence of flame lift against the velocity difference between flame ports type 1 and 2 for different prototype families: L9-2 (triangle), L9-3 (square), L9-4 (diamond) and the definitive crown burner (circle).The closed symbols represent the burners not affected by the flame lift instability.

No clear correlation was found between the velocity at the main flame ports and the flame lift quantification. As discussed in the context of Fig. 1.14, it is also possible to plot the velocity boundary gradients computed by the numerical simulations for the flame lift instability. Fig. 5.4 depicts these critical velocity gradients for type 1 flame ports of different burner crowns, showing that it is nearly impossible to draw a blow-off limit curve in order to filter out the burners influenced by the flame lift instability from the unaffected ones.

As explained in § 1.3, the concept of flame lift for a Bunsen burner (i.e. one flame port) can be attributed to the fact that the stream velocity through the flame port is not balanced by the burning velocity of the fuel/air mixture. In the case of a multi-flame port design, the flames interact with one another and the lift cannot be described by the velocity out of the flame ports only. The correlation of flame lift is therefore disputable and a robust numerical prediction criteria is not identified without including a combustion model in the numerical investigation. As for the results obtained experimentally by PIV without flame, the flame lift phenomenon is not predicted by the virtual prototype when the flame is not modeled. Indeed, the interaction between the flame ports and the influence of the secondary air should be implemented in the numerical model to

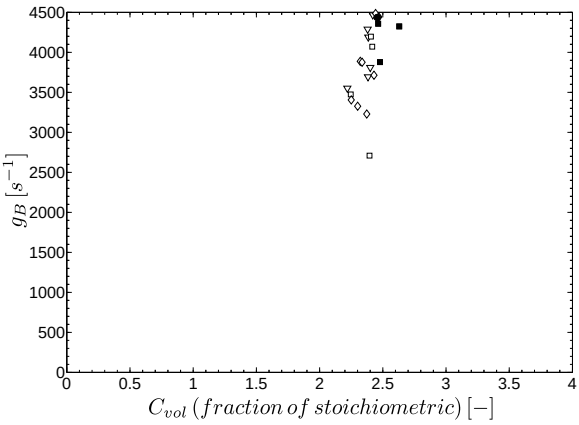

Figure 5.4: Numerical correlation for CH_4 in cold conditions between the volume gas concentration (fraction of stoichiometric) and the critical boundary velocity gradient in type 1 flame ports for different prototype families: L9-2 (triangle), L9-3 (square), L9-4 (diamond) and the definitive crown burner (circle). The closed symbols represent the burners not affected by the flame back instability.

capture this phenomenon. A more correct investigation regarding the flame lift instability was performed, and is presented in the next chapter, in which the numerical model was improved by means of a combustion process modelization.

5.4 Experimental Investigation

As discussed in the previous section, the flame lift instability cannot be investigated without involving a combustion process. However, a further experimental analysis was required to understand this phenomenon completely and to verify the prediction performances of the numerical model. Indeed, the available investigations of the flame lift instability in domestic gas burners were based on certification tests. These experiments often refer to different conditions or configurations during the test (i.e. different burner crown geometries, hobs, working gases, etc.), making it almost impossible to compare them to understand the phenomena. Moreover, these tests were performed from the European standard point of view, by applying the certification procedure without providing a more comprehensive scientific result (the instability was verified and certified only by direct observation). Therefore, it was not possible to take advantage of a previous database of results.

Experimentally the flame lift instability can be observed either in a steady or in a transient state. It can be characterized by a lifted flame placed at a constant height from the burner rim or the phenomenon can include a transient time in which the flame can initially be detached from the burner crown and subsequently be re-attached. Moreover, the flame lift can be considered an aleatory instability in terms of space, because its repeatability at different burner crown flame ports is almost arbitrary. Of course, in order to perform a scientific investigation, the repeatability of the experiment has to be guaranteed. To better understand its phenomenology and for safety reason too, the instability has to be kept under control.

From the literature review, it is possible to note that the flame lift is affected by the formation and the homogenization of the reactive mixture and by the flame interaction with the burner wall and the other surrounding flames. Most important of all, the instability could be highlighted in the same burner for particular equivalence ratios (i.e. primary aerations). Therefore, the scientific investigation performed in this work, started from a simple idea: to force this instability by starting from a flame that was quite stable. To reach this target, the domestic gas burner crown already in production was adopted because it was unaffected by the instability during its normal functioning. This burner crown was developed for a nominal heat power of $3kW$. To force and control the flame lift, the domestic appliance was modified to avoid all the possible causes of uncertainty linked with the characteristics of the mixture. The fuel gas jet and the entrainment process were thus replaced by a premixing circuit in which the characteristics of the mixture were imposed by the user. In this way, it was possible to know the equivalence ratio and the velocity of the feeding mixture, in order to be able to replicate the instability and obtain a scientific investigation. To capture the instability, a visualization technique based on direct photographs and OH images was adopted.

5.4.1 Experimental setup

The experimental setup consists of a flow control system, a cylindrical burner and a measurement system, as schematically shown in Fig. 5.5.

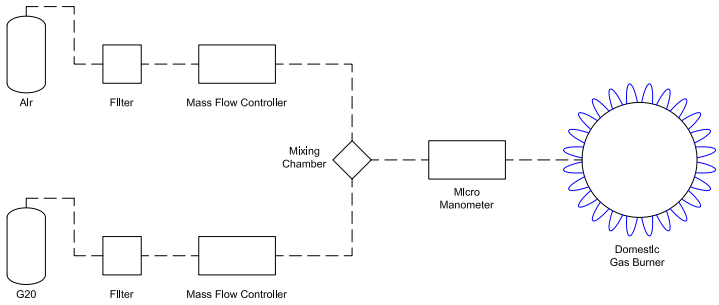

Figure 5.5: Schematic of the experimental setup.

The flow control system is composed of two mass flow controllers and a mixing chamber. The desired gas mixture is prepared by controlling the mass flow rate of the air and the fuel lines. The fuel was chemically pure grade $G20$ (>99%) without any dilution. These flow rates are directly set and measured for each experiment by using the flow bus interface linked with a PC. A simple T valve provided the flow mixing between the two streams. In order to feed the appliance with a controlled and known gaseous mixture, the burner crown was modified by replacing the bowl and the injector with a tube directly connected to the venturi neck. As illustrated in Fig. 5.6, the gaseous mixture flows in this tube (1), enters the burner crown, then discharges through the flame ports (2). By comparing Fig. 1.4 with Fig. 5.6 it is clearly visible that the test appliance is deeply simplified compared to the traditional one, in which the entrainment of the primary air by the fuel gas jet plays a key role in the mixture formation, affecting its flow rate and concentration.

For all the flames studied, the flow was laminar and fully developed at the burner entrance. Furthermore, a micro-manometer was used to measure the static pressure upstream of the burner inlet. To minimize disturbances from the ambient air, an enclosure was placed around the burner. The effect of this enclosure on the flame aspect was found to be negligible and all of the flames were seen to be well within the laminar regime. Indeed, the Reynolds number based on the cold gas properties at the fuel exit varies between 130 and 450 for the analyzed flames.

The visualization setup consisted of a high speed camera (PCO, CCD Camera 12bit cooled), whereas the measurement of the chemiluminescence intensity was performed by the same CCD camera equipped with an optical interference filter.

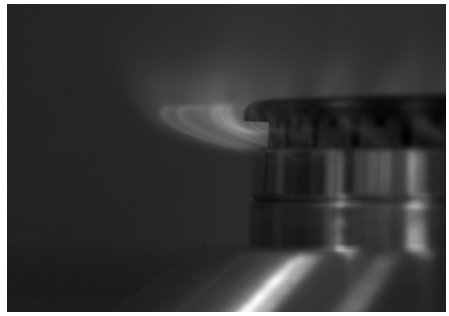

(a) Flames close up

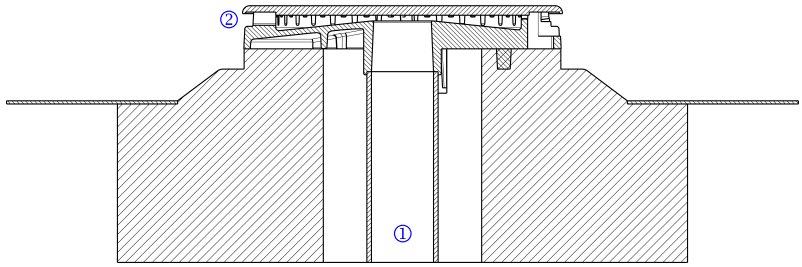

(b) Ensemble section

Figure 5.6: Test domestic gas burner. The section view shows its main components: (1) mixture supply tube, (2) flame port exit.

The video camera was furnished with a lens (50mm focal lens, f 1:28) and was located about 1 meter from the burner in the front configuration and 2 meters above the burner in the top configuration. The measurement window was represented by 1280x1024 pixels, providing a spatial resolution of 0.09mm and 0.13mm for the front and top visualizations respectively.

5.4.2 Experimental procedure

For a fixed heat power input, operating conditions were varied by keeping the rate of fuel flow constant and changing the air flow rate to achieve different equivalence ratios. The reactant flow rates for each equivalence ratio of the flames studied are listed in Tab. 5.1.

The equivalence ratio of a system is defined as the ratio of the fuel to oxidizer ratio to the stoichiometric fuel to oxidizer ratio. Mathematically:

$$\Phi = \frac{(m_F/m_O)}{(m_F/m_O)_{st}} \tag{5.2}$$

where m_F and m_O represent the mass of fuel and oxidant respectively, whereas the subscript st stands for stoichiometric condition. An advantage of using the

	Heat Power $3kW$		Heat Power $4kW$		Heat Power $5kW$	
Φ	$\dot{m}_{G20}$	$\dot{m}_{air}$	$\dot{m}_{G20}$	$\dot{m}_{air}$	$\dot{m}_{G20}$	$\dot{m}_{air}$
-	(l/min)	(l/min)	(l/min)	(l/min)	(l/min)	(l/min)
1.2	4.76	37.73	6.34	50.38	7.93	63.01
1.4	4.76	32.35	6.34	43.22	7.93	54.00
1.6	4.76	28.37	6.34	37.83	7.93	47.19
1.8	4.76	25.17	6.34	33.57	7.93	42.02
2.0	4.76	22.65	6.34	30.24	7.93	37.84

Table 5.1: Reactant flow rates.

equivalence ratio is that ratios lower than one represent a fuel-lean mixture, ratios equal to one a complete combustion (stoichiometric reaction) and ratios greater than one a fuel-rich mixture, irrespective of the fuel and oxidizer being used. The experimental procedure was planned as follow: for a fixed heat power, after a preheating time of 20 minutes to obtain a temperature steady trend, the mixture equivalence ratio was gradually decreased and flame pictures were sequentially acquired every 6 minutes. Therefore, both direct and chemiluminescence photographs were captured by the high speed camera at each equivalence ratio change. As demonstrated clearly in Fig. 5.7, each experiment was therefore defined by a fixed heat power, equivalence ratio, wall temperature and inlet pressure.

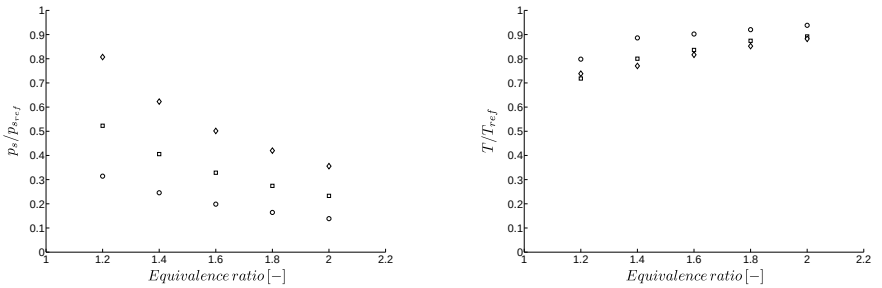

(a) Pressure (b) Temperature

Figure 5.7: Experimental inlet pressure and crown temperature for 3kW (circle), 4kW (square) and 5kW (diamond) heat power input.

The experimental uncertainty for the mass flow rates was 1%. The temperature uncertainty was ±3°C; a k type thermocouple [145] located on the radial diffuser of the domestic gas burner was used.

5.4.3 Flame photographs

The present study has provided qualitative experimental visualizations which describe the visible appearance of the flames. Cross-sectional planes of the burner flame port, perpendicular to the flame axis (Fig. 5.8, Fig. 5.10 and Fig. 5.12), were acquired, and used as primary mode of flow visualization. The flame was also visualized from the top of the burner to acquire a more complete understanding of the flame interactions (Fig. 5.9, Fig. 5.11 and Fig. 5.13).
Data were recorded by saving 50 images for each test condition.

The simplest method for finding the flame front is one in which the luminous part of the flame is observed: this represents the region where reaction and heat release take place. Since the luminous zone is produced mainly by the hot incandescent products of combustion, the flame surface recorded by direct photography is closer to the "post flame" region [160]. The flames depicted in Fig. 5.9, Fig. 5.11 and Fig. 5.13 clearly indicate that there is a luminous conical region within which reaction and heat release are taking place. Underneath the luminous cone, there is a dark zone within which the unburned gas molecules change their flow direction from the initially longitudinal direction to outward directions. Immediately beneath the luminous cone, the unburned gases are heated to a critical temperature at which a rapid chemical reaction starts. The burned gases expand as they leave the flame zone and are diluted and cooled by the surrounding air [26].
These photographs present a double flame structure in which the inner cone corresponds to the flame front of the reaction zone, and the outer cone corresponds to the diffusion flame where excess oxidisable constituents (mainly CO and H_2) burn. The two zones of the flame obviously have a strong influence on each other. For rich mixtures, the mantle above the inner cone can be considered as a very hot region where there is an equilibrium concentration of radicals like CH and C_2, which can give thermal radiation in the visible region [46]. The colour of the luminous zone changes with the fuel/air ratio. The high temperature burned gases usually show a reddish glow, which arises from CO_2 and water vapour radiation. When the mixture is adjusted to be very rich (high equivalence ratios), an intense yellow radiation can appear. This radiation is continuous and can be attributed to the presence of solid carbon particles. For hydrocarbon-air mixtures that are fuel lean (low equivalence ratios), a deep violet radiation due to excited CH radicals appears. When the mixture is fuel rich, the green radiation found is due to excited C_2 molecules [26]. Moreover, by decreasing the equivalence ratio, the combustion becomes more premixed, leading to a less luminous flame. As confirmed by [161], this decreasing luminosity is probably due to the monotonic decrease of the soot concentration with increased premixing. Furthermore, the decreasing of the equivalence ratio stretches the pale blue cone of the inner flame, from a paraboloidal shape to a conical one, and it avoids any yellow tipping of the flame.

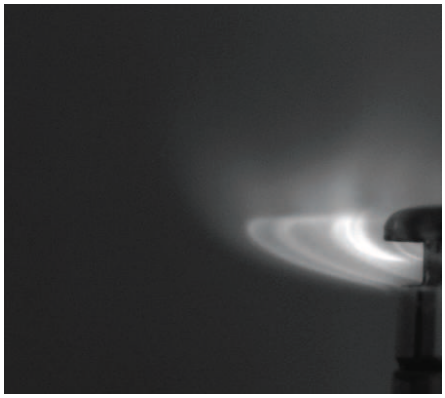

(a) $\Phi = 2.0$

(b) $\Phi = 1.8$

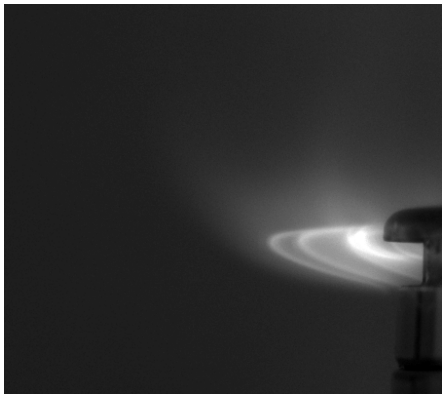

(c) $\Phi = 1.6$

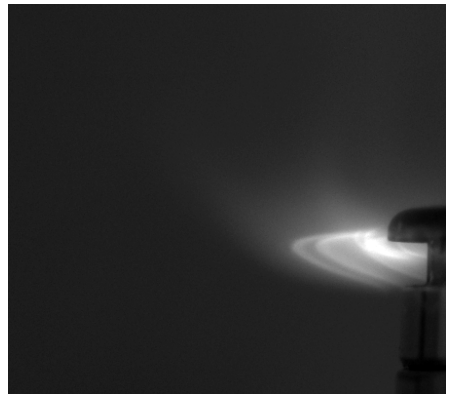

(d) $\Phi = 1.4$

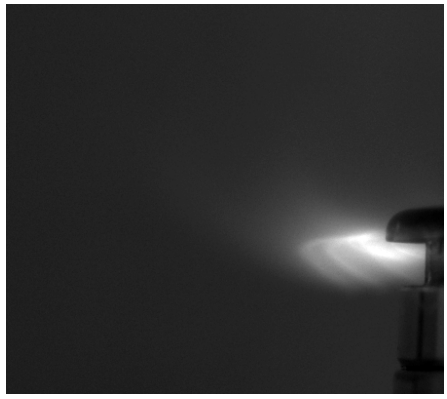

(e) $\Phi = 1.2$

Figure 5.8: Flame images for different equivalence ratios at 3kW (visualizations from the front).

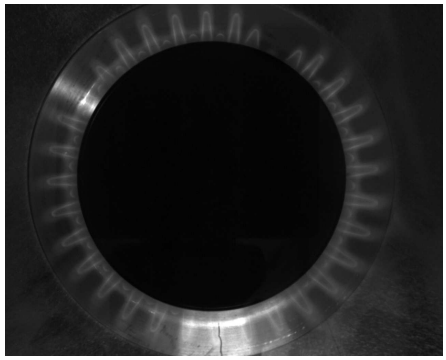

(a) $\Phi = 2.0$

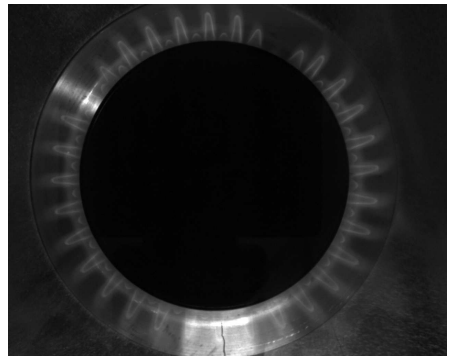

(b) $\Phi = 1.8$

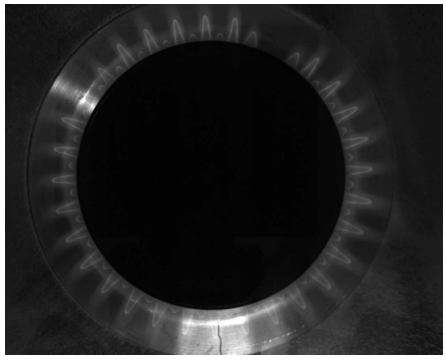

(c) $\Phi = 1.6$

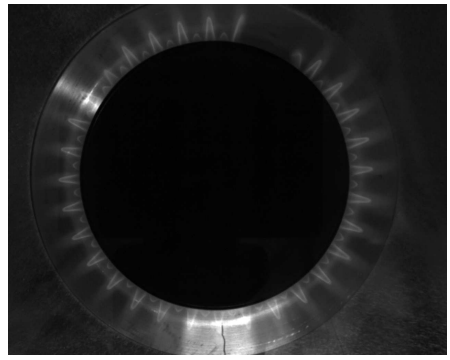

(d) $\Phi = 1.4$

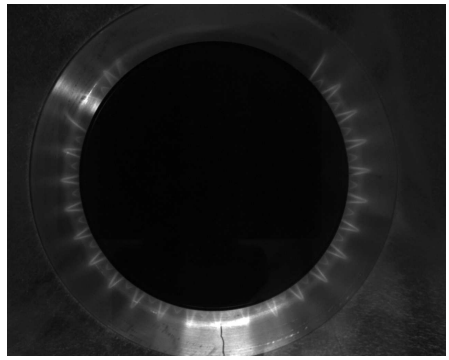

(e) $\Phi = 1.2$

Figure 5.9: Flame images for different equivalence ratios at 3kW (visualizations from the top).

(a) $\Phi = 2.0$

(b) $\Phi = 1.8$

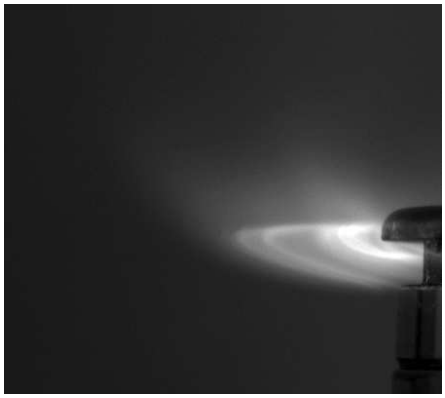

(c) $\Phi = 1.6$

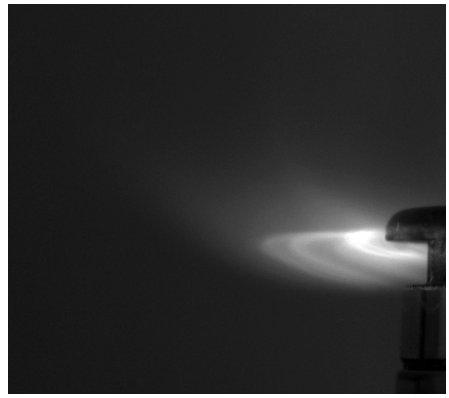

(d) $\Phi = 1.4$

(e) $\Phi = 1.2$

Figure 5.10: Flame images for different equivalence ratios at 4kW (visualizations from the front).

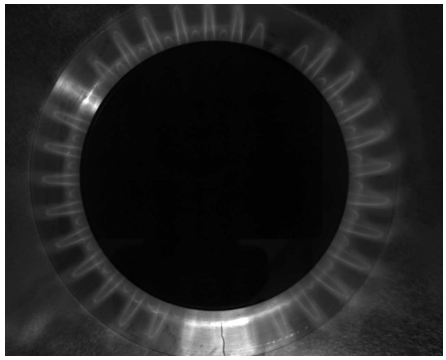

(a) $\Phi = 2.0$

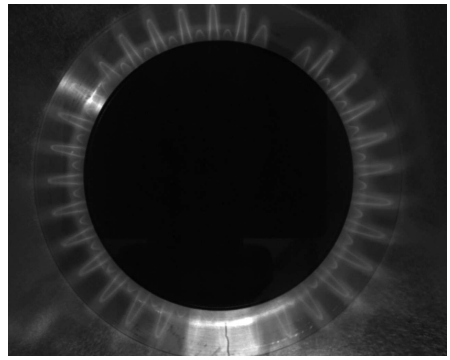

(b) $\Phi = 1.8$

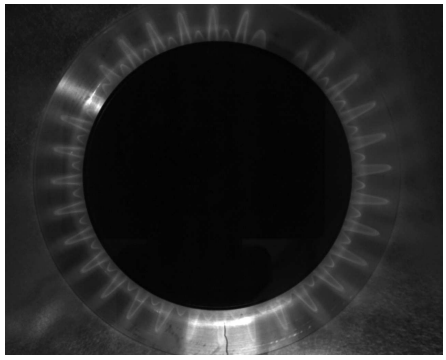

(c) $\Phi = 1.6$

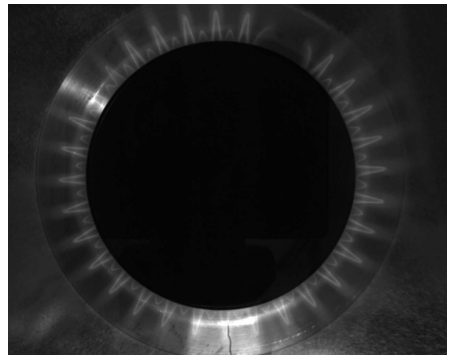

(d) $\Phi = 1.4$

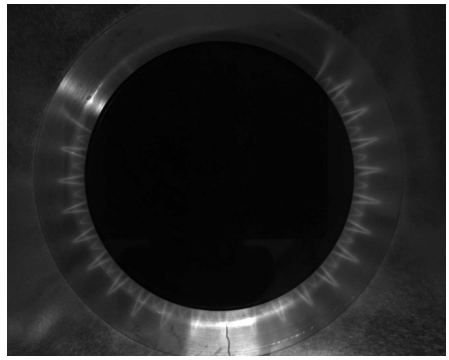

(e) $\Phi = 1.2$

Figure 5.11: Flame images for different equivalence ratios at 4kW (visualizations from the top).

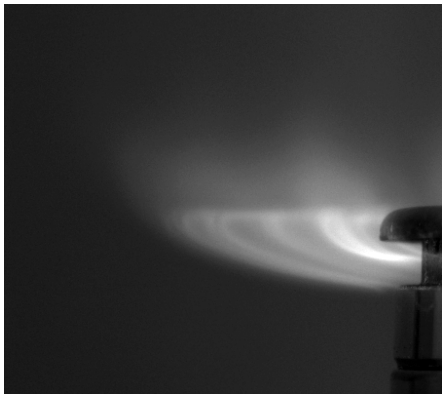

(a) $\Phi = 2.0$

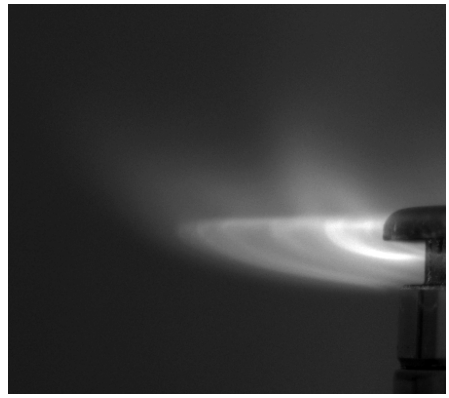

(b) $\Phi = 1.8$

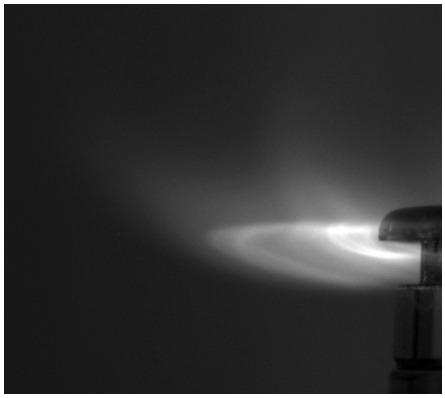

(c) $\Phi = 1.6$

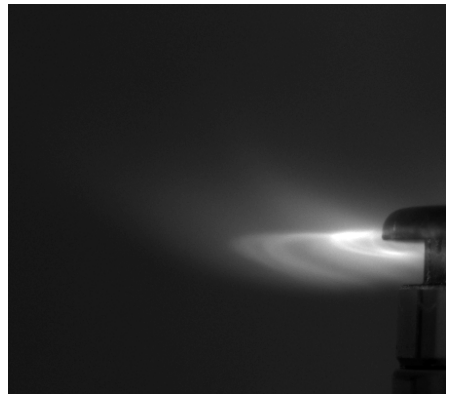

(d) $\Phi = 1.4$

(e) $\Phi = 1.2$

Figure 5.12: Flame images for different equivalence ratios at 5kW (visualizations from the front).

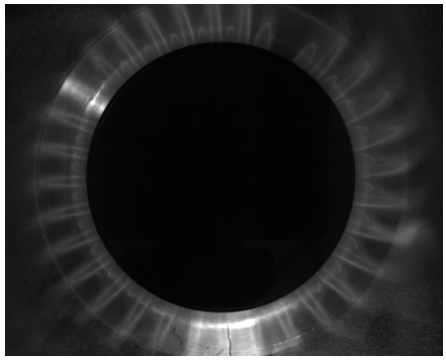

(a) $\Phi = 2.0$

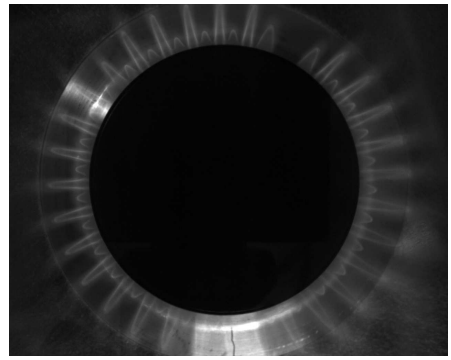

(b) $\Phi = 1.8$

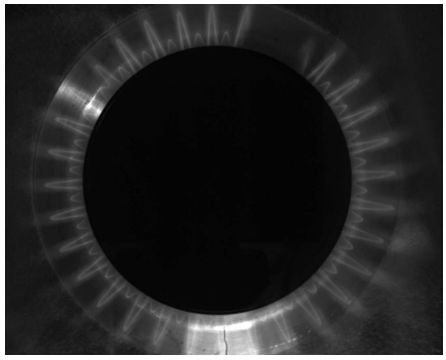

(c) $\Phi = 1.6$

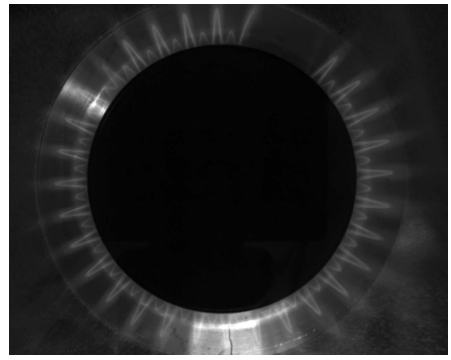

(d) $\Phi = 1.4$

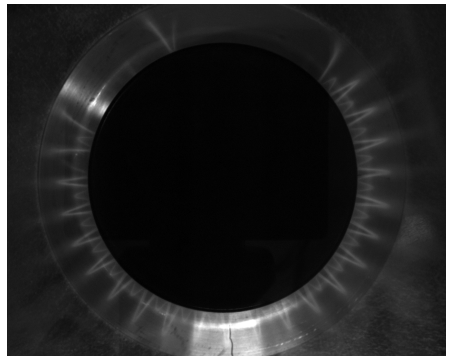

(e) $\Phi = 1.2$

Figure 5.13: Flame images for different equivalence ratios at 5kW (visualizations from the top).

The direct photographs presented in Fig. 5.8, Fig. 5.10 and Fig. 5.12 also show that the base the flame does not coincide with the burner crown wall. This dead space near the rim of the domestic gas burner is a consequence of heat loss (and possibly loss of active chain carriers) from the flame to the metallic wall. Such a loss quenches the reaction and causes the dead space just below the cone. In this region, the back pressure distorts the parabolic velocity profile, therefore the base of the inner cone is appreciably modified from its theoretical shape. The back pressure of a flame is due to the acceleration of the flame gases as they pass through the reaction zone and it depends on the burning velocity. Due to this pressure inside the cone, slightly larger than that outside, it is possible for fresh mixture to escape unreacted through the dead space into the room air. This causes the well known overhang of the flame.
The apex of the flames is rounded off as depicted in both the front and the top visualizations. As the radius of curvature of the flame front becomes comparable in magnitude with the flame thickness, heat and active particle diffusion become more intense. This will increase the fundamental flame speed. Because of this, at the apex of the cone, the flame tends to push harder into the fresh mixture and the observed apex rounds o ff.
Therefore, two primary agents responsible for flame propagation in gas mixtures are conduction of heat and diffusion of some unstable intermediate active atoms and radicals (which promote chain reactions), from the flame zone into the fresh mixture. The relative importance of these two agents differs for different mixtures under different circumstances. The effect of the back pressure is relatively greater for a slow initial gas flow which gives a wide angle cone and big overhang. In the same way, at very low pressures, the flame front will be thicker and the rounding of the apex becomes particularly noticeable [160].
Considering the influence at different equivalence ratios of a fixed power input, the changes in the visual appearance of these flames suggest that partial premixing decreases the flame height. All the luminous cones are compressed towards the burner as the equivalence ratio is reduced. Since the CH_4 flow rate is held constant, the flame length will decrease because the higher the partial premixing, the smaller the amount of secondary air that must diffuse inward to create a stoichiometric mixture, and thus the smaller the axial distance required for this diffusion to occur. On the other hand, the bottom flame edge does not seem to be influenced by the partial premixing until flame lift-off occurs. At low injection velocities, this edge flame is attached to, or stabilized very close to the burner. As mentioned above, the flames are stabilized at the location of highest reactivity, where the higher flame temperature occurs. Although the gas accelerates as a result of the lower density in this region, the overall increase in speed is significantly small and thus does not affect the lift-off distance. At a higher injection speed, this flow acceleration forces the flame to adjust its location at a more favorable position. Therefore the flame lift-off occurs due to the balance between the laminar burning velocity and the unburnt reactant velocity. However, as mentioned

in § 1.5.2.9, the greater stability of a fuel-rich flame compared to a stoichiometric flame, appears also to be due to the interaction between the primary (premixed) and secondary (diffusive) combustion zone. The secondary combustion zone acts as a pilot flame and retains the primary zone [29].
As the input power increases the flame length increases. However, the behavior of the flame tip and of the bottom flame edge location are the same for the different heat powers: the tip moves downstream, whereas the bottom edge moves upstream. Therefore, the transition from the stable flame to the unstable one is believed to be caused by the fact that, as the equivalence ratio is decreased, the resulting increase in the laminar flame speed reduces the flame standoff distance, which in turn increases the heat loss to the burner wall and thereby enhances the propensity for flame front instability.

5.4.4 OH-radical imaging

In past decades, most of the experimental effort was dedicated to the visualization of flame front position and structure in turbulent flames. Imaging of reactive flow fields has provided new views into the complex chemical and fluid mechanical phenomena typically found in combustion devices. The most popular two dimensional imaging techniques used in combustion studies derive their signal from Lorenz-Mie scattering [162], Rayleigh scattering [163], natural light emission from free radicals (e.g., [164, 165]), or laser induced fluorescence (LIF) (see, e.g., [166, 167]). Most of the investigations were therefore concentrated on spatially resolved species-specific measurements in combustion experiments, with the goal of providing some detailed data concerning the local progress of the flame chemistry and dynamics [168, 169]. In this context, optical emission signatures from combustion experiments represent a convenient chemically based diagnostic for a variety of applications. Optical flame emissions, like the familiar blue color of a gas stove, are the result of specific molecular electronic transitions from excited states produced in non-equilibrium concentrations by specific chemical reactions. This radiative emission given off by chemically excited reactive species is named chemiluminescence. Chemiluminescence measurements are widely used in estimating global heat release rates in hydrocarbon flames [46] because their intensities of chemiluminescence are roughly proportional to the reaction intensity [170, 46, 129]. The intensity of the chemiluminescent radiation varies also linearly with fuel flow rate at a constant equivalence ratio [171]. As a result, this experimental approach was extensively used to study different unsteady combustion phenomena. Since the chemiluminescent emission arises from chemical reactions, examining the spectral content of the light and identifying the signatures of the species present provides an insight into the chemical reactions occurring during each different configuration devised in this investigation. Therefore, the chemiluminescent emission may be interpreted as a signature of chemical reaction of the domestic gas burner flames and can be used to delimit regions

of reaction and heat release [172–176]. Many other researchers have shown that chemiluminescence of flame species such as CH, C_2, OH and CO_2 can be used as a qualitative and/or quantitative combustion diagnostic tool [177]. Certain radicals, for example C_2 and CH, appear almost exclusively in reactive zones and their concentrations are always small and their lifetimes quite short [173]. Moreover C_2 will qualitatively indicate rich regions, whereas CH will be found over a broader equivalence ratio region [178]. Finally, in recent investigations [179, 180], it was found that C_2 and CH disappear in regions of high curvature and high rates of strain. On the other hand, OH is formed in a later phase of the combustion reaction, has a longer lifetime and diffuses into the hot burned gases, describing the broader zone of reaction rather than just the reactive interface [46]. Therefore, measuring radical intensity in the flame can determine whether the regions near the wall are rich and those near the axis of symmetry are lean. Furthermore, the CH chemiluminescence, located in the visible range, is also superimposed on the solid-body light emission of soot particles, whereas the OH chemiluminescence is free from background luminosity because it is located in the UV range [181].
Concerning the influence of the fluid dynamics phenomena on the optical flame emission of these radicals, Najm et al. [182] presented a well developed argument that CH, CO_2 or OH chemiluminescence are poor indicators of the global heat release rate in a flame characterized by highly turbulent combustion. In contrast, for laminar or weakly turbulent partially premixed flames, such as the hydrocarbon-air flames of the domestic burner, most light comes from OH at 306 nm [183, 184]. Therefore, the experimental simplicity of optical emission diagnostics, combined with the flexibility of species selectivity, makes chemiluminescence a very useful diagnostic in modern combustion research. A limitation of classical visualization methods of this kind concerns its spatial resolution in flows that are not two-dimensional with respect to the optic axis. The information is collected over the optical path along the line of sight, and the image is not easily deconvolved. Because the domestic gas burner is at least partly three-dimensional, this diagnostic technique provides a spatial resolution that is only adequate for a qualitative interpretation. Chemiluminescence thus suffers from being a line-of-sight technique with limited spatial resolution; small-scale structures and local heat release rates cannot be resolved. Chemiluminescence is also inadequate for studying the detailed interactions between reaction layers and turbulent flow structures, which can result in localized variations in strain and heat loss, as well as extinction [185].
The general arrangement used in this study for emission imaging is shown in Fig. 5.14. The chemiluminescence imaging integrates the flame radiation over the line of sight of the camera.

The emission image is formed by collecting the light emission with a fixed CCD camera equipped with a filter. The specification of the optical interference filter is given in (Fig. 5.15).

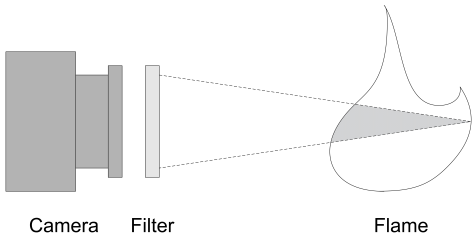

Figure 5.14: Line of sight integration.

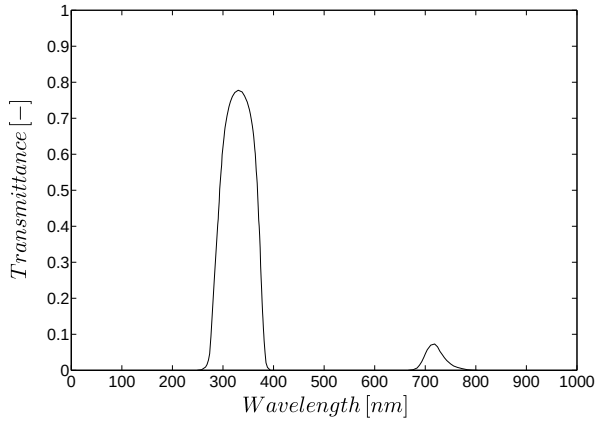

Figure 5.15: OH interference filter specification.

This process yields the spatial distribution of the light emission of the OH radical. The images of the emission of this free radical were acquired with the same set-up as for the flame photographs. Data were recorded by averaging 50 images pixel-by-pixel in order to minimize turbulent fluctuations; therefore each point represents a mean normalized emission intensity value calculated from 50 separate images.
The OH emission signal is therefore represented by an intensity image that was post-processed to point out the structure of the reaction zone. By using multilevel thresholding, the intensity image was converted to an indexed image to highlight the different pixel intensity range. The plot, depicted in Fig. 5.16, shows the chemiluminescence intensity, in Arbitrary Units (AU,) of the averaged OH images with respect to the predicted heat power based on the reactant flow rate. This correlation shows a linear relationship between the heat release rate and the chemiluminescence image: the emission image, proportional to the formation of OH, can therefore be used as a qualitative rate measure of the flame chemistry [182, 186].

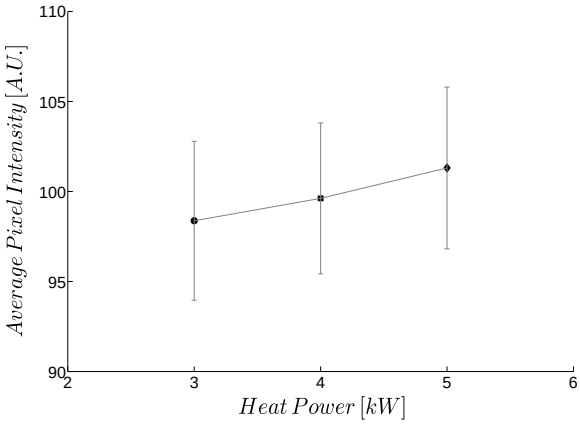

Figure 5.16: OH chemiluminescence intensity for $3kW$ (circle), $4kW$ (square) and $5kW$ (diamond) heat power input.

Therefore, the excited OH free radical intensity varies linearly with the volumetric heat release. The same procedure was also applied to create a contour plot of the OH image data. Fig. 5.17, Fig. 5.18 and Fig. 5.19 show a composite image of the captured data in which separate images at different equivalent ratios are combined for a heat power input of 3kW, 4kW and 5kW respectively. Since these images taken by the CCD camera are integrated over the line of sight, it is not possible to point out a single main flame issuing from the burner. A single image presents different superimposed flames. The central portion of the field of view is therefore dominated by OH chemiluminescence, the intensity of which shows that methane is burning in this region. However, the flame front is poorly

reproduced because the OH diffuses into the hot burned gases [187]. Moreover, not only the flames from the main flame ports are shown, but also the ones issuing from the smaller grooves (pilot flames). Of course the OH footprint is located on the upper side out of the flame ports, due to the optical emissions of the various main and pilot flames. Therefore these images confirm the presence of a main flame represented by an outer emission region and a pilot flame characterized by a smaller brighter central zone close to the burner wall. As discussed in the context of Fig. 5.8-Fig. 5.13, for a fixed heat power the maximum luminosity occurs at higher partial premixing. In addition, by decreasing the equivalence ratio, the chemiluminescence signal moves closer to the burner wall. It is evident that the OH emission intensity of the flame is strongly influenced by the injection velocity; therefore the OH radiation decreases by increasing the inlet mixture mass flow rate. This effect is highlighted by the inner OH contour that gradually reduces its curve by becoming more and more aligned with the flame port centerline. This kind of alignment represents the marker of the flame lift instability.

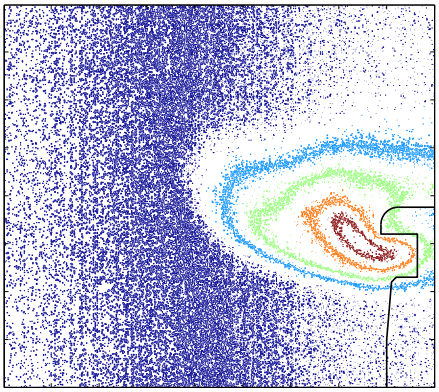

(a) $\Phi = 2.0$

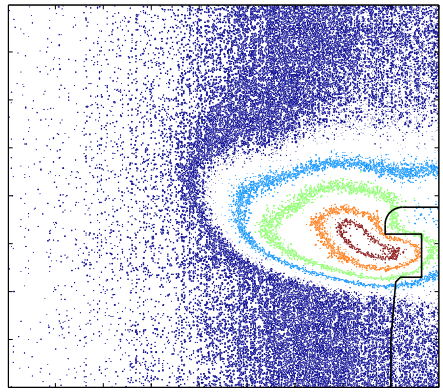

(b) $\Phi = 1.8$

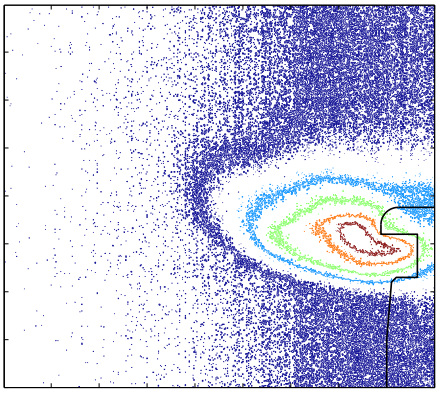

(c) $\Phi = 1.6$

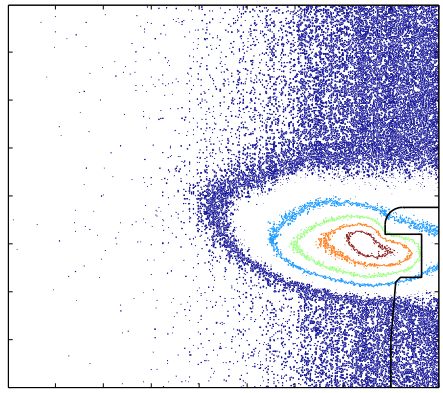

(d) $\Phi = 1.4$

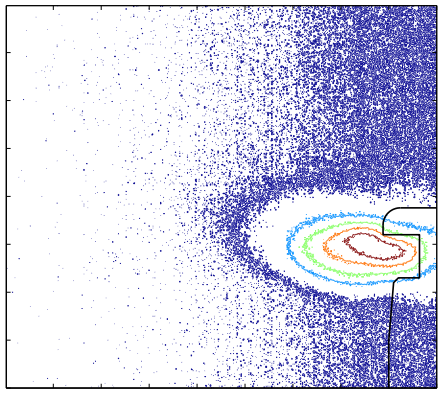

(e) $\Phi = 1.2$

Figure 5.17: Visualization of OH chemiluminescence iso-contour levels for different equivalence ratios at 3kW. The burner edges are also sketched (black line).

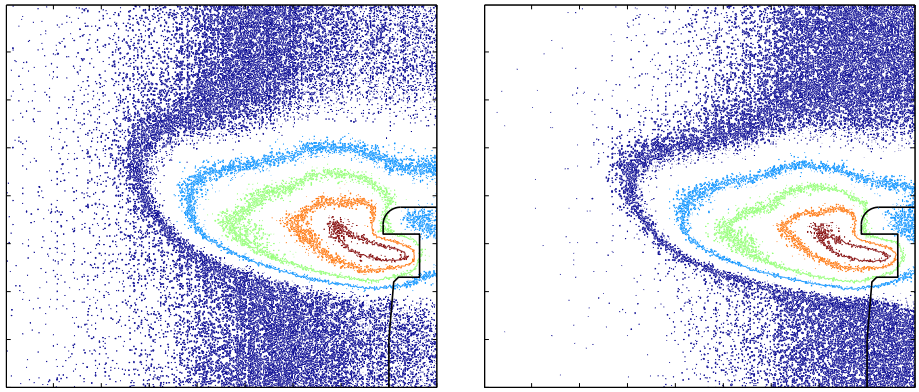

(a) $\Phi = 2.0$

(b) $\Phi = 1.8$

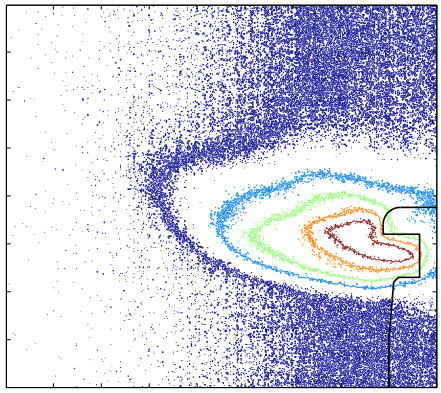

(c) $\Phi = 1.6$

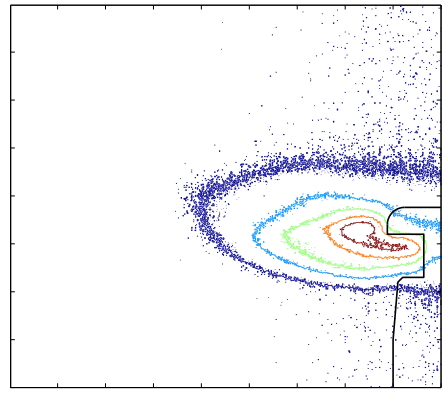

(d) $\Phi = 1.4$

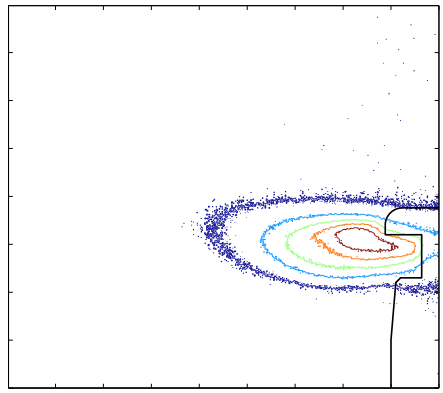

(e) $\Phi = 1.2$

Figure 5.18: Visualization of OH chemiluminescence iso-contour levels for different equivalence ratios at 4kW. The burner edges are also sketched (black line).

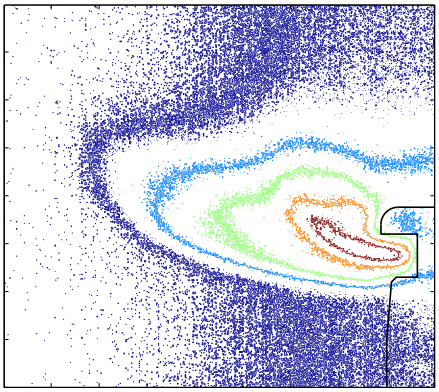

(a) $\Phi = 2.0$

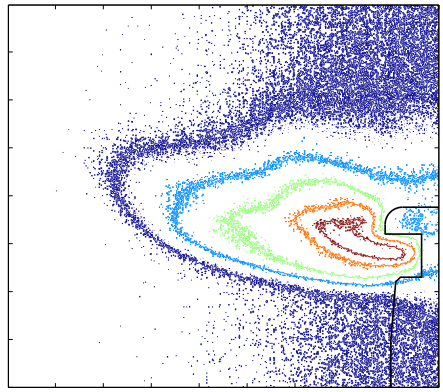

(b) $\Phi = 1.8$

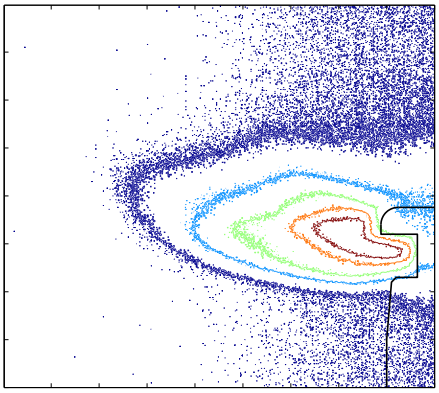

(c) $\Phi = 1.6$

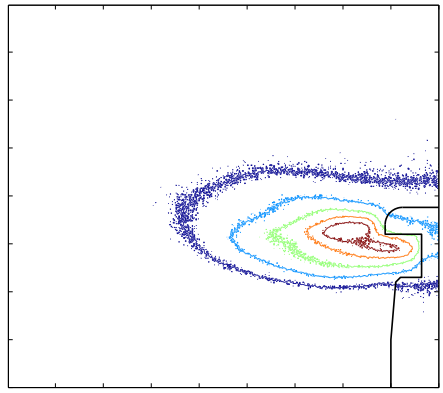

(d) $\Phi = 1.4$

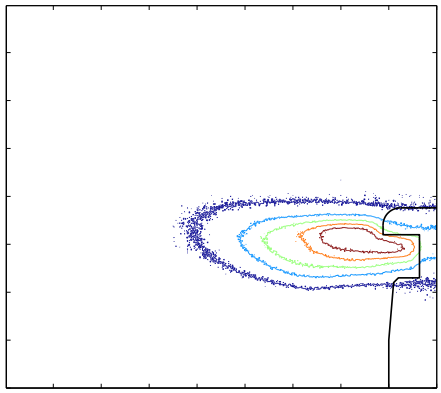

(e) $\Phi = 1.2$

Figure 5.19: Visualization of OH chemiluminescence iso-contour levels for different equivalence ratios at 5kW. The burner edges are also sketched (black line).

5.5 Numerical Investigation

The major challenge in the use of combustion modeling technology is confiding that a comprehensive modeling approach adequately characterizes, both qualitatively and quantitatively, the combustion process of interest. This is accomplished by comparing code predictions with the experimental data presented in the previous section, measured from the domestic gas burner flames. Consequently, data from these flame visualizations are necessary to validate the adequacy of code predictions and to establish the degree of precision that the code can reach in simulating not only the behavior of the domestic gas burner, but most of all the flame lift instability phenomena. For this investigation, the same experimental simulations presented in Tab. 5.1 were carried out, by using the finite volume *Model B*. The numerical results provided by the comprehensive combustion model are divided in several parts and they always refer to the primary flame port (i.e. type 1 flame port). The first part focuses on the model validation based on the flame length and lift-off height. In order to reach a better understanding of the combustion process and the flame lift instability phenomena, a detailed post-processing of the numerical data is presented in the following.

5.5.1 Flame Length and Lift-off Height

The changes in the visual appearance of the flames suggest that partial premixing affects the flame length. As discussed by [161], different formulations can be used to define this quantity:

- H_f, the mixture-strength flame height, is defined as the location at which the centerline local equivalence ratio is one;
- H_t, a surrogate of H_f, is defined as the location where the maximum centreline temperature occurs;
- H_v, the visible flame height, is defined as the length corresponding to the yellow tip (location at which soot oxidation is completed) or the length corresponding to the inner premixed flame tip.

H_f and H_t can be considered almost equal. As the partial premixing increases, less secondary air is required to create a stoichiometric mixture at the centerline, because, as stated by Roper's theory [188, 189], less time is needed for diffusional mixing. Therefore H_f decreases as the partial premixing is increased. H_v shows the same trend, but it decreases more rapidly due to the combined effects of decreasing soot concentration and the earlier onset of oxidation due to decreasing H_f. The appropriate flame length for the purpose of this investigation is the visible flame height, measured as the distance between the burner flame port and the inner premixed cone tip. In the numerical simulation, this inner premixed cone tip is represented by the maximum heat release rate around the tip. To obtain the flame length and the lift-off height, classical image processing was used on all images for each configuration. The reference visible flame height was obtained by averaging the camera record of the flames over 50 frames, whereas the standard deviation was computed by the visible flame height shown in each single image. In order to validate the numerical prediction concerning the flame length, a comparison between the numerical simulations and the experimental measurement was performed. Flow visualizations were provided by acquiring cross-sectional planes of the burner flame port, perpendicular to the flame axis, by means of direct photography. Of course, due to the cylindrical shape of the gas burner, it was not possible to isolate a single flame front during the experimental measurements.

As discussed in the previous sections, the flame tip moves downstream whereas the bottom edge of the flame remains nearly constant until flame lift-off occurs, then it abruptly moves away downstream. The position of the double point thus represents a marker for the evolution of flame lift-off. It is possible to account for the compression of the flame towards the burner wall by representing each configuration as a flame length. In particular, two flame elements were investigated: the length of the inner rich premixed flame and the length of the leading edge of the flame at the bottom. The former can be considered as the flame length of

the whole flame, whereas the latter as its liftoff height. Fig. 5.20 and 5.21 show the comparison between the numerical simulations and the experiments showing the effect of the Reynolds number on the flame length and lift-off height, respectively. As depicted in Fig. 5.20, the agreement between the numerical simulations and the experiments is only acceptable for the configurations at a low Reynolds number (i.e. higher equivalence ratios). At a higher Reynolds number, quantitative but also qualitative differences between the predicted and measured flame length are present. As discussed in the context of Fig. 5.8-Fig. 5.13, the flame length decreases linearly with R_e. On the contrary, the numerical model is not able to simulate this trend by presenting an increased flame length as the Reynolds number is increased. This opposite prediction may be due to an incorrect prediction of the laminar burning velocity at the tip of the flame. This, the velocity at which the flame propagates through the unburnt mixture, is mainly a function of pressure, temperature and equivalence ratio. Therefore the correct simulation of these parameters plays a fundamental role in the stability balance of the flame. A further validation of the model should be performed in order to achieve a better agreement with the experiments. On the other hand, Fig. 5.21 shows a very good agreement between the numerical results and the experimental measurements concerning the lift-off height. From the point of view of flame stability, this result represents a key factor considering the role of the flame bottom edge in the flame lift phenomena. Therefore, the correct simulation of the lift-off height allows the formulation of a prediction criterion for this kind of instability.

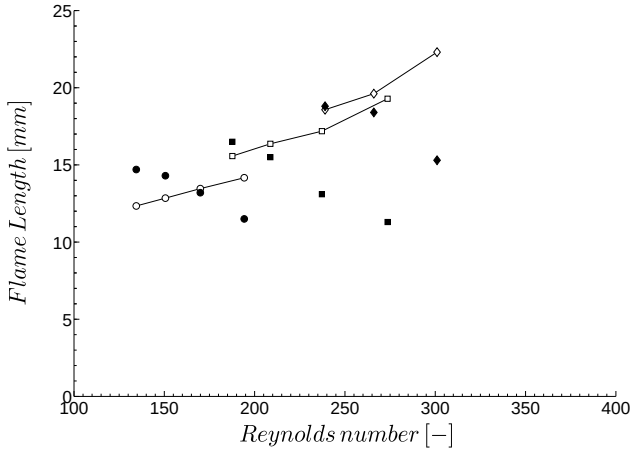

Figure 5.20: Flame length versus Reynolds number for 3kW (circle), 4kW (square) and 5kW (diamond) heat power input. The open and closed symbols represent the numerical and experimental results, respectively.

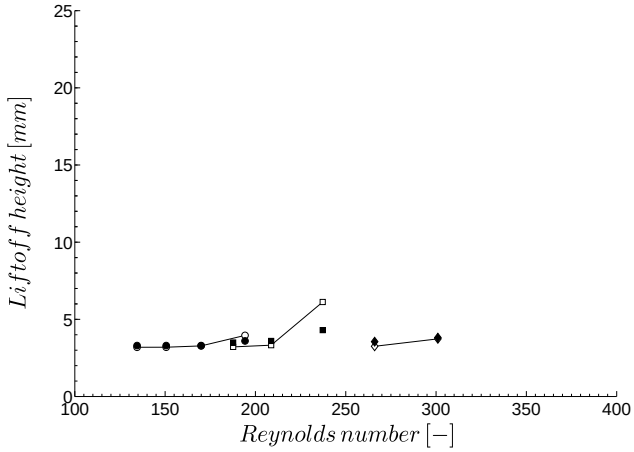

Figure 5.21: Liftoff height versus Reynolds number for 3kW (circle), 4kW (square) and 5kW (diamond) heat power input. The open and closed symbols represent the numerical and experimental results, respectively.

5.5.2 Major Species

The premixed flame structure usually consists of a broad preheat zone followed by a much narrower reactive zone. The preheat zone is dominated by diffusive and convective phenomena, whereas the reaction zone is mainly diffusive. Specifically, in the methane-air premixed flame, the single reaction zone structure is replaced by a structure with two reaction zones. Therefore, the methane-air flame is assumed to consist of three layers: (1) the upstream, chemically inert, preheat zone; (2) a thin, fuel consumption layer, also called the inner layer; and (3) another thin oxidation layer. Downstream of the oxidation layer, the equilibrium, fully reacted state of the mixture is achieved. Therefore chemical activation and heat release occur in different spatial locations: the fuel consumption layer and the oxidation layer. To be more specific, in the fuel consumption layer the primary fuel CH_4 reacts with the H atom to form the secondary fuels, H_2 and CO, through the following steps:

$$3H_2 + O_2 \leftrightarrows 2H_2O + 2H \tag{5.3}$$

$$CH_4 + 2H + H_2O \leftrightarrows CO + 4H_2 \tag{5.4}$$

In the oxidation layer these secondary fuels are converted to the products H_2O and CO_2 by means of reaction (5.3) and:

$$H + H + M \leftrightarrows H_2 + M \tag{5.5}$$

$$CO + H_2O \leftrightarrows CO_2 + H_2 \tag{5.6}$$

Since the characteristic reaction rate of step 5.4 is much faster than the rates of 5.5 and 5.6, the fuel consumption layer is thinner than the oxidation layer. Moreover, the H atoms needed for fuel consumption are supplied through back diffusion from the oxidation layer.
The reaction mechanism within the Eddy Break Up Model consists of two forward reactions, presented in §2.4.3. Therefore, reaction 2.23 represents the fuel consumption layer, whereas 2.24 corresponds to the oxygen consumption layer. Adopting this two-step reaction mechanism, the predicted major species concentrations at different equivalence ratios are compared in Fig. 5.22, 5.23 and 5.24, corresponding to the input powers of 3kW, 4kW and 5kW, respectively. Further evidence of the flame structure is provided by plotting the predicted heat release rates. In order to identify the global flame structure, previous investigations [94, 190, 191] used heat release rate profiles, which exhibited two distinct peaks, indicating the double flame structure. The species and heat release profiles are plotted along an ideal line that represents the partially premixed flame centerline: from the main flame port to the tip of the premixed flame cone. The profiles

in Fig. 5.22, 5.23 and 5.24 have several common features for both the burner-attached and lifted flames. The initial concentrations of CH_4 and O_2 persist to a large distance above the burner surface, as indicated by the longer flat region at the start of each profile. Then their mole fractions decrease rapidly in the preheat zone and the combustion products are formed near the stoichiometric surface. The O_2 concentration is small until all of the CH_4 has been consumed, at which point it starts rising rapidly. Therefore, CH_4 decomposes forming CO and H_2O on the rich side of the flame front. The CO oxidation then forms CO_2 mainly at the top of the flame. The double flame structure effects can be also observed in the CO mole fraction profiles. The presence of a marked peak followed by a second smaller one denotes two main zones of CO production: the former peak is located in the zone of the inner premixed reactions, whereas the latter peak represents the nonpremixed reaction zone in which CO is transported and consumed as it is gradually depleted downstream. The profiles of the CO_2 and H_2O mole fractions have a similar trend. The CO_2 concentration peaks in the highest temperature region, which is located downstream of the inner premixed reaction zone. Nevertheless, most of the H_2O is produced on the inner flame front. These observations demonstrate that CH_4 and O_2 are converted to H_2O and CO in the inner premixed flame, while the conversion of CO to CO_2 occurs in the outer nonpremixed flame. As the equivalence ratio decreases, the initial concentration of CH4 decreases, while that of O_2 increases, due to dilution by primary air. Moreover, as the level of premixing increases, the reactants (CH_4 and O_2) need less time before they start to react. Partial premixing significantly affects the concentration of CO: its mass fraction peak increases with the level of premixing, whereas the smaller peak slowly disappears. Moreover, as the level of partial premixing is increased, there is an increase in the concentrations H_2O and CO_2 further downstream. This behavior is a result of the reduced radial transport of chemical species formed off-axis, due to a reduction in the radial inward flow (coflow entrainment) as the inlet mass flow rate increases [89]. As the input power increases, an increasing flow rate of primary air is required in order to achieve the same equivalence ratio. Therefore, an unbalance between the unburnt reactant velocity and the laminar burning velocity occurs. This leads to a global downstream shifting of the concentration and heat release profiles because the flame front moves away from the burner wall. Moreover, the higher the level of partial premixing, the earlier is the onset of flame lift-off. The presence of this flame instability can be predicted by noting the disappearance of the second peak in the CO mass fraction. Its disappearance represents the transition between a mainly diffusive flame and a mainly premixed flame. As discussed in Ref. [34], this change in flame topology can be used as an indicator for flame instability. It is possible to show the disappearance of the second peak at different equivalence ratio for the different input powers: 3kW ($\Phi = 1.2$), 4kW (from $\Phi = 1.4$) and 5kW (from $\Phi = 1.4$). Lastly, as the input power is increased, a wider flame is observed, as indicated by a broader CO concentration profile for all the equivalence

ratios.

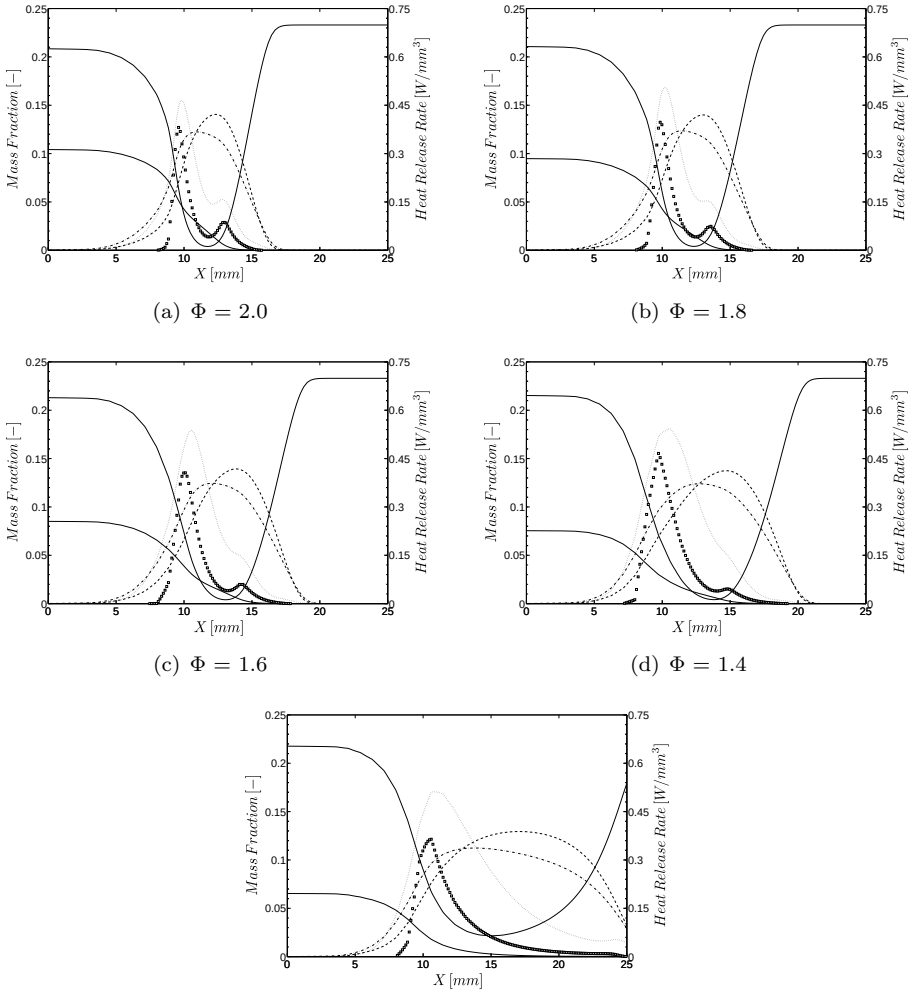

(a) Φ = 2.0

(b) Φ = 1.8

(c) Φ = 1.6

(d) Φ = 1.4

(e) Φ = 1.2

Figure 5.22: Predicted profiles of major species (CH_4: bold solid line, O_2: solid line , CO: dotted line, CO_2: dashed line, H_2O: dash dotted line) and heat release rate (square marker) for different equivalence ratios at 3kW.

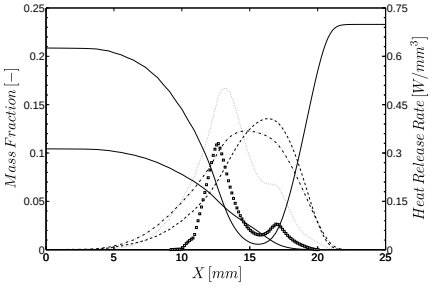

(a) $\Phi = 2.0$

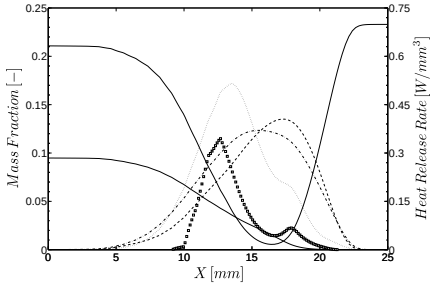

(b) $\Phi = 1.8$

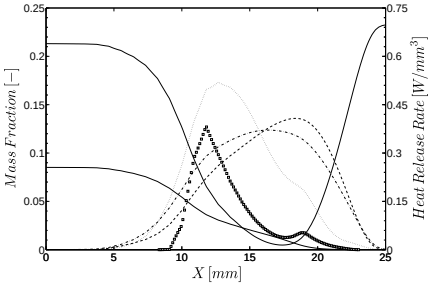

(c) $\Phi = 1.6$

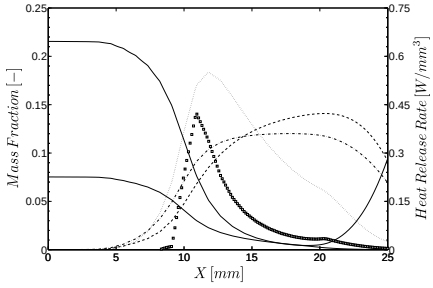

(d) $\Phi = 1.4$

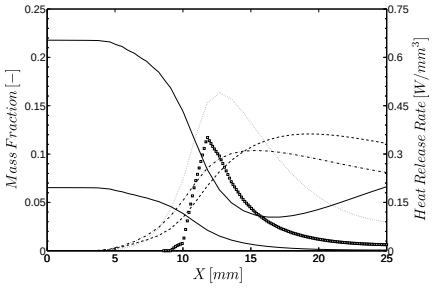

(e) $\Phi = 1.2$

Figure 5.23: Predicted profiles of major species (CH_4: bold solid line, O_2: solid line , CO: dotted line, CO_2: dashed line, H_2O: dash dotted line) and heat release rate (square marker) for different equivalence ratios at 4kW.

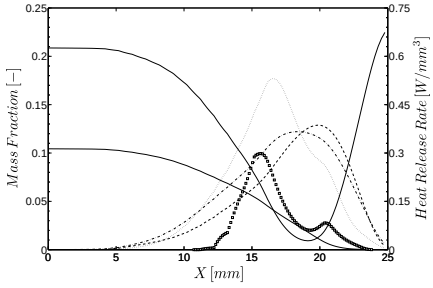

(a) $\Phi = 2.0$

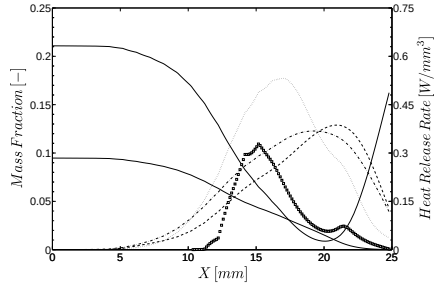

(b) $\Phi = 1.8$

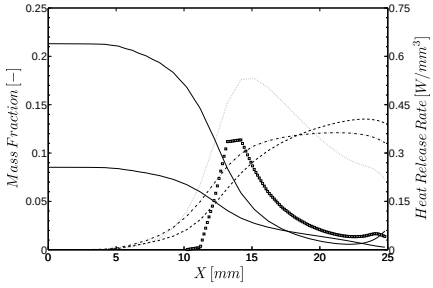

(c) $\Phi = 1.6$

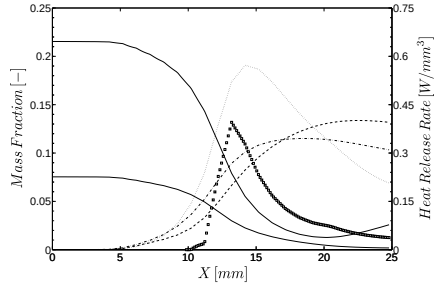

(d) $\Phi = 1.4$

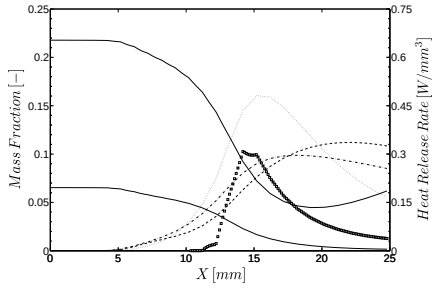

(e) $\Phi = 1.2$

Figure 5.24: Predicted profiles of major species (CH_4: bold solid line, O_2: solid line , CO: dotted line, CO_2: dashed line, H_2O: dash dotted line) and heat release rate (square marker) for different equivalence ratios at 5kW.

5.5.3 Flame Index

In order to understand the structure of the flame, previous investigations regarding partially premixed flames divided the various reaction zones according to their spatial locations. To spatially resolve its various reaction zones more clearly, a flame indicator based on the scalar product of fuel and oxidizer mass fraction gradients was first proposed by Takeno et al [192]:

$$G_{FO} = \nabla Y_F \cdot \nabla Y_O \tag{5.7}$$

where Y_s is the mass fraction of chemical species s. The flame structure corresponds to a premixed flame for $G_{FO} > 0$ and to a diffusion flame for $G_{FO} < 0$. This flame index is useful for distinguishing between the premixed and non-premixed reaction zones. Domingo et al. [193] derived a normalized flame index as:

$$G_{|FO|} = \frac{1}{2}\left(1 + \frac{G_{FO}}{|G_{FO}|}\right) \tag{5.8}$$

This flame index has a value of one and zero in premixed and nonpremixed reaction zones, respectively. Note that the identification of reaction zones is relevant in regions of high reactivity, i.e., where the heat release rates are significant. The flame index therefore was only computed in the spatial locations where the heat release rate is at least 1% of the maximum heat release rate. The use of the modified flame index to identify different reaction zones in a partially premixed flame is illustrated in Fig. 5.25 for different equivalence ratios at the input power of 3kW. The green and blue surfaces in this figure correspond to premixed and diffusion flames, respectively. In this visualization, it is possible to highlight four flame elements: (1) a leading edge of the flame at the bottom, (1) a leading edge of the flame at the top, (3) an inner rich premixed flame, and (4) an outer diffusion flame island. As the equivalence ratio is reduced the outer diffusion flame changes more significantly. At the condition for $\Phi = 1.4$, the flame index contours clearly indicate the lift-off of the bottom leading edge of the flame. When the flame at the bottom leading edge is completely extinguished, the unburned fuel-air mixture flows downstream as a fuel jet entraining the surrounding air to produce a premixed flame in the downstream flow. This premixed flame remains attached to the cap of the burner because of the presence of the pilot flame. Therefore, the partially premixed flames exhibit a double flame structure for all equivalence ratios except for $\Phi = 1.2$, where the presence of only the green contour indicates the premixed nature of the flame. Further evidence of the transition of the double flame is provided in Fig. 5.26 and Fig. 5.27, which present the modified flame index contours for different equivalence ratios at the input power of 4kW and 5kW, respectively. As for the 3kW flames, all the four flame elements are still present in 5.26, but in the case of higher power input, the flame starts to lift off at $\Phi = 1.6$ (Fig. 5.26(c)). Subsequently, by further decreasing,

the quenching of the flame edge at the bottom occurs and the transition to a premixed flame pushed downstream can be observed (Fig. 5.26(d) and 5.26(e)). Similarly, Fig. 5.27 shows the same trend exhibited by the flame at lower power. However, for a higher power input, the flame lift-off occurs at a higher equivalence ratio, $\Phi = 1.8$, and the leading edge of the flame at the bottom can be considered completely detached from the burner wall at $\Phi = 1.6$.

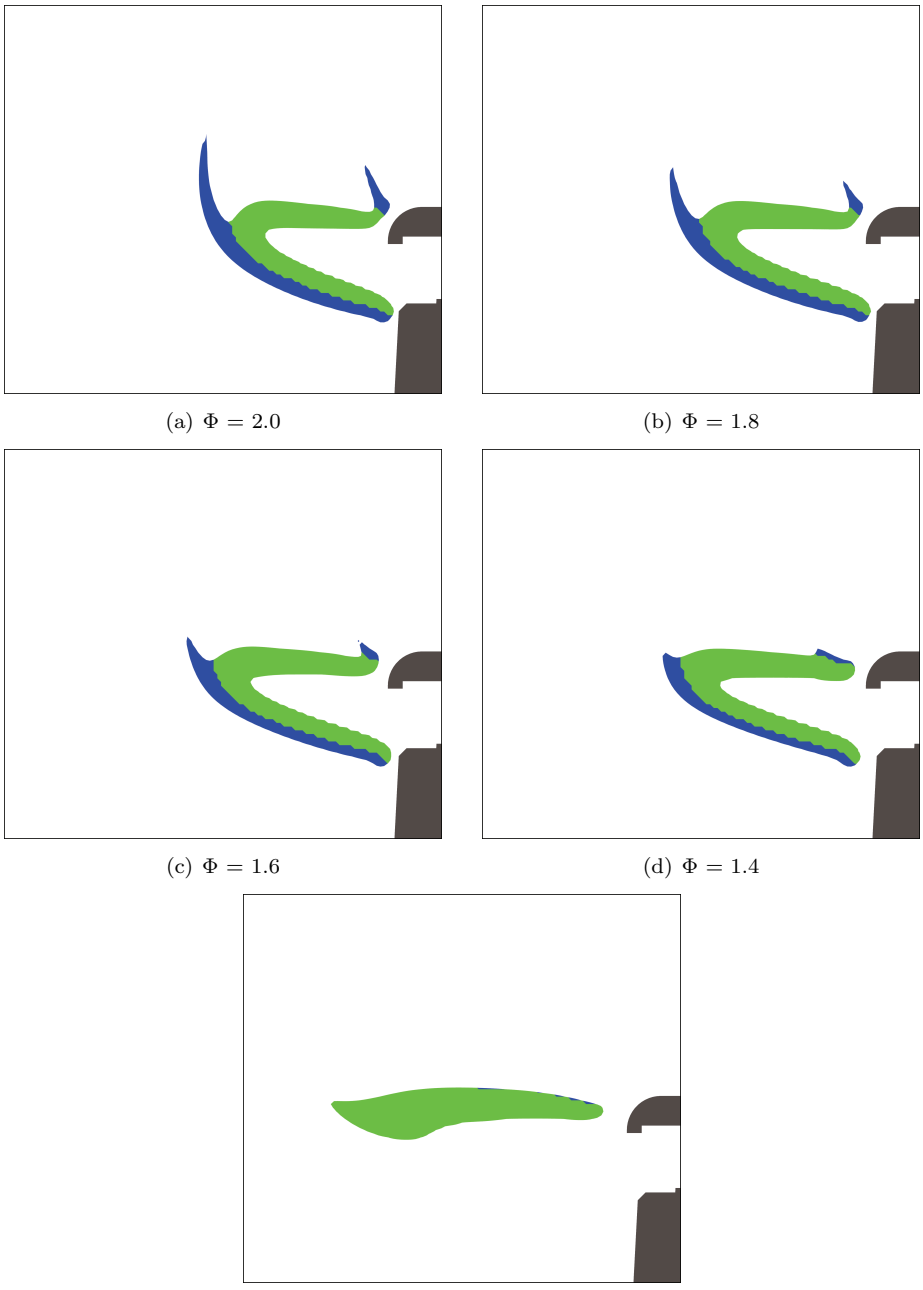

(a) $\Phi = 2.0$

(b) $\Phi = 1.8$

(c) $\Phi = 1.6$

(d) $\Phi = 1.4$

(e) $\Phi = 1.2$

Figure 5.25: Modified flame index for 3kW partially premixed flames at different equivalence ratios; green and blue surfaces correspond to premixed and diffusion flames, respectively.

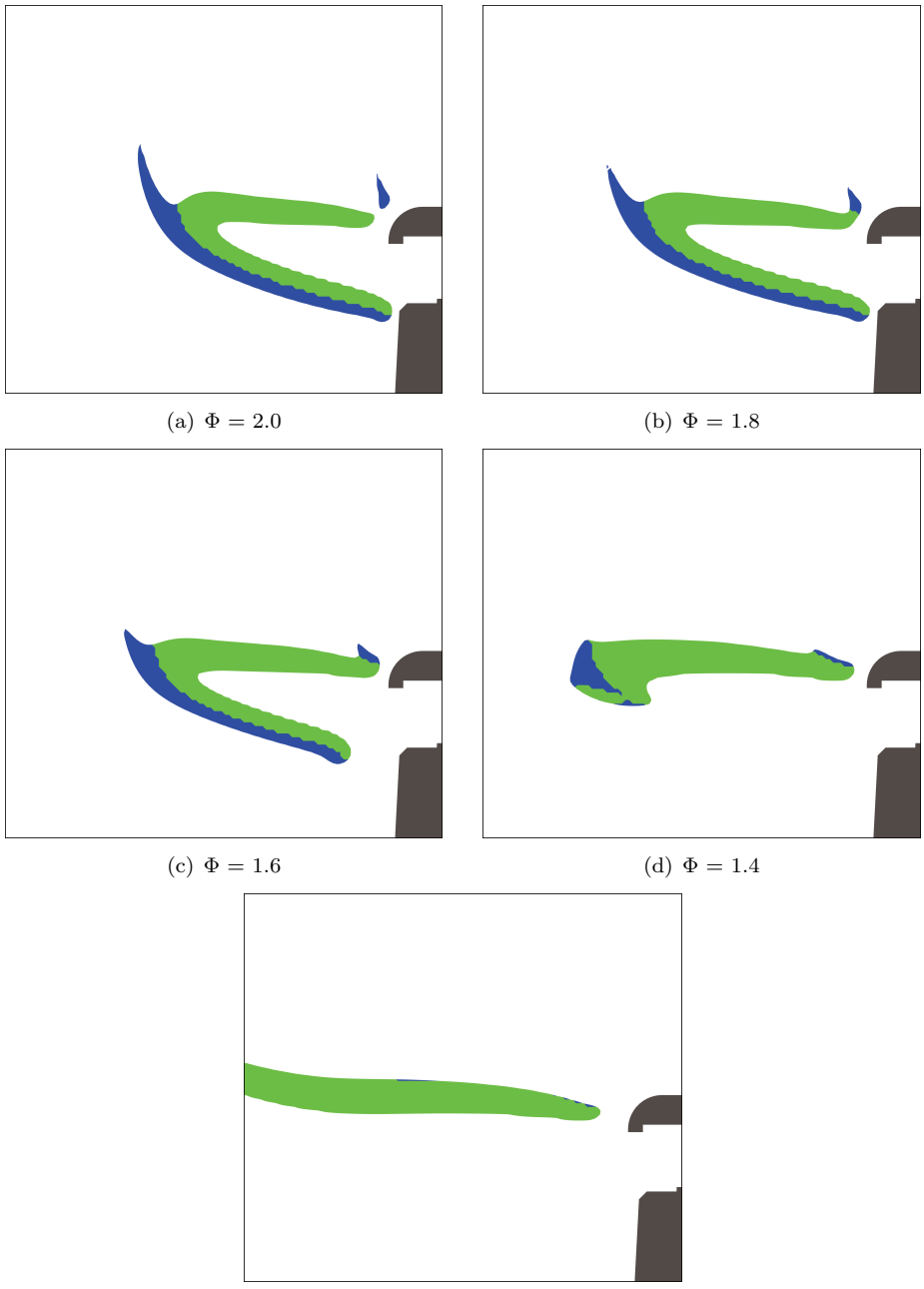

(a) $\Phi = 2.0$ (b) $\Phi = 1.8$

(c) $\Phi = 1.6$ (d) $\Phi = 1.4$

(e) $\Phi = 1.2$

Figure 5.26: Modified flame index for 4kW partially premixed flames at different equivalence ratios; green and blue surfaces correspond to premixed and diffusion flames, respectively.

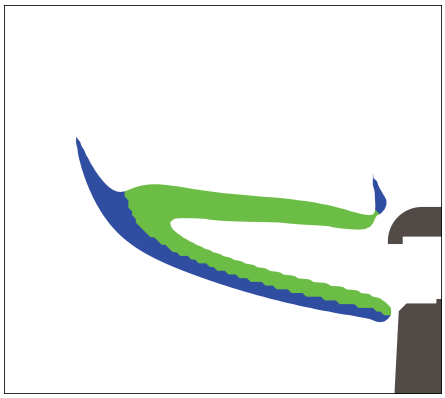

(a) $\Phi = 2.0$

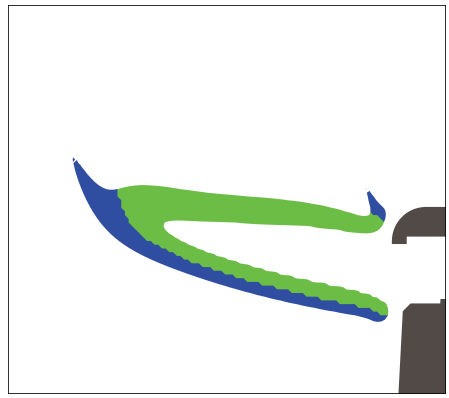

(b) $\Phi = 1.8$

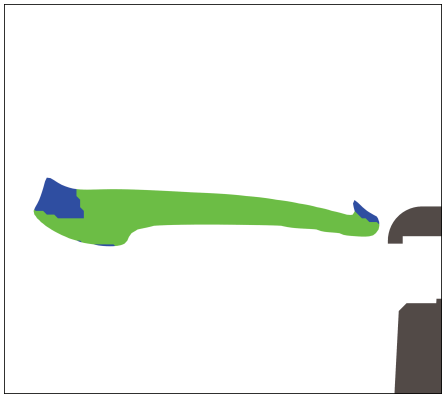

(c) $\Phi = 1.6$

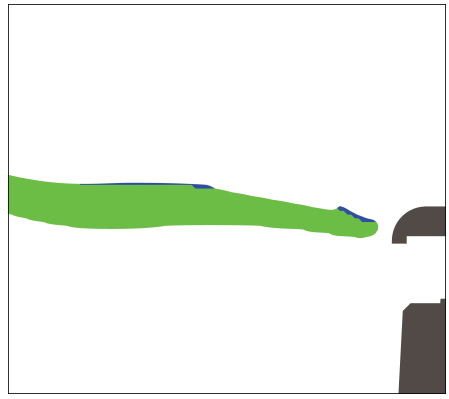

(d) $\Phi = 1.4$

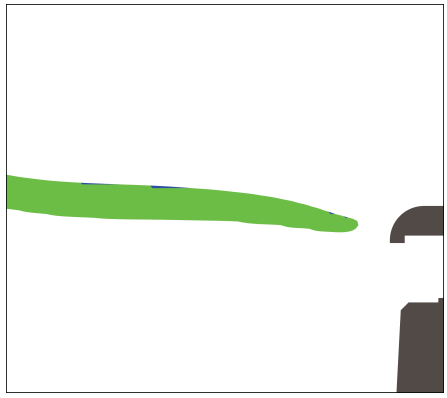

(e) $\Phi = 1.2$

Figure 5.27: Modified flame index for 5kW partially premixed flames at different equivalence ratios; green and blue surfaces correspond to premixed and diffusion flames, respectively.

5.5.4 Mixture and Volume Fraction

In a partially premixed system, the weigh of the reactant is generally specified by means of fractions. In this investigation two definitions are presented: the mixture fraction and the volume fraction. The mixture fraction is a conserved scalar that represents the mixing state of the reacting flow system. Consider a partially premixed methane-air flame in which the mole fractions of the following species are predicted by the finite volume model: CH_4, CO, O_2, CO_2, H_2O and N_2. The mixture fraction ξ can therefore be expressed in terms of the mole fractions of the measured species. This quantity is defined as a linear combination of the elemental mass fractions on the basis of the formula suggested by Bilger [194]. Although there is no unique definition of the mixture fraction for multicomponent systems due to differential diffusion, the definition suggested by Bilger captures the stoichiometric lines properly. Therefore, the sum of the mass fractions of the carbon, hydrogen and oxygen associated with each species, yields

$$\xi = \frac{2Z_C/MW_C + 0.5Z_H/MW_H + (Z_{O,2} - Z_O)/MW_O}{2Z_{C,1}/MW_C + 0.5Z_{H,1}/MW_H + (Z_{O,2} - Z_{O,1})/MW_O} \tag{5.9}$$

where MW_i represents the molecular weight of the element i and Z_i indicates the mass fraction of the element i (C, H and O refer to carbon, hydrogen, and oxygen, respectively) and the subscripts 1 and 2 refer to the fuel and oxygen reference states. Substituting for the mass fractions:

$$Z_C = \frac{MW_C \cdot Y_{CH_4}}{MW_{CH_4}} + \frac{MW_C \cdot Y_{CO}}{MW_{CO}} + \frac{MW_C \cdot Y_{CO_2}}{MW_{CO_2}} \tag{5.10}$$

$$Z_H = \frac{4MW_H \cdot Y_{CH_4}}{MW_{CH_4}} + \frac{2MW_H \cdot Y_{H_2O}}{MW_{H_2O}} \tag{5.11}$$

$$Z_O = \frac{MW_O \cdot Y_{H_2O}}{MW_{H_2O}} + \frac{MW_O \cdot Y_{CO}}{MW_{CO}} + \frac{2MW_O \cdot Y_{CO_2}}{MW_{CO_2}} \tag{5.12}$$

The fuel and air sides are indicated by $\xi = 1$ and $\xi = 0$, respectively. For the non premixed methane-air flames, the stoichiometric value of the mixture fraction, ξ_s, is equal to 0.055 [194]; for partially premixed flames the mixture fraction reaches stoichiometry when the reactants are completely consumed; it varies therefore with the equivalence ratio, and can be expressed by:

$$\xi_s = \frac{Z_{O,2}/MW_O}{2Z_{C,1}/MW_C + 0.5Z_{H,1}/MW_H + (Z_{O,2} - Z_{O,1})/MW_O} \tag{5.13}$$

On the other hand, another definition that is commonly adopted by domestic gas burner designers is based on the volume fraction or volume concentration. By considering Eq. 1.3, another volume fraction formulation can be introduced. C_{vol} can be computed locally from the mass fraction Y_i as follows:

$$C_{vol} = \frac{\frac{Y_{CH_4}}{MW_{CH_4} \cdot P_s/T}}{\frac{Y_{CH_4}}{MW_{CH_4} \cdot P_s/T} + \frac{Y_{O_2}}{MW_{O_2} \cdot P_s/T} + \frac{Y_{N_2}}{MW_{N_2} \cdot P_s/T}} \tag{5.14}$$

where P_s is the local pressure [Pa] and T the local temperature [K]. The stoichiometric value of C_{vol} does not change with the equivalence ratio, and always corresponds to 0.092. The above mixture fraction and volume fraction account for important effects of stoichiometry and flame stretch in linking the turbulent flame structure to that of laminar flame. Therefore, in this work an investigation concerning the volume fraction is performed in order to highlight flame structure parameters such as the flame double point. The double point at the flame base is defined as the location of the intersection of the stoichiometric volume fraction surface and the flame surface. The location of this point acts as an indicator of the stabilization mechanism of lifted flame in the near field of domestic gas burner flame ports. As indicated in Fig. 5.28 for the input power of 3kW, as the level of partial premixing is increased, the double point position remains nearly constant until flame lift-off occurs at $\Phi = 1.4$; subsequently the blowout condition is reached at Φ =1.2. In the same manner, Fig. 5.29 shows the double point positions for the 4kW input power. As mentioned above, in order to achieve the same equivalence ratios of the 3kW configuration, the increase in the mass flow rate causes the flame lift-off to occur at a higher equivalence ratio. The flame lift occurs now at $\Phi = 1.6$, followed by an increase in the liftoff height (Φ =1.4) and by the consequent detachment of the leading edge of the flame at the bottom (blow-out at $\Phi = 1.2$). For the 5kW case, the double point seems to indicate flame liftoff at $\Phi = 1.8$; the flame then abruptly moves away from the burner surface (Φ =1.6) as depicted in Fig. 5.30. At this input power the condition $\Phi = 1.4$ represents an almost complete blowout of the flame because the two iso-contours intersect each other weakly. Moreover, according to the predictions shown in the context of Fig. 5.28-5.30, the blow-off instability can be pointed out when the flame surface iso-contour and the stoichiometric volume fraction iso-contour do not intersect each other (i.e. $\Phi = 1.2$ for the all input powers). However, the present investigation focuses on methane, which has a Schmidt number smaller than one. Therefore, by following the double point location, a lifted flame is observed only in the near field:therefore the non-existence of a stationary lifted flame in the far field of a coflow jet (burner ports) for Schmidt < 1 is confirmed [38, 78, 195]. Therefore, the Schmidt number of the fuel plays a crucial role in the existence of lifted flames in laminar jets: stationary lifted flames cannot exist for Schmidt < 1. Consequently, the flame could blow off directly from the port as the jet velocity increases. This situation is avoided by means of the pilot flame that keeps the upper flame attached to the burner crown. Otherwise, the presence of a stationary flame would be seriously compromised, as indicated by the behavior of the leading edge of the flame at the bottom. In addition to the various double point positions observed in Fig. 5.28-5.30, it can be also observed that the CO profile becomes broader and it gradually shifts downstream as the level of partial premixing is increased. This is due to the increased mass flow rate through the burner ports, as discussed in the context of Fig. 5.22-5.24.

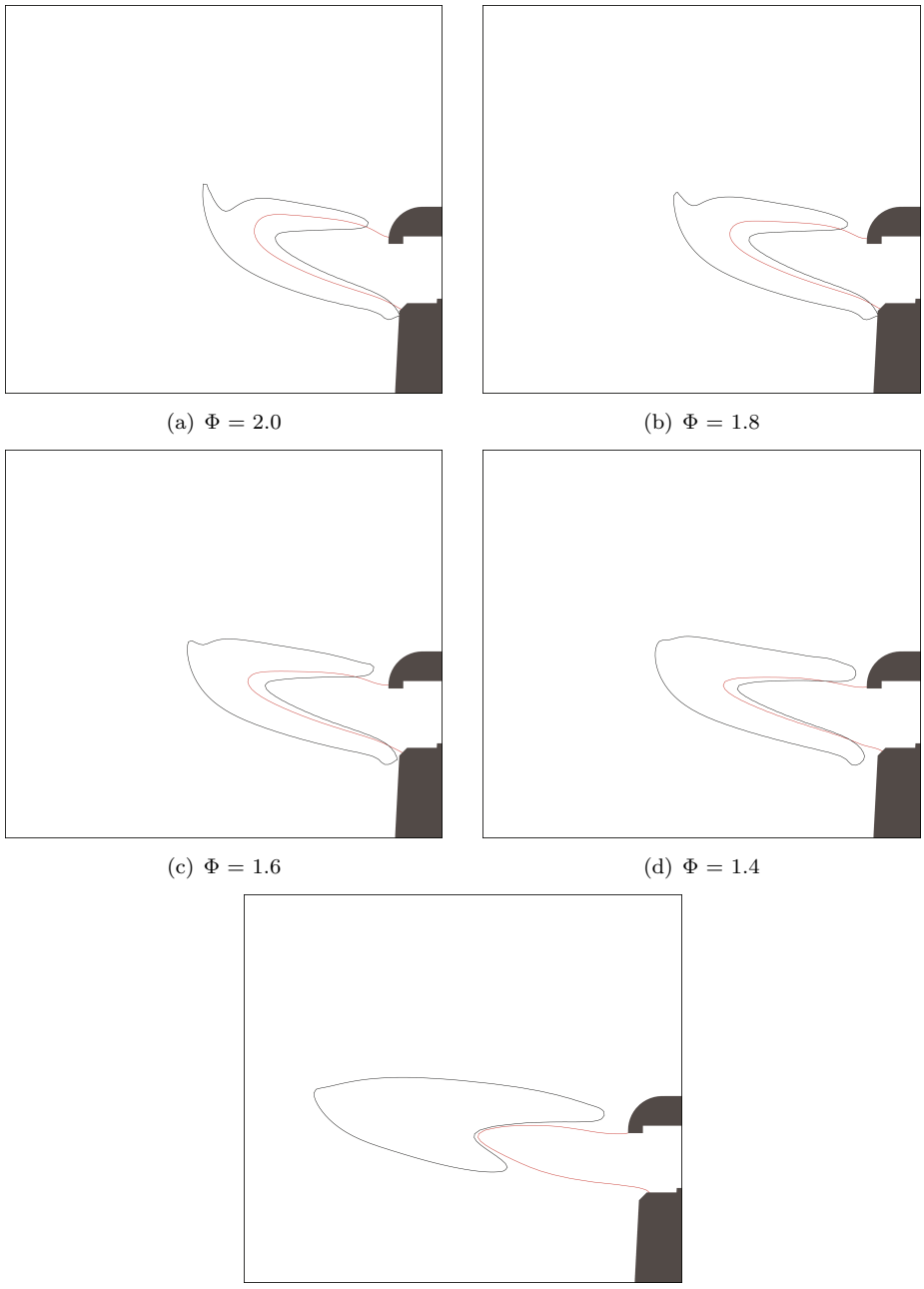

(a) $\Phi = 2.0$

(b) $\Phi = 1.8$

(c) $\Phi = 1.6$

(d) $\Phi = 1.4$

(e) $\Phi = 1.2$

Figure 5.28: Volume fraction iso-contours at $C_{vol} = 0.0952$ (red line) and CO iso-contour at $Y_{CO} = 0.004$ (black line), for different equivalence ratios at 3 kW.

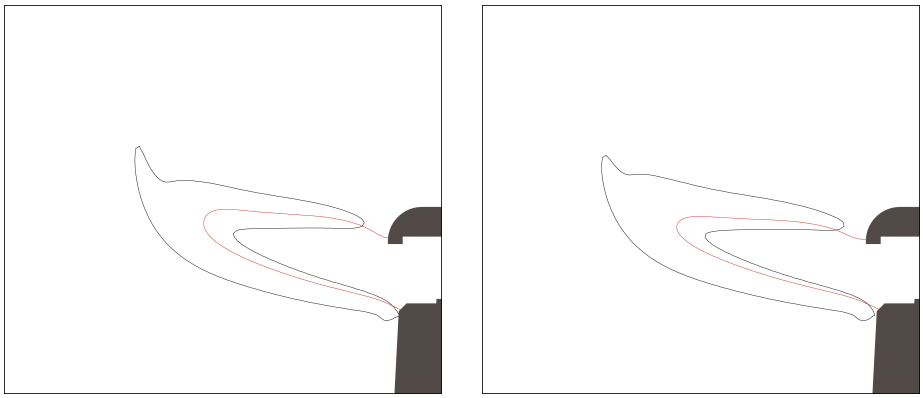

(a) $\Phi = 2.0$

(b) $\Phi = 1.8$

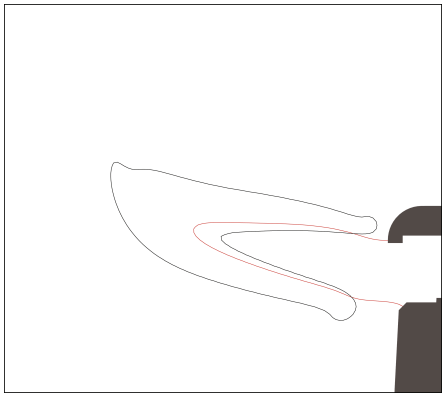

(c) $\Phi = 1.6$

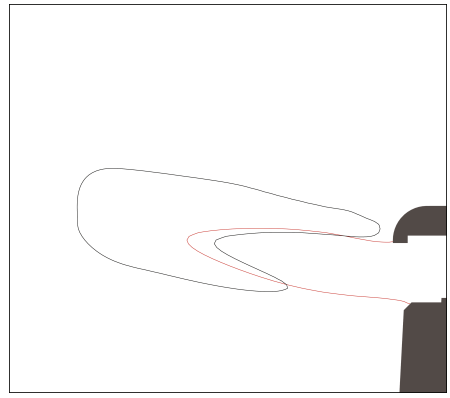

(d) $\Phi = 1.4$

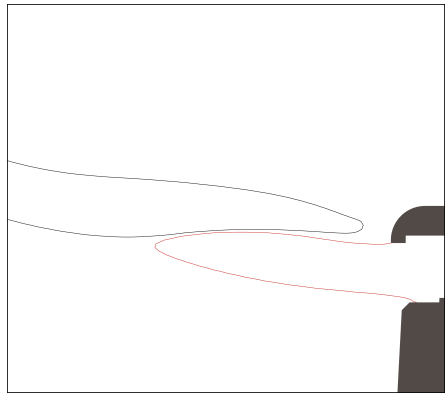

(e) $\Phi = 1.2$

Figure 5.29: Volume fraction iso-contours at $C_{vol} = 0.0952$ (red line) and CO iso-contour at $Y_{CO} = 0.004$ (black line), for different equivalence ratios at 4 kW.

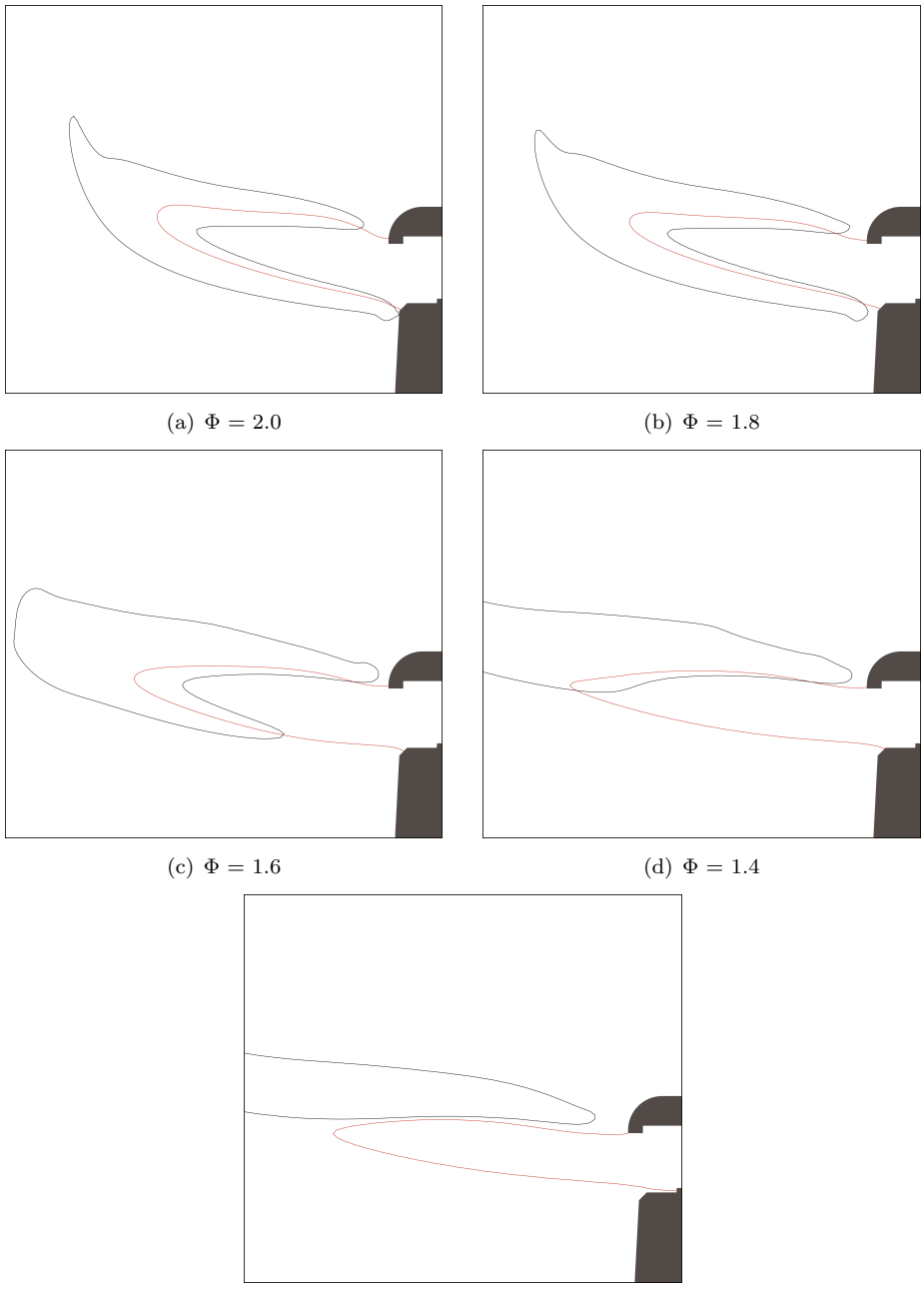

(a) $\Phi = 2.0$ (b) $\Phi = 1.8$

(c) $\Phi = 1.6$ (d) $\Phi = 1.4$

(e) $\Phi = 1.2$

Figure 5.30: Volume fraction iso-contours at $C_{vol} = 0.0952$ (red line) and CO iso-contour at $Y_{CO} = 0.004$ (black line), for different equivalence ratios at 5 kW.

In order to achieve a better understanding of the role of the flame bottom edge in the flame lift-off instability, it is possible to present the partially premixed flame in terms of heat release rate contours, streamlines and volume fraction contours. Fig. 5.31-5.33 shows these quantities for different equivalence ratios at 3kW, 4kW and 5kW respectively. These contours show a common trend: in all of them, the position of the leading edge of the flame at the bottom is determined by the balance among reaction, upstream diffusion and convection. The flame edge represents the maximum reaction zone intensity and heat release rate. Therefore, as suggested by Takahashi [81], the flame stabilizes at the location of the highest reactivity. Therefore the edge of the flame lies close to the stoichiometric volume fraction iso-surface, where the effective reaction time is minimum due to higher flame temperatures [196]. At blow-off condition this reaction kernel at the flame base disappears. Moreover, before the reaction zone, the unburned gas particles change flow direction, from the initial radial one to outward directions. Of course, by decreasing the equivalence ratio there is less turning of the streamlines due to the combined effect of the increasing mass flow rate and increasing density (decreasing temperature) of the unburned flow imposed as boundary conditions. Therefore the flame becomes more symmetric with respect to the stoichiometric volume fraction iso-contour. In the same way, for a fixed equivalence ratio, increasing the input power (Fig. 5.31-5.33) implies a higher mass flow rate through the burner flame ports, that nose down the streamlines. Obviously, changing the inlet parameters (i.e. mass flow rate and equivalence ratio) leads to a different spatial location of the flame. The lean and rich flammability limits for a methane-air premixed flame correspond to volume fraction values of 0.05 and 0.15 respectively. For the flames discussed in this investigation it is possible to show that the rich flammability limit gradually moves upstream as the equivalence ratio is decreased until it disappears inside the flame port, as depicted in Fig. 5.31-5.33 (from $\Phi = 1.6$). Similarly, the lean flammability limit moves closer to the burner surface as the partial premixing is increased. This indicates that less secondary air is needed to complete combustion. However, as partial premixing increases, the heat release rate increases on the inner flame front, whereas it decreases on the outer flame front. This trend can be observed in Fig. 5.31-5.33, and it was also reported in previous investigations [161].

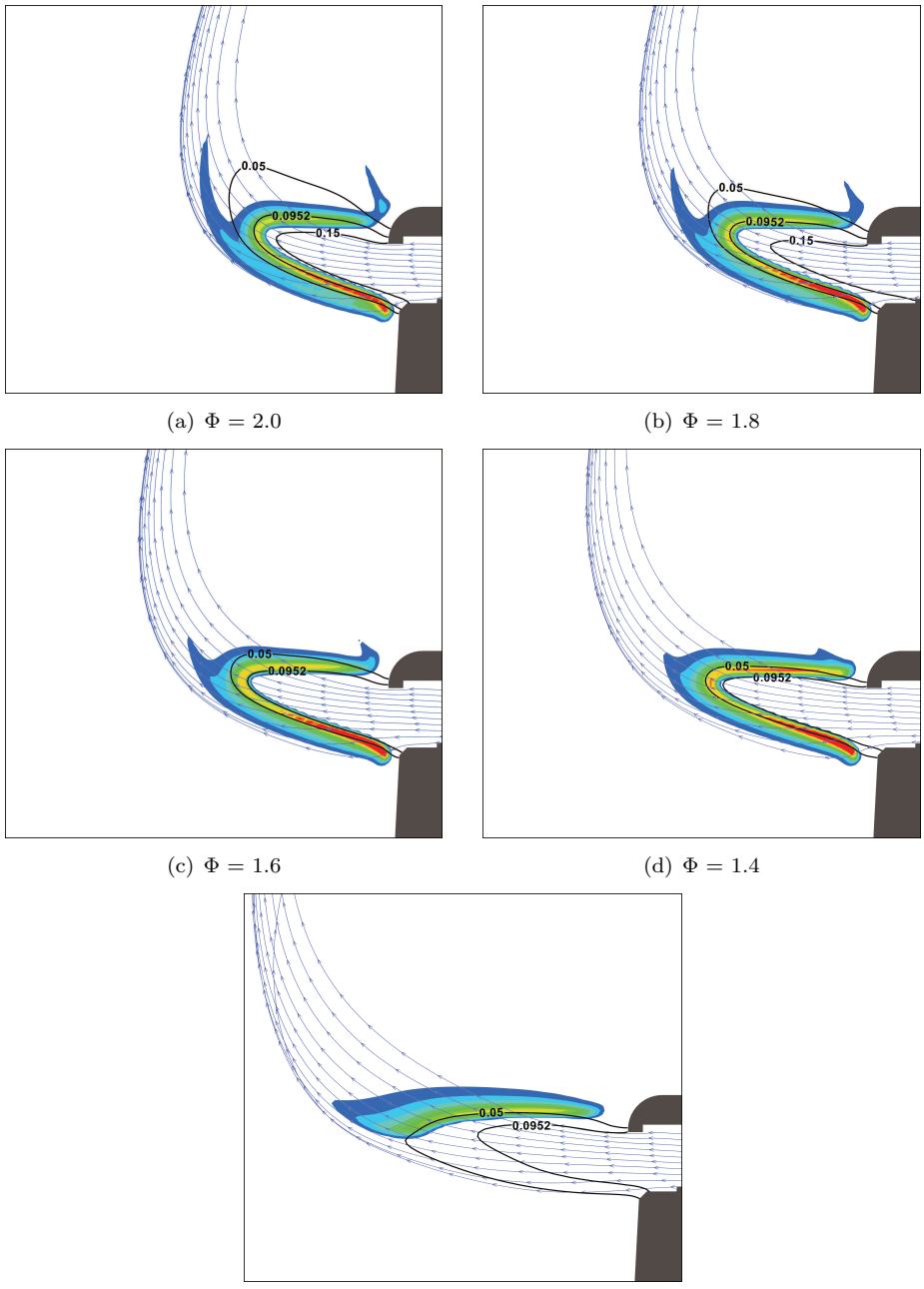

(a) $\Phi = 2.0$ (b) $\Phi = 1.8$

(c) $\Phi = 1.6$ (d) $\Phi = 1.4$

(e) $\Phi = 1.2$

Figure 5.31: Computed heat release rate contours (rainbow scheme), volume fractions iso-contours (black lines) and flow field streamlines (blue lines) for different equivalence ratios at 3kW.

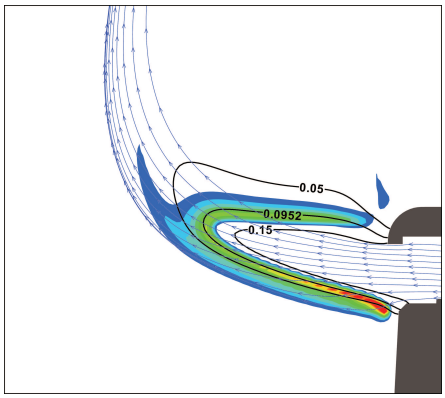

(a) $\Phi = 2.0$

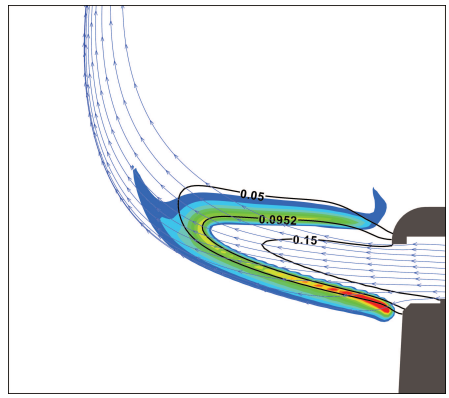

(b) $\Phi = 1.8$

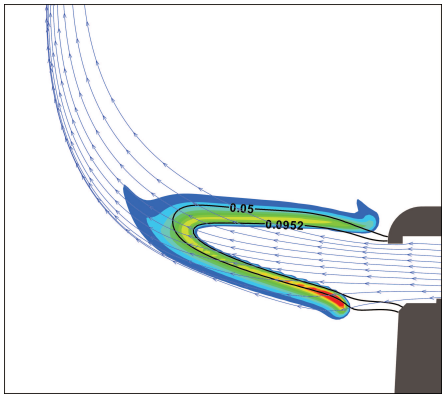

(c) $\Phi = 1.6$

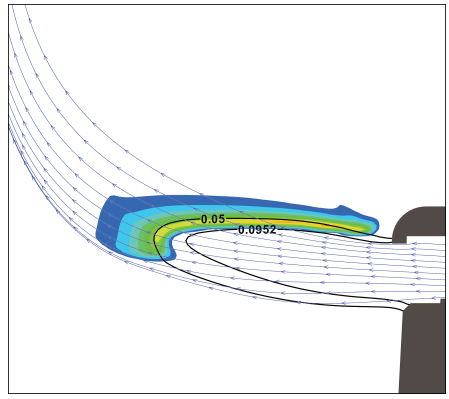

(d) $\Phi = 1.4$

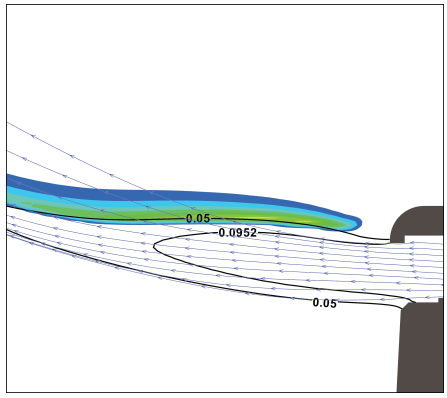

(e) $\Phi = 1.2$

Figure 5.32: Computed heat release rate contours (rainbow scheme), volume fractions iso-contours (black lines) and flow field streamlines (blue lines) for different equivalence ratios at 4kW.

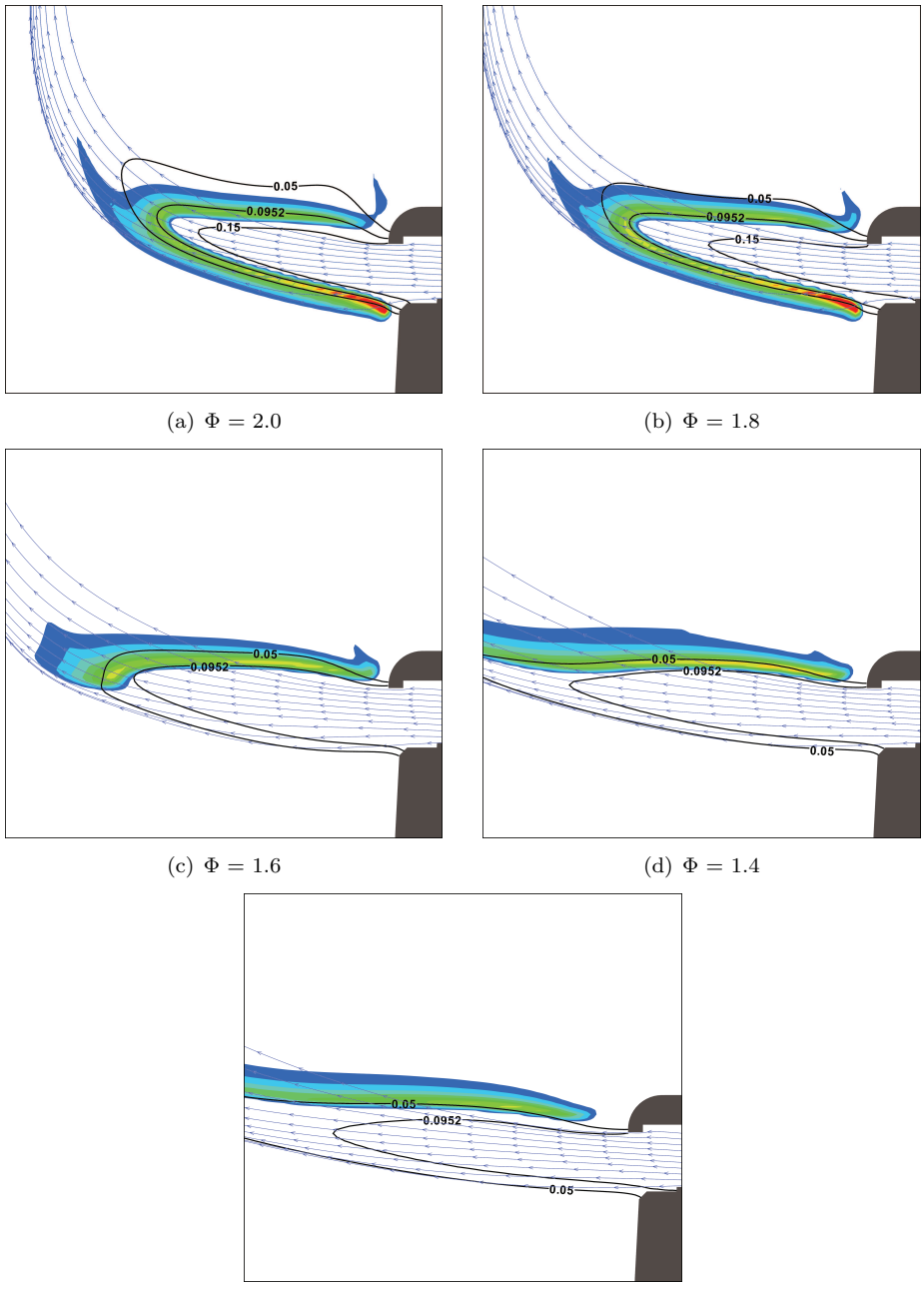

(a) $\Phi = 2.0$ (b) $\Phi = 1.8$

(c) $\Phi = 1.6$ (d) $\Phi = 1.4$

(e) $\Phi = 1.2$

Figure 5.33: Computed heat release rate contours (rainbow scheme), volume fractions iso-contours (black lines) and flow field streamlines (blue lines) for different equivalence ratios at 5kW.

5.5.5 Flame Stretch

Chemical reactions, convection and diffusion are the factors that affect the structure and propagation of laminar premixed flames. In order to understand the influence of these phenomena, early investigations moved in two directions. The first focused on the aerodynamics of the flame, in which transport and chemistry are not taken into account. Therefore, the flame is treated as a structurless surface with a given constant speed. According to the composition of the mixture, this surface releases a specific amount of heat, which is passively convected by the surrounding flow field. In contrast, the second approach focused on the study of the flame structure allowing for transport and chemical processes. Such analyses usually kept the aerodynamic description at the simplest level. One of the main results reached by this approach is the speed at which the flame propagates, which represents the constant flame speed needed by the aerodynamic analysis. Of course, the influence of aerodynamics on the characteristics of premixed flames was recognized quite early. In particular, flame instability phenomena, such as lift-off and blow-out, are profoundly affected by the surrounding flow field, and cannot be described if the flame is characterized by an imposed constant flame speed. According to previous studies, two important parameters to characterize the flow field and mixing effects are scalar dissipation rate and flame stretch. The scalar dissipation rate represents the degree of scalar mixing and is commonly used in describing the behaviour of diffusion flame. The flame stretch is a more direct indicator of the convective flow strain and is used to characterize premixed flame propagation and structure response to an external flow. In response to these concerns, the concept of flame stretch was introduced. This is an important characteristic of flame behavior that arises because of the combined effects of aerodynamic strain rate and flame curvature. The flame stretch formally comprises individual or collective contributions of aerodynamic straining (non-uniform flow along the flame), flame curvature, and flame/flow unsteadiness. These influences are particularly strong in the presence of mixture nonequidiffusion because of the resulting modification of the flame temperature. Moreover, it is well known that stretch has a profound effect on the local flame speed through the coupled effects of unequal heat and mass diffusion. In the case of a premixed reaction zone, the flame stretch influences the propagation speed and stabilization, the reaction front instabilities, flammability limits, and the reaction zone temperature [197]. Theoretical studies of stretched laminar premixed flames are an important part of combustion theory and provide an improved understanding of the phenomena of premixed combustion. Historically, the concept of flame stretch was proposed by Karlovitz, who first introduced it with other authors in a phenomenological description of flame quenching by strong velocity gradients (nonuniform flow fields) [62]. He was followed by several pioneering investigators like Lewis and von-Elbe [65] and Markstein [198]. In order to describe the observed flamefront cellular instability phenomenon, Markstein allowed the flame speed to vary with the flame

curvature. Therefore, he first proposed a linear relation between flame speed and flame stretch to address the effect of curvature on flame speed. Subsequently, Williams characterized the flame stretch as the fractional rate of change of an area element on a flame surface [199], whereas Strehlow and Savage defined the flame stretch by assuming an infinitesimally thin hypothetical flame that had a definable preheat zone thickness and a normal burning velocity, which were both invariant with curvature. To obtain a general expression for flame stretch, Buckmaster specified the flame surface in spatial coordinates [200]. Over the years, significant progress has been made in flame theory and in the structure and dynamics of stretched flame. Therefore, Karlovitz's definition of flame stretch as caused by flow nonuniformity has been generalized to include flame curvature and flame/flow unsteadiness. Two main definitions can thus be found in literature: the thin and thick flame approach. In the thin flame methodology the flame is identified with a surface and the flame stretch expression is based on the relation proposed by Matalon [201] and Chung and Law [202]. These formulations are equivalent and are based on a multidirectional flow velocity that is separated in the analyses into normal and tangential components at the flame front. On the other hand, the thick flame (mass-based) approach assumes that the flame surface lies within a reacting zone of finite thickness. The stretch field is thus defined within this flame volume and the expressions concerning the flame stretch are derived by De Goey et al. [203] and De Goey and Boonkkamp [204] based on mass conservation. Therefore, both approaches require the identification of a surface along which the stretch and the flame speed must be evaluated, but in the thick flame definition this surface spans a finite volume. In this work the thin flame approach is used. This approach provides an expression for flame stretch that contains the various factors which contribute to the influence of stretch. In order to demonstrate these stretch sources, the flame stretch will be expressed in terms of the dynamics of a general surface defined by $x(p, q, t)$, as explained in [205, 206]. The evolution of the flame surface is shown in Fig. 5.34, where p and q are the two orthogonal curvilinear coordinates on the surface.

Since the flame surface has a velocity V_{flame}, the instantaneous velocity is expressed by:

$$V_{flame}(p, q, t) = \frac{\partial x(p, q, t)}{\partial t} \tag{5.15}$$

Therefore, at the time $t + \delta t$, the flame surface can be represented as:

$$x(p, q, t + \delta t) = x(p, q, t) + V_{flame}(p, q, t)\delta t \tag{5.16}$$

A general definition of flame stretch at any point on this surface was suggested by Williams [199]:

$$k = \frac{1}{A}\frac{dA}{dt} \tag{5.17}$$

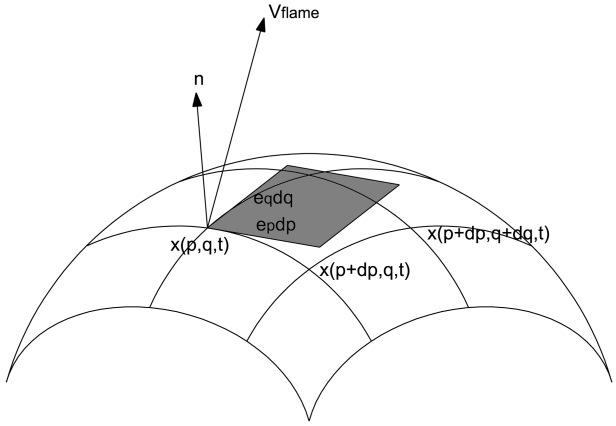

Figure 5.34: Flame surface evolution

where A consists of the points on the flame surface, which have the same normal velocity as the flame surface and the same tangential velocity as the local fluid particles. The elemental area $A(p,q,t)$ of the surface at time t can be approximated as the area of parallelogram on the tangential plane:

$$A(p,q,t) = e_p dp \times e_q dq = (dpdq)\hat{n} \tag{5.18}$$

where e_p and e_q are the unit vectors in the direction of p and q, while $\hat{n} = e_p \times e_q$ is the unit vector of the elemental surface pointed in the direction in which the surface is propagating. Hence the surface area at time $t + \delta t$ becomes:

$$A(p,q,t+\delta t) = \left[e_p + \left(\frac{\partial V_{flame}}{\partial p}\right)\delta t\right] \times \left[e_q + \left(\frac{\partial V_{flame}}{\partial q}\right)\delta t\right] dpdq \tag{5.19}$$

Therefore, with $A = A \cdot n$, the stretch rate can be expressed as:

$$k = \frac{1}{A(t)} \lim_{\delta t \to 0} \frac{A(t+\delta t) - A(t)}{\delta t} = \left[e_p \cdot \left(\frac{\partial V_{flame}}{\partial p}\right) + e_q \cdot \left(\frac{\partial V_{flame}}{\partial q}\right)\right] \tag{5.20}$$

Decomposing V_{flame} into its tangential and normal components as:

$$V_{flame} = V_{flame,t} + (V_{flame} \cdot \hat{n})\hat{n} \tag{5.21}$$

yields:

$$\left(\frac{\partial V_{flame}}{\partial p} \times \frac{\partial x}{\partial p}\right)\hat{n} = \left[\frac{\partial V_{flame,t}}{\partial p} \times \frac{\partial x}{\partial p} + (V_{flame} \cdot \hat{n})\frac{\partial \hat{n}}{\partial p} \times \frac{\partial x}{\partial p} + \frac{\partial}{\partial p}(V_{flame} \cdot \hat{n})\hat{n} \times \frac{\partial x}{\partial p}\right] \cdot \hat{n} \tag{5.22}$$

Hence,

$$\left(\frac{\partial V_{flame}}{\partial p} \times \frac{\partial x}{\partial p}\right) \hat{n} = \left[\frac{\partial V_{flame,t}}{\partial p} \times \frac{\partial x}{\partial p} + (V_{flame} \cdot \hat{n}) \frac{\partial \hat{n}}{\partial p} \times \frac{\partial x}{\partial p}\right] \cdot \hat{n} \quad (5.23)$$

Similarly:

$$\left(\frac{\partial V_{flame}}{\partial q} \times \frac{\partial x}{\partial q}\right) \hat{n} = \left[\frac{\partial V_{flame,t}}{\partial q} \times \frac{\partial x}{\partial q} + (V_{flame} \cdot \hat{n}) \frac{\partial \hat{n}}{\partial q} \times \frac{\partial x}{\partial q}\right] \cdot \hat{n} \quad (5.24)$$

Combining Eq. 5.23 and Eq. 5.24 of the above expressions yields:

$$\left[\left(\frac{\partial V_{flame,t}}{\partial p} \times \frac{\partial x}{\partial p} + \frac{\partial V_{flame,t}}{\partial q} \times \frac{\partial x}{\partial q}\right) + (V_{flame} \cdot \hat{n}) \left(\frac{\partial \hat{n}}{\partial p} \times \frac{\partial x}{\partial p} + \frac{\partial \hat{n}}{\partial q} \times \frac{\partial x}{\partial q}\right)\right] \cdot \hat{n} \quad (5.25)$$

By using the following identity:

$$a \cdot (b \times c) = b \cdot (c \times a) = c \cdot (a \times b) \quad (5.26)$$

it is thus possible to obtain:

$$\left(\frac{\partial V_{flame,t}}{\partial p} \times \frac{\partial x}{\partial p}\right) \cdot \hat{n} = \left(\hat{n} \times \frac{\partial V_{flame,t}}{\partial p}\right) \cdot \frac{\partial x}{\partial p} = \frac{\partial V_{flame,t}}{\partial p} \cdot \frac{\partial x}{\partial p} \quad (5.27)$$

Other terms can be treated in the same way to give Eq. 5.25 the following form:

$$\left(\frac{\partial x}{\partial p} \cdot \frac{\partial V_{flame,t}}{\partial p} + \frac{\partial x}{\partial q} \cdot \frac{\partial V_{flame,t}}{\partial q}\right) + (V_{flame} \cdot \hat{n}) \left(\frac{\partial x}{\partial p} \cdot \frac{\partial \hat{n}}{\partial p} + \frac{\partial x}{\partial q} \cdot \frac{\partial \hat{n}}{\partial q}\right) \quad (5.28)$$

Hence, the flame stretch becomes:

$$k = \nabla_t \cdot V_{flame,t} + (V_{flame} \cdot \hat{n})(\nabla_t \cdot \hat{n}) \quad (5.29)$$

where ∇_t is the tangential gradient operator over the flame surface. Assuming that the tangential component of V_{flame} is equal to the tangential component of the flow velocity at the flame ($V_{fluid,t}$), the flame stretch becomes:

$$k = \nabla_t \cdot V_{fluid,t} + (V_{flame} \cdot \hat{n})(\nabla_t \cdot \hat{n}) \quad (5.30)$$

The above equation shows the two stretch contributions affecting the flame. The first term represents the influence of the flow nonuniformity along the flame surface. Since $V_{fluid,t} = \hat{n} \times (V_{fluid} \times \hat{n})$, this first term embodies the effects due to flow nonuniformity, through V_{fluid}, and flame curvature through the variation in $\hat{n}$. Furthermore, it exists only if the flow is oblique to the flame surface so that $V_{fluid} \times \hat{n} \neq 0$. This non-orthogonality requirement of $V_{fluid} \times \hat{n} \neq 0$ indicates the importance of diffusive transport in the dynamics of stretched flames because heat and mass diffusion exist in the direction of $\hat{n}$. The second term in Eq. 5.30 represents stretch experienced by a nonstationary flame through V_{flame};

although this flame also has to be curved because $\nabla \cdot \hat{n}$ vanishes otherwise. These three stretch-induced effects can be separately referred to as those caused by aerodynamic straining, flame curvature, and flame motion. Since $\nabla = \nabla_t + \nabla_n$, where ∇_n is the normal component of the gradient operator on the surface and of course $\nabla_n \cdot V_{fluid,t} \equiv 0$. The flame stretch expression can be alternatively expressed as:

$$k = \nabla \cdot V_{fluid,t} + (V_{flame} \cdot \hat{n})(\nabla \cdot \hat{n}) \tag{5.31}$$

where $(\nabla \cdot \hat{n})$ represents the curvature of the flame front. By specifying,

$$V_{fluid,t} = V_{fluid} - (V_{fluid} \cdot \hat{n})\hat{n} \tag{5.32}$$

This gives,

$$\nabla \cdot V_{fluid,t} = \nabla \cdot V_{fluid} - \nabla \cdot [(V_{fluid} \cdot \hat{n})\hat{n}] \tag{5.33}$$

$$\nabla \cdot V_{fluid,t} = \nabla \cdot V_{fluid} - \nabla(\hat{n}\hat{n} \cdot V_{fluid}) \tag{5.34}$$

$$\nabla \cdot V_{fluid,t} = \nabla \cdot V_{fluid} - \hat{n}\hat{n} : \nabla V_{fluid} - V_{fluid} \cdot (\nabla \cdot \hat{n}\hat{n}) \tag{5.35}$$

$$\nabla \cdot V_{fluid,t} = \nabla \cdot V_{fluid} - \hat{n}\hat{n} : \nabla V_{fluid} - (V_{fluid} \cdot \hat{n})(\nabla \cdot \hat{n}) - V_{fluid} \cdot (\hat{n} \cdot \nabla \hat{n}) \tag{5.36}$$

in which obviously, $\hat{n}\hat{n} : \nabla V_{fluid} = \sum_i \sum_j \hat{n}_i \hat{n}_j \frac{\partial V_i}{\partial x_j}$. Hence, the expression for flame stretch becomes:

$$k = \nabla \cdot V_{fluid} - \hat{n}\hat{n} : \nabla V_{fluid} - (V_{fluid} \cdot \hat{n})(\nabla \cdot \hat{n}) + (V_{flame} \cdot \hat{n})(\nabla \cdot \hat{n}) \tag{5.37}$$

$$k = \nabla \cdot V_{fluid} - \hat{n}\hat{n} : \nabla V_{fluid} - [(V_{flame} - V_{fluid}) \cdot \hat{n}](\nabla \cdot \hat{n}) \tag{5.38}$$

The term $(V_{flame} - V_{fluid}) \cdot \hat{n}$ refers to the velocity of the flame surface relative to the fluid. This is defined as the flame Speed S_d. Therefore the flame stretch can be expressed as:

$$k = \nabla \cdot V_{fluid} - \hat{n}\hat{n} : \nabla V_{fluid} - S_d(\nabla \cdot \hat{n}) \tag{5.39}$$

Of course the above expression requires the identification of the flame surface. This expression points out the different sources of stretch a flame is subjected to. The first two terms comprise the strain rate tensor (tangential strain rate), therefore they represent the effect of a non uniform tangential flow field along the flame surface. The term hydrodynamic stretch, k_h, is commonly used to represent them. The last term represents the flame stretch rate due to flame curvature (displacement speed multiplied by the flame curvature) and is commonly named

curvature-induced stretch, k_c. Therefore, determining curvature and stretch requires (i) the identification of a flame surface and (ii) the application of analytical expressions for burning velocity, stretch, and curvature to that surface.
In reality, a flame possesses a finite thickness and a single flame surface has no precise meaning. Still it is possible to identify a particular surface that represents the flame, although admittedly it is difficult to provide a unique definition for a flame surface. Therefore, the definition of the front can be somewhat arbitrary and it is important to realize that the results for the displacement speed or the flame stretch depend on the choice of this surface. Lewis and Von Elbe [65] identified the flame front as the locus of the inflection points of the temperature profile across the flame. However, Mikolaitis, while dealing with stagnation point flame, observed that the definition of the flame surface as the location of the inflection point is not always adequate [207]. Moreover, it seems to be unwise to use the temperature as flame surface quantity because local temperature variations along the flame contours induced by stretch effects may be of interest. Markstein [208], Sivashinsky [209] and Matalon and Matkowsky [210] modeled the flame as a surface of hydrodynamic discontinuity. Williams [48] represented the flame as a level surface of a scalar transport quantity, an approach that has been subsequently adopted by several researchers. Since the flame has a finite thickness in which various layers of individual species exist at different locations, there is ambiguity as to the choice of the particular isoline used to evaluate the displacement speed. While Najm and Wyckoff [211], Najm et al. [182], De Goey et al. [203] and T. Echekki and J. H. Chen [212] used a particular value of the fuel mass fraction to identify the flame surface, Zhong et al. [213] used the mixture fraction to characterize the surface. Im and Chen [214] initially used a mass fraction contour of a product species (water) to describe the flame in their studies on premixed hydrogen-air triple flames; subsequently they adopted a reactant species (oxygen) as flame marker [215, 216]. To define the flame surface in the present investigation, the CO isocontour was selected because it clearly identifies the premixed and diffusive reaction zones, and thus represents a good reaction zone marker. For the purpose of evaluating the double point location, the flame surface is located by the isocontour of the CO mass fraction at $Y_{CO} = 0.004$.
Past research gives no single definition of burning velocity. The common approaches to compute this quantity can be mainly summarized in two formulations: global consumption speed and local displacement speed. The former characterizes the burning velocity as an indicator of the mass flow rate of reactant consumed. The latter defines how rapidly the flame surface will traverse a certain distance. Before discussing these formulations, it should be understood that for any specific flame, these definitions present different magnitudes, and thus are not equal [217, 218]. Therefore, a global consumption speed can be pointed out, S_c, proportional to the total mass flow rate of the reactants $\dot{m}_R$:

$$S_c = \frac{\dot{m}_R}{\rho_R \cdot A_L} \tag{5.40}$$

Here ρ_R is the density of the reactants and AL is defined as the area of unwrinkled flame surface [219]. Of course, to use this formulation it is necessary that all of the reactants should pass trough the flame surface. Moreover, a formulation for local consumption speed can be found in literature [219], stating that to achieve a rapidly propagating flame it is desirable to have a large value of the product of maximum surface density and flame thickness. The local displacement speed is defined by:

$$S_d = (V_{flame} - V_{fluid}) \cdot \hat{n} \tag{5.41}$$

where V_{flame} is the velocity of the flame in the laboratory coordinate system and V_{fluid} is the velocity in the laboratory frame of the gas into which the wave is propagating. The velocities and the normal n are defined to be the values that occur at the flame surface. In the present work the displacement speed formulation is adopted, therefore its derivation is briefly reviewed. On a flame surface that moves with a velocity V_{flame}:

$$\frac{d\varphi}{dt} = \frac{\partial \varphi}{\partial t} + V_{flame} \cdot \nabla \varphi = 0 \tag{5.42}$$

The normal to the flame surface is defined as:

$$\hat{n} = \pm \frac{\nabla \varphi}{|\nabla \varphi|} \tag{5.43}$$

There is some disagreement in literature regarding the direction of the positive normal vector. The generally accepted sign convectionis that the curvature of the flame front, defined as $\nabla \hat{n}$, is considered positive for a flame surface if it is concave toward the unburned side. The sign on the right hand side of Eq. 5.43 is decided by the particular scalar chosen to represent the flame surface. In the present investigation, by using the Eq. 5.42 and Eq. 5.43 it is possible to obtain the relation:

$$V_{flame} \cdot \hat{n} = \frac{1}{|\nabla \varphi|} \frac{\partial \varphi}{\partial t} \tag{5.44}$$

The displacement speed of a flame is defined as the normal component of the speed of the flame front relative to the local fluid velocity, i.e.:

$$S_d = (V_{flame} - V_{fluid}) \cdot \hat{n} = \frac{1}{|\nabla \varphi|} \left(\frac{\partial \varphi}{\partial t} + V_{fluid} \cdot \nabla \varphi \right) \tag{5.45}$$

For stationary flames $\partial \varphi / \partial t = 0$. Consequently, the flame displacement speed is:

$$S_d = \frac{1}{|\nabla \varphi|} V_{fluid} \cdot \nabla \varphi \tag{5.46}$$

This relation thus gives the propagation speed of a progress variable isosurface along its normal, oriented towards the unburnt gas. An alternative expression

for the burning speed can be obtained by using the conservation equation for the transported scalar φ:

$$\frac{d\varphi}{dt} + V_{fluid} \cdot \nabla\varphi = \frac{1}{\rho}[\nabla \cdot (\Gamma_\varphi \nabla_\varphi) + \omega_\varphi] \tag{5.47}$$

In the above equation, Γ_φ represents the diffusion coefficient for the scalar and ω_φ represents the volumetric rate of generation or destruction of the scalar. Substituting the above equation, the resultant expression for flame speed is:

$$S_d = \frac{1}{\rho\,|\nabla\varphi|}[\nabla \cdot (\Gamma_\varphi \nabla_\varphi) + \omega_\varphi] \tag{5.48}$$

This displacement speed is determined by equating the transport equation for a scalar variable with the Hamilton-Jacobi equation for the scalar field, in order to obtain the relative progression velocity of the isoscalar surface. The advantage of using this alternative expression for flame speed is that an identical expression is applicable for both stationary and propagating flames [220]. Moreover, to minimize thermal expansion effects across the flame, a nondimensional density-weighted displacement speed formulation can be defined as in [212]:

$$S_d = \frac{\rho S_d}{\rho_u} \tag{5.49}$$

where ρ_u denotes the density of the unburnt mixture. This density-weighted formulation is used as a measure of the effects of stretch/curvature/preferential diffusion on the flame speed, relative to the laminar flame speed. In addition, the concept of global flame speed at any point in the flow can be used to investigate the effect of heat release on the propagation speed. Since the displacement speed represents the local flame speed and it is important in terms of the chemistry (by determining the rate of chemical reaction), the global flame speed U_f is identified with the propagation of the flame structure as a whole. The difference between the local and global flame speeds is due to the particular flow field that characterizes double and triple flames along the stoichiometric volume fraction iso-contour. As reported by [221], in addition to the rise in velocity throughout the flame, the horizontal (radial) velocity component reaches a minimum before the flame. The mechanism responsible for this difference in velocity is thermal expansion. Due to the heat released by the flame, the component of the velocity perpendicular to the flame increases across the flame surface because of the presence of a high density gradient across the flame front. Therefore the density across the flame decreases and the velocity component perpendicular to the flame has to increase to maintain mass continuity across the flame. On the other hand, the tangential component remains unchanged due to small temperature variations along the flame. The jump in the normal velocity component causes a redirection of the flow toward the stoichiometric volume fraction line. This redirection effect bends the streamlines, which diverge upstream of the flame front, resulting in a decrease

in the flow velocity in front of the flame. The local velocity jump across the flame is strongly related to the local reaction rate, which is, in turn, affected by the local mixture fraction. Therefore, as discussed in the context of Fig. 5.31-5.33, the reason for different streamline patterns as one moves away from stoichiometric conditions can be also attributed to the distribution of the reaction rate along the premixed wing as well as to the increment in the reactants mass flow rate. In the domestic gas burner flame, the redirection in the flow is less pronounced because the reaction rate drops off as one moves along the premixed wing. Therefore the reaction rate drops off quickly moving away from the stoichiometric conditions due to a small mixing thickness. Following [214] and [222] the global flame speed can be expressed as:

$$V_{flame,o} = U_f - U_o \tag{5.50}$$

where $V_{flame,o}$ is the flame velocity, considering a fixed coordinate system, and U_o is the local maximum flow velocity along the stoichiometric volume fraction line upstream of the flame. Similarly, the flame velocity $V_{flame,o}$ can be also defined as:

$$V_{flame,o} = S_d - U_e \tag{5.51}$$

where U_e is the local minimum flow velocity along the stoichiometric volume fraction upstream of the flame front. If the flame were to be stabilized as a lifted flame, $V_{flame,o} = 0$, then:

$$U_f = |U_o| \tag{5.52}$$

$$S_d = |U_e| \tag{5.53}$$

The ratio U_f/S_d is the normalized far field flame speed; it is a function of the Damköhler number (D_a), it decreases as D_a decreases, and is also influenced by thermal expansion [196]. Moreover, in the case of small mixture fraction gradients this ratio is proportional to the square root of the density ratio [214, 221]:

$$\frac{U_f}{S_d} \propto \sqrt{\rho_u/\rho_b} \tag{5.54}$$

where the subscripts u and b refer to the unburned and burned regions of the flows. The displacement speed formulation adopted in this investigation is based on Eq. 5.46. This expression is obtained by tracking a surface of a constant mass fraction that represents the flame reaction zone; therefore one disadvantage of this definition is that the displacement speed depends on the choice of the iso-surface. However, it was observed [223] that the variation in burning velocity is relatively small when the iso-level surface is near the reaction zone.
Poinsot et al. [224] have shown that the increase in displacement speed in a

stretched flame occurs primarily due to hydrodynamic and diffusion effects rather than through effects related to chemistry. Therefore, the use of a two-step global reaction mechanism is here appropriate. Tables 5.2-5.4 provide the values of some relevant properties of the double point for five different equivalence ratios, for heat power equals to 3kW, 4kW and 5kW respectively. In order to maintain the same input power, the fuel flow rate is held constant. Therefore, the reduced equivalence ratio is achieved by increasing the amount of air added to the mixture and the velocity through the domestic gas burner diffuser (V_{in}), and the Reynolds number (R_e) at the flame ports, increase with the partial premixing. These tables also show that the displacement speed (S_d) is smaller than the axial flow velocity V_a. Moreover, S_d gradually increases as the level of partial premixing is increased. However, S_d never becomes equal to V_a. For each heat power configuration, the double flame structure is very clear when V_a is small, but the two flames approach each other as V_a is increased and the duplicity becomes indistinct for a large value of V_a, to give one combined flame structure [225]. In order to obtain a better understanding of this phenomenon, the analysis of the flame stretch is proposed. As the equivalence ratio is decreased, both the hydrodynamic (k_h) and the curvature-induced stretch (k_c), and consequently the total stretch (k), increase considerably. The increase in k_h can be attributed to the increased heat release rate at the flame base, which in turns increases the normal component of flow velocity across the flame front, as reported by [97]. Nevertheless, k_c increases slightly due to the increase in flame curvature. The overall stretch is hence positive and increases as the partial premixing is increased. Therefore, while the total stretch is predominantly due to k_h at high equivalence ratios, both k_h and k_c contribute equally to the total stretch at low equivalence ratios. As a matter of fact, when the flame lifts ($\Phi = 1.4$, $\Phi = 1.6$ and $\Phi = 1.8$ for 3kW, 4kW and 5kW respectively), the flame stretch exhibits an abrupt rise. This is mainly due to the curvature-induced component that has small negative values for a stable attached flame, whereas it reaches high positive values when the flame lifts off. It is worth mentioning that these results are in agreement with those reported by [226] for partially premixed flames. For instance, at higher strain rates, a flame that could otherwise be premixed in character (as discussed in the context of Fig. 5.25-5.27) may not have enough time to form on the fuel side, because the fluid dynamic time scales have become too short. This may also be considered as the "merging" of a premixed flame with a stagnation region diffusion flame. Therefore the premixed flame appears to merge with the diffusion flame due to the curvature effect as also reported by [196].

The fundamental understanding of the partially premixed flame was limited to the knowledge that the flame front instability was primarily convective in nature, and was caused by a dynamic imbalance between the mixture gas velocity and the burning velocity. The reported data also present the flame lift instability as a diffusional and thermal instability, caused by imbalances in the diffusion rates of heat and of the reactant species as the mixture approaches the flame fronts. An

Φ	R_e	V_{in}	V_a	S_d	$\nabla \cdot \hat{n}$	$divV$	k_h	k_c	k
-	-	(m/s)	(m/s)	(m/s)	(mm^{-1})	(s^{-1})	(s^{-1})	(s^{-1})	(s^{-1})
1.2	237	0.761	3.003	-	-	-	-	-	-
1.4	194	0.664	2.779	0.983	1223	199	566	1202	1768
1.6	170	0.593	2.535	0.618	63	205	709	43	752
1.8	151	0.536	2.342	0.435	-296	168	607	-121	487
2.0	134	0.491	2.208	0.339	-453	143	558	-146	412

Table 5.2: Flame characteristics at the double point at 3kW

Φ	R_e	V_{in}	V_a	S_d	$\nabla \cdot \hat{n}$	$divV$	k_h	k_c	k
-	-	(m/s)	(m/s)	(m/s)	(mm^{-1})	(s^{-1})	(s^{-1})	(s^{-1})	(s^{-1})
1.2	342	1.054	4.008	-	-	-	-	-	-
1.4	274	0.887	3.515	2.438	1239	-336	-1221	1811	589
1.6	237	0.791	3.210	1.432	1979	99	601	2835	3436
1.8	209	0.714	2.974	0.449	-9	444	729	-22	706
2.0	188	0.655	2.779	0.310	-380	397	592	-99	493

Table 5.3: Flame characteristics at the double point at 4kW

Φ	R_e	V_{in}	V_a	S_d	$\nabla \cdot \hat{n}$	$divV$	k_h	k_c	k
-	-	(m/s)	(m/s)	(m/s)	(mm^{-1})	(s^{-1})	(s^{-1})	(s^{-1})	(s^{-1})
1.2	427	1.297	4.874	-	-	-	-	-	-
1.4	352	1.109	4.277	-0.634	342	-497	-414	-213	-627
1.6	301	0.987	3.934	0.954	1143	-333	-1056	1034	-22
1.8	266	0.894	3.646	0.642	380	457	816	252	1068
2.0	239	0.819	3.401	0.336	-279	423	674	-63	611

Table 5.4: Flame characteristics at the double point at 5kW

important system parameter which can significantly influence the flame response is expected to be the domestic gas burner flame port, represented by the burner crown exit geometry and its assembly with the lip of the burner cap, because in the neighborhood of this rim the flame is stabilized. The influence can be classified according to the modification in concentration caused by entrainment, aerodynamic stretching and the heat transfer effect.

Concerning the modification in concentration, as a result of the atmospheric entrainment, a fuel-lean mixture is made leaner whereas a fuel-rich mixture is made more stoichiometric. Since diffusional-thermal instability is promoted when the deficient species is also the more mobile one (i.e. lean methane/air mixture), a modification in concentration in the rim region can either enhance or suppress the onset of instability.

Concerning flame stretching, it is noted that the flame segment situated downstream to the burner rim (i.e. flame bottom edge) suffers low or negative hydrodynamic stretch (i.e. compression). A theoretical study by [209] showed that the diffusional thermal instability is suppressed in a positively hydrodynamic stretched flow. Since the flow at the flame bottom edge suffers negative k_h, the onset of instability is expected to be promoted.

Finally, the flame lift instability is promoted in the presence of heat loss. This heat transfer is not simulated in this investigation, but is forced by the temperature boundary condition imposed to the appliance wall.

5.6 Flame lift prediction criteria

The flame lift prediction criteria can be formulated on the basis of different post-processing analyses performed on the numerical results. These investigations are major species concentration profiles along the flame, flame index contours, mixture and volume fraction contours and flame stretch analysis.
In order to achieve a stable flame attached to the appliance rim, the domestic gas burner designer has to ensure that:

- the flame presents a double flame structure;
- the double point represented by the bottom edge of the flame is close to the burner wall;
- the reaction kernel of high reactivity is located at the flame base;
- the flame stretch value at the double point is below a threshold value.

The double flame nature of the flame can be quantitatively highlighted by the major species concentrations along the flame, mainly by looking at the CO mole fraction profiles. The presence of a marked peak followed by a second smaller one denotes two main zones of CO production, and therefore clearly shows the double nature of the flame. Moreover, the same feature can be qualitatively explained by the flame index contour. The presence of the two reaction zones based on their spatial location zones identifies the double flame nature of the flame.
The spatial location of the bottom edge of the burner flame characterizes the tendency of the flame to lift. The closer the double point distance is to the wall, the greater is the possibility for the flame to remain attached to the burner rim. The position of the double point at the flame base is defined as the location of the intersection of the stoichiometric volume fraction surface and the flame surface. Among several configurations, the designer can thus post-process the numerical simulation result, and screening between the different double point positions, can choose the one closest to the wall as an indicator of a lower risk geometry.
The flame edge represents the maximum reaction zone intensity and heat release rate. This high reactivity kernel provides radicals and serves as flame stabilization. In order to ensure the constant presence of this kernel on the leading edge of the flame at the bottom, the heat release rates contour with superimposed volume fraction isolines and streamlines can be analyzed.
Finally, the analysis of the flame stretch at the double point can indicate a threshold value from which to judge quantitatively the onset of the flame lift instability. For the domestic gas appliance analyzed in this work, characterized by mass flow rates and temperatures different from the traditional gas burner (i.e. gaseous mixture generated by the mixing process due to the fuel jet entrainment), the flame stretch value k should be kept below 700 s^{-1} to avoid the risk of flame lift. Therefore the numerical tool can provide a better insight into the flame lift phenomenon by means of different post-processing techniques. In this way useful

guidelines can be defined for the design of practical devices aiming to achieve a more stable operation with the $G20$ working fluid.

Concluding remark and outlook

Flame stability is an essential part of the operation of all domestic burners. In this work an experimental and numerical investigation was performed on gas-fired cooktops, in which special attention was given to the prediction of two flame instabilities: flame back and flame lift. A flame issuing from a domestic gas burner port can be stabilized between two limiting values of the gas flow rates. The stability range of the flame of a domestic appliance is therefore known to be limited by the influence of the fresh gases trough the flame ports on the critical flow velocity. When the flow rate of the gas falls below a certain minimum threshold value, the flame is not capable of anchoring itself to the burner rim and moves into the burner. This minimum threshold value of the gas flow rate is known as the flashback limit. On the other hand, when the gas flow rate exceeds a certain maximum value, the flame gets detached from the burner ports. This phenomenon is called the lift off of the flame. On the other hand, if the gas flow rate is increased further, a threshold value is reached at which the flame may leave the domain of interest. This maximum value of the gas flow rate is known as the blowoff limit. Due to the complex flow field that characterizes the appliance and drives its performances, the prediction criteria associated with these instabilities were analyzed by means of numerical simulations. A commercial finite volume code was used in association with unstructured grids to provide RANS based simulations. The turbulence model adopted is a standard k-E with low Reynolds approach. The simulation of the combustion is only applied in the analysis of the flame lift instability and the proposed model is a variation of the Eddy Break Up combustion model, i.e. the combined time scale approach. In order to validate the appliance virtual prototype, a preliminary investigation was carried out on the internal fluid dynamics of the gas stove. Different experimental measurements were performed in order to point out the agreement with the numerical prediction and to calibrate the simulation code properly.

The capacity of CFD to simulate the internal fluid dynamics of the domestic gas burner correctly was analyzed by checking the volume flow rate of the gas through different injectors and the pressure recovery on the radial diffuser of the burner crown. The numerical error of the prediction of these quantities was verified to be always less than 5%. However, the pressure prediction concerning the stagnation region on the burner cap always shows the worst agreement with

the experimental data, due to the overestimation of the turbulent kinetic energy. A further validation was carried out by comparing the numerical results with a set of data obtained in a previous research by planar PIV performed in the flow region outside the flame port using non reactive flows. A good agreement is observed; however, the primary flame ports are always overestimated by the numerical model, whereas the small flame ports are underestimated. This unbalance in the prediction of the numerical velocity profiles is emphasized in the simulations adopting a lighter mixture, probably due to a non-optimized setting of turbulence parameters at the inlet boundary. Furthermore, the comparison between the main flame port and the flame port velocity profiles for the three different burner crowns showed that the velocity out of the secondary flame ports, can be correlated with the flame back effect, verifying that this flame instability can be predicted by means of an investigation in cold conditions. The possibility of predicting the flame back phenomenon in the domestic gas burner without involving the combustion process goes to support the mainly aerodynamic origin of this instability. Unluckily, the velocity out of the flame ports does not describe the flame lift phenomenon in cold conditions. In this case the combustion process must be taken into account.

In order to achieve a better understanding of the flame back instability, a post-processing investigation of an experimental plan based on DoE was performed. The DoE was experimentally carried out by Electrolux to highlight the different fluid dynamic behaviour due to the different geometric dimensions of the domestic gas burner crowns. This experimental plan was performed numerically in order to correlate the direct observation of the flame back with the numerical predictions. As pointed out in literature, the flame back instability is found to be influenced by the velocity and the composition of the mixture through the small flame ports. Thus it was possible to formulate a prediction criterion for this instability based only on the post processing of the numerical results. Furthermore, the composition of the gaseous mixture through the flame ports was checked in association with the laminar burning velocity curve of the fuel. This criterion of dynamic stability between the laminar burning velocity and the velocity magnitude of the unburned mixture was based on the extrapolated data of the laminar burning velocity curve. The prediction criterion was formulated as follows: the flame back occurs when (1) the laminar burning velocity exceeds the flow velocity through the burner; (2) the composition of the mixture is outside the flammability limits. Therefore, the gas volume concentration, pressure and temperature were monitored at different radii at the flame port exits in order to evaluate this dynamic stability criterion. In this way it was possible to highlight the boundaries of the stable flame regimes defined by the limit of flame back instability. This result provided a useful guideline for the design of domestic gas burners aiming to achieve a more stable operation with the butane working fluid.

As expected, the flame lift is affected by the formation and the homogenization of the reactive mixture and by the interaction of the flame with the burner

wall and the other surrounding flames. The structure and aerodynamics of the flame generated by a cooking appliance was thus characterized by experimental and numerical investigations, in which the flame behaviour, in conditions ranging from a stable reference case to blow-out, was studied by varying the flow inlet conditions. Considering the influence at different equivalence ratios of a fixed input power, the changes in the visual appearance of these flames suggest that a partial premixing decreases the flame height. Since the methane flow rate is held constant, the flame length will decrease since the higher is the partial premixing, the smaller is the amount of secondary air that must diffuse inward to create a stoichiometric mixture, and thus the smaller is the axial distance required for this diffusion to occur. On the other hand, the bottom flame edge does not seem to be influenced by the partial premixing until the flame lift-off occurs. At low injection velocities, this edge flame is attached or stabilized very close to the burner. On the other hand, at a higher injection speed, this flow acceleration forces the flame to adjust its location at a more favourable position. Therefore the flame lift-off occurs because of the balance between the laminar burning velocity and the unburnt reactant velocity. However, the greater stability of a fuel-rich flame, compared to a stoichiometric flame, also appears to be influenced by the interaction between the primary (premixed) and secondary (diffusive) combustion zone. Indeed, the secondary combustion zone acts as a pilot flame and retains the primary zone. As a result, the prediction criterion was formulated on the basis of different post-processing analyses performed on the numerical results in order to point out the variations of the flame structure. These investigations consisted of major species concentration profiles along the flame, flame index contours, mixture and volume fraction contours and flame stretch analysis. Each of them provides a complementary insight into the flame lift instability. In order to prevent this kind of instability the domestic gas burner flame should therefore present (1) a double flame structure; (2) the double point close to the burner wall; (3) the reaction kernel of high reactivity located at the flame base and (4) a flame stretch value below a threshold value at the double point. The double-flame nature of the flame is indeed quantitatively and qualitatively highlighted by the major species concentrations along the flame and the flame index contour, respectively. The spatial location of the double point of the flame bottom edge is characterized by the intersection of the stoichiometric volume fraction surface and the flame surface. The maximum reaction zone intensity and heat release rate represented by the reaction kernel can be observed in the heat release rates contour with superimposed volume fraction isolines and streamlines, showing the influence on the kernel position due to the balance between reaction, upstream diffusion and convection. Finally, the analysis of the flame stretch at the double point indicated a threshold value that determines the onset of the flame lift instability. All these numerical techniques have to be jointly adopted to provide a good prediction of flame stability in the context of the onset of flame lift.

Several future works can be carried out in order to provide a better insight

into, and foresight of, the features of domestic gas burners. Concerning the experimental analysis, a gas volume concentration measurement should be considered a necessary step during the development of a new domestic gas burner. Despite the difficulties in acquiring this kind of measurement, the value of the mixture concentration represents the key factor in order to understanding and predicting the features of the appliance, because it could clarify and quantify the uncertainty concerning the air entrainment process. Moreover, the validation of this measurement by the numerical model can be considered the missing information that would make numerical simulation a robust process. Furthermore, a comprehensive investigation of the flow field by means of PIV using reactive gas could be suggested. From the numerical point of view, several improvements can be pointed out too. Initially, the complete re-run of the DoE prototype families should be performed by implementing the combustion model; in this way the concept of flame stabilization based on critical boundaries will also be expanded to include the flame lift instability, allowing the formulation of a robust prediction criteria. Moreover, the implementation of the solid part in the model represents a further development in the numerical simulation because it allows to free the designer from the constrain to impose the temperature on the wall. In this way a temperature distributions on the different appliance components will be available through the domestic gas burner components. The numerical domain can be also improved by adding to the appliance configuration also the grids and, perhaps, the pot. In this way a complete simulation of a cooking top can be performed. Moreover, the application of a new combustion process, involving more (reversible) reactions and more chemical species will produce a more detailed flame solution and, most of all, the possibility to decouple the reaction velocities from the turbulence model. Furthermore, a time dependent simulation can increase the range of applicability of the model to investigate different domestic gas burner features (i.e., ignition process, turn down ratio, transient instability). Obviously, all these improvements regarding the numerical tool require high computational cost or long time to achieve a convergent simulation, that usually cannot be afford by an industry during the development phase of a new product. Maybe, due to greatly enhanced computer power, in few years this kind of simulations will become the daily run of a CFD engineer, and a number of new ideas and design solutions will appear.

Acknowledgments

First of all I would like to thank my main advisors Professor Alessandro Talamelli And Professor Franco Persiani from Bologna University for giving me the great opportunity to carry out this Ph.D. thesis and for the help I received during my work.
The best part of these three years was not anything I might have learned but all the fantastic people I met along the way, especially at II Facoltá di Ingenegneria Aerospaziale di Forlí.

A very special thanks goes out to Cédric Catalogne. He provided me with direction, technical support and became more of a mentor and friend, than a colleague.
I thank Marco Starnini for generously offering insightful and critical comments that have helped this research.
I also would like to thank Jean-Yves Noel for his significant contributions during this work and his thorough review of this thesis.
It was a pleasure for me to work with all the wonderful people in CTI and GTC.

My thanks extends to everyone involved with this Ph.D. from University of Illinois at Chicago. I would like to offer my sincere gratitude to Professor Suresh K. Aggarwal, Sibendu and Anita for their support and patience. I wish to thank Mirko, Andrea and Maria for making Chicago a home away from home.

A special thank to Riccardo Rossi. The support and sharing of our lives kept me grounded and helped me grow.

Forlí, 17 March 2009

Lorenzo Gattei *(lorenzo.gattei@gmail.com)*

List of Figures

List of Tables

Bibliography

[1] Pascale Domingo and Luc Vervisch. In *Proceedings of the Combustion Institute*, volume 26, pagine 233–240. The Combustion Institute, 1996.

[2] H.R.N. Jones. *Appliance of Combustion Principles to Domestic Gas Burner Design*. Taylor & Francis Books Ltd, 1990.

[3] C.E.N. *Domestic cooking appliances burning gas – Part1–1: Safety – General*. European Standard EN 30-1-1, 1997.

[4] C.E.N. *Test gases. Test pressures. Appliance categories*. European Standard EN 437, 2003.

[5] G. N. Abramovich. *The Theory of Turbulent Jets*. The MIT Press, 1963.

[6] R. Viskanta. Heat Transfer to Impinging Isothermal Gas and Flame Jets. *Experimental Thermal and Fluid Science*, 6:111–134, 1993.

[7] Lorenzo Gattei. *Jets*. Technical report, Electrolux Major Appliances Europe – CTI, 2006.

[8] Coleman duP. Donaldson and Richard S. Snedeker. A study of free jet impingement. Part 1. Mean properties of free and impinging jets. *Journal of Fluid Mechanics*, 45:281–319, 1971.

[9] A.J. Yule. Large scale structure in the mixing layer of a round jet. *Journal of Fluid Mechanics*, 89:413–432, 1978.

[10] K. Kataoka. Impingement heat transfer augmentation due to large scale eddies. *Proceedings of 9th Int. Heat Transfer Conference*, 1:255–273, 1996.

[11] Peter S. Bernard and James M. Wallace. *Turbulent Flow: Analysis, Measurement and Prediction*. Wiley, 2002.

[12] N. Blacker, R. Cowling, K. Parker, and J. Soria. A comparison between pulsed and continuous round jets. *International Symposium on Applications of Laser Techniques to Fluid Mechanics*, 13, 2006.

[13] Brice Prosperi, Jerôme Helie, and Rudy Bazile. FPIV Study of Density Effect on Air Entrainment in Gasoline Dense Sprays. *International Symposium on Applications of Laser Techniques to Fluid Mechanics*, 13, 2006.

[14] A.A. Townsend. The mechanism of entrainment in free turbulent flows. *Journal of Fluid Mechanics*, 26:689–715, 1966.

[15] W.M. Pitts. Reynolds number effects on the mixing behavior of axisymmetric turbulent jets. *Experiments in Fluids*, 11:135–141, 1991.

[16] S. Russ and P.J. Strykowski. Turbulent structure and entrainment in heated jets: The effect of initial conditions. *Physics of Fluids A*, 5:3216–3225, 1993.

[17] I. Serres, B.Sarh, C. Cheauveau, and I. Gokalp. Développement d'un jet à masse volumique variable impactant sur une plaque. *9º Congrès Francophone de Vélocimétrie Laser*, 2004.

[18] Baki M. Cetegen and Nazri Mohamad. Experiments on liquid mixing and reaction in a vortex. *Journal of Fluid Mechanics*, 249:391–414, 1993.

[19] P.J. Ashman, R. Junus, J.F. Stubington, and G.D. Sergeant. The Effects of Load Height on the Emissions from a Natural Gas-Fired Domestic Cooktop Burner . *Combustion Science and Technology*, 103:283–298, 1994.

[20] Rosita Junus, John Frank Stubington, and Geoffrey David Sergeant. The effects of design factors on emissions from natural gas cooktop burners. *International Journal of Environmental Studies*, 45:101–121, 1994.

[21] John Stubington, Geoffrey Sergeant, Rosita Junus, Gregory Beashel, Terence Murphy, Peter Ashman, and Ibrahim Tas. Methodology for the simultaneous measurement of emissions and efficiency for natural gas-fired cooktop burners. *International Journal of Environmental Studies*, 48:117–133, 1995.

[22] Yung-Chang Ko and Ta-Hui Lin. Emissions and efficiency of a domestic gas stove burning natural gases with various compositions. *Energy Conversion and Management*, 44:3001—-3014, 2003.

[23] Shuhn-Shyurng Hou and Yung-Chang Ko. Effects of heating height on flame appearance, temperature field and efficiency of an impinging laminar jet flame used in domestic gas stoves. *Energy Conversion and Management*, 45:1583—-1595, 2004.

[24] Shuhn-Shyurng Hou and Yung-Chang Ko. Influence of oblique angle and heating height on flame structure, temperature field and efficiency of an impinging laminar jet flame. *Energy Conversion and Management*, 46:941—-958, 2005.

[25] Shuhn-Shyurng Hou, Chien-Ying Lee, and Ta-Hui Lin. Efficiency and emissions of a new domestic gas burner with a swirling flame. *Energy Conversion and Management*, 48:1401—-1410, 2007.

[26] Irvin Glassman. *Combustion, Third Edition.* Academic Press, San Diego, 1997.

[27] Stuart B. Reed. An approach to the prediction of aerated-burner performance. *Combustion and Flame*, 13:583–595, 1969.

[28] P. Datta, B.M. Hayward, and S.B. Reed. A flame structure study of the stabilizing region of a near-stoichiometric laminar burner flame. *Combustion and Flame*, 17:399–408, 1971.

[29] Parimal Datta and Stuart B. Reed. A flame structure study of the stabilizing region of a fuel-rich flame and the effects of vitiation. *Combustion and Flame*, 19:89–99, 1972.

[30] D.L. van Oostendorp, C.E. van der Meij, and H.B. Levinsky. Entrainment and the effectiveness of retention flames in the burners of domestic cookers. *Journal of the Institute of Energy*, 66:17–19, 1993.

[31] R. Junus, J.E. Vierkant, J.F. Stubington, G. D. Sergeant, and I. Tas. The effects of the design of the cap of a natural gas-fired cooktop burner on flame stability. *International Journal of Energy Research*, 22:175–184, 1998.

[32] Luca Casarsa. *Experimental analysis of the fluid dynamics of a domestic gas burner by means of Particle Image Velocimetry technique.* Technical report, DIPARTIMENTO di ENERGETICA e MACCHINE, Universitá degli Studi di Udine, UDINE, Italy, 2006.

[33] Piero Pinamonti. *Experimental analysis of the fluid dynamics of a domestic gas burner by means of Particle Image Velocimetry technique.* Technical report, DIPARTIMENTO di ENERGETICA e MACCHINE, Universitá degli Studi di Udine, UDINE, Italy, 2004.

[34] Corine Lacour. *Stabilité de flammes laminaires partiellement prémélangées - Application aux brûleurs domestiques.* Ph.D. Thesis, CNRS UMR 6614 – CORIA, Université de Rouen, 2006.

[35] C. Lacour, D. Honore, A. Boukhalfa, and R. Hauguel. Stabilization Mechanisms of Laminar Partially Premixed Flames from Domestic-Like Burner. *Combustion Science and Technology*, 180:156–175, 2008.

[36] S.L. Plee and A.M. Mellor. Review of Flashback Reported in Prevaporizing/Premixing Combustors. *Combustion and Flame*, 32:193–203, 1978.

[37] A.A. Putnam, D.A. Ball, and A. Levy. Effect of fuel composition on relation of burning velocity to product of quenching distance and flashback velocity gradient. *Combustion and Flame*, 37:193–196, 1980.

[38] S.T. Lee and J.S. T'ien. A numerical analysis of flame flashback in a premixed laminar system. *Combustion and Flame*, 48:273–285, 1982.

[39] Y. Sommerer, D. Galley, T. Poinsot, S. Ducruix, F. Lacas, and D. Veynante. Large eddy simulation and experimental study of flashback and blow-off in a lean partially premixed swirled burner. *Journal of Turbulence*, 5:1–37, 2004.

[40] J.0. Keller, L. Vaneveld, D. Korschelt, G.L. Hubbard, A.F. Ghoniem, J.W. Daily, and A.K. Oppenheim. Mechanism of Instabilities in Turbulent Combustion Leading to Flashback. *AIAA Journal*, 20:254–262, 1982.

[41] R.W. Pitz and J.W. Daily. Combustion in a turbulent mixing layer formed at a rearward-facing step. *AIAA Journal*, 21:1565–1570, 1983.

[42] L. Vaneneld, K. Hom, and A.K. Oppenheim. Secondary effects in combustion instabilities leading to flashback. *AIAA Journal*, 22:81–82, 1984.

[43] Denis Thibaut and Sebastien Candel. Numerical Study of Unsteady Turbulent Premixed Combustion: Application to Flashback Simulation. *Combustion and Flame*, 113:53–65, 1998.

[44] O. Lucca-Negro and T. O'Doherty. Vortex breakdown: a review. *Progress in Energy and Combustion Science*, 27:431–481, 2001.

[45] Forman A. Williams. *Combustion Theory.* Addison-Wesley Publishing Company, INC., 1965.

[46] A.G. Gaydon and H.G. Wolfhard. *Flames: Their Structure, Radiation and Temperature, Third Edition.* Chapman & Hall, New York, 1979.

[47] Bernard Lewis and Guenther von Elbe. Stability and Structure of Burner Flames. *Journal of Chemical Physics*, 11:75–97, 1943.

[48] Guenther von Elbe and Morris Mentser. Further Studies of the Structure and Stability of Burner Flames. *Journal of Chemical Physics*, 13:89–100, 1945.

[49] K. Wohl. In *Proceedings of the Combustion Institute*, volume 4, pagine 68–89. The Combustion Institute, 1953.

[50] Henry C. Barnett and Robert R. Hibbard. *NACA Report 1300*. Technical report, NACA, 1957.

[51] A. L. Berlad and A. E. Potter. Relation of boundary velocity gradient for flash-back to burning velocity and quenching distance. *Combustion and Flame*, 1:127–128, 1957.

[52] P.F. Kurz. Some factors influencing stability limits of Bunsen flames. *Combustion and Flame*, 1:162–168, 1957.

[53] V.S. Babkin. Convective mechanism for quenching the flame of a bunsen burner. *Fizika Goreniya i Vzryva*, 9, 1973.

[54] Gary M. Hieftje. Burner Design Criteria and Variables Affecting Flash-back of Acetylene Flames. *Applied Spectroscopy*, 25:653–659, 1971.

[55] M.R.S. Nair and M.C. Gupta. Measurement of flame quenching distances in constant volume combustion vessels. *Combustion and Flame*, 21:321–324, 1973.

[56] S.H. Sohrab and C.K. Law. Influence of burner rim aerodynamics on polyhedral flames and flame stabilization. *Combustion and Flame*, 62:243–254, 1985.

[57] V.N. Kurdyumov, E. Fernández, and A. Li nán. In *Proceedings of the Combustion Institute*, volume 28, pagine 1883—1889. The Combustion Institute, 2000.

[58] V. Kurdyumov, E. Fernández-Tarrazo, J.M. Truffaut, J. Quinard, A. Wangher, and G. Searby. In *Proceedings of the Combustion Institute*, volume 31, pagine 1275–1282. The Combustion Institute, 2007.

[59] P.F. Kurz. Stability limits of flames of ternary hydrocarbon mixtures. *Combustion and Flame*, 1:3–13, 1957.

[60] P.F. Kurz. Influence of diborane on blow-off limits of hydrocarbon flames. *Combustion and Flame*, 1:212–216, 1957.

[61] P.F. Kurz. Behaviour of inverted propane-hydrogen sulphide flames at the blow-off limits. *Combustion and Flame*, 1:257–263, 1957.

[62] B. Karlowitz, D.W. Denniston, D.H. Knapschaefer, and F.E. Wells. In *Proceedings of the Combustion Institute*, volume 4, pagina 613. The Combustion Institute, 1953.

[63] Stuart B. Reed. Flame stretch — A connecting principle for blow-off data. *Combustion and Flame*, 11:177–189, 1967.

[64] Harry Edmondson and Michael Peter Heap. The correlation of burning velocity and blowoff data by the flame stretch concept. *Combustion and Flame*, 15:179–187, 1970.

[65] B. Lewis and G. von Elbe. *Combustion, Flames and Explosion of Gases.* Academic Press, Orlando, 1987.

[66] Takeshi Kawamura, Katsuo Asato, Tamotsu Mazaki, Tsuneo Hamaguchi, and Hirofumi Kayahara. Explanation of the blowoff of inverted flames by the area-increase concept. *Combustion and Flame*, 35:109–116, 1979.

[67] Takeshi Kawamura, Katsuo Asato, and Tamotsu Mazaki. Reexamination of the blowoff mechanism of premixed flames — inverted flames. *Combustion and Flame*, 45:225–233, 1982.

[68] N. Peters and F.A. Williams. Liftoff characteristics of turbulent jet diffusion flames. *AIAA Journal*, 21:423–429, 1983.

[69] W.M. Pitts. In *Proceedings of the Combustion Institute*, volume 22, pagine 809–816. The Combustion Institute, 1988.

[70] O. Savaş and S.R. Gollahalli. Stability of lifted laminar round gas-jet flame. *Journal of Fluid Mechanics*, 165:297–318, 1986.

[71] Douglas Feikema, Ruey-Hung Chen, and James F. Driscoll. Enhancement of flame blowout limits by the use of swirl. *27th Aerospace Sciences Meeting, January 9-12, Reno (Nevada)*, pagine 1–9, 1989.

[72] S.H. Chung and B.J. Lee. On the characteristics of laminar lifted flames in a nonpremixed jet. *Combustion and Flame*, 86:62–72, 1991.

[73] P.N. Kioni, B. Rogg, K.N.C. Bray, and A. Li nán. Flame spread in laminar mixing layers: The triple flame. *Combustion and Flame*, 95:276–290, 1993.

[74] B.J. Lee and S.H. Chung. Stabilization of lifted tribrachial flames in a laminar nonpremixed jet. *Combustion and Flame*, 109:163–172, 1997.

[75] Indrek S. Wichman and Bassem Ramadan. Theory of attached and lifted diffusion flames. *Physics of Fluids*, 10:3145–3154, 1998.

[76] L. Vervisch. In *Proceedings of the Combustion Institute*, volume 28, pagine 11—24. The Combustion Institute, 2000.

[77] Sandip Ghosal and Luc Vervisch. Stability diagram for lift-off and blowout of a round jet laminar diffusion flame. *Combustion and Flame*, 124:646–655, 2001.

[78] B. J. Lee and S. H. Chung. Characteristics of reattachment and blowout of laminar lifted flames in partially premixed propane jets. *Combustion and Flame*, 127:2194–2204, 2001.

[79] H. Phillips. In *Proceedings of the Combustion Institute*, volume 10, pagina 1277. The Combustion Institute, 1965.

[80] Yung-Cheng Chen and Robert W. Bilger. Stabilization mechanisms of lifted laminar flames in axisymmetric jet flows. *Combustion and Flame*, 122:377–399, 2000.

[81] F. Takahashi, W.J. Schmoll, and V.R. Katta. In *Proceedings of the Combustion Institute*, volume 27, pagine 675—684. The Combustion Institute, 1998.

[82] F. Takahashi and V.R. Katta. In *Proceedings of the Combustion Institute*, volume 28, pagine 2071—2078. The Combustion Institute, 2000.

[83] N.I. Kim, J.I. Seo, K.C. Oh, and H.D. Shin. In *Proceedings of the Combustion Institute*, volume 30, pagine 367—374. The Combustion Institute, 2005.

[84] M. I. Hassan, K. T. Aung, and G. M. Faeth. Measured and predicted properties of laminar premixed methane/air flames at various pressures. *Combustion and Flame*, 115:539–550, 1998.

[85] X.J. Gu, M.Z. Haq, M. Lawes, and R. Woolley. Laminar burning velocity and Markstein lengths of methane–air mixtures. *Combustion and Flame*, 121:41–58, 2000.

[86] H.S. Xue and Suresh K. Aggarwal. Effects of reaction mechanisms on structure and extinction of partially premixed flames. *AIAA Journal*, 39:637–645, 2001.

[87] Suresh K. Aggarwal and Ishwar K. Puri. Flame structure interactions and state relationships in an unsteady partially premixed flame. *AIAA Journal*, 36:1190–1199, 1998.

[88] K.A. Watson, K.M. Lyons, J.M. Donbar, and C.D. Carter. Observations on the leading edge in lifted flame stabilization. *Combustion and Flame*, 119:199–202, 1999.

[89] Beth Anne V. Bennett, Charles S. McEnally, Lisa D. Pfefferle, and Mitchell D. Smooke. Computational and experimental study of axisymmetric coflow partially premixed methane/air flames. *Combustion and Flame*, 123:522–546, 2000.

[90] Chun W. Choi and Ishwar K. Puri. Contribution of curvature to flame-stretch effects on premixed flames. *Combustion and Flame*, 126:1640–1654, 2001.

[91] Xiao Qin, Ishwar K. Puri, and Suresh K. Aggarwal. In *Proceedings of the Combustion Institute*, volume 29, pagine 1565—1572. The Combustion Institute, 2002.

[92] Xiao Qin, Chun W. Choi, Achintya Mukhopadhyay, Ishwar K. Puri, Suresh K. Aggarwal, and Viswanath R. Katta. Transition of propagating triple flames to burner attached flames in an axisymmetric jet. *38th AIAA/ASME/SAE/ASEE Joint Propulsion Conference and Exhibit, July 7-10, Indianapolis (IN)*, 2002.

[93] Xiao Qin, Ishwar K. Puri, Suresh K. Aggarwal, and Viswanath R. Katta. Effect of Gravity on Burner-Stabilized and Lifted Partially Premixed Flames. *41th Aerospace Science Meeting and Exhibit, January 6-9, Reno (NE)*, 2003.

[94] Andrew J. Lock, Alejandro M. Briones, Xiao Qin, Suresh K. Aggarwal, Ishwar K. Puri, and Uday Hegde. Liftoff characteristics of partially premixed flames under normal and microgravity conditions. *Combustion and Flame*, 143:159–173, 2005.

[95] A. Briones and S.K. Aggarwal. A Numerical Investigation Of Flame LiftOff And Stabilization. *44th Aerospace Science Meeting and Exhibit, January 9-12, Reno (NE)*, 2006.

[96] A. Briones, S.K. Aggarwal, and V.R. Katta. Characteristics of Propagating H_2-Enriched CH_4-Air Flames. *45th Aerospace Science Meeting and Exhibit, January 8-11, Reno (NE)*, 2007.

[97] Alejandro M. Briones, Suresh K. Aggarwal, and Viswanath R. Katta. Effects of H_2 enrichment on the propagation characteristics of CH_4–air triple flames. *Combustion and Flame*, 153:367–383, 2008.

[98] Andrew Lock, Suresh K. Aggarwal, Ishwar K. Puri, and Uday Hegde. "Suppression of fuel and air stream diluted methane–air partially premixed flames in normal and microgravity. *Fire Safety Journal*, 43:24–35, 2008.

[99] Riccardo Azzoni, Stefano Ratti, Suresh K. Aggarwal, and Ishwar K. Puri. The structure of triple flames stabilized on a slot burner. *34th AIAA/ASME/SAE/ASEE Joint Propulsion Conference and Exhibit, July 13-15, Cleveland (OH)*, 1998.

[100] Ishwar K. Puri, Suresh K. Aggarwal, Stefano Ratti, and Riccardo Azzoni. On the similitude between lifted and burner-stabilized triple flames: a numerical and experimental investigation. *Combustion and Flame*, 124:311–325, 2001.

[101] Chun W. Choi, Ranjan Ganguly, Andrew J. Lock, Ishwar K. Puri, Suresh K. Aggarwal, and Uday Hedge. Gravity Effects on Partially Premixed Flames. *41th Aerospace Science Meeting and Exhibit, January 6-9, Reno (NE)*, 2003.

[102] A. Wason, W. Carnell, M. Quinn, and M. Renfro. Lift-off Behavior and Flame Structure of Interacting Edge Flames. *42nd AIAA Aerospace Sciences Meeting and Exhibit, January 5-8, Reno (NE)*, 2004.

[103] S. Kostka, W. Carnell, and M. Renfro. Numerical Study of Neighboring Edge Flame Interactions. *45th Aerospace Science Meeting and Exhibit, January 8-11, Reno (NE)*, 2007.

[104] I.K. Puri and S.K. Aggarwal. Partially Premixed Flames: Applications and Issues. *45th Aerospace Science Meeting and Exhibit, January 8-11, Reno (NE)*, 2007.

[105] K.K. Kuo. *Principles of Combustion, Second Edition*. Wiley & Sons LTD., 2005.

[106] E. Caffo and C. Padovani. Flashback in premixed air flames. *Combustion and Flame*, 7:331–337, 1963.

[107] Madhav S. Phadke. *Quality engineering using robust design*. Prentice Hall, 1989.

[108] Douglas C. Montgomery. *Introduction to statistical quality control*. Wiley, 2004.

[109] Douglas C. Montgomery. *Design and analysis of Experiments*. John Wiley & Sons., 2000.

[110] Phillip J. Ross. *Taguchi Techniques for Quality Engineering*. McGraw-Hill Professional, 1995.

[111] Stefano Strada. *New Burner Crown Project*. Technical report, Electrolux Major Appliances Europe – GTC, 2004.

[112] R.B. Bird, W.E. Stewart, and E.N. Lightfoot. *Transport phenomena*. Wiley, New York, 1960.

[113] R.W. Bilger. Turbulent jet diffusion flames. *Progress in Energy and Combustion Science*, 1:87–109, 1975.

[114] David C. Wilcox. *Turbulence modeling for CFD*. DCW Industries Inc., 1988.

[115] David G. Sloan, Philip J. Smith, and L. Douglas Smoot. Modeling of swirl in turbulent flow systems. *Progress in Energy and Combustion Science*, 12:163–250, 1986.

[116] N. Djilali, I. Gartshore, and M. Salcudean. Enhancements Of The Simple Method For Predicting Incompressible Fluid Flows. *Numerical Heat Transfer*, 16:189–212, 1989.

[117] Lorenzo Gattei, Cédric Catalogne, and Mirko Agnetti. *CFDesign-Burner06 CFD Model calibration and validation*. Technical report, Electrolux Major Appliances Europe – CTI, 2006.

[118] W.P. Jones and B.E. Launder. The prediction of laminarization with a two-equation model of turbulence. *International Journal of Heat and Mass Transfer*, 15:301–314, 1972.

[119] Gaz de France. *Combustibles gazeux et principe de la combustion*. Technical report, Gaz de France BT 104, 1992.

[120] M. Nallasamy. *Survey of Turbulence Models for the Computation of Turbulent Jet Flow and Noise*. Technical report, NASA/CR-1999-206592, 1999.

[121] C.C. Chieng and B.E. Launder. On The Calculation Of Turbulent Heat Transport Downstream From An Abrupt Pipe Expansion. *Numerical Heat Transfer*, 3:189–207, 1980.

[122] R.S. Amano. Development of A Turbulence Near-Wall Model And Its Application To Separated And Reattached Flows. *Numerical Heat Transfer*, 7:59–75, 1984.

[123] Brian E. Launder. Second–moment closure: present... and future? *International Journal of Heat and Fluid Flow*, 10:282–300, 1989.

[124] P.G. Huang and P. Bradshaw. Law of the wall for turbulent flows in pressure gradients. *AIAA Journal*, 33:624, 1995.

[125] P. Bradshaw, B. E. Launder, and J. L. Lumley. Collaborative Testing of Turbulence Models. *Journal of Fluids Engineering*, 118:243–247, 1996.

[126] T. Rung. Formulierung universeller Wandrandbedingungen für Transportgleichungsturbulenzmodelle. *Hermann Fottinger Institut fur Stromungsmechanik, Technische Univesritat at Berlin*, Institutsbericht Nr. 02/99, 1999.

[127] CD-Adapco. *Star-CD v3.26 Methodology Manual*. CD-Adapco, 2005.

[128] A.M. Eaton, L.D. Smoot, S.C. Hill, and C.N. Eatough. Components, formulations, solutions, evaluation, and application of comprehensive combustion models. *Progress in Energy and Combustion Science*, 25:387–436, 1999.

[129] Craig T. Bowman and Daniel J. Seery. Chemiluminescence in the high-temperature oxidation of methane. *Combustion and Flame*, 12:611–614, 1968.

[130] K. N. C. Bray. Turbulent flows with premixed reactants. *Turbulent Reacting Flows. Topic in Applied Physics*, 44:115, 1980.

[131] B. F. Magnussen and B. H. Hjertager. In *Proceedings of the Combustion Institute*, volume 16, pagine 719–729. The Combustion Institute, 1976.

[132] D.B. Spalding. In *Proceedings of the Combustion Institute*, volume 13, pagine 649–657. The Combustion Institute, 1971.

[133] J.M. Duclos, D. Veynante, and T. Poinsot. A Comparison of Flamelet Models for Premixed Turbulent Combustion. *Combustion and Flame*, 95:101–117, 1993.

[134] J. Abraham, F.V. Bracco, and R.D. Reitz. Comparisons of computed and measured premixed charge engine combustion. *Combustion and Flame*, 60:309–322, 1985.

[135] C.K. Westbrook and F.L. Dryer. Simplified reaction mechanisms for the oxidation of hydrocarbon fuels in flames. *Combustion Science and Technology*, 27:31–43, 1981.

[136] Weihong Yang and Blasiak Wlodzimierz. Flame entrainments induced by a turbulent reacting jet using high-temperature and oxygen-deficient oxidizers. *Energy & fuels*, 19:1473–1483, 2005.

[137] A. Bentebbiche, K. Bouhadef, D. Veynante, and E. Esposito. Numerical investigation for prediction of pollutants formation type CO and NO in premixed turbulent flame using an extended coherent flame model. *Forschung im Ingenieurwesen*, 69:236–245, 2005.

[138] J.I. Ramos. *Numerical modeling in combustion.* Taylor and Francis, Washington DC, 1993.

[139] T.J. Chung. *Numerical modeling in combustion.* Taylor and Francis, Washington DC, 1993.

[140] S.V. Patankar. *Numerical heat transfer and fluid flow.* Hemisphere Publishing Corp., Washington DC, 1980.

[141] Charles Hirsch. *Numerical computation of internal & External Flows, Second Edition.* Elsevier, 2007.

[142] Cédric Catalogne. *Optimal gas burner – Design criteria for flame stability and combustion performance.* Technical report, Electrolux Major Appliances Europe – CTI, 2005.

[143] Michael Casey and Torsten Wintergerste. *Special interest group on Quality and Trust in Industrial CFD – Best Practice Guidelines.* ERCOFTAC, 2000.

[144] Charles E. Baukal Jr., Vladimir Y. Gershten, and Xianming Li. *Computational Fluid Dynamics in Industrial Combustion.* CRC Press, 2001.

[145] B. Lawton and G. Klingenberg. *Transient temperature in engineering and science.* Oxford University Press, 1996.

[146] Lorenzo Gattei. *Pressure and Temperature Measurements.* Technical report, Electrolux Major Appliances Europe – CTI, 2006.

[147] AIAA Guide for the Verification and Validation of Computational Fluid Dynamics Simulations. *AIAA Standards Series*, 1998.

[148] Arthur Rizzi and Jan Vos. Toward Establishing Credibility in Computational Fluid Dynamics Simulations. *AIAA Journal*, 36:668–675, 1998.

[149] John D. Anderson. *Fundamentals of Aerodynamics.* McGraw Hill Higher Education, 2001.

[150] Ertan Baydar. Confined impinging air jet at low Reynolds numbers. *Experimental Thermal and Fluid Science*, 19, 1999.

[151] T.J. Craft, H. Iacovides, and J.H. Yoon. "Progress in the Use of Non-linear Two-Equation Models in the Computation of Convective Heat-Transfer in Impinging and Separated Flows. *Flow, Turbulence and Combustion*, 63:59–80, 1999.

[152] Yan Zhang, Jing yu Fan, and Johan Liu. *Numerical investigation based on CFD for air impingement heat transfer in electronic cooling.* Technical report.

[153] S. Ashforth-Frost and K. Jambunathan. Numerical Prediction Of Semi-Confined Jet Impingement And Comparison With Experimental Data. *International Journal for Numerical Methods in Fluids*, 23:295–306, 1996.

[154] S. Senthooran, Dong-Dae Lee, and S. Parameswaran. A computational model to calculate the flow-induced pressure fluctuations on buildings. *Journal of Wind Engineering and Industrial Aerodynamics*, 92:1131—-1145, 2004.

[155] Lorenzo Gattei. *Thermo physical properties.* Technical report, Electrolux Major Appliances Europe – CTI, 2006.

[156] Lorenzo Gattei. *Instability of Partially Premixed Flame: a review on flame back and flame lift.* Technical report, Electrolux Major Appliances Europe – CTI, 2006.

[157] J. Warnatz, U. Maas, and R.W. Dibble. *Combustion. Physical and Chemical Fundamentals, Modeling and Simulation, Experiments, Pollutant Formation.* Springer, 2006.

[158] Li Qiao, Yongxian Gu, Werner J.A. Dahm, Elaine S. Oran, and Gerard M. Faeth. In *Proceedings of the Combustion Institute*, volume 31, pagine 2701—-2709. The Combustion Institute, 2007.

[159] Gaz de France. *Combustibles gazeux et principes de combustion. BT No.104.* Gaz de France, Paris, 1992.

[160] A. Murty Kanury. *Introduction to Combustion Phenomena.* Gordon and Breach Science Publisher, 1984.

[161] Charles S. McEnally and Lisa D. Pfefferle. Experimental study of nonfuel hydrocarbon concentrations in coflowing partially premixed methane/air flames. *Combustion and Flame*, 118:619–632, 1999.

[162] L. Boyer. Laser tomographic method for flame front movement studies. *Combustion and Flame*, 39:321–323, 1980.

[163] M. C. Escoda and M. B. Long. Rayleigh Scattering Measurements of the Gas Concentration Field in Turbulent Jets. *AIAA Journal*, 21:81–84, 1983.

[164] N. Darabiha, V. Giovangigli, A. Trouve, S. Candel, and E. Esposito. In *Proc. France-USA Joint Workshop on Turbulent Combustion, Turbulent Reactice Flows, R. Borghi and S. N. B. Murthy, Eds.*, pagine 591–637, 1989.

[165] S. Candel, D. Veynante, F. Lacas, E. Maistret, N. Darabiha, and T. Poinsot. In *Recent Advances in Combustion Modelling, World Scientific, Singapore*, pagine 19–64, 1991.

[166] R. K. Hanson. In *Proceedings of the Combustion Institute*, volume 21, pagine 1677–1691. The Combustion Institute, 1986.

[167] R. K. Hanson. Planar Laser-Induced Fluorescence. *J. Quant. Spectrosc. Radiat. Transfer*, 40:343–362, 1988.

[168] A. Eckbreth. *Laser Diagnostics for Combustion Temperature and Species*. Abacus Press, Cambridge MA, 1988.

[169] K. Kohse Hoinghaus. Laser techniques for the quantitative detection of reactive intermediates in combustion systems. *Progress in Energy and Combustion Science*, 20:203–279, 1994.

[170] M. J. Dyer and D. R. Crosley. In *Proc. (International) Conference Lasers '84*, pagine 211–216, 1985.

[171] J.G. Lee and D.A. Santavicca. Experimental Diagnostics for the Study of Combustion Instabilities in Lean Premixed Combustors. *J. Propuls. Power*, 19:735–750, 2003.

[172] M. Barrère and S. Barrère. Etude Spectrographique d'une Flamme Stabilisée dans un Ecoulement. *Rech. Aerosp.*, 67:11–19, 1958.

[173] R.W. Dibble, M.B. Long, and A. Masri. Two-Dimensional Imaging of C_2 in Turbulent Nonpremixed Jet Flames. *Prog. Astronaut. Aeronaut.*, 105:99–109, 1986.

[174] R.J. John, E.S. Wilson, and M. Summerfield. Studies of the Mechanism of Flame Stabilization by a Spectral Intensity Method. *Jet Propulsion*, 25:535, 1955.

[175] R.J. John and M. Summerfield. Effect of Turbulence on Radiation Intensity from Propane-Air Flames. *Jet Propulsion*, 27:169–179, 1957.

[176] C.L. Beyler and F.C. Gouldin. In *Proceedings of the Combustion Institute*, volume 18, pagine 1011–1019. The Combustion Institute, 1981.

[177] B. Higgins, M. Q. McQuay, F. Lacas, and S. Candel. An experimental study on the effect of pressure and strain rate on CH chemiluminescence of premixed fuel-lean methane/air flames. *Fuel*, 80:1583–1591, 2001.

[178] Trinh K. Pham, Derek Dunn-Rankin, and William A. Sirignano. In *Proceedings of the Combustion Institute*, volume 31, pagine 3269–3275. The Combustion Institute, 2007.

[179] Y. Hardalupas and M. Orain. Local measurements of the time-dependent heat release rate and equivalence ratio using chemiluminescent emission from a flame. *Combustion and Flame*, 139:188–207, 2004.

[180] Quang-Viet Nguyena and Phillip H. Paul. In *Proceedings of the Combustion Institute*, volume 26, pagine 357–364. The Combustion Institute, 1996.

[181] Shohji Tsushima, Hiroyasu Saitoh, Fumiteru Akamatsu, and Masashi Katsuki. In *Proceedings of the Combustion Institute*, volume 27, pagine 1967–1974. The Combustion Institute, 1998.

[182] Habib N. Najm, Phillip H. Paul, Charles J. Mueller, and Peter S. Wyckoff. On the Adequacy of Certain Experimental Observables as Measurements of Flame Burning Rate. *Combustion and Flame*, 113:312–332, 1998.

[183] Bengt Johansson, Magnus Christensen, Anders Hultqvist, Mattias Richter, Marcus Alden, and Axel Franke. A Study of the Homogeneous Charge Compression Ignition Combustion Process By Chemiluminescence Imaging. *Society of Automotive Engineers (SAE)*, 1999-01-3680, 1999.

[184] B. Kim, M. Kaneko, Y. Ikeda, and T. Nakajima. In *Proceedings of the Combustion Institute*, volume 29, pagine 671—677. The Combustion Institute, 2002.

[185] B.O. Ayoola, R. Balachandran, J.H. Frank, E. Mastorakos, and C.F. Kaminski. Spatially resolved heat release rate measurements in turbulent premixed flames. *Combustion and Flame*, 144:1–16, 2006.

[186] Zhuang Shua, Brady J. Krassa, Chun W. Choia, Suresh K. Aggarwala, Viswanath R. Katta, and Ishwar K. Puri. In *Proceedings of the Combustion Institute*, volume 27, pagine 625—-632. The Combustion Institute, 1998.

[187] A. Fayoux, K. Zähringer, O. Gicquel, and J.C. Rolon. In *Proceedings of the Combustion Institute*, volume 30, pagine 251–257. The Combustion Institute, 2005.

[188] F. G. Roper, C. Smith, and A. C. Cunningham. The prediction of laminar jet diffusion flame sizes: Part II. Experimental verification. *Combustion and Flame*, 29:227–234, 1977.

[189] F. G. Roper. Soot Escape from Diffusion Flames: A Comparison of Recent Work in this Field. *Combustion Science and Technology*, 40:323–329, 1984.

[190] Hongsheng Guo, Fengshan Liu, and Gregory J. Smallwood. A numerical study on NO_x formation in laminar counterflow CH_4/air triple flames. *Combustion and Flame*, 143:282–298, 2005.

[191] Alejandro M. Briones, Sibendu Som, and Suresh Aggarwal. Effect of multistage combustion on NO_x emissions in methane–air flames. *Combustion and Flame*, 149:448–462, 2007.

[192] H. Yamashita, M. Shimada, and T. Takeno. In *Proceedings of the Combustion Institute*, volume 26, pagine 27–34. The Combustion Institute, 1996.

[193] Pascale Domingo, Luc Vervisch, and Julien Réveillon. DNS analysis of partially premixed combustion in spray and gaseous turbulent flamebases stabilized in hot air. *Combustion and Flame*, 140:172–198, 2005.

[194] R.W. Bilger. In *Proceedings of the Combustion Institute*, volume 22, pagine 475–488. The Combustion Institute, 1988.

[195] S.H. Won, J. Kim, K.J. Hong, M.S. Cha, and S.H. Chung. In *Proceedings of the Combustion Institute*, volume 30, pagine 339–347. The Combustion Institute, 2005.

[196] Kevin T. Walsh, Joseph Fielding, Mitchell D. Smooke, Marshall B. Long, and Amable Liñán. In *Proceedings of the Combustion Institute*, volume 30, pagine 357–365. The Combustion Institute, 2005.

[197] C.K. Law. In *Proceedings of the Combustion Institute*, volume 22, pagine 1381–1402. The Combustion Institute, 1988.

[198] G. H. Markstein. *Nonsteady Flame Propagation, First Edition.* The Macmillan Company, Pergamon Press, New York, 1964.

[199] F.A. Williams. In *AGARD Conference Proceedings*, volume No. 164, 1975.

[200] Roger A. Strehlow and Lester D. Savage. The concept of flame stretch. *Combustion and Flame*, 32:209–211, 1978.

[201] Moshe Matalon. On Flame Stretch. *Combustion Science and Technology*, 31:169–181, 1983.

[202] S. H. Chung and C. K. Law. An invariant derivation of flame stretch. *Combustion and Flame*, 55:123–125, 1984.

[203] L. P. H. de Goey, R. M. M. Mallens, and J. H. M. Ten Thije Boonkkamp. An evaluation of different contributions to flame stretch for stationary premixed flames. *Combustion and Flame*, 110:54–62, 1997.

[204] L. P. H. De Goey and J. H. M. Ten Thije Boonkkamp. A Mass-Based Definition of Flame Stretch for Flames with Finite Thickness. *Combustion Science and Technology*, 122:399–405, 1997.

[205] Anurag Jhalani. *A numerical study of stretch in partially pemixed flames.* Master Thesis, University of Illinois at Chicago, Chicago, Illinois, U.S.A., 2001.

[206] C. K. Law. *Combustion Physics.* Cambridge University Press, 2006.

[207] David W. Mikolaitis. Strained Laminar Premixed Flames. *Combustion Science and Technology*, 53:203–216, 1987.

[208] G. H. Markstein. *Nonsteady Flame Propagation, Second Edition.* The Macmillan Company, Pergamon Press, New York, 1975.

[209] Gregory I. Sivashinsky, Chung K. Law, and Guy Joulin. On Stability of Premixed Flames In Stagnation - Point Flow. *Combustion Science and Technology*, 28:155–159, 1982.

[210] M. Matalon and B. J. Matkowsky. Flames as gasdynamic discontinuities. *Journal of Fluid Mechanics*, 124:239–259, 1982.

[211] Habib N. Najm and Peter S. Wyckoff. Premixed flame response to unsteady strain rate and curvature. *Combustion and Flame*, 110:92–94, 1997.

[212] Tarek Echekki and Jacqueline H. Chen. Unsteady strain rate and curvature effects in turbulent premixed methane-air flames. *Combustion and Flame*, 106:184–190, 1996.

[213] R. Zhong, S. E. Elghobashi, and O. N. Boratav. Surface topology of a buoyant turbulent nonpremixed flame. *Physics of Fluids*, 12:2091–2100, 2000.

[214] H. G. Im and J. H. Chen. Structure and propagation of triple flames in partially premixed hydrogen–air mixtures. *Combustion and Flame*, 119:436–454, 1999.

[215] J.H. Chen and H.G. Im. In *Proceedings of the Combustion Institute*, volume 28, pagine 211—218. The Combustion Institute, 2000.

[216] H. G. Im and J. H. Chen. Preferential diffusion effects on the burning rate of interacting turbulent premixed hydrogen-air flames. *Combustion and Flame*, 131:246–258, 2002.

[217] R. K. Cheng I. G. Shepherd. The burning rate of premixed flames in moderate and intense turbulence. *Combustion and Flame*, 127:2066–2075, 2001.

[218] C.J. Lawn and R.W. Schefer. Scaling of premixed turbulent flames in the corrugated regime. *Combustion and Flame*, 146:180–199, 2006.

[219] James F. Driscoll. Turbulent premixed combustion: Flamelet structure and its effect on turbulent burning velocities. *Progress in Energy and Combustion Science*, 34:91–134, 2008.

[220] Anurag Jhalani, Achintya Mukhopadhyay, and Ishwar K. Puri. In *Meeting of Western State Section of Combustion Institute*, volume Paper No. 01F-3, 2001.

[221] G. R. Ruetsch, L. Vervisch, and A. Li nàn. Effects of heat release on triple flames. *Physics of Fluids*, 7:1447–1454, 1995.

[222] G. R. Ruetsch and J. E. Broadwell. Effects of confinement on partially premixed flames. Center for Turbulence Research, Stanford University, 1995.

[223] J.H. Chen and H.G. Im. In *Proceedings of the Combustion Institute*, volume 27, pagine 819—826. The Combustion Institute, 1998.

[224] T. Poinsot, T. Echekki, and M. G. Mungal. A Study of the Laminar Flame Tip and Implications for Premixed Turbulent Combustion. *Combustion Science and Technology*, 81:45–73, 1992.

[225] M. Nishioka, S. Nakagawa, Y. Ishikawa, and T. Takeno. NO emission characteristics of methane-air double flame. *Combustion and Flame*, 98:127–138, 1994.

[226] M. A. Tanoff, M. D. Smooke, R. J. Osborne, T. M. Brown, and R. W. Pitz. In *Proceedings of the Combustion Institute*, volume 26, pagine 1121–1128. The Combustion Institute, 1996.